

Behavior of reinforcing steel and reinforced concrete undergoing stray current

Chen, Zhipei

DOI

[10.4233/uuid:8ed1e48a-5c00-47d9-b1bf-ef7d06fab048](https://doi.org/10.4233/uuid:8ed1e48a-5c00-47d9-b1bf-ef7d06fab048)

Publication date

2021

Document Version

Final published version

Citation (APA)

Chen, Z. (2021). *Behavior of reinforcing steel and reinforced concrete undergoing stray current*. [Dissertation (TU Delft), Delft University of Technology]. <https://doi.org/10.4233/uuid:8ed1e48a-5c00-47d9-b1bf-ef7d06fab048>

Important note

To cite this publication, please use the final published version (if applicable).
Please check the document version above.

Copyright

Other than for strictly personal use, it is not permitted to download, forward or distribute the text or part of it, without the consent of the author(s) and/or copyright holder(s), unless the work is under an open content license such as Creative Commons.

Takedown policy

Please contact us and provide details if you believe this document breaches copyrights.
We will remove access to the work immediately and investigate your claim.

Behavior of reinforcing steel and reinforced concrete undergoing stray current

Proefschrift

ter verkrijging van de graad van doctor
aan de Technische Universiteit Delft,
op gezag van de Rector Magnificus Prof.dr.ir. T.H.J.J. van der Hagen,
voorzitter van het College voor Promoties,
in het openbaar te verdedigen op
Woensdag 24 February 2021 om 15:00 uur

door

Zhipei CHEN

Master of Engineering in Structural Engineering, Dalian University of
Technology, P.R. China
geboren te Hengshui, Hebei, P.R. China

Dit proefschrift is goedgekeurd door:

Promotor: Prof. dr. ir. K. van Breugel

Copromotor: Dr. ir. D. A. Koleva

Samenstelling promotiecommissie bestaat uit:

Rector Magnificus,	Voorzitter
Prof.dr.ir. K. van Breugel	Delft University of Technology, promotor
Dr.ir. D.A. Koleva	Delft University of Technology, copromotor

Onafhankelijke leden:

Prof.dr. B.M. Wang	Dalian University of Technology
Prof.dr.ir. E.A.B. Koenders	Technical University of Darmstadt
Prof.dr. C. Andrade	International Centre for Numerical Methods in Engineering
Prof.dr.ir. R.P.B.J. Dollevoet	Delft University of Technology
Prof.dr.ir. H.E.J.G. Schlangen	Delft University of Technology

Keywords: Stray current, anodic polarization, steel rebar, corrosion, mortar, interface, bond, electrochemical response, rebar orientation.

Printed by: Gildeprint - The Netherlands

Cover design: Zhipei Chen

ISBN: 978-94-6419-150-9

Author email: zhipeichen@outlook.com

An electronic version of this dissertation is available at
<http://repository.tudelft.nl/>

Copyright © 2021 by Zhipei Chen

All rights reserved. No part of the material protected by this copyright notice may be reproduced or utilized in any form or by any means, electronic or mechanical, including photocopying, recording or by any information storage and retrieval system, without written permission from the author.

To my family

To my father Baoyou Chen (陈宝友)

To my mother in heaven Baoju Zhao (赵宝菊)



Springtime 1990, Jianguo zhongxue, Jianguo Town, Hengshui City, Hebei Province, P.R. China.

Propositions

Accompanying the PhD Thesis

Behavior of reinforcing steel and reinforced concrete undergoing stray current

By

Zhipei Chen

Delft, February 2021

1. Stray current induces both anodic polarization and cathodic polarization on steel rebar. Therefore only testing anodic polarization is not sufficient to judge on stray current effects. (This thesis)
2. Stray current induces back flow in steel rebar, after the stray current is just turned off. This implies the interconversion between anode and cathode induced by stray current, i.e., post-stray current effect. (This thesis)
3. No wind is favorable if you do not know which port you are sailing to.
4. Perfectionism is luxury, expedience is essence.
5. Everybody has things she/he is good in.
6. What does not kill me, makes me stronger. (Friedrich Wilhelm Nietzsche, German philosopher)
7. No one is born to be lonely.
8. Everything we understand seems easy.
9. All grown-ups were once children, but only few of them remember it. (Antoine de Saint Exupéry, French writer)
10. If you want to build a roof, you have to build a foundation first.

These propositions are regarded as opposable and defendable, and have been approved as such by the promotor Prof. dr. ir. Klaas van Breugel and copromotor Dr. ir. Dessi Koleva.

Summary

Currents flowing along paths not being elements of a purpose-built electric circuit, are called stray currents. Various types of reinforced concrete structures (such as viaducts, bridges and tunnels) in the neighborhoods of railways may be subjected to stray current leaking from the rails. In these cases the concrete pore solution acts as an electrolyte, and the reinforcing rebars (or pre-stressed steel wires) embedded in concrete act as conductors, which can “pick up” the stray current and can corrode.

The understanding of stray current-induced corrosion of steel rebar in concrete still remains unclear, as it is challenging to inspect in detail the full scale of steel rebar, as embedded in concrete. Most of previous understanding and preventive measures for stray current corrosion refer to investigations or field tests on pipelines. Besides, it is difficult to rebuild or repair the structures under or near rail transits. All above reasons reflect that stray current corrosion of reinforced concrete structures is in need of more in-depth investigation and understanding.

As an expansion of the current body of knowledge of stray current corrosion of steel rebar in cement-based materials, this research aims to be a step forward towards for a better understanding of stray current corrosion mechanisms, a basis of feasible preventive measures for stray current-induced corrosion of reinforced concrete structures.

The conditions for the steel rebar to pick up stray current are analyzed in Chapter 3. A concrete culvert under railway line is referred to as a practical case to illustrate the issue. The existing means for reducing stray current corrosion of concrete infrastructure are discussed. On the basis of literature review and practical cases, remaining scientific challenges related with stray current corrosion of steel in reinforced concrete structures are summarized.

For simulating stray current-induced corrosion of metals, most researchers just supplied anodic polarization on samples. However, stray current induces both cathodic polarization and anodic polarization. Chapter 4 deals with this issue by studying experimentally the performance of reinforced concrete specimens under different types of currents. A comparison between stray current and anodic polarization effects on the corrosion behavior of embedded steel is performed, for both fresh (24 hour-cured/24h-cured) and hardened matrix (28 day-cured/28d-cured), in chloride-free (Cl-free) and chloride-containing (Cl-containing) environments. It is found that in all conditions anodic polarization leads to significantly different electrochemical performance of the steel rebar, compared to stray current.

Very few investigations reported on the influence of stray current-induced corrosion on the bond of steel-concrete or steel-mortar interface. Chapter 5 presents test results on the bond strength of reinforced mortar undergoing stray current and anodic polarization, while conditioned in either Cl-free or Cl-containing medium. The bond behavior of the steel-mortar interface, derived by the pull-out tests, is correlated to the electrochemical response of the steel rebar and the properties of bulk matrix. The effect of stray current on bond strength versus the effect of anodic polarization is discussed. The effects of the curing regimes (in terms of duration of curing) and starting point of stray current (e.g. stray current applied at 24h or 28d) are also investigated. It is found that stray current (level of 0.3 mA/cm^2) exerts bond strength degradation in all cases, irrespective of the presence or absence of a corroder (Cl^-) in the external medium.

The reinforcement in reinforced concrete elements usually consists of a steel rebar cage. Stray current flowing in reinforced concrete can then be parallel or orthogonal to the steel rebar. Chapter 6 investigates the stray current corrosion on steel rebar in different orientations (relative to the direction of the stray current). Based on the test results, it is clear that the geometrical position of the steel bar undergoing stray current affects the electrochemical response of steel rebar. A more significant corrosion state is observed when the steel bar is parallel to the direction of the current, compared to the situation of a steel bar is orthogonal to the electrical current. These outcomes are further clarified through the recorded level of stray current picked-up by steel rebar. It is found that, although the supplying stray current is constant, the level of current actually picked-up by the steel rebar is decreasing. At the instant when the stray current supply is just turned off, an opposite current flow (back flow) is recorded. It is caused by the stray current-induced potential difference between anode and cathode.

According to the test results of this research, some recommendations for the practice and future research are summarized as below:

Only testing anodic polarization is not sufficient to judge stray current effects on steel-concrete interface. The evaluation of both electrochemical phenomena of steel rebar and properties of concrete bulk, will allow a more accurate appraisal of stray current effects on steel-concrete interface. Stray current effects on reinforced concrete structures with different mixtures/additives should be studied, because the different mixtures/additives lead to different properties of bulk matrix surrounding steel, and influence the stray current effects on steel-concrete interface.

Stray current effects on the fatigue, deflections and ductility of reinforced concrete elements (for instance, beams) are worthy to be investigated. This is because stray current leads to the degradation of steel-concrete interface, which determines the above properties of reinforced concrete elements.

The back flow induced by stray current is of importance in stray current induced-corrosion of rebar. For modeling or predicting the bond property of steel-concrete interface affected by stray current, the back flow should be considered, as the back flow re-distributes the corrosion product after the stray current interference. Sectionalization of reinforced concrete structures is a possible solution for mitigating the stray current effect, as it is found that the longer length of steel rebar leads to more severe corrosion damage.

Table of Contents

Summary	I
 Chapter 1 General Introduction	 1
1.1 Research background	1
1.2 Scope of this research.....	3
1.3 Objectives of this research	3
1.4 Research strategy and outline of this thesis	4
 Chapter 2 Literature Review	 7
2.1 Introduction	7
2.2 Sources of stray current.....	7
2.2.1 Electrified traction system.....	7
2.2.2 Cathodic protection (CP) system.....	10
2.2.3 High voltage power lines.....	10
2.2.4 Disturbances of the earth's magnetic field	12
2.2.5 Stray current underwater	12
2.2.6 Electrolysers and bus ducts	12
2.2.7 Other sources.....	12
2.3 Characteristics of stray current.....	13
2.4 Corrosion of steel caused by stray current	14
2.4.1 Steel corrosion caused by stray alternating current (AC)	14
2.4.2 Mechanism of stray direct current (DC) induced corrosion.....	15
2.5 Monitoring and evaluation of stray current.....	16
2.6 Concluding remarks	17
 Chapter 3 Conditions for rebar to pick up stray current and means for reducing stray current effects	 19
3.1 Introduction	19
3.2 Stray current corrosion in reinforced concrete culvert under railway.....	19
3.3 Steel rebar in culvert under railway subjected to stray current	21
3.4 Means for reducing stray current effects	24

3.4.1	Measures on stray current sources	24
3.4.1.1	<i>Track</i>	24
3.4.1.2	<i>Railway earthing systems</i>	24
3.4.2	Measures on ambient conditions	25
3.4.2.1	<i>Stray current collection system</i>	25
3.4.2.2	<i>Electrical drainage bond</i>	26
3.4.2.3	<i>Electrical shield</i>	26
3.4.3	Measures on interfered structure itself	27
3.4.3.1	<i>Insulating couplings</i>	27
3.4.3.2	<i>Intentional anodes and cathodic protection</i>	28
3.4.3.3	<i>Application of coatings</i>	28
3.4.3.4	<i>Electrical discontinuity</i>	29
3.5	Challenges to be dealt with in this thesis	29

Chapter 4 Corrosion of reinforcing steel undergoing stray current and anodic polarization31

4.1	Introduction	31
4.2	Experimental	33
4.2.1	Materials and specimen preparation.....	33
4.2.2	Curing and conditioning.....	34
4.2.3	Experimental methods.....	35
4.3	Results and discussion.....	36
4.3.1	OCP and R_p evolution	36
4.3.1.1	<i>OCP and R_p of 24 hours-cured specimens</i>	37
4.3.1.2	<i>OCP and R_p of 28 days-cured specimens</i>	39
4.3.2	Curing effect reflected by EIS response.....	41
4.3.3	Competitive mechanisms of stray current and Cl^- at early age	44
4.3.4	EIS response indicating difference between stray current and anodic polarization.....	47
4.3.5	Potential decay monitoring over 24 hours.....	52
4.4	Conclusions	55

Chapter 5 Bond of steel-mortar interface interfered by stray current and anodic polarization57

5.1	Introduction	57
-----	--------------------	----

5.2	Experimental	58
5.2.1	Materials and specimen preparation.....	58
5.2.2	Curing and conditioning.....	59
5.2.3	Testing Methods.....	60
5.2.3.1	<i>Electrochemical measurements</i>	60
5.2.3.2	<i>Pull-out test</i>	61
5.3	Results and discussion.....	61
5.3.1	OCP and R_p	62
5.3.2	Pull-out test results	64
5.3.2.1	<i>Typical bond-slip relationship curves</i>	64
5.3.2.2	<i>Bond behavior</i>	65
5.3.3	PDP.....	70
5.3.3.1	<i>PDP response of Cl-free specimens</i>	70
5.3.3.2	<i>PDP response of Cl-containing specimens</i>	72
5.3.4	EIS	73
5.3.4.1	<i>General consideration for EIS fitting</i>	73
5.3.4.2	<i>EIS response of Cl-free specimens</i>	77
5.3.4.3	<i>EIS response of Cl-containing specimens</i>	78
5.3.5	Summary of mechanisms for stray current inducing bond loss	79
5.4	Conclusions	80

Chapter 6 Stray current corrosion as determined by geometrical orientation of steel rebar..... 81

6.1	Introduction	81
6.2	Experimental	82
6.2.1	Materials and Specimens.....	82
6.2.2	Testing Methods.....	83
6.2.2.1	<i>Electrochemical tests</i>	83
6.2.2.2	<i>Potential change monitoring on individual specimens</i>	83
6.2.2.3	<i>Picked-up current levels in a stray current electrical field</i>	84
6.2.2.4	<i>Microstructural observation on corrosion product distribution</i> ...	86
6.3	Results and discussion.....	87
6.3.1	OCP and R_p evolution	87
6.3.2	PDP and EIS.....	88
6.3.3	Potential change monitoring on individual reinforced mortar specimens....	92

6.3.4	Mechanism of stray current-induced corrosion initiation with respect to geometrical orientation of the bar	94
6.3.5	ESEM observation.....	96
6.3.6	Picked-up current monitoring.....	99
6.3.7	Summary of effects of steel rebar orientation on stray current-induced corrosion.....	101
6.4	Conclusions	102
Chapter 7	Retrospection, Conclusions and Prospects	103
7.1	Retrospection.....	103
7.2	Conclusions	105
7.3	Contributions to science and recommendations to engineering.....	106
7.4	Prospects for further investigations.....	108
Appendix	111
A	EIS response evolution of specimens in various conditions as involved in Chapter 4	111
A.1	EIS response of 24h-cured groups.....	111
A.2	EIS response of 28-cured groups.....	117
B	Schematics of different effects of stray current and anodic polarization at early and later age	123
C	An example of EIS fitting procedure involved in Chapter 5	129
References	131
List of Publications	149
Acknowledgements	151
Curriculum Vitae	153

Chapter 1

General Introduction

1.1 Research background

In modern industrial countries, infrastructure makes out at least 50% of the nation's national wealth. Construction materials continuously communicate with their environment and never reach a condition of rest [1]. These ongoing communications make the ageing of infrastructure inherent. Ageing of infrastructure assets threatens the reliability and proper functioning of industrialized societies and is a financial burden on the society [1]. Corrosion of metal accelerates the ageing of infrastructure.

Corrosion, from the Latin “corrodere”, means “to chew away”, “to attack” a material as a result of chemical and/or physical interaction between this material and its environment. Corrosion of the reinforcing steel has been identified as one of the main reasons for reduced service life of reinforced concrete structures [2].

Steel reinforced concrete is the most widely used construction material, and forms an important part of infrastructure worldwide. The synergy of both materials, i.e., concrete and steel, provides a combination of high compressive strength (of concrete) and high tensile properties (of steel). Upon proper construction work and adequate maintenance, steel corrosion of reinforced concrete structures will be limited during the overall designed service life.

However, penetration of aggressive substances and specific environmental factors can lead to a premature degradation of reinforced concrete structures due to steel corrosion. The ultimate consequence of reinforcement corrosion is failure of the whole structure. Embedded reinforcing steel corrodes mainly because of: (1) Carbonation of the concrete cover and bulk matrix, subsequently loss of alkalinity at the steel-concrete interface; (2) The presence of chloride ions (Cl^-) in sufficient amounts in the vicinity of the steel surface. The schematic illustration of the corrosion cell formation on reinforcing steel in concrete is shown in Figure 1.1.

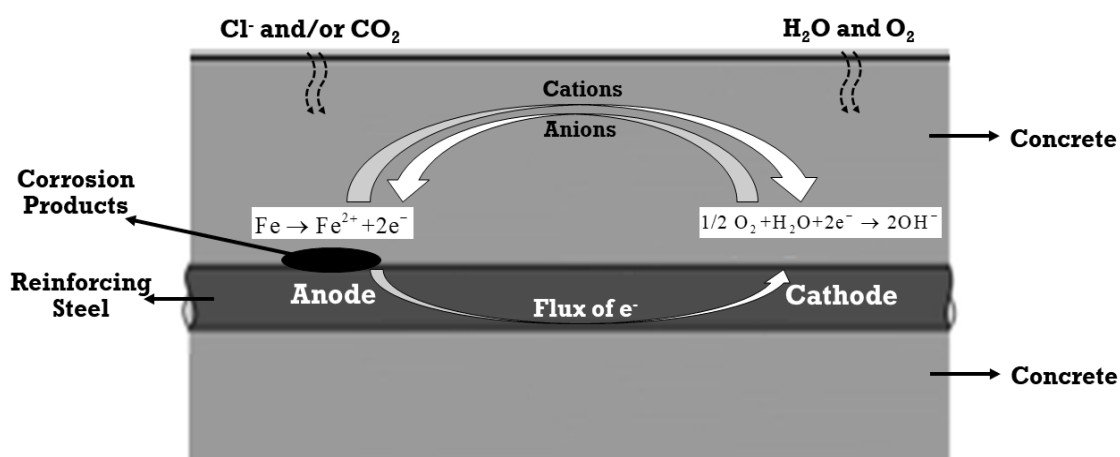


Figure 1.1: Schematic illustration on corrosion of reinforcing steel in concrete.

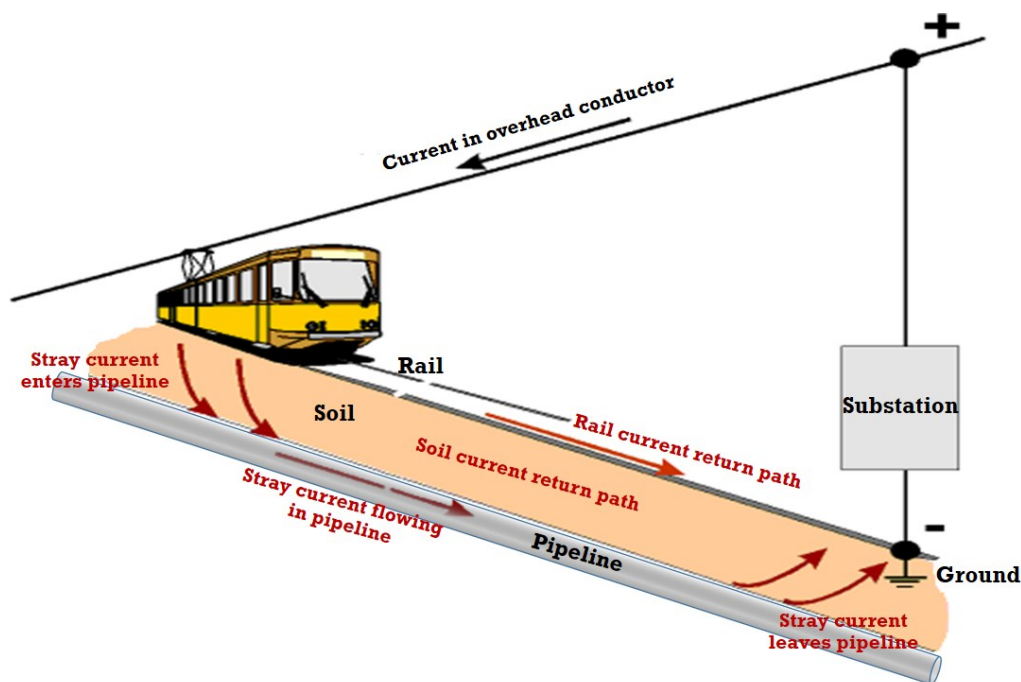


Figure 1.2: Example of stray current from a railway line picked-up by pipeline.

Besides Cl^- and reduced pH of the pore solution due to carbonation, other factors can also induce corrosion of reinforcing steel in concrete. Stray current arising from power sources and circulating in metal structures may initiate corrosion or accelerate existing corrosion processes [3-5]. Usually, this corrosion attack is localized and induces serious damage on the metallic structure.

Electric currents flow along different paths, in the earth (e.g. through soil, rock) and through conductive materials (e.g. metallic objects). Part of these currents, flowing along paths not being elements of a purpose-built electric circuit, are called stray currents [3, 6-14]. Stray current can originate from electrified traction systems, offshore structures, marine platforms, cathodic protection systems, etc. In close proximity or remote locations of these power sources, stray current can be picked-up by metallic parts of nearby infrastructure (reinforcement in concrete, buried pipelines and tanks, for instance). One of the typical examples for stray current scenario can be seen in Figure 1.2.

Stray current corrosion is one of the most severe damage forms for buried structures (such as tunnels and underground pipelines), as the matrix surrounding the metal (soil surrounding pipeline or concrete cover surrounding steel rebar) can offer a conductive path for the stray current [15, 16]. At the end of the 19th and beginning of the 20th century, when the technical revolution with emergence of electric traction was launched, the world was confronted with accelerated corrosion due to stray currents [17]. Later, with the intensive development of the petroleum and gas industry (about 8% of the world's production of metals is used in oil and gas production, storage, transport, and processing), corrosion of buried oil or gas pipelines induced by stray current has been found more and more frequently all over the world [18-26].

Stray currents can also flow into and circulate in reinforced concrete structures near the railways [27-34]. In 1906 and 1907, first attention was given to the damage of reinforced

concrete structures caused by stray currents from electric railways (or other power sources) in the USA [35]. Early laboratory experiments found that the passage of electric currents in concrete structures gave rise to serious corrosion of the reinforcing steel, and subsequent cracking and splitting of the surrounding concrete cover [36, 37].

Since then, further laboratory experiments and field investigations have been carried out, all tending to understand the earlier observations regarding the corrosion induced by stray current [38-41]. However, the range of unwanted interference of stray currents is much broader than generally recognized [3, 6-8]. The more specific effects of stray current on reinforced concrete are still unclear and less reported. Identical and reliable testing methods for evaluating or monitoring stray current corrosion are missing. This research aims to be a step forward for better understanding the stray current corrosion of reinforcing steel embedded in cement-based materials, like concrete.

1.2 Scope of this research

Nowadays, the accelerating urbanization all over the world is still prosperous. To relieve the traffic pressure, electrified traction systems (rail transit or subway) are becoming main transportation means due to the faster speed and greater passenger travel capacity. Various types of reinforced concrete structures (such as viaducts, bridges and tunnels) in the neighborhoods of railways may be subjected to stray current leaking from the rails [42-46].

Compared with stray current-induced corrosion of pipelines, reinforced concrete has more problems to deal with: difficult to inspect for the corrosion status of the embedded reinforcing steel in full and complete scale; the volume of corrosion product gradually increases, hence the normal stress (radial pressure) between the steel surface and the concrete is induced; the subsequently induced stress can force the surrounding concrete to split, possibly result in cracking, spalling or delamination, etc. Additionally, stray currents can also affect the microstructural properties of the concrete matrix [47-53]. As it is difficult to rebuild or repair the structures under or near rail transits, this kind of corrosion of reinforced concrete structures is in urgent need of more in-depth investigation.

In terms of inducing corrosion, stray direct currents (DC) are known to be much more dangerous than stray alternating currents (AC) [54-57]. The DC traction powers for railway electrification system are used in a variety of countries (for instance, 3kV DC in Belgium and Spain, 1.5 kV DC in Netherlands, 0.75 kV DC in Southern England, etc). Therefore, in this research the experimental investigations focus on stray DC.

1.3 Objectives of this research

Stray direct current (DC) is composed of both cathodic polarization and anodic polarization. However, in terms of simulating stray direct current (DC) induced corrosion of metals, most references just supplied anodic polarization on samples: Ref. [49, 50, 58-72] applied anodic polarization for simulating stray current effects, Ref. [22, 27, 73, 74] applied stray current. Although the stray current leads to corrosion by inducing anodic polarization, the effects of cathodic polarization should also be judged. The different effects of stray current and anodic polarization on the corrosion behavior of reinforcing steel are not investigated yet. The distribution, morphology and microstructure of stray current-induced corrosion products at the

1 steel-concrete interface are still unclear. Existing strategies for monitoring a stray current attack are not optimized. All these issues lead to uncertainty, i.e., overestimation or underestimation of service life predictions of reinforced concrete structures. Additionally, during the design stage of reinforced concrete structures the possible degradation of bond induced by stray current is generally not considered. Bond degradation induced by stray current corrosion leads to wider crack width and enhances the penetration of corrosive substances, in turn accelerates the corrosion of the embedded steel. This cycle significantly reduces the durability and service life of reinforced concrete structures.

Considering the foregoing aspects, this research aims to establish a basis for further understanding the mechanism of stray current-induced corrosion of reinforcing steel embedded in cement-based materials. The main objectives of the present work are:

1. To create a suitable setup for optimum stray current application at laboratory scale.
2. To compare the effect of anodic polarization to that of stray current on the corrosion behavior of reinforcing steel.
3. To illuminate the different effects of stray current and anodic polarization on bond strength of the steel-concrete interface.
4. To correlate the bond strength to corrosion status of steel surface, in both stray current and anodic polarization conditions.
5. To clarify the importance of the geometric orientation of reinforcing steel in view of stray current-induced corrosion damage.
6. To find out the link between steel rebar orientation and amount/distribution of stray current corrosion product on steel surface.
7. To elucidate the time-dependent behavior of steel rebar response, in the sense of potential shift and current actually picked-up by steel, in condition of stray current.

1.4 Research strategy and outline of this thesis

The research strategy following in this thesis is summarized in Figure 1.3. The investigated samples are reinforced mortar prisms and cubes; construction steel (rebar) FeB500HKN (6 mm diameter) is embedded in mortar prisms or cubes. The supplied levels of stray current in this study are 0.3 mA/cm² (on reinforced mortar prisms, Chapter 4 and 5), and 3 mA/cm² (on reinforced mortar cubes, Chapter 6). Different external environments are involved: the specimens are immersed in water or 5% NaCl solution, after curing in fog room for 24 hours (24h) or 28 days (28d).

As shown in Figure 1.3, this dissertation includes 7 chapters. This Chapter 1 is presenting the background, scope, objectives, and outline of this dissertation.

Chapter 2 presents a literature review related to: sources of stray current, and characteristics and mechanisms of stray current-induced corrosion. Methods and techniques for evaluation and monitoring of stray current-induced corrosion are also presented and discussed.

The conditions for steel rebar (concrete culvert under railway line as a practical case) to pick up stray current will be analyzed in Chapter 3. The means for reducing stray current corrosion in practice are discussed. Subsequently the challenges to be dealt with in this thesis are summarized.

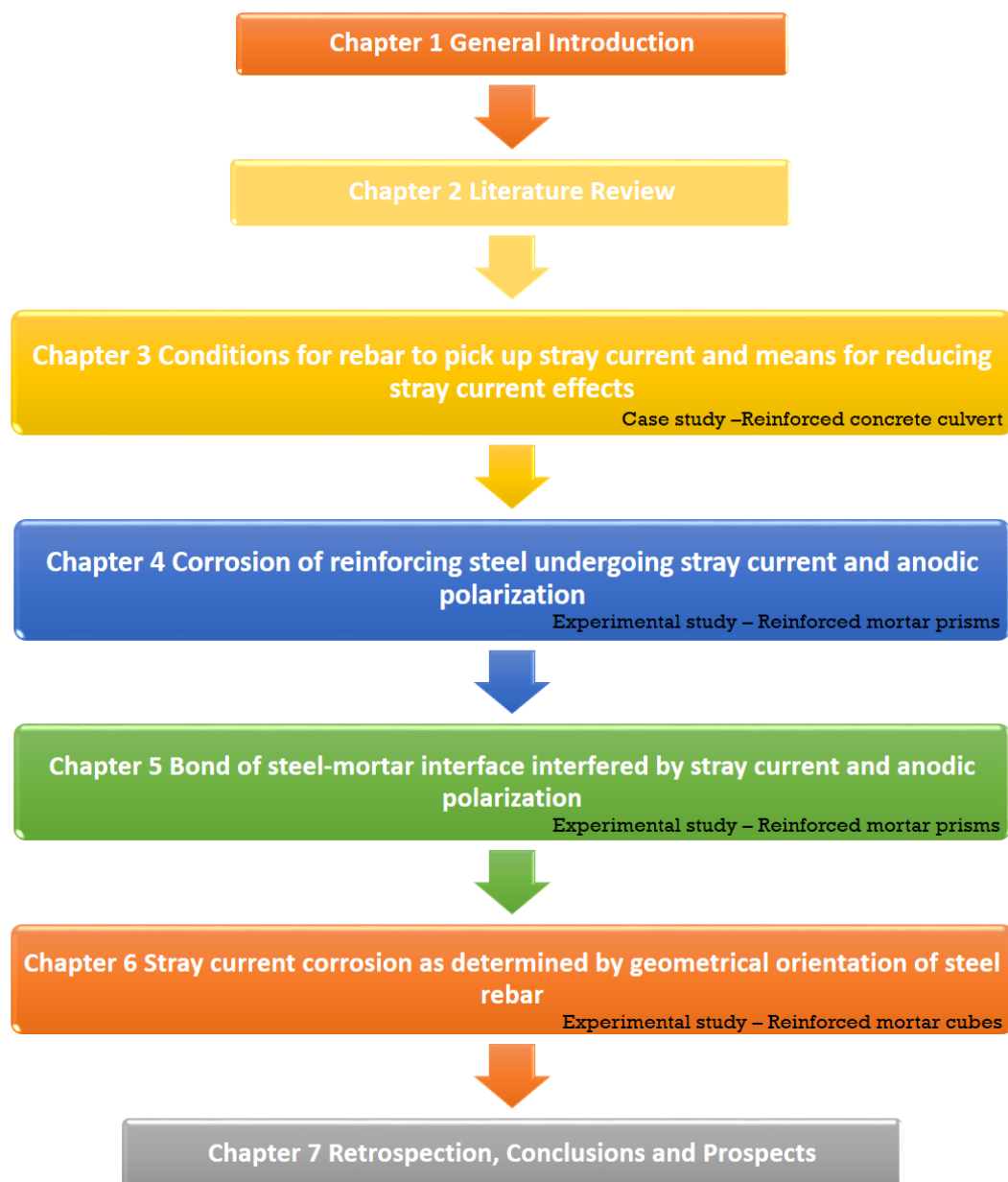


Figure 1.3: Outline of this thesis.

In Chapter 4 the different effects of stray current and anodic polarization on reinforcing steel in mortar specimens are presented. The corrosion state of steel, embedded in mortar and in conditions of stray current is discussed from an electrochemical view point.

The aim of Chapter 5 is to correlate the electrochemical response/corrosion state of steel undergoing stray current/anodic polarization with bond property at the steel-mortar interface. The pull-out test (based on ASTM C234-91a) which relates the bond stress to the slip is adopted.

Chapter 6 elucidates the effect of steel rebar orientation (i.e., steel bar parallel or orthogonal to the current direction) on stray current-induced corrosion. The distribution and morphology of corrosion products due to stray current at the steel-mortar interface are investigated as well.

1 The potential shift of steel rebar and the level of current picked-up by steel rebar are recorded. The different time-dependent behavior of steel response in a series of tests is shown and discussed.

Finally, the results and conclusions of this thesis are drawn in Chapter 7. Recommendations for further research related with stray current corrosion are given as well.

Chapter 2

Literature Review

2.1 Introduction

The objective of this chapter is to review stray current-induced corrosion of steel in infrastructure, with regard to sources of stray current, characteristics of stray current, and mechanism of stray current corrosion. Methods and techniques for evaluation and monitoring of stray current corrosion are also presented and discussed.

2.2 Sources of stray current

2.2.1 Electrified traction system

In electrified traction systems the current drawn by the vehicles returns to the traction power substation through the rails (see Figure 2.1). Owing to the longitudinal resistance of the rails (about 40-80 m Ω /km of rail [75], forming a voltage drop along the rail, $\phi_1 - \phi_4$, see Figure 2.1) and their imperfect insulation to ground (typically 2-100 Ω /km [75-77]), part of the return current leaks out from the running rails.

The leaked current flows along parallel circuits (either directly through the soil or through buried conductors) before returning onto the rail (nearby the negative terminal of the substation), forms the stray current [43, 78-80].

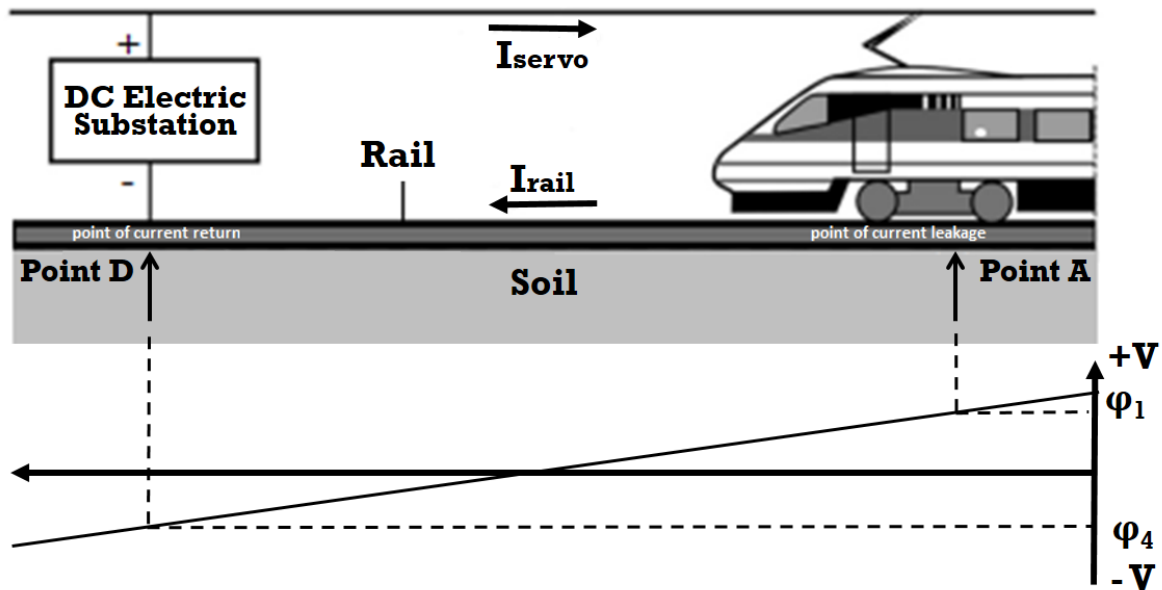


Figure 2.1: Schematic of rail-to-earth voltage profile for rail system - modified from [81].

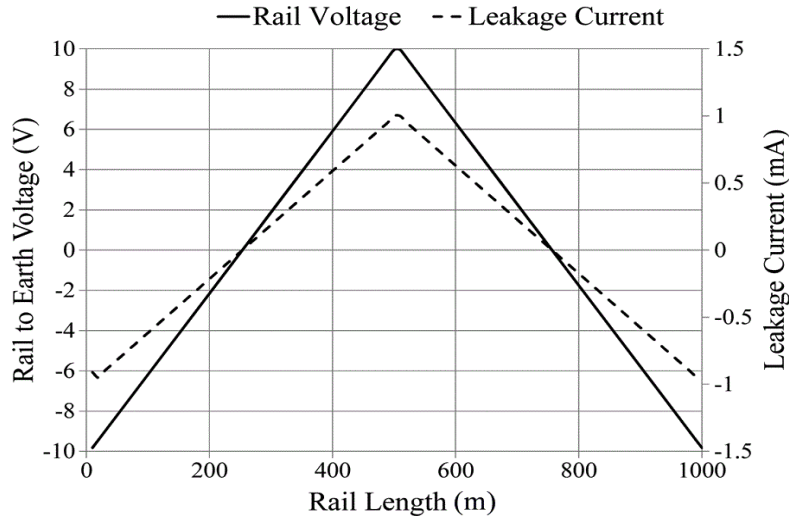


Figure 2.2: Simulated rail-to-earth voltage and leakage current [82].

Although measures are normally taken to avoid stray current from tracks, stray current leaking from rails is inevitable. The distribution of rail potential and the leaked current level along the rail length has been evaluated by Charalambous & Aylott [82]. The result of this numerical simulation is presented in Figure 2.2, showing that the level of leakage current was positively correlated with rail-to-earth voltage.

As any underground metallic structure has (in general) a lower electrical resistance than soil, the stray current can flow through it. Similarly, stray current will flow through the conductive portion of a reinforced concrete structure, which is the reinforcing steel. The example of stray current from a DC railway line picked-up by reinforcement in concrete is illustrated in Figure 2.3.

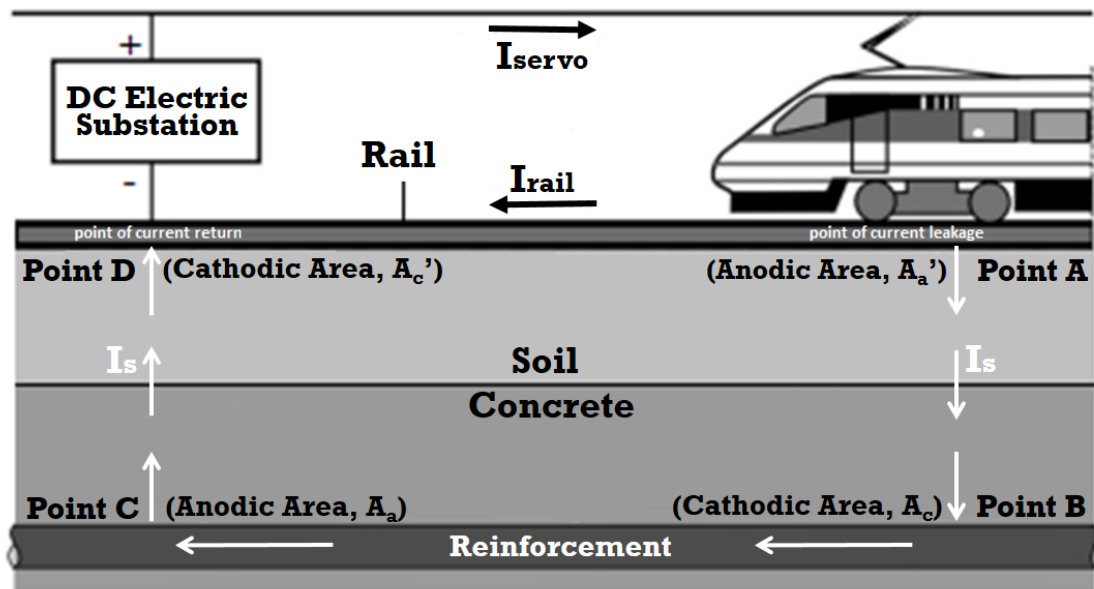


Figure 2.3: Example of stray current (I_s) from a DC railway line picked-up by steel reinforcement in concrete - modified based on [81].

Given that the current flow in a metallic conductor is an electron flow, while that through electrolytes such as soil, concrete, etc., is ionic, there must be an electron to ion transfer when the current leaves the rails and flows into the soil. Where a current leaves the rail oxidation occurs (loss of electrons). Where the current returns onto the rail, there must be a reduction or electron-consuming reaction [75, 83].

The schematic representation of the anodic area (Point A) and cathodic area (Point D) on a rail is illustrated in Figure 2.3, in conditions when current leaks out and returns to the rail. A corrosion characteristic produced by the contact of the tie plate with the rail in the presence of stray current is shown in Figure 2.4. Where the current leaks out from the rail (point A, with the area of A'_a , anodic current density of i'_a), anodic area forms. When the current returns back onto the track at point D, a cathodic current is present, with the area of A'_c , cathodic current density of i'_c .

The relationship between them can be expressed as follow:

$$I_s = i'_c \cdot A'_c = i'_a \cdot A'_a \quad 2.1$$

In industrial sectors, current leakage from electric traction systems (rails) constitutes the major and most frequent cause of the induction of strong stray currents [7, 84]. As a special case for this situation, stray current issue in coal mining has attracted much attention [85, 86]. The underground mining haulage systems (electric traction networks), operating in much the same manner as described for railway transit systems, can also induce stray current and then lead to corrosion of the surrounding embedded metallic structures.

Besides the corrosion problem, the presence of stray currents in the mining industry, particularly in underground excavations, may also produce the following risks:

1. Hazards during blasting, possible accidental firing of the detonator due to a stray current of sufficient intensity entering the circuit;
2. Risk of explosion as result of stray voltages in intrinsically safe circuits, or as a result of sparking, which can occur when two bodies under stray voltage are in contact;
3. Fire danger as a result of the long-lasting flow of stray current (In South Africa, coal seams fire caused by stray currents was found [87]), resulting in the ignition of coal dust or methane due to local heating up to the ignition temperature;
4. Hazards due to the disturbances caused by the interference of stray current (and stray voltages) into the control, monitoring and warning circuits of mining equipment [85, 86].



Figure 2.4: View of a section of 115-lb rail showing severe corrosion at the base of the rail [88].

2.2.2 Cathodic protection (CP) system

Impressed current cathodic protection systems can cause stray current interference on adjacent metallic structures, depending on the location of the ground beds, the exact location of the metal structure, and the operating characteristics of the CP system [89-96]. Any metallic structure buried in soil represents a low-resistance current path and is vulnerable to the effects of stray currents.

One of the cases for this situation is illustrated in Figure 2.5: the current path originating from the components of the CP system flows through the soil (from the anode to the cathode e.g. a steel tank to be protected) and can be picked-up by a low-resistance metallic object, as a pipeline. Depending on the soil resistivity, part of the current flown through the anode of this impressed current CP system, will just flow into another conductor (the steel pipe nearby); accordingly, in the neighborhood of the protected structure (the cathode or the steel tank in this case), the picked-up current leaves the pipeline and returns to the closed circuit of protection current. The existence of stray current can also reduce the efficiency of the cathodic protection system, since the current supposed to protect the intended structure is attenuated.

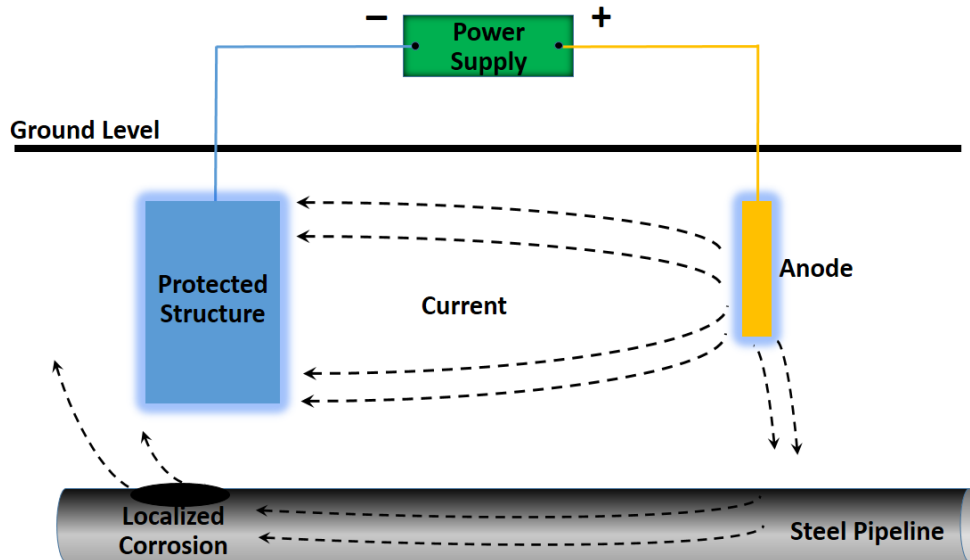


Figure 2.5: Stray current resulting from cathodic protection.

2.2.3 High voltage power lines

Municipal and industrial developments require the transport of considerable amounts of energy over long distances, which enhances the importance of the power lines as an essential link between energy generators and final consumers.

Power lines, supported by power towers with foundations, can be found almost everywhere. In these systems, high corrosion rate of the semi-underground foundations is usually detected. It is believed that corrosion results from stray currents that flow through the ground to close the loop between neighboring towers [97-101]. Stray currents here originate in the rod cables of the power line towers, induced by the strong electromagnetic and electric fields of the energized power lines [102-104].

This kind of stray current does not only attack buried foundations, but also flows into the ground accessory structures near the power supply system. For instance, it is well known that a power supply system along a railway is necessary, and the electric wiring of this system in general, is supported by wire poles.

This is also found along railways near Utrecht (The Netherlands) [105]. In this case the wire poles are fixed by the steel wire connected to a reinforced concrete block (Figure 2.6). It is found that the anchors in the block used to connect the steel wiring and the reinforcement in the block suffer from corrosion at an extremely high rate. In some exceptional cases, the blocks with the design service life of 80 years, were damaged totally only after 3 years, due to steel corrosion and corrosion-induced cracks around the anchors (Figure 2.7). The rebars in the block were also corroded. According to the investigation [105], the corrosion damage here was also induced by stray current from the electric wiring.

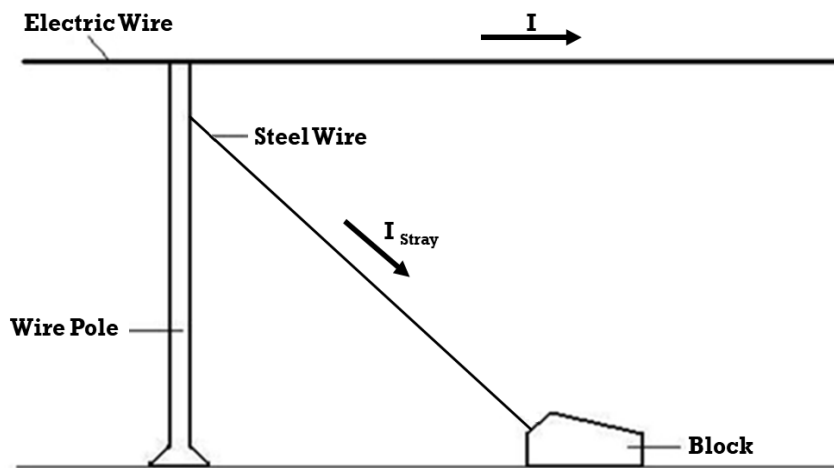


Figure 2.6: Schematic of the setup of block, steel wiring, wire pole and electric wire.



Figure 2.7: Damaged block due to the corrosion of anchor induced by stray current [105].

2.2.4 Disturbances of the earth's magnetic field

Occasionally, varying potential and current distribution of buried structures will be encountered in areas where there is no known source of “man-made” stray current. These variations are usually associated with disturbances in the earth's magnetic field: a voltage is generated on a buried metallic structure (for instance, a pipeline) due to the variations in the earth's magnetic field along the pipeline route. Stray current induced by transient earth's geomagnetic activity is also termed telluric. Telluric effects may be identified with recording instruments, and are classified into quiet, unsettled, and active conditions.

Such disturbances have been found most active during periods of severe sun activity [106-109]. Fortunately, although occasionally intense, telluric current effects on buried metallic structures are seldom of long duration and may not even be localized at specific pickup or discharge areas. However, where the condition occurs frequently enough and is of serious intensity, corrective measures should be adapted to counteract the telluric effects. For instance, grounding or cathodic protection can be adapted. Cathodic protection has been used on the Trans-Alaska pipeline in the form of a sacrificial zinc ribbon anode [107].

2.2.5 Stray current underwater

Although the occurrence of stray current in water is much less probable than in the ground, stray current has also been found underwater [110-114]. Owing to the relatively low conductivity of fresh water compared to sea water, stray currents from identical source are less dangerous in the former case and with a potentially higher risk in the latter case [16, 55, 56].

Stray current in marine environment can come from welding operations, inadequate electrical systems, and boats with different grounding polarities [110, 115-117]. For instance, when the grounding current of a boat flows through water to the ground point, another nearby boat could provide a path of lower resistance. Once part of grounding current flows through the boat as stray current, corrosion of the boat's hull will be induced. The anodic areas, where oxidation occurs, will be the location where the current leaves the hull and flows into the surrounding water; the cathodic areas will be the location where the stray current “enters” the boat.

2.2.6 Electrolysers and bus ducts

Special standards exist for determining the stray current reduction measures in reinforced concrete structures of electrochemical plants of the chemical and metallurgic industry. Electrolyzers and bus ducts are the major stray current sources in these plants [118]. Overlaps, platforms for the maintenance of electrolyzers, columns and beams for supporting bus ducts, as well as underground structures of reinforced concrete, are the objects of the attack by stray currents [16].

2.2.7 Other sources

Stray currents have also been found elsewhere, and in some situations these other causes may also be of importance. They may include:

1. Communication networks, control and warning circuits [119];

2. Means of communication using radio transmitters;
3. Local galvanic cells, which are formed by metallic masses in wet compartments;
4. Static electricity;
5. Atmospheric discharges;
6. Spontaneous polarization induced electric fields by ferroelectric materials [7];
7. Grounded photovoltaic (PV) systems [120];
8. Electrical submersible pump (ESP) motors [121].

Irrespective of the source of stray current, stray current could be conducted through nearby metallic structures, since the metal represents a low resistance path. Stray currents will enter the metallic structure and then leave to surrounding soil or water (solution). Stray current-induced corrosion or acceleration of existing corrosion on these metallic structures will occur.

2.3 Characteristics of stray current

Depending on the stray current source, a classification is made into stray direct current (DC) and stray alternating current (AC), with different frequency (for AC), continuity, fluctuation and current density [69, 122-142].

A railway electrification system may induce different kinds of stray current. As shown in Figure 2.8, a variety of traction powers are used in European countries [143]. The main electrification systems currently used are: 15 kV AC 16.7 Hz, used in Sweden and Germany for example; 25 kV AC 50 Hz, used in France and part of Netherlands; 2x25 kV AC 50 Hz, used in France on high speed lines; 3kV DC in Belgium and Spain for instance; 1.5 kV DC in Netherlands; and 0.75 kV DC in Southern England [143-146]. The reasons for so many different systems are mainly historical [147].

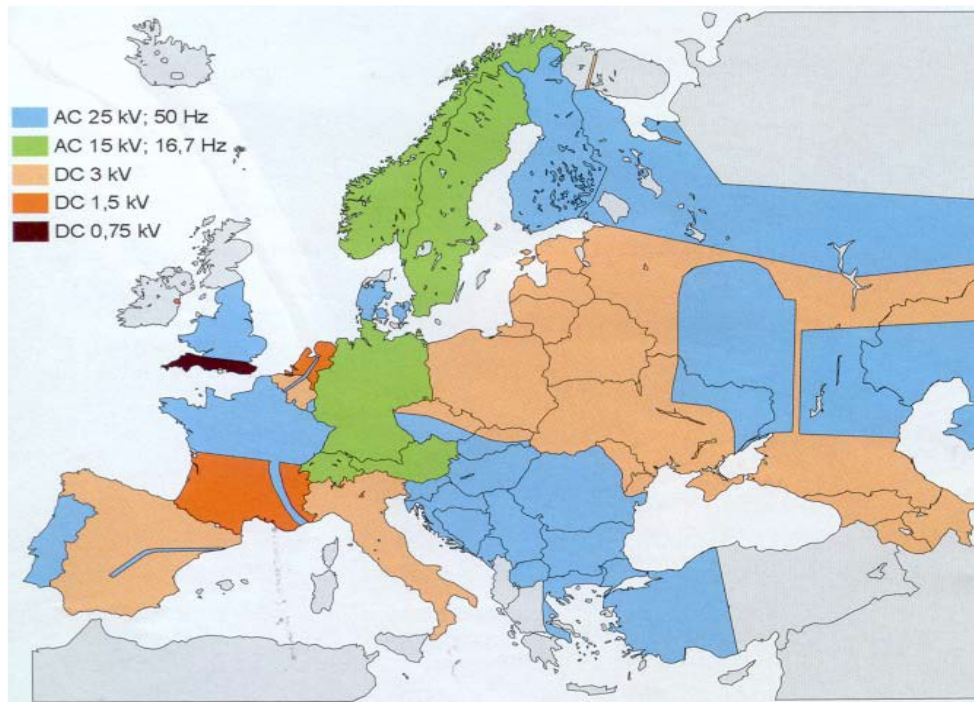


Figure 2.8: Distribution of traction power for railways in Europe [143].

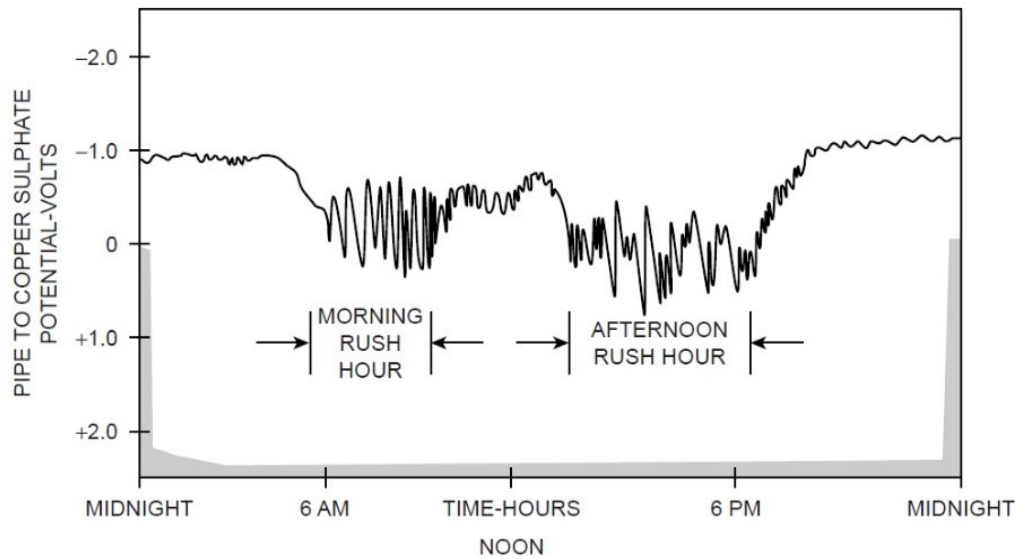


Figure 2.9: Pipe-to-earth potential at traction system stray current discharge area [85].

Nowadays a lot of old systems are still used because it is very expensive to change an electrification system and because each of them has its advantages. The DC has been, for many years, simpler for railway traction purposes; the AC is better over long distances and cheaper to install but, until recently, more complicated to control [144, 148, 149]. Consequently, the stray current arising from these electrified traction systems may be stray direct current (DC) or stray alternating current (AC), where both can induce corrosion of nearby metal structures.

Stray currents produced by industrial platforms have relatively stable intensity in time. In contrast the stray currents leaked from electrical tractions are fluctuating in both intensity and duration [17, 92, 150-159]. Stray currents derived from the electrical traction systems may fluctuate over short or long intervals of time, parallel to the varying load of the power source. This is also in contrast to galvanic or cathodic protection currents, which are relatively stable.

Figure 2.9 presents results from potential fluctuations in the discharge area of a pipeline, subjected to stray current due to its proximity to a transit system. The chart shows that the pipeline is affected by stray current activity when the transit system is in operation, especially during the morning and afternoon rush hour periods [85]. In Chen et al. 's study [15] it is also found that stray currents produced by rail traction systems are non-stationary. The effect of interruptions of stray current should be taken into account in some particular situations, e.g. where the stray currents leaked from electrical tractions are intermittent.

2.4 Corrosion of steel caused by stray current

2.4.1 Steel corrosion caused by stray alternating current (AC)

Corrosion caused by stray alternating current (AC) was firstly reported back in the early 1900s [160-169]. It is found that stray AC induced corrosion is moderate compared to stray DC induced corrosion. In the experiments conducted by R. Radeka et al. on ship construction steel, stray AC caused 4.35-17.57% corrosion damage of the equivalent DC [54]. Other researchers

estimated that for metals like steel, lead, and copper, AC causes less than 1% of the damage caused by an equivalent DC [55, 56, 170].

In practice, it is not easy to predict stray AC-induced corrosion rate by considering parameters such as alternating induced voltage. It was reported that the most rapid corrosion did not always occur at the points of the highest induced alternating voltage (AV) on the pipeline [171-174]. The relationship between AC density, frequency of AC and corrosion rate reported on literature will be summarized below.

In terms of stray AC induced corrosion, the higher the density of stray AC with the same frequency, the more serious the corrosion damage will be. Based on experimental results on carbon and low alloy steels [175-177], what can be summarized is: The higher the AC density, the higher the corrosion rate. No significant corrosion state was observed at AC density lower than 30 A/m^2 . Therefore, most authors suggest an AC critical current density of 30 A/m^2 , above which corrosion will be significant [172, 175-181].

The influence of various AC current densities on stress corrosion cracking (SCC) behavior of pipeline steel was also investigated by M. Zhu et al. [161, 162] and X. Wang et al. [21]. With increasing level of AC current density, the susceptibility to SCC increases. The thermal activation (the temperature rise within the test cells) created by AC current was also considered to play an important role in AC corrosion [182].

Corrosion induced by stray AC was reported to be more detrimental at low frequency [54]. A set of experiments was conducted by Pagano et al. [163] at various frequencies (5–500 Hz). It was found that with increasing frequency from 5 to 500 Hz (with the same AV of 1000 mV), there was a sharp drop in corrosion rate.

Overall, stray AC induced corrosion increases with the increase of current density, but decreases with increasing frequency. Stray AC corrosion was only a fraction of that induced by an equivalent stray DC.

2.4.2 Mechanism of stray direct current (DC) induced corrosion

The concept of stray current related with reinforcement was already illustrated in Figure 2.3. The stray current (I_s) inducing reinforcement corrosion in a reinforced concrete element is illustrated in Figure 2.10.

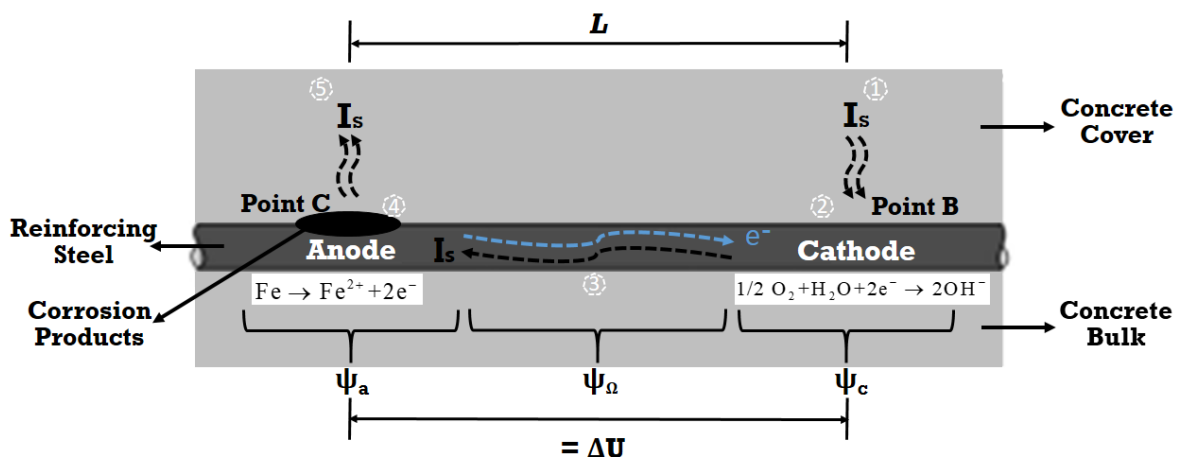


Figure 2.10: Schematic of the stray current interference (I_s) on reinforcement in concrete.

In this case, stray current originates from the positive terminal of a foreign DC electrical source, and flows to an alternative path (underground reinforced concrete element) through the soil and concrete cover (position ① in Figure 2.10). Due to the low resistivity of the steel rebar, if compared to the surrounding concrete, the stray current can easily be picked-up by the embedded reinforcement [183]. At the point ② where the stray current enters the reinforcement, a cathodic area is generated, where a cathodic reaction occurs and corresponds to a relevant cathodic polarization (ψ_c in Figure 2.10). In an environment of neutral or high pH, the cathodic reaction is predominantly oxygen reduction, as shown in Figure 2.10.

The stray current would flow along the reinforcement between cathodic and anodic areas (③ in Figure 2.10), where the ohmic drop (ψ_Ω in Figure 2.10) would also be present. An anodic reaction (metal dissolution) will occur where the stray current flows out (is discharged) from the reinforcement (anodic area, point ④/point C). At this location, anodic polarization induced by the current outflow (ψ_a in Figure 2.10) will be relevant. This means that the process of (stray current-induced) steel corrosion is initiated and accelerated at this location. The current outflow would return to the negative terminal of the foreign DC source, “passing” through the concrete cover and soil (site ⑤), and closing the electrical circuit.

If stray current can be “picked-up” by the steel reinforcement, a driving voltage (ΔU , see Figure 2.10) has to be present:

$$\Delta U = \psi_c + \psi_a + \psi_\Omega \quad 2.2$$

This voltage equals the sum of cathodic (ψ_c) and anodic (ψ_a) polarizations, in case the ohmic drop (ψ_Ω) through the reinforcement is negligible because of the low resistivity of the steel rebar:

$$\Delta U = \psi_c + \psi_a \quad 2.3$$

The anodic and cathodic areas may not have the same area, as has been assumed so far. The driving voltage ΔU may decrease when the cathodic area is significantly larger than the anodic area, such that the current density on the cathodic site is negligible compared to that of the anodic site, and thus $\psi_c \rightarrow 0$, so that $\Delta U \rightarrow \psi_a$. Therefore, under particular circumstances, ΔU may be relatively low, in other words, it will be easier for the stray current to be picked-up by the reinforcement.

2.5 Monitoring and evaluation of stray current

Although the stray current leakage can be controlled by some measures, its existence is sometimes inevitable [184-196]. In cases where a corrosion possibility due to stray DC interference exists, analysis of the situation shall include electrical properties and the location of the possible source of interference as well as recorded anomalies. Intuitively, monitoring of stray current corrosion can be performed as qualitative assessments, for instance using Faraday’s laws, in order to assess the cumulative mass loss of steel over the targeted operating period. The application of Faraday’s law, however, requires the current outflow level/density to be known. Measuring the stray current flowing through the metallic structures is problematic

due to the impossibility of breaking off the metallic structures, which forms closed circuits of metallic conductors. According to the related Ref. [11, 73, 196-261], it can be summarized that there are four principal ways to identify stray current interference:

1. Structure-to-electrolyte potential fluctuations;
2. Deviations of structure-to-electrolyte potentials;
3. Voltage gradients in the electrolyte;
4. Line currents in coupons [196, 218, 242].

Compared to pipelines, the assessment of stray current corrosion of reinforced concrete structures is even more complicated. This is due to: ramification of bars inside the concrete, impossibility of breaking off the reinforcement (which form closed circuits of metallic conductors inside the concrete) to measure stray current values; dependence of current distribution on the humidity of the concrete at different sites of the structure, etc. Additionally, in the case of pre-stressed concrete structures, the expected cathodic areas should also be monitored in order to investigate the risk of hydrogen embrittlement.

Monitoring of stray current in reinforced concrete may be carried out by embedding permanent reference electrodes at positions identified as critical, in order to trace the presence of stray currents, determine the direction of flow, locate anodic and cathodic areas, etc. For example, a stray current sensor with cylindrical twisted fiber was proposed [262] to monitor the presence of stray current. Other measures that can help in detecting the presence of stray current in reinforced concrete are based on the potential difference present between different parts of the structure, due to the ohmic drop (IR drop) produced by the stray current.

However, in some cases it is impossible to measure the stray current on site, so some other methods for stray currents calculation have been proposed. Such as: Back Propagation (BP) neural network predictive models, novel or numerical predictive models, software tools, etc [66, 100, 263-308]. Methods based on unequivocal and precise hazard criteria have also been suggested in view of evaluation or prediction of the corrosion degree of metallic materials caused by stray current [123].

Due to the generally limited number of reference electrodes, it is also necessary to predict the corrosion status of the metal materials in an area without reference electrodes. In this regard, Wang et al. [217] approximated the nonlinear mapping between characterization parameters and influential parameters, using a Radial Basis Function (RBF) neural network.

Besides, mathematical models based on different concepts (FEM, boundary element method, data mining technique, etc.) have been established to assess the stray current corrosion [72, 309-316]. These models have been applied on: ductile iron pipe (DIP) located in the vicinity of cathodically protected steel pipe [309]; unprotected structures undergoing stray current arising from a nearby cathodic protection system [310]; underground steel structures through traction power systems producing stray current [311, 312], etc.

2.6 Concluding remarks

This literature review outlines and brings together the main aspects with regard to stray current-induced corrosion, namely, the sources of stray current, characteristics and mechanism of stray current corrosion in view of electrochemical aspects. Methods and techniques for evaluation

and monitoring of stray current corrosion of steel in infrastructure were summarized in Section 2.5. Based on the reviewed literature, some concluding remarks can be drawn as follows.

Stray current can easily and unexpectedly arise from electrified traction systems, making stray current-induced corrosion one of the most severe forms of damage to buried structures, such as tunnels and underground pipelines. Irrespective of the origin of stray current, it is easily “picked-up” by metallic conductive paths and later-on discharged, causing stray current corrosion.

Nevertheless, the understanding of stray current-induced corrosion still remains unclear. The danger of stray current is still not sufficiently recognized in practice, despite the far-reaching range and scale of dangerous or unwanted interactions of stray currents. More scientific mechanisms and practical approaches are necessary in order to thoroughly understand the process of stray current-induced corrosion.

Based on the information derived from the literature review, the conditions for embedded steel rebar to pick up stray current will be analyzed and proposed in the next chapter. A situation (reinforced concrete culvert under a railway line) suspected to be attacked by stray current arising from rail will be demonstrated as a specific example. The aim of this contribution is to further clarify the stray current-induced corrosion process in practice. The challenges to be dealt with in this thesis will be proposed in Chapter 3.

Chapter 3

Conditions for rebar to pick up stray current and means for reducing stray current effects

3.1 Introduction

The primary objective of understanding the mechanism of a hazard is to prevent and reduce the damages induced by this hazard. Based on the introduction on the stray current mechanism in theory in Chapter 2, this chapter further goes through the more practical aspects of stray current, i.e., conditions for a steel rebar to pick up stray current and the potential means for reducing stray current corrosion in practice.

The process of stray current corrosion is a function of electrical/electrochemical and chemical/physical parameters [150]. The better the understanding of the parameters involved, the better the possibilities for mitigating stray current corrosion. These parameters can be classified into 3 categories [269, 280, 317-331]:

1. Sources of stray current;
2. Ambient conditions (soil, concrete, etc.);
3. Interfered structure itself (reinforcement in concrete structures, for instance).

Accordingly, the means for reducing stray current corrosion are also related to the above 3 categories. As for the order of importance of these factors, as mentioned by British Standard - BS EN 50162:2004 [332] back in 2005: “measures taken to minimize the effects of stray current interference should commence with the source of the stray current interference”. If measures taken to mitigate the effect of stray current sources are impractical or ineffective, the attention should be focused on the external environment and the interfered structure itself [333-335].

More details of these will be discussed in the next sections of this chapter. The reinforced concrete culvert under a railway line, suspected to be attacked by stray current arising from rail, will be demonstrated as a specific case.

3.2 Stray current corrosion in reinforced concrete culvert under railway

The most frequent stray current sources are rail transits, which are also main traffic tools with accelerating urbanization all over the world. Stray currents from these systems may easily flow into the nearby structures, making stray current corrosion one of the most severe forms of damage of these structures.

Railway lines frequently cross cut and fill transitions [82]. In these locations culverts are often used as vehicular or pedestrian crossings (sometimes also as wildlife corridors, water distribution structures) in both conventional and high-speed railway lines. These solutions have

been used since the 1800s (a traditional stone arch culvert is shown in Figure 3.1a) [336-342]. Nowadays, culverts under railway lines are usually made with reinforced concrete rectangular boxes, which are cast-in-situ (Figure 3.1b) or precast (Figure 3.1c) [343].

As transition zones in railway lines, the culverts may introduce localized stiffness variations [343, 344]. The dynamic train loads over culverts lead to a number of interactions between the track and the culvert, as well as between the sidewalls and the backfill (i.e. soil-structure interactions) [345-351]. As concrete elements inside the railway track subgrade, the culverts may promote differential settlements in the track [343, 352-354].

Similar to level crossings of railway lines, the concrete culverts are also highly susceptible to stray current effects [355-357]. Because of safety concerns, it is inevitable that vehicles need to brake and accelerate at these transition zones, which means that the servo current is higher than in normal situations. Subsequently, the density of the return current in the rail and leaked-out current (stray current) are higher [215]. Due to poor rail insulated boots attributed to vibrations, the stray current can leak out more easily from the rail foot. As the concrete culverts are usually embedded in soil, the stray current leaked from rail may flow into culverts through the surrounding soil [285, 358].

The stray current corrosion of reinforcement in culverts represents a dangerous condition for the culverts themselves, but also for the track integrity and, eventually for the safety of transit systems. Because of the concurrences of stray current corrosion, combined road/railroad loadings, inconvenience for repair, high cost and disturbance of traffic and railroad operations at culverts, it is necessary to pay more attention to these locations.

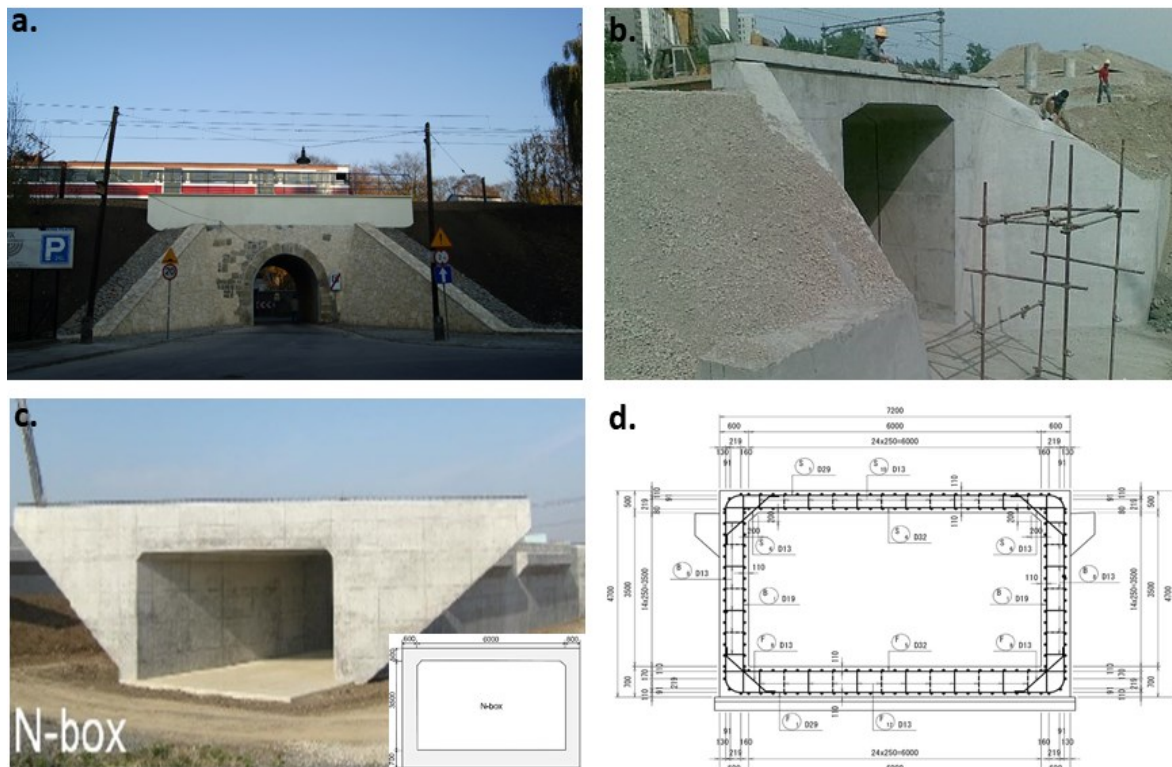


Figure 3.1: a). A traditional railway culvert (stone arch), Miodowa street, Kazimierz, Krakow, Poland [359]; b). Construction of a concrete box culvert under railway [360]; c). A precast reinforced concrete box culvert [337]; d). Detailed reinforcement drawing of culvert in Figure 3.1c [337].

3.3 Steel rebar in culvert under railway subjected to stray current

The scenario of stray current arising from rail and then flowing into a culvert under railway is shown in Figure 3.2. The returning current (I_{rail}) leaks out from point A of the rail, then flows directly through soil and buried reinforced concrete culvert, before returning into point D on the rail.

The equivalent electrical circuit relevant to this scenario is shown in Figure 3.3, where: R_{rail} , R_{rebar} , $R_{\text{soil},1}$, $R_{\text{soil},2}$, $R_{\text{concr},1}$, and $R_{\text{concr},2}$ are the electrical resistances of the rail, reinforcement, soil and concrete cover/matrix at different positions; I_s is the stray current flowing into the reinforcement. This equivalent electrical circuit is to describe the flowing paths of stray current picked-up by steel. In other words, the other part of stray current flowing in concrete (but not picked-up by steel) is not involved.

In this case, the supply voltage (ΔE) is raised by the potential difference between point A and point D on the track, where stray current leaks out and returns back, respectively. Of course, depending on the different types of stray current source, the supply voltage for stray current varies.

The distance between point A and D is denoted L_{rail} (m). φ_1 and φ_4 are the potentials at points A and D on the rail. For a resistance per unit length (r_{rail} Ω/m) of rail, there will be a resulting voltage drop (ΔE) caused by the returning current along the distance L_{rail} of rail:

$$\Delta E = \varphi_1 - \varphi_4 = L_{\text{rail}} \cdot r_{\text{rail}} \cdot I_{\text{rail}} \quad 3.1$$

If i_c and i_a are the stray current densities where stray current flows into (at Point B, cathodic area with the area of A_c) and flows out (at Point C, anodic area with the area of A_a) the reinforcement, the relationship between the overall stray current I_s and the anodic and cathodic currents can be expressed as follows:

$$I_s = i_c \cdot A_c = i_a \cdot A_a \quad 3.2$$

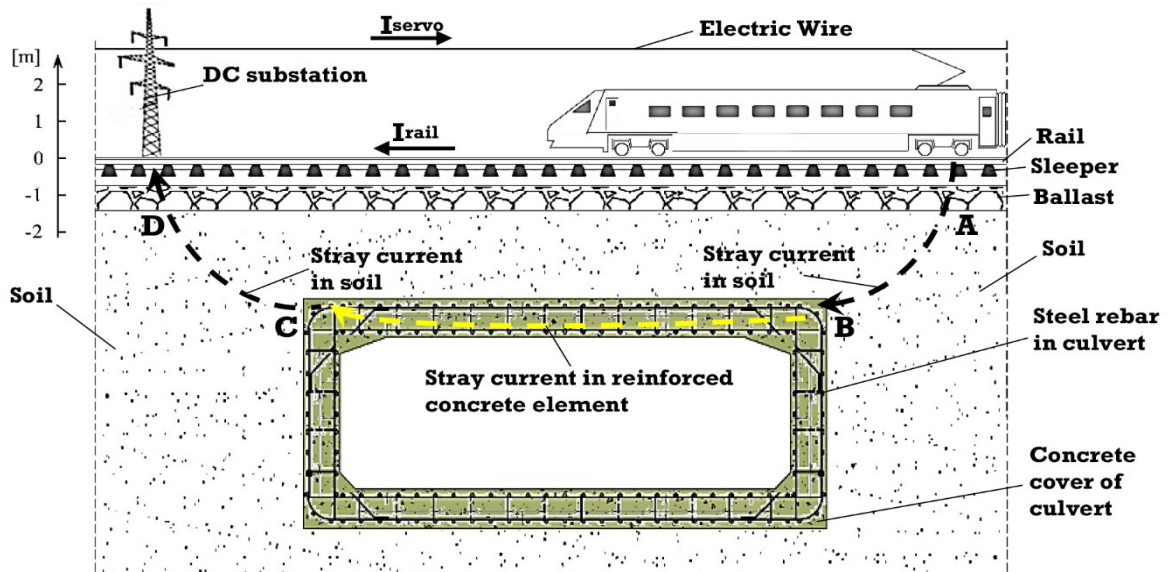


Figure 3.2: Transverse section of reinforced concrete box culvert under railway line undergoing stray current arising from the track.

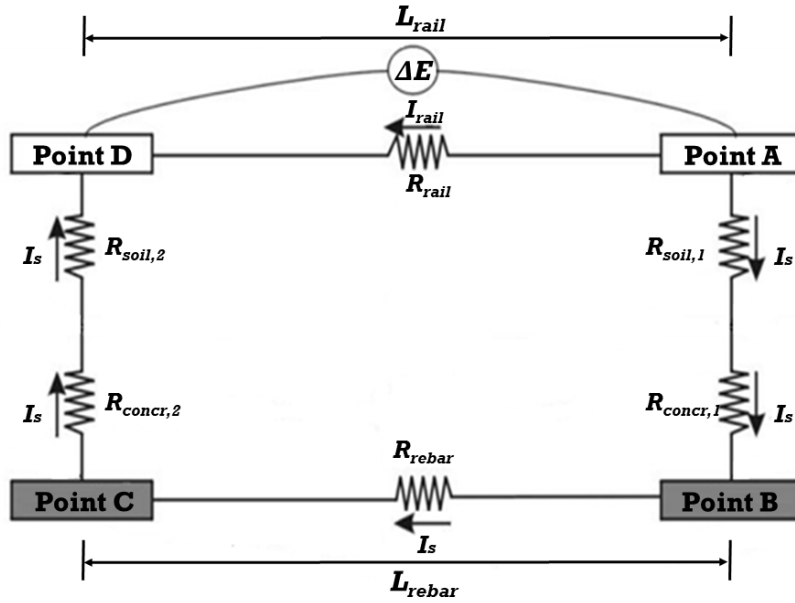


Figure 3.3: Equivalent electrical circuit to the scenario shown in Figure 3.2.

Considering ohmic drops due to resistance and polarization on both rail and reinforcement (when stray current leaks out or flows into), the equivalent electrical circuit representing stray current arising from rail is shown in Figure 3.4. This equivalent circuit can be simulated by series of two electrolytic cells I and II (see Figure 3.5). The distance between point B and C is denoted L_{rebar} (m). φ_2 and φ_3 are potentials at point B and C on the reinforcement, respectively. For resistance per unit length R_{rebar} (Ω/m) of rebar, there will be a potential drop between point B and C:

$$\varphi_2 - \varphi_3 = L_{rebar} \cdot R_{rebar} \cdot I_s \quad 3.3$$

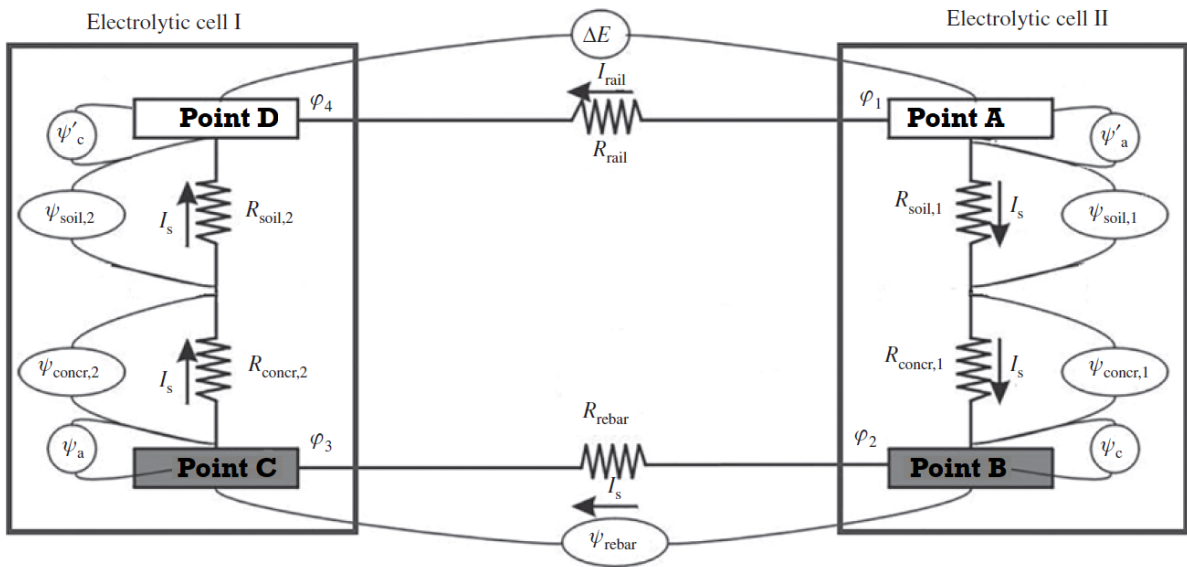


Figure 3.4: Schematic of stray current path considering the polarization and ohmic drop.

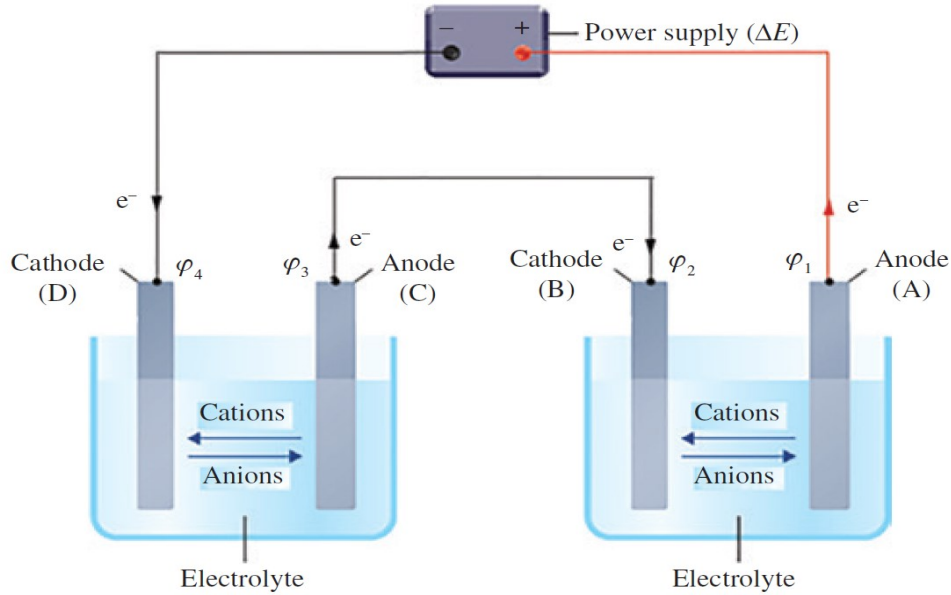


Figure 3.5: Series of electrolytic cells.

Based on the mechanism of an electrolytic cell, the driving force for cell II is $\phi_1 - \phi_2$. To force the anodic and cathodic reactions to occur, the minimum electric potential (driving force) is the sum of the absolute potential value of the macro cell ($E'_{corr} - E_{corr}$), the polarizations in anodic and cathodic areas (ψ'_a, ψ_c) and the ohmic drop ($\psi_{soil,1}, \psi_{conc,1}$):

$$\phi_1 - \phi_2 = E'_{corr} - E_{corr} + \psi'_a + \psi_c + \psi_{soil,1} + \psi_{conc,1} \quad 3.4$$

For the electrolytic cell I, the same argument holds:

$$\phi_3 - \phi_4 = E_{corr} - E'_{corr} + \psi_a + \psi'_c + \psi_{soil,2} + \psi_{conc,2} \quad 3.5$$

From the Equations 3.1, 3.3, 3.4 and 3.5, the relationship of the factors can be given in equations as follows, i.e. the condition required for stray current to be picked-up by the reinforcement in concrete near electrified traction system is:

$$L_{rail} \cdot r_{rail} \cdot I_{rail} = \psi_a + \psi_c + \psi'_a + \psi'_c + I_s \cdot R_{soil,1} + I_s \cdot R_{conc,1} + I_s \cdot R_{soil,2} + I_s \cdot R_{conc,2} + I_s \cdot L_{rebar} \cdot r_{rebar} \quad 3.6$$

ψ_a, ψ_c, ψ'_a and ψ'_c can be expressed as functions of stray current (I_s) according to the polarization definition:

$$\psi_a = F_a(i_a) = F_a(I_s / A_a) \quad 3.7$$

$$\psi_c = F_c(i_c) = F_c(I_s / A_c) \quad 3.8$$

$$\psi'_a = F'_a(i'_a) = F'_a(I_s / A'_a) \quad 3.9$$

$$\psi'_c = F'_c(i'_c) = F'_c(I_s / A'_c) \quad 3.10$$

Hence Equation 3.6 can be described as follows in Equation 3.11:

$$L_{\text{rail}} \cdot r_{\text{rail}} \cdot I_{\text{return}} = F_a \left(\frac{I_s}{A_a} \right) + F_c \left(\frac{I_s}{A_c} \right) + F'_a \left(\frac{I_s}{A'_a} \right) + F'_c \left(\frac{I_s}{A'_c} \right) + I_s \cdot R_{\text{soil},1} + I_s \cdot R_{\text{conc},1} + I_s \cdot R_{\text{soil},2} + I_s \cdot R_{\text{conc},2} + I_s \cdot L_{\text{rebar}} \cdot r_{\text{rebar}} \quad 3.11$$

Based on above analyses, it can be seen that when the electrochemical state of a system (including rail, reinforced concrete and surrounding environment) satisfies the criterion expressed by Equation 3.11, stray current will be picked-up by the reinforcement in concrete near railways. Once this takes place, corrosion will occur at locations where the stray current leaves the reinforcement. Any factors related to the subentries of Equation 3.11 can affect the probability for the stray current to be picked-up by reinforcement. For reducing stray current corrosion, impact factors of stray current corrosion should be modified accordingly.

3.4 Means for reducing stray current effects

3.4.1 Measures on stray current sources

3.4.1.1 Track

Means for reducing stray current corrosion should also be tailored according to which source the stray current comes from. As the most frequent stray current source, the electric power traction system will be taken as the example in this part. The essential elements of a transit system are the rails, power supply and vehicles. The design and placement of all these dictate the stray current effects in terms of the total stray current leaving the rails.

As aforementioned, owing to the longitudinal resistance of rails and their imperfect insulation to ground, part of the return current leaks out from the running rails and flows along parallel circuits, before returning onto the rail and the negative terminal of the substation, forming the stray current. Apparently, the higher the contact resistance between the rails and the ground (insulation) and the less the longitudinal resistance of the rail, the lower are the leakage currents from the railway into the ground.

Reduction of the longitudinal resistance can be attained by the connection of adjacent joints using flexible copper wire or other conductors [361, 362]. According to existing standards, in the case of increasing the contact resistance between the rails and ground, rails should be bedded in broken stone, gravel or other equivalent (regarding their insulating properties) ballast. Wooden ties must be impregnated with non-conductive oil antiseptics, while at the time of application of ties of reinforced concrete, it is necessary to insulate them from the rails [16, 363, 364].

Reducing the distances between traction substations is another measure that can be taken for mitigating stray current. However, this solution increases the construction cost, so the optimum placement of traction substations should be carried out on the basis of peak service conditions [32].

3.4.1.2 Railway earthing systems

The railway earthing system has significant effect on the magnitude of stray currents. Schemes adopted in the earthing of a railway system include solid (direct) earthed, floating (unearthed),

and diode earthed [272, 279, 326]. Based on analysis of the grounding strategies, it was found that various earthing schemes can change the stray current intensity to a different extent [32, 75, 365, 366].

Simulation results clearly indicate that stray currents and rail potentials are closely related in both unearthed and earthed systems. Generally, the rail potential of the rail in the unearthed system is higher, but it would decrease considerably when the substations are earthed. However, it was shown that the stray current increases where direct earthing of rails is implemented [32].

Diode-earthed-schemes represent a compromise between earthed and direct-earthed-schemes. They are often used to eliminate the problems of stray current corrosion from a direct-earthed system. However, the practical and theoretical studies have shown that diode earth strategies may result in high touch potentials and stray currents at the same time. As a result, among the three available approaches, the unearthed scheme (floating) is the most effective in view of levels of stray currents and rail potential.

3.4.2 Measures on ambient conditions

3.4.2.1 Stray current collection system

If the total stray current for a given system is high, considerable corrosion of the supporting infrastructure may occur. In this situation, a stray current collection system (current collection mat or cable) may be needed to control the path through which the stray current returns to the substation. As shown in Figure 3.6, a stray current collection system can be constructed under the rails in order to "capture" the stray. Such collection systems usually take the form of reinforcement in the concrete track bed of a traction system.

The performance of a stray current collection system is highly dependent on the conductivity of the system itself and of the neighboring soil. Extremely high efficiencies can be achieved when the material, surrounding the stray current collection system, is highly resistive [367]. The arrangement of a reinforcement mat, being bonded electrically back to the substation through parallel conductors, has therefore a dual function: (1) To prevent corrosion of the reinforcement bars themselves, and (2) To act as a secondary level of protection against stray currents penetrating the surrounding earth and possibly into buried services [367].

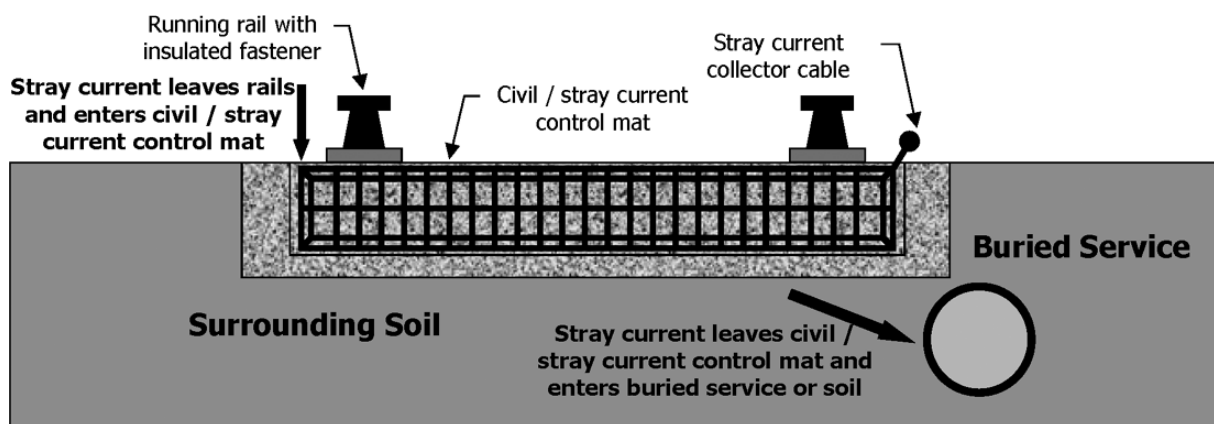


Figure 3.6: Stray current collection system under the rail [75].

3.4.2.2 Electrical drainage bond

As mentioned before, corrosion only occurs when stray current leaves the metallic structure. It does not occur at the section where current enters the structure or when it leaves the structure to another metallic structure, other than to enter the soil or concrete (i.e., electrolyte). To mitigate the corrosion effects of stray current, a so-called drainage bond can be used [368]. Therefore, by diverting most of the current into the drainage bond rather than into the soil, the amount of corrosion of the metal structure will be reduced. A drainage bond (Figure 3.7) is a metallic joint between the structure and rail that provides an alternative path for the stray current to return to the rail [367].

For complex systems in practice, the design of bonds is not easy. The drainage bond connection to the underground structure should be located where the railway and the structure cross or where they are closest together.

In addition, the location should be convenient for checking the equipment and where it does not interfere with traffic [367]. Stray currents sometimes tend to be dynamic in nature, with the direction of current reversing from time to time. In such cases, simple bonding is insufficient, and additional installation of diodes will be required to protect a critical structure at all times [55, 106].

Until recent years it was considered sufficient to rely on the traditional tie-wires used to assemble a reinforcement mesh to provide bonding. But as a result of some failures in practice, this view no longer holds for structures of DC traction systems. Where weldable steelworks are used, spot welding may provide the best solution, though the effect of this on the structural properties of the systems needs careful evaluation [184].

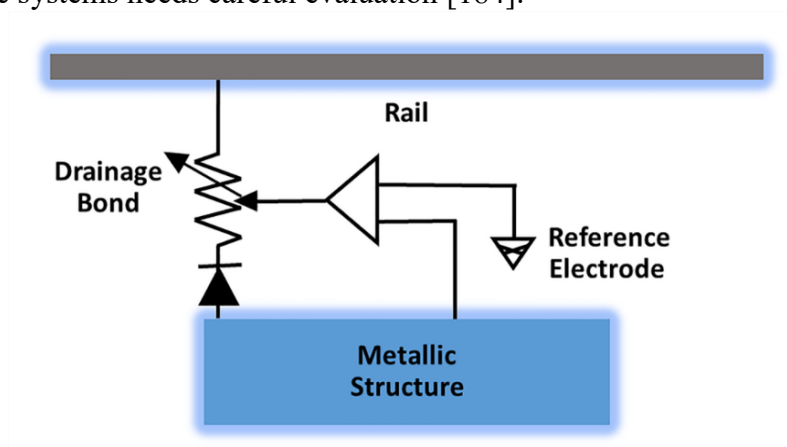


Figure 3.7: Schematic of drainage bond for mitigating the corrosion effects of stray current [367].

3.4.2.3 Electrical shield

Where a metallic structure is located nearby a stray current source, it is possible to reduce the amount of picked-up stray current by using electrical shields. A metallic barrier (or “shield”) that is polarized cathodically is positioned in the path of the stray current, as shown in Figure 3.8. In cathodic shielding, the aim is to minimize the amount of stray current reaching the structure at risk (i.e., the steel pipeline as shown in Figure 3.8). The shield represents a low-resistance preferred path for the stray current, thereby minimizing the flow of stray current onto the interfered structure.

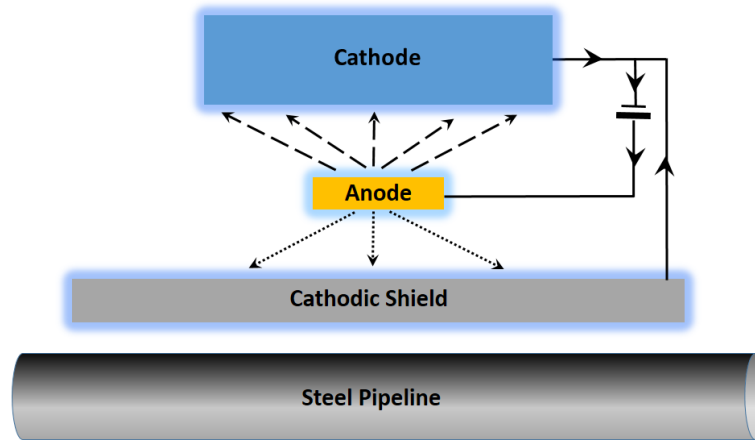


Figure 3.8: Schematic of a cathodic shield to minimize anodic interference.

The effects of location and the manner of installing a metallic shield for mitigating the effects of stray current were studied experimentally by Du et al. [185]. The metallic shield was connected with the cathode of the interference source and the picked-up stray current value was monitored. If the shield is connected to the negative terminal of the power supply of the interfering structure, its effects on the protection levels of the interfering structure have to be considered; these will obviously be reduced for a given rectifier output [106].

Though the shields can reduce the stray current pickup, interference current can still be expected to flow away from the pickup area to remote discharge points at which the interfered metallic structure will be corroded. This current flow needs to be reversed. This may be done with galvanic anodes or bonds, if the shields have reduced stray current pickup to a reasonably small magnitude [85].

3.4.3 Measures on interfered structure itself

3.4.3.1 Insulating couplings

By installing one or more insulating couplings, the pipeline becomes a less favorable path for stray currents. Such couplings are often useful for minimizing stray current damage. But they are less useful if voltages are so large that current is induced to flow around the insulating joint, causing corrosion near the couplings as shown in Figure 3.9 [55].

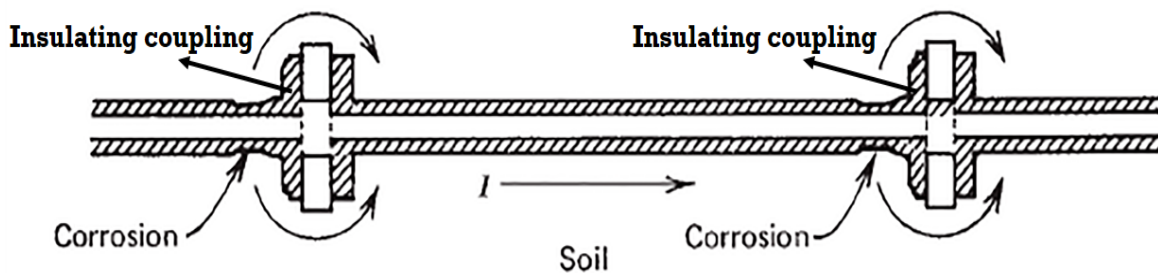


Figure 3.9: Effect of current flowing along a buried pipeline on corrosion near insulated couplings [55].

3.4.3.2 Intentional anodes and cathodic protection

Sacrificial anodes can be installed at the current discharge areas of the interfered structures to mitigate stray current corrosion. Stray currents then cause corrosion only on the intentional anode, which can easily be replaced at low cost. This mitigation method is used frequently in pipeline exposed to stray current, and is most applicable in cases of relatively low levels of stray currents [106].

As shown in Figure 3.10, the current is discharged from these anodes rather than from the structure at risk. The importance of placing the anodes close to the interfering structure is obvious: to minimize the resistance to current flowing from the anodes. The less noble anodes will generate a cathodic protection current, thereby compensating for small amounts of residual stray currents that continue to be discharged from the interfered structure.

Cathodic protection is installed when the intentional anode is not sufficient to overcome all corrosion caused by stray currents [55]. The materials applied for manufacturing grounding anodes in cathodic protection (by impressed current) are various. Dissolution of steel anodes at current outputs is close to 100%. Consequently, steel grounding anodes, designed for a long-term service life, should have enough weight [16].

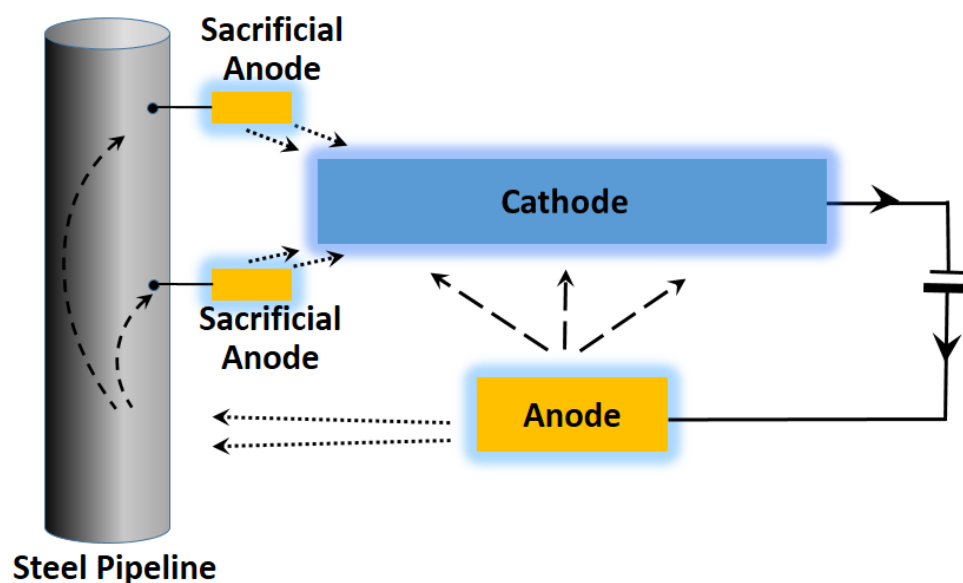


Figure 3.10: Schematic of sacrificial anodes to mitigate cathodic interference.

3.4.3.3 Application of coatings

The most important component of the protection system for underground structures is the insulation coating. The higher the construction-ground resistance (the better the quality of the insulating coating of the construction), the smaller the stray current magnitudes penetrating to the construction.

Application of water proof coatings to buried reinforced concrete structures may reduce the stray current flowing through the concrete [333]. To prevent stray current from flowing into the reinforced concrete structures in plants using electrochemical methods, standards forbid the

application of materials that are capable of absorbing moisture (concrete, non-glazed porcelain, ceramics, etc.) in these plants, without special treatment by water-repellent and insulating compositions [16].

The use of coatings to mitigate the influence of stray currents should only be considered at the current pickup areas. It is not recommended to rely on additional coatings at current discharge areas, because rapid penetration of substances and localized corrosion is to be expected at any coating defects. In general, if a macroscopic anode and cathode exists on a structure, coatings should never be applied to the anode alone in view of corrosion protection [106].

3.4.3.4 *Electrical discontinuity*

In practical applications, it is impossible to completely exclude defects in coatings, applied on large structures. Therefore, alongside the application of insulating coatings, the longitudinal resistance of pipelines should be increased, to decrease the magnitude of stray currents, as well as to minimize the effect of defects. For this purpose, electric sectionalization of pipelines can be executed. This consists of the application of insulating flanges and the insertion of insulating material into the pipelines. In this way, it is possible to significantly lower the magnitude of stray current flowing into the pipeline.

However, along with a decrease of the stray current density, the number of anodic zones, where the current is draining off from the pipeline into the ground, increases. This number is equal to the number of sections, “breaking” the current flow along the pipeline. Therefore, sectionalization is usually carried out together with the application of grounded current taps [16].

Other than pipeline networks, reduction of stray currents for various structures can also be achieved by sectionalization, e.g., for maintenance platforms of electrolyzers or underground reinforced concrete structures. For instance, overlaps of the installation for electrolyzers should be separated by insulation seams from adjoining walls, columns and other elements of the building.

3.5 Challenges to be dealt with in this thesis

The literature review and introduction about the stray current mechanism have been presented in Chapter 2. To further clarify the challenges that may be encountered in practice, the reinforced concrete culvert under a railway line suspected to be attacked by stray current arising from rail was demonstrated. The conditions for a steel rebar to pick up the stray current were analyzed. Subsequently the means for reducing stray current corrosion of the practical infrastructure were summarized.

On the basis of the literature review and practical cases, a number of scientific challenges related to stray current corrosion of steel in reinforced concrete structures can be listed as below:

1. It is found that a lot of previous studies actually supply anodic polarization to simulate stray current. Thus in this work, the effect of anodic polarization and stray current will be studied and compared in Chapter 4.
2. Bond of steel-concrete interface is an important structural property for reinforced concrete elements. The bond between steel surface and surrounding concrete assures the concrete

and the reinforcement can work together as composite material. However, the role which stray current plays in bond degradation of steel-concrete interface has not been studied in detail yet. Therefore, the effect of stray current corrosion on bond strength will be investigated in Chapter 5 of this thesis.

3. In reinforced concrete structures the steel rebar orientation always varies corresponding to location or function of a specific element (see Figure 3.1). Thus the direction of a rebar can be parallel or orthogonal to the stray current. However, very rare investigations compare the corrosion behavior of steel rebar undergoing stray current in different directions. This aspect is of significance in view of the corrosion degree and the location of corrosion cells formed on the steel rebar surface. Therefore, the importance of cell geometry, i.e. the effect of steel orientation with respect to the electrical field (placed parallel or orthogonal to the stray current direction) will be studied in Chapter 6. The effect of rebar length undergoing stray current (related to the electrical discontinuity in practice, as introduced in Section 3.4.3.4) will be studied as well.
4. In view of picked-up stray current level and induced potential shift of rebar, Chapter 6 also aims to simulate a stray current electrical field on a steel rebar embedded in mortar, and monitor the time-dependent response (both potential shift and stray current flowing within the steel rebar) of the steel rebar undergoing stray current at the laboratory scale. Specifically, the effect of rebar positioning (steel bar placed parallel or orthogonal to the stray current direction) on potential shift and picked-up stray current level, will be clarified.

Chapter 4

Corrosion of reinforcing steel undergoing stray current and anodic polarization

4.1 Introduction

To study the effects of stray current on the corrosion behavior of steel in concrete, various works report on different approaches [58-68, 183]. However, most of the investigations actually reported the results on anodic polarization, rather than stray current-induced corrosion of steel in reinforced concrete specimens [49, 50, 58-68]. The main objective of this chapter is to experimentally justify the different effects of stray current and anodic polarization, on reinforcing steel embedded in “fresh” (24 hour-cured) and “matured” mortar (28 day-cured).

Polarization (imposed in this work) refers to a potential shift away from the former corrosion potential (open circuit potential) of a corroding system. Corrosion potential is an important parameter related to the corrosion state of metals. Corrosion potential is a mixed potential at which the metal is in a state of dynamic equilibrium, where the rates of oxidation and reduction reactions on the metal surface are equal, hence, the net current of the system is zero. A change of this initial dynamic equilibrium (due to altered electrochemical state or externally imposed) is reflected by a change in the corrosion potential. A potential shift in a positive direction from the initial equilibrium (corrosion) potential is called anodic polarization, while a negative potential shift is cathodic polarization.

Although stray current leads to the generation of anodic locations on a steel surface, meaning that the degradation itself is linked to anodic currents and oxidation, the influence of stray current is not just anodic polarization. As presented in Figure 2.10 (Chapter 2) the stray current effect is composed of both anodic polarization and cathodic polarization on a metal (steel) surface. Hence, stray current and its effects are more complex than only anodic polarization. Except exerting effects on the metallic conductor (steel specifically), stray current will also trigger ion migration in a cement-based matrix. Cations would migrate in the direction of current, but anions (e.g. Cl^-) migrate in the opposite direction.

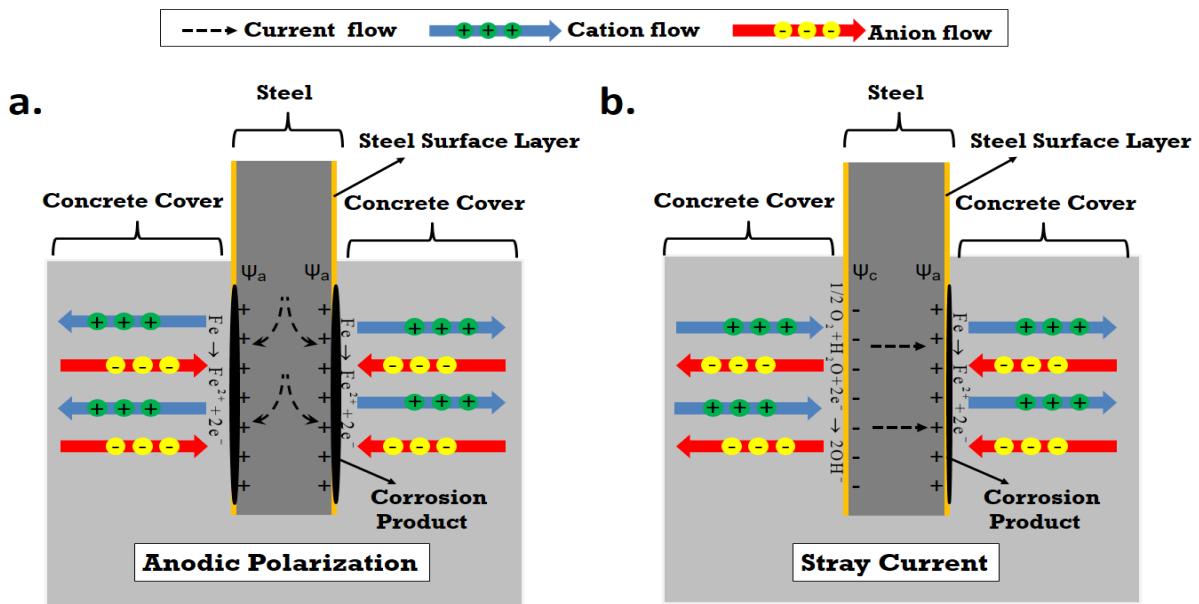
If anodic polarization is applied to steel in concrete (Figure 4.1a), anions (Cl^- for instance, as present in seawater, where Cl^- ions ingress is common for reinforced concrete structures in these environmental conditions) will be attracted to the steel surface (anode), while cations (Ca^{2+} , Na^+ , K^+ , etc.) will be repelled towards the cathode (or an external conductor, e.g. counter electrode polarizing the anode). In conditions of stray current, a separation of charge will be relevant (as previously introduced in Chapter 2, as well as here depicted in Figure 4.1b), where anions would be similarly attracted to the anode and cations to the cathode. In such situations the corrosion activity at the anode would be further accelerated by a combined mechanism of

stray current-induced corrosion (in the sense of oxidation due to anodic polarization) and localized corrosion attack induced by Cl^- .

Nevertheless, as for the stray current flowing within a reinforced concrete structure, the concentration of Cl^- nearby the steel surface is not expected to be as significant as the case of anodic polarization, although this will very much depend on the level of stray current, as well as the pore network (bulk matrix) characteristics of the concrete bulk.

Ion migration in electrolyte is an ion transport mechanism that can only occur in an electrical field. Ion migration (or its co-existence with diffusion, capillary suction, etc.) in cement-based materials is through the connected pores [51, 369-371]. Thus the transport process is related to the porosity and pore network connectivity of the bulk, which is also determined by the age/maturity of a concrete matrix. Fresh concrete at very early age is considered as a viscoelastic material [372, 373]. From mixing until the initial setting time, cement hydration takes place and makes the concrete harden. During this period, ion migration, due to electrical field, would additionally influence the cement hydration process and product layer formation on the steel surface. Specifically, current flow in the fresh (non-mature) cement matrix with high porosity and permeability, can easily lead to enhanced water and ion transport due to accelerated ion migration. Consequently, cement hydration will be enhanced, leading to a faster development of the cementitious microstructure, assisting a more rapid stabilization of the pore solution and hydration products at the steel-mortar interface.

In this chapter, stray current and anodic polarization are both applied and monitored in identical reinforced mortar specimens. The specimens are cured in fog room (98% RH, 20 °C) for only 24 hours (24h) to produce “fresh” bulk matrix, or standard 28 days (28d) for hardened matrix. For a period of 243 days of conditioning, a comparison between stray current and anodic polarization effects on the corrosion behavior of embedded steel is performed for both fresh (24h-cured) and hardened matrix (28d-cured), in Cl-free and Cl-containing environment.



4.1a: Anodic polarization.

4.1b: Stray current.

Figure 4.1: Ion migration in reinforced concrete undergoing: a). Anodic polarization; b). Stray current.

4.2 Experimental

4.2.1 Materials and specimen preparation

Stray current and anodic polarization were applied on reinforced mortar prisms (of $40 \times 40 \times 160$ mm³). The specimens were cast from Ordinary Portland Cement (OPC) - CEM I 42.5 N, and normed sand. The water-to-cement (W/C) ratio was 0.5; the cement-to-sand (C/S) ratio was 1:3. Construction steel (rebar) FeB500HKN ($d=6$ mm), with an exposed length of 40 mm (with an exposed steel surface area of 7.54 cm²) was centrally embedded in the mortar prisms. The schematic presentation of the specimens' geometry is depicted in Figure 4.2.

Prior to casting, the steel rebars were cleaned electrochemically by cathodic current of 100 A/m², where the steel rebar was the cathode, stainless steel was the anode. This process was performed in a solution of 75 g NaOH, 25 g Na₂SO₄, 75 g Na₂CO₃ (reagent water to make 1000 mL), according to ASTM G-1 [374, 375]. After that the two ends of the rebar were covered by a heat-shrinkable tube. This aimed to avoid or minimise crevice corrosion and confine the effect of the experimental conditions to identical geometry and exposed steel surface. More details on specimen preparation for pull-out test will be further introduced in Chapter 5.

The two cast-in Ti electrodes (MMO Ti mesh, 40×160 mm²) served as terminals for anodic polarization and/or stray current application. When anodic polarization and/or stray current supplies were interrupted (min 24h before electrochemical tests), the two Ti electrodes (connected with each other) served as counter electrode in a general 3-electrode set-up, where the rebar was the working electrode and an external Saturated Calomel Electrode (SCE) served as a reference electrode.

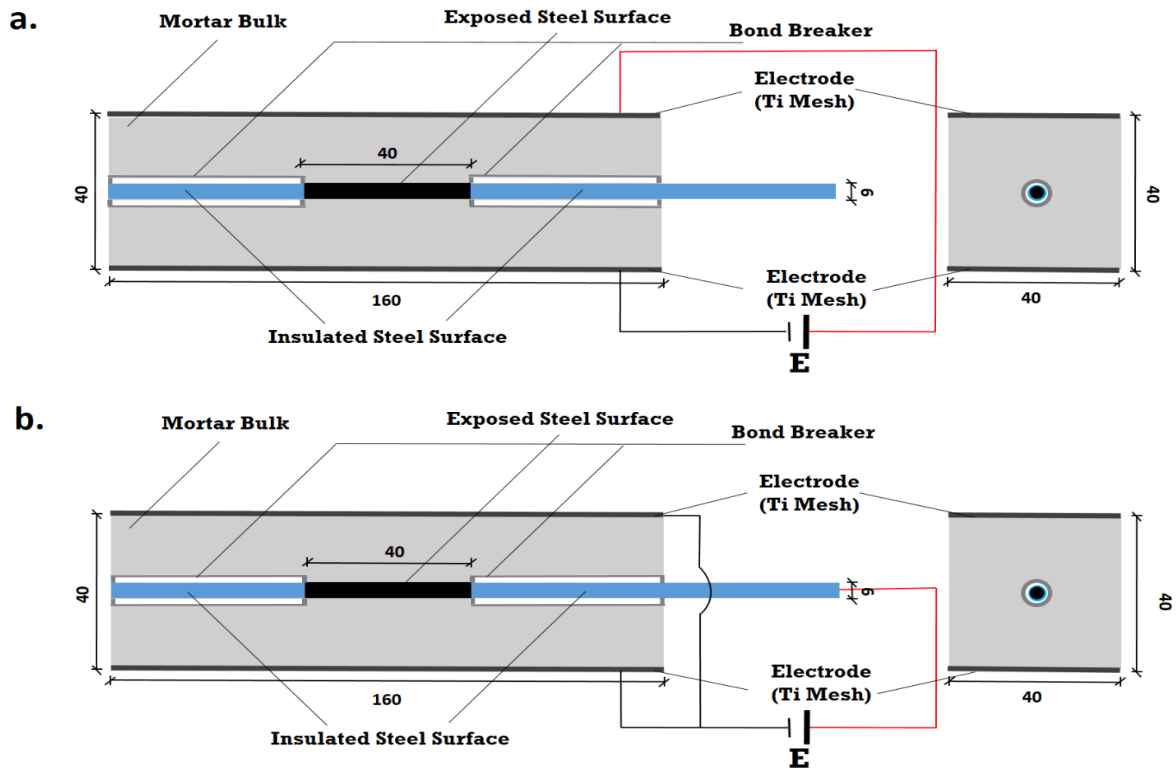


Figure 4.2: Experimental set-up for current supply and position of electrodes: a). Stray current; b). Anodic polarization.

The level of stray current and anodic polarization were both set at 0.3 mA/cm², applied as an external DC electrical field. The current density was calculated according to the exposed steel surface area. This level of current density was chosen to account for a hypothetical 10% weight loss of steel rebar, as analytically calculated via Faraday's law, for a period of 28 days in the relevant experimental conditions:

$$i = ZFr\rho\eta_s / 2At \quad 4.1$$

Where t is time of corrosion (28 days = 2419200 s), Z is the valence of the iron ions taking part in the anodic reaction ($Z = 2$), F is Faraday's constant (96500 As), r is the radius of corroded bar (0.3 cm), ρ is the density of iron ($\rho = 7.87$ g/cm³), η_s is the mass loss ratio (10%), A is the atomic mass of iron ($A = 56$ g), and i is the impressed current density (A/cm²). Based on this calculation the level of anodic polarization corresponding to 10% mass loss over 28d is 0.1744 mA/cm². Considering the fact that the supplied anodic current may be partially limited if any resistive components in the circuit would arise within the mortar bulk, the final chosen current level was increased to 0.3 mA/cm².

4.2.2 Curing and conditioning

Table 4.1 summarizes the relevant curing and conditioning regimes, and specimens designation. After casting, all specimens were cured in a fog room (98% RH, 20 °C) for 24 hours (24h) or 28 days (28d) until demoulding. Next, the specimens were lab-conditioned (lab air). The specimens were immersed in water (Cl-free) or 5% NaCl solution (Cl-containing), with 2/3rd of height.

Table 4.1*: Summary of curing and conditioning regimes.

Group	Curing	Immersion Environment (2/3 rd)		Electrical Field	
		Water	5% NaCl	Stray Current (0.3 mA/cm ²)	Anodic Polarization (0.3 mA/cm ²)
R-24h	24h	✓			
C-24h			✓		
S-24h		✓		✓	
CS-24h			✓	✓	
A-24h		✓			✓
CA-24h			✓		✓
R-28d	28d	✓			
C-28d			✓		
S-28d		✓		✓	
CS-28d			✓	✓	
A-28d		✓			✓
CA-28d			✓		✓

* R-24h: Reference; C-24h: Corroding (NaCl medium); S-24h: Stray Current; CS-24h: Corroding (NaCl) + Stray Current; A-24h: Anodic Polarization; CA-24h: Corroding (NaCl) + Anodic Polarization – after 24h curing.

R-28d: Reference; C-28d: Corroding (NaCl medium); S-28d: Stray Current; CS-28d: Corroding (NaCl) + Stray Current; A-28d: Anodic Polarization; CA-28d: Corroding (NaCl) + Anodic Polarization – after 28d curing.

4.2.3 Experimental methods

Electrochemical measurements were performed at Open Circuit Potential (OCP), using a SCE as reference electrode (as above specified, the counter electrode was the initially embedded MMO Ti mesh). The OCP values were recorded at each time interval prior to electrochemical measurements. The OCP evolution, in general, provides information for transitions from passive to active state, and vice versa. For steel embedded in a cement-based material, a threshold value of -200 ± 70 mV (vs SCE) [375] has been accepted, i.e. more anodic OCP values would reflect passive state, whereas more cathodic values are linked to an active (corroding) state [376].

However, OCP only provides an indication of the corrosion state, rather than giving quantitative information, e.g. corrosion rate. Hence, more cathodic OCP values would not always be related to increased corrosion rates. The OCP response of the steel can be affected by a number of factors, such as relative humidity, oxygen availability, the presence of highly resistive layers. For instance, limited oxygen availability (as in submerged conditions) can be reflected in a more cathodic OCP value. Hence, the interpretation of OCP values in such conditions, would be more complex and cathodic OCP would not indicate enhanced corrosion activity.

Linear Polarization Resistance (LPR) was performed in the range of ± 20 mV (vs OCP), at a scan rate of 0.1 mV/s ($= 6$ mV/min). It is found that the sweep rates of 2.5 - 10 mV/min give reliable results (suitability obtained by comparison to gravimetric losses, as reported in Ref. [377]). This range of scan rate makes sure the R_p achieves a constant value (i.e., the stationary value), because within this scan rate the recorded i (vs E) is already constant after the attenuation of varying current (this process is controlled by the attenuation rate, which is governed by the time constant of the working electrode) [377, 378].

This method allows determination of polarization resistance (R_p). The R_p values are used for a quantitative assessment, through calculating corrosion current by employing the Stern-Geary equation, i.e., $i_{\text{corr}} = B/R_p$ [379, 380]. The R_p value was experimentally derived, whereas for the constant B the reported values for passive ($B = 52$ mV/dec) or active ($B = 26$ mV/dec) were employed [381, 382]. Since R_p is inversely proportional to the corrosion current, quantification of corrosion resistance can be performed by a comparative analysis of R_p values only, as used and discussed in this work.

Electrochemical Impedance Spectroscopy (EIS) was employed in the frequency range of 50 kHz - 10 mHz, by superimposing an AC perturbation voltage of 10 mV (rms). As a non-destructive electrochemical technique, EIS provides qualitative and quantitative information of both the steel reinforcement and the bulk matrix. The high frequency (HF) range (i.e., MHz to approx. 10 kHz) offers information for the contribution of the bulk matrix (solid and pore network). High to middle frequency ranges (10 kHz to 1 kHz), reflects the contribution of the pore network and steel-cement paste interface, while middle (MF) to low frequency (LF) range (< 1 kHz to 10 mHz) corresponds to the electrochemical response of the embedded steel [383-387].

For the 24h-cured specimens, both LPR and EIS tests were performed at the age of 3, 7, 14, 28, 56, 141 and 215 days. For the 28d-cured cases, LPR and EIS tests were conducted at the age of 28 (after 1d conditioning), 35 (after 7d conditioning), 42 (after 14d conditioning), 56 (after 28d conditioning), 169 (after 141d conditioning) and 243 (after 215d conditioning) days. In other words, the time periods of testing and conditioning for both 24h-cured and 28d-cured

specimens were identical, but the hydration age of the specimens at the specific time interval varied, reflecting the 24h and 28d curing.

For specimens undergoing stray current or anodic polarization, a 24-hour de-polarization (potential decay) was performed prior to any further testing. The experimental protocol and the sequence of tests are meant to verify: (1) if stray current indeed flows into the steel; (2) if 24-hour potential decay is sufficient to result in stability of the electrochemical state of steel (i.e., if a stable OCP was achieved), so that electrochemical tests can follow after the decay. During the decay and within electrochemical tests, the specimens were immersed fully in the relevant medium (in water or 5% NaCl). The used equipment for electrochemical tests in this work was Metrohm Autolab (Potentiostat PGSTAT302N), combined with a FRA2 module.

4.3 Results and discussion

To experimentally justify the different effects of stray current and anodic polarization on reinforcing steel embedded in “fresh” (24h-cured) and “matured” mortar (28d-cured), the electrochemical performance of steel in different curing regimes and conditions will be shown and discussed. The electrochemical state of the embedded steel in this work is firstly discussed based on the OCP and LPR records. EIS results are discussed as a qualitative assessment in view of bulk matrix properties and steel surface active/passive state. Finally, the recorded 24-hour potential decay at the age of 95 days will be shown, supporting the results and discussion in the preceding sections.

4.3.1 OCP and R_p evolution

The evolution of OCP and polarization resistance R_p values (recorded via LPR measurements) for the group of 24h-cured specimens are presented in Figure 4.3 and 4.4. Figure 4.5 and 4.6 depict the OCP and LPR records of the 28d-cured specimens. Besides the environment and the conditioning regimes (stray current or anodic polarization), the following factors affect the observed behavior: (1) the steel surface properties prior to conditioning; (2) the properties of the mortar bulk matrix, such as maturity and pH of the pore solution; (3) the porosity and pore network connectivity of the mortar bulk determining ion migration, as well as water transport and oxygen penetration.

The steel surface property is a factor, relevant for both 24h and 28d-cured groups. This aspect is of importance in the sense that clean steel surface would be relatively more active, if compared to oxide layer-covered (“as received”) steel. This factor will dominate until a stable passive layer is formed (as in the non-corroding specimens), in the high pH environment of the mortar pore network.

The effects linked to changes in cement-based material properties, together with their influence on passive film formation, would be more significant in the 24h-cured group. If the stray current supply (or anodic polarization) starts at very early age (e.g. at age of 24h), water transport and leaching-out effects, due to ion migration, will be more evident, because of the high porosity and pore network connectivity of a fresh bulk. Hence, if the hydration process and pore network characteristics are influenced by the foregoing factors, these will further affect the stability of the passive and/or corrosion product layer.

4.3.1.1 OCP and R_p of 24 hours-cured specimens

As can be observed in Figure 4.3, until the 28 days of age, the majority of OCP values for specimens R-24h (control case) and S-24h (stray current case) fall in the cathodic region and are far beyond the passivity threshold, i.e., more cathodic than the generally accepted -200 ± 70 mV (vs SCE) for reinforced mortar/concrete systems [375, 376]. These OCP values account for active state of the steel reinforcement, for at least until 28 days of age.

This performance is due to the surface condition of the embedded steel (clean surface), the fresh mortar matrix. Specifically, the electrochemical cleaning of the embedded steel performed prior to casting, results in a “bare” steel surface, which will be active in alkaline environment of $\text{pH} > 13.5$ at very early age, until a passive layer is formed and the pH of the environment (pore solution) stabilizes at around 12.9.

As can be observed in Figure 4.4, relatively low R_p values are initially recorded for the control specimen R-24h, and increase to $60 \text{ k}\Omega\cdot\text{cm}^2$ at the end of the test. This result was not as expected, although in line with the OCP evolution for R-24 in Figure 4.4. Until 141 days, higher R_p values (in the range of $40\text{--}70 \text{ k}\Omega\cdot\text{cm}^2$) for S-24h (compared to R-24h) are recorded. For specimen A-24h, very low R_p values are recorded, below $10 \text{ k}\Omega\cdot\text{cm}^2$, with an increasing trend towards $30\text{--}40 \text{ k}\Omega\cdot\text{cm}^2$ between 14d and 141d. A significant reduction of R_p values for A-24h, below $5 \text{ k}\Omega\cdot\text{cm}^2$, is observed at the end of the test (at 215 days).

In the period of 3 days until 28 days for the 24h-cured groups, the OCP records reflect the steel electrochemical response within a gradually refined pore network, a steel-cement paste interface development, characteristic for a cement-based system at early hydration stage. These are in terms of pore solution chemistry alterations as well as passive layer stabilization (for control cases) or corrosion initiation (for corroding cases). The development of the passive layer and further stabilization is illustrated by the initial fluctuations of OCP values for the control group R-24h and stabilization further on, towards more anodic OCP values and higher R_p values after prolonged conditioning (see Figure 4.3, after age of 215 days).

A factor related to the above observations, which contributes to an impeded passive layer formation, is the leaching-out effect. If a cement-based material is in a prolonged contact with water, dissolution of cement hydrates will occur (due to alkali ions - Ca^{2+} , Na^+ , K^+ leaching) [263, 388-398]. The transport of sodium and potassium is faster than that of calcium ions, and more pronounced at early stages (a fresh bulk matrix, means a non-mature, more open pore structure), whereas stable and/or negligible with longer treatment [399, 400]. Leaching of calcium ions promotes coarsening of the pore structure, leads to increased transport properties (permeability, diffusivity) and decrease in mechanical properties [400].

Generally, the leaching process starts with a total dissolution of portlandite (calcium hydroxide, CH), ettringite, followed by a progressive decalcification of the calcium-silicate-hydrate (C-S-H) phase [401-403]. From 1 day of age onwards (after 24h curing in moulds), the 24h-cured specimen (R-24h) was conditioned in water, which is likely to result in leaching-out and altered transport properties of the bulk matrix. Hence, stabilization of the passive layer in a fresh (24h only cured) cement-based system, as in specimen R-24h, takes a significantly longer period - after 141 days of conditioning (see Figure 4.3), when OCPs tend towards more anodic values.

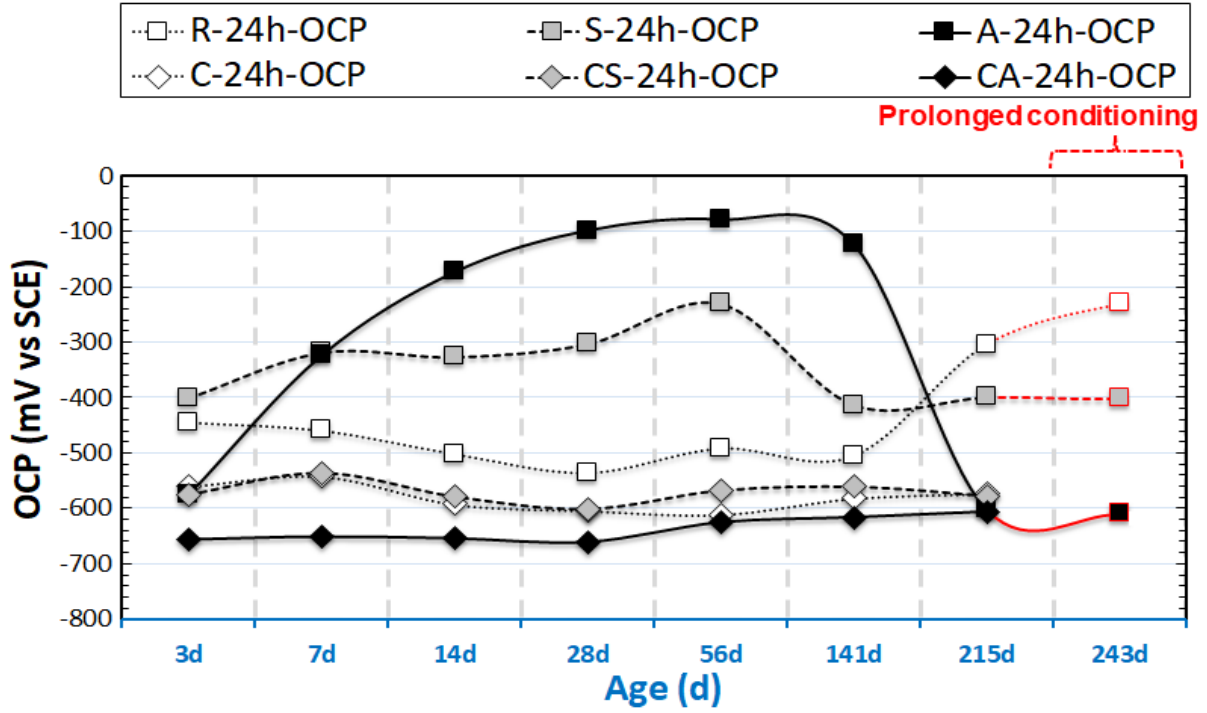


Figure 4.3: OCP evolution of samples with time: R-24h: Reference; S-24h: Stray Current; A-24h: Anodic Polarization; C-24h: Corroding (NaCl medium); CS-24h: Corroding (NaCl) + Stray Current; CA-24h: Corroding (NaCl) + Anodic Polarization – after 24h curing.

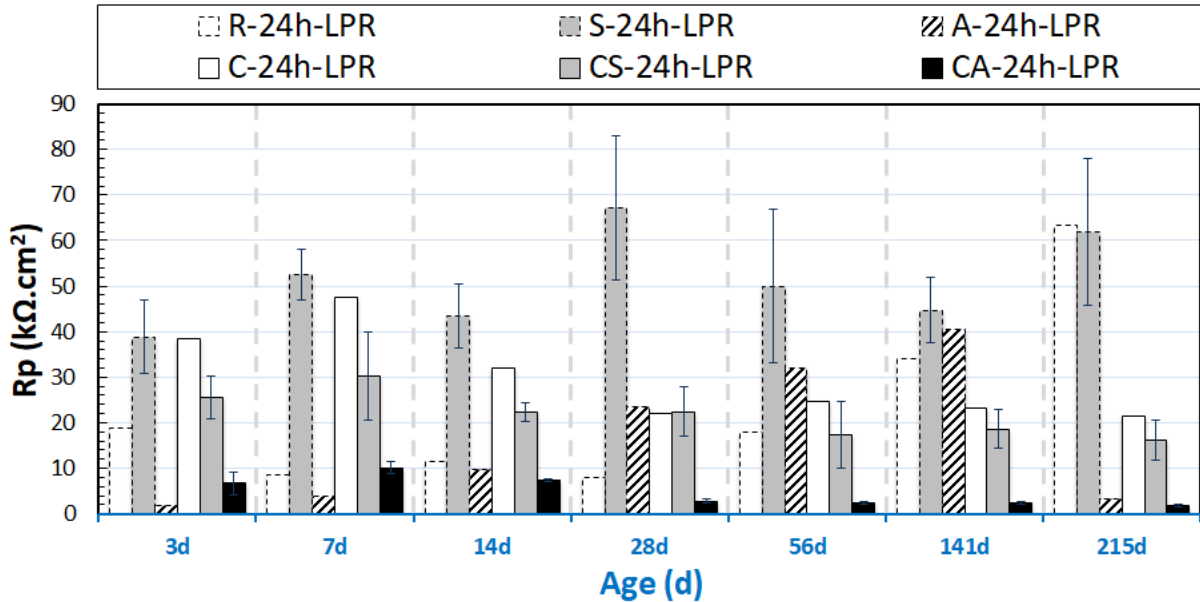


Figure 4.4: R_p evolution of samples with time: R-24h: Reference; C-24h: Corroding (NaCl medium); S-24h: Stray Current; CS-24h: Corroding (NaCl) + Stray Current; A-24h: Anodic Polarization; CA-24h: Corroding (NaCl) + Anodic Polarization – after 24h curing.

It can be noted that the recorded R_p values of C-24h are higher than that for the control group R-24, especially in the first period of 3-28 days (Figure 4.4). This phenomenon is due to the effect of NaCl as accelerator of cement hydration (especially at early age before 28 days) [404-406]. In case of NaCl additions, Friedel's salt is formed, accompanied by a release of NaOH, which is attributed to the chemical action between NaCl and $3\text{CaO} \cdot \text{Al}_2\text{O}_3 \cdot 6\text{H}_2\text{O}$. Consequently the pH in the pore solution will increase. The increased pH will further accelerate the hydration process and modify the pore structure towards a finer one. This will lead to a more stable product layer on the steel surface, which in turn will delay Cl-induced corrosion damage. Therefore initially higher R_p values are recorded for C-24h at early age. After 28 days, the R_p values of C-24h remain at stable and lower values towards the end of the test, indicating the corroding state of C-24h after prolonged conditioning in 5% NaCl.

Until 141 days, the OCPs of specimens A-24h and S-24h are more noble than those for R-24h (in the range of -300 to -400 mV for S-24h, and -300 to -100 mV for A-24h). A significant cathodic drop in the OCP value i.e. increased corrosion activity, for specimen A-24h is observed at the end of the test, establishing an OCP at around -600 mV. The OCP value for specimens S-24h remain stable over most of the test duration, with a cathodic shift and stabilisation (around -400 mV) at the end of the test.

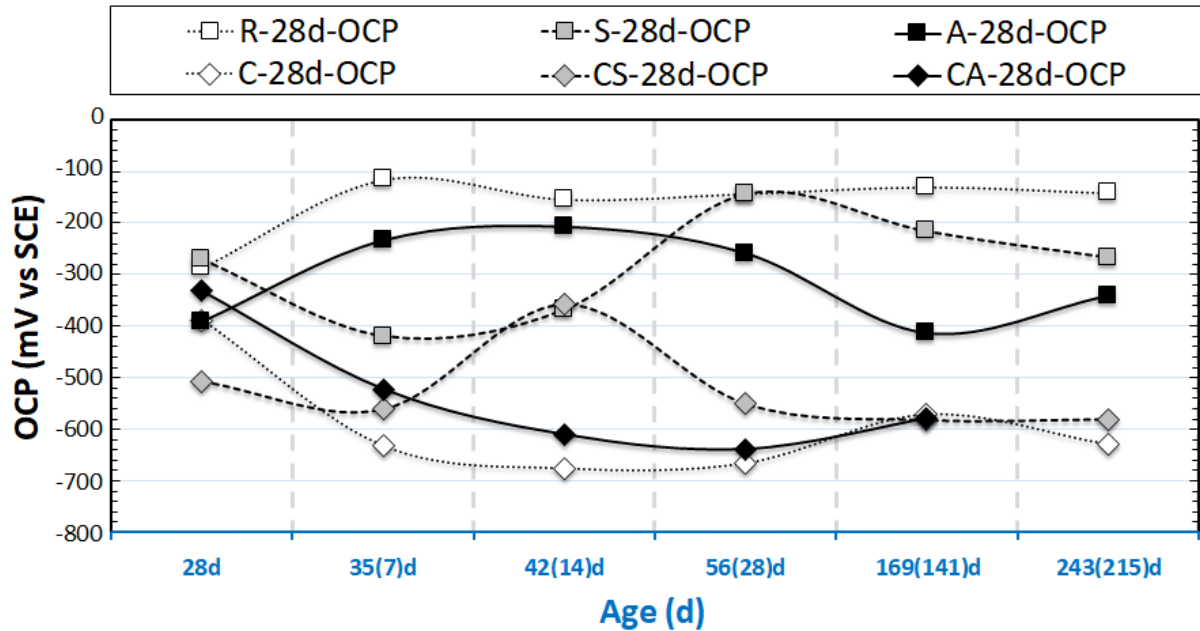
The stray current in Cl-free condition (group S-24h, cured for only 24h) was expected to have a negative effect on steel corrosion resistance at early age. This, however, is not observed. On the contrary, the recorded OCP values (as shown in Figure 4.3) of specimen S-24h are more anodic than those for specimen R-24h (before 141d) and maintain stability (corresponding to higher R_p values of S-24h than those of R-24h, before 141 days, see Figure 4.4), suggesting intensified process of passive layer formation/stabilization of S-24h at early age. The more anodic OCP of S-24h can also be due to microstructural changes (e.g., a denser bulk matrix) at early age. This will lead to an improved steel-mortar interface and a more stable passive layer.

Again, this observation reflects the effect of a “fresh” matrix on the properties of the steel-mortar interface. For group S-24h, stray current flow through the fresh (non-mature) cement matrix, leads to enhanced water and ion transport due to a potential gradient. Consequently, cement hydration will be enhanced, leading to a faster development of the pore network, assisting a more rapid stabilization of the pore solution and hydration products at the steel-mortar interface. Previously reported and known are the early stage beneficial effects of stray current on cement-based matrix properties [47].

4.3.1.2 OCP and R_p of 28 days-cured specimens

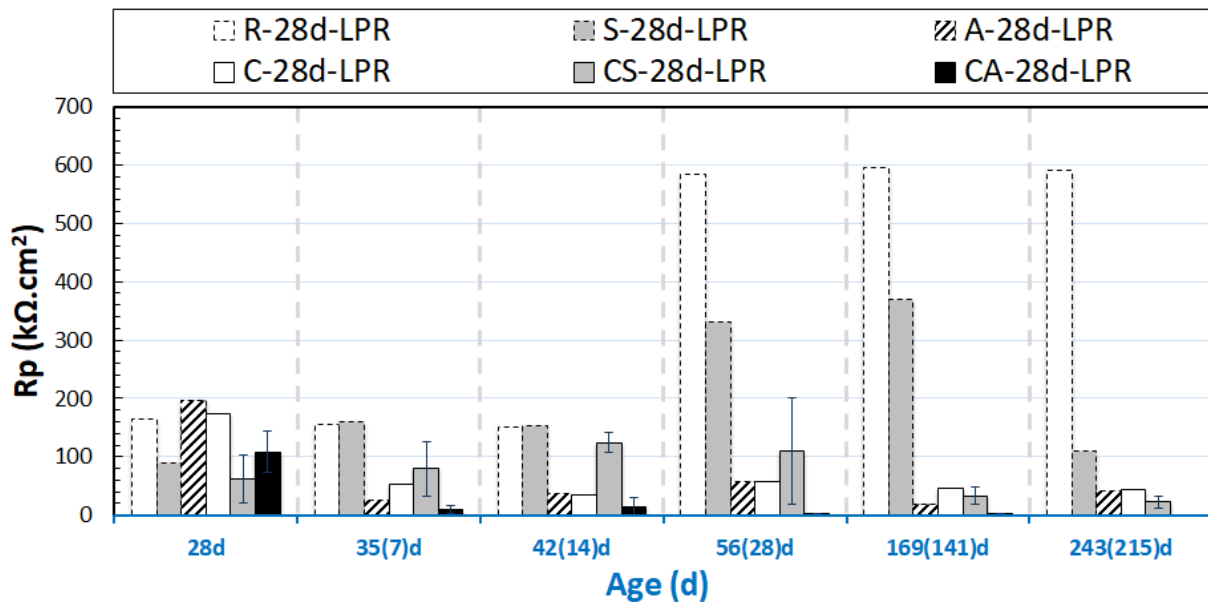
The outflow of stray current from the steel “body” accelerates corrosion on the steel surface (as shown in Figure 2.10 and 4.1b). This is relevant for all tested series related to stray current (i.e., “S” specimens), irrespective of the curing duration (in fog room) prior to conditioning. However, the effect of stray current for the previously discussed S-24h specimen, is already different for the S-28d specimen (cured for 28d). For S-28d, the stray current was applied when the bulk matrix was already hardened. In this situation, ion and water transport cannot be as significantly enhanced, as this would be in a fresh matrix (e.g. as in S-24h). Therefore, the effect of stray current on cement hydration of S-28d is slight, and the stray current effect would be mainly on the properties of the product layer on the steel surface of S-28d. As can be observed in Figure 4.6, the R_p values of S-28d show a trend towards lower R_p ($110 \text{ k}\Omega \cdot \text{cm}^2$, at 243 days), i.e., lower corrosion resistance, if compared to the control specimen R-28d ($590 \text{ k}\Omega \cdot \text{cm}^2$, at 243

days). In line with the R_p records and compared to control conditions (R-28d), more cathodic OCP values of ca. -290 mV are observed for group S-28d at the time interval of 243 days.



* The number in brackets denotes the conditioning duration.

Figure 4.5*: OCP evolution of samples with time: R-28d: Reference; S-28d: Stray Current; A-28d: Anodic Polarization; C-28d: Corroding (NaCl medium); CS-28d: Corroding (NaCl) + Stray Current; CA-28d: Corroding (NaCl) + Anodic Polarization – after 28d curing.



* The numbers in brackets denote the conditioning duration.

Figure 4.6*: R_p evolution of samples with time: R-28d: Reference; C-28d: Corroding (NaCl medium); S-28d: Stray Current; CS-28d: Corroding (NaCl) + Stray Current; A-28d: Anodic Polarization; CA-28d: Corroding (NaCl) + Anodic Polarization – after 28d curing.

The R_p values of R-28d (Figure 4.6) are higher than that for R-24h (see Figure 4.4) over the testing period. These, together with the more noble OCP values of R-28d, show the more resistive steel surface of R-28d, and reflect that a sufficient curing leads to a stable product layer formation on steel surface in Cl-free environment. The expected beneficial effect of sufficient curing is also reflected by the higher R_p values of A-28d specimen, compared to those of A-24h.

The corroding specimens cured for 28d (C-28d, CS-28d and CA-28d), exhibit cathodic OCP values at the end of conditioning. In accordance with these cathodic OCPs, the R_p values of C-28d and CS-28d are much lower than R-28d and S-28d. Lower R_p is recorded for CS-28d (25 $k\Omega \cdot cm^2$ at 243 days), compared to C-28d (about 40 $k\Omega \cdot cm^2$ at 243 days). The result illustrates the effect of both Cl-induced corrosion and the additional stray current contribution in the case of CS specimen. The most active steel surface is observed for CA-28d (the lowest R_p values are recorded for CA-28d after 28 days).

Based on the OCP and LPR results, it can be concluded that stray current and anodic polarization exert significantly different effects on the corrosion behavior of steel embedded in mortar, in both 24h-cured (samples cured in fog room for only 24 hours) and 28d-cured (samples cured in fog room for the standard 28 days) conditions. This will be discussed in more detail together with EIS response in the next sections.

4.3.2 Curing effect reflected by EIS response

If a prompt evaluation of the corrosion state of steel embedded in a cement-based material is aimed at, together with a simplified assessment of the electrical properties of the bulk matrix, qualification of the EIS response is a useful approach. This is especially the case if specimens conditioned in different environments and hence, are expected to present significant variation in properties and response. For instance, a reinforced mortar specimen conditioned in NaCl will logically perform differently in time, if compared to a control specimen conditioned in water. This is due to the expected Cl-induced steel corrosion in the former case, and stabilization of the passive state of the steel reinforcement in the latter case.

Additionally, alterations in the electrical properties of the cement-based matrix, e.g., increased electrical resistivity over time would be expected in all conditions, due to the cement hydration and matrix densification [407-409]. Similarly, factors such as chemical composition of the external environment, ion and water penetration into the bulk matrix, pore interconnectivity of bulk matrix, variation in bulk matrix diffusivity, etc., will determine changes in the electrical properties of the bulk matrix over time [404, 410, 411]. These will be reflected by the high to middle frequency of EIS response.

All these features in an experimental EIS response are well visible, and can be compared qualitatively for systems as in this work - control and corroding reinforced mortar specimens. The EIS responses at time intervals of most significant interests will be presented and discussed in this chapter. The EIS responses (in both Nyquist and Bode formats) of all specimens at all intervals are given in Appendix A.

The EIS responses overlay in Nyquist format of R-24h and R-28d are shown in Figure 4.7. The responses for 24h-cured groups (R-24h and S-24h) are presented in Figure 4.8. These cases are chosen here to address the effect of curing (Figure 4.7), on one hand. On the other

hand, the comparison of R-24h and S-24h cases (Figure 4.8) would specifically address the aspect of the stray current effect.

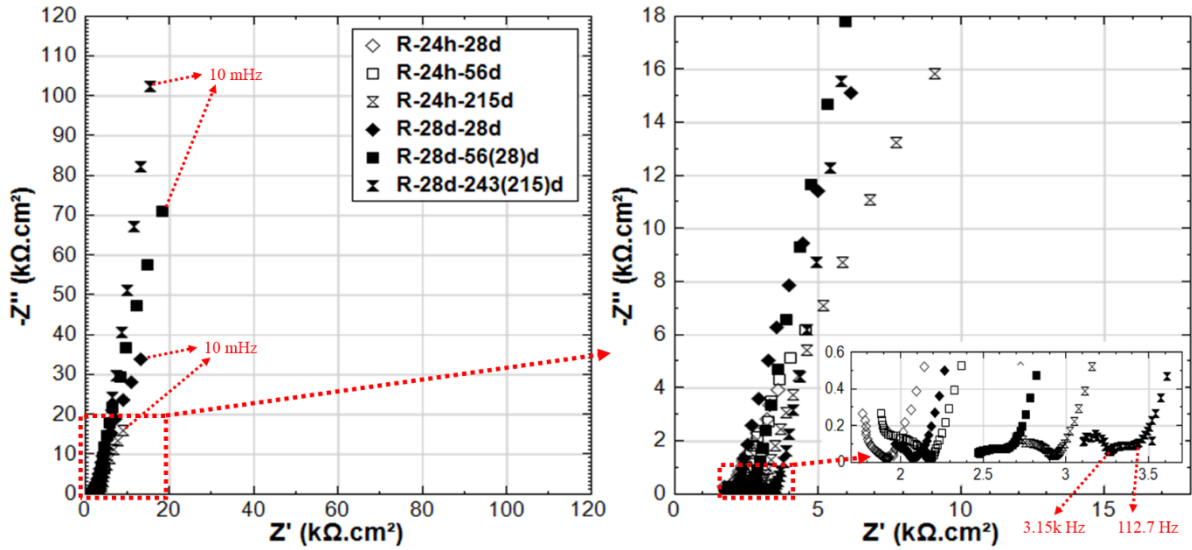


Figure 4.7: EIS responses overlay in Nyquist format of R-24h and R-28d (R-24h: Reference, 24h-cured specimen treated in water; R-28d: Reference, 28d-cured specimen treated in water).

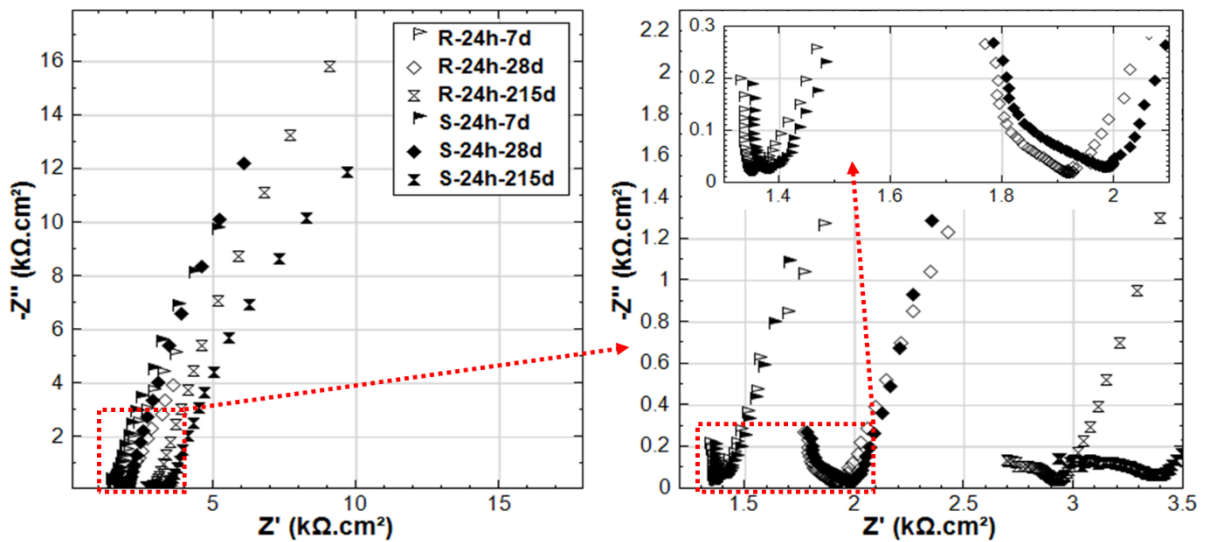


Figure 4.8: EIS responses overlay in Nyquist format of R-24h and S-24h (R-24h: Reference, S-24h: Stray Current, 24h-cured specimens treated in water).

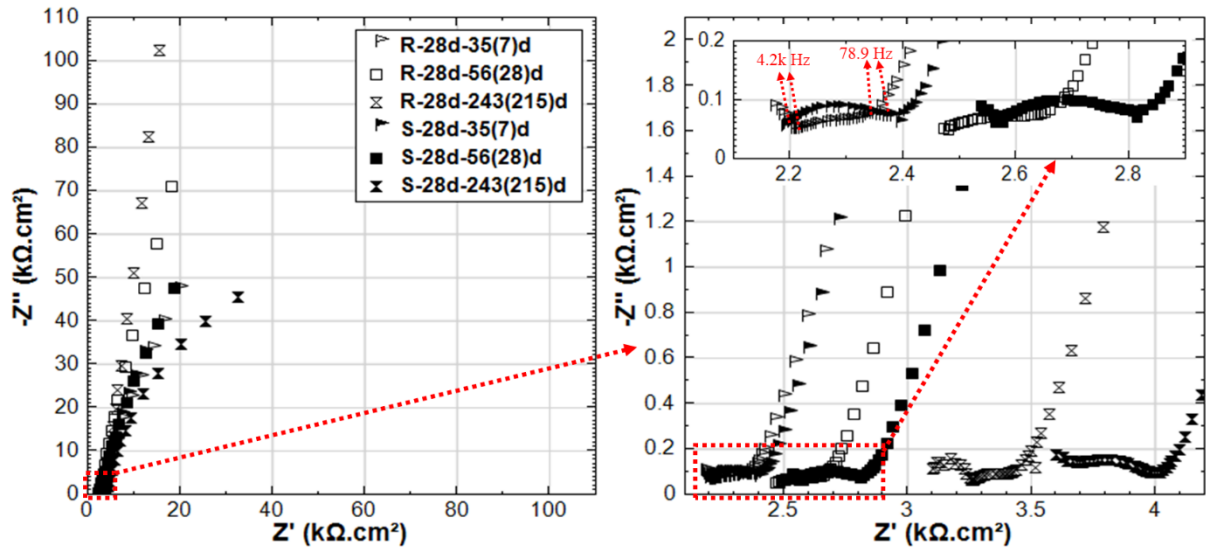


Figure 4.9: EIS responses overlay in Nyquist format of R-28d and S-28d (R-28d: Reference, S-28d: Stray Current, 28d-cured specimens treated in water).

For group R-24h, the shape of the experimental curves reflects the typical response of steel in a Cl-free cement-based environment (alkaline medium) [412, 413]. The response depicts curves inclined to the imaginary y-axis, specifically in the LF EIS response range, reflecting a capacitive-like behavior, or passive state of the steel reinforcement. This is relevant for both R-24h and R-28d at the end of conditioning, denoting the stabilization of the passive layer over time.

A stable passive state would be related to R-28d from the beginning of the test (28d response), but stability of the passive layer for the R-24h group would develop over time of conditioning, as can be observed in Figure 4.7 for the 215d response. Figure 4.7 also depicts variation in bulk matrix properties for the 24h and 28d-cured groups, reflected by the HF EIS response (Figure 4.7, inlet). As can be observed, the magnitude of real $|Z|$ increases over time (due to cement hydration in both cases), but ends-up higher for the 28d group at 215d of conditioning. Besides, for the last time intervals (after 215d conditioning), an additional time constant (in the range of 3.15 kHz-112.7 Hz, Figure 4.7 inlet) can be observed in the HF response of R-28d, while not observed for R-24h. This time constant of R-28d reflects a more developed bulk matrix, steel-mortar interface and product layer on the steel surface. Evidently a more corrosion resistive product layer is formed in R-28d, as also reflected by the LF response for this specimen (Figure 4.7). All these results show the importance of sufficient curing duration for the development of both bulk matrix properties and passive layer formation at steel-mortar interface.

Related to ion transport in the bulk matrix, the main difference between R-24h and S-24h is the effect of ion and water migration (as in “S” cases), compared to diffusion controlled processes only (as in “R” cases). Ion migration is logically expected to affect both pore network properties and passive layer formation. As can be seen in Figure 4.8, the Z' values in the HF EIS response (inlet in Figure 4.8) increase with time of conditioning for both R-24h and S-24h, indicating the increase of bulk matrix resistance due to the on-going cement hydration. For specimen S-24h, the magnitude of HF Z' is slightly higher than that for R-24h at the initial time

intervals of 7-28 days. In the meanwhile the LF responses of S-24h (at 7 and 28 days) reflect a more corrosion resistant steel surface, compared to R-24h. Both LF and HF responses before 28 days for specimens R-24h and S-24h are in line with the OCP and R_p values, where the more noble potential and higher R_p are recorded for S-24h. All these results suggest an intensified process of cement hydration and passive layer formation/stabilization of S-24h at earlier ages, if compared to the control condition (R-24h).

In contrast to the above performance, the responses of S-24h and R-24h change towards the end of the test, namely: the LF response for S-24h depicts a reduction of $|Z|$, which is well in line with the more cathodic OCP (Figure 4.3) and lower R_p (Figure 4.4) for the same time interval. Corrosion resistance of R-24 increases at the end of conditioning, reflected by the increasing $|Z|$ in the LF (Figure 4.7), the more noble OCP (Figure 4.3) and an increasing trend of the R_p (Figure 4.4). All these mean that the stray current (negative) effect is observed, but at already later stages for the group of 24h-cured specimens.

The experimental impedance responses for the 28d-cured specimens R-28d and S-28d can be seen in Figure 4.9. With regard to group R-28d, the curves reflect passivation of the steel reinforcement [414-416]. It can be noted that, the time constant (in the range of 4.2k-78.9 Hz, as marked in inset of Figure 4.9) is relevant for both R-28d and S-28d. In this frequency window the time constant reflects bulk matrix characteristics, showing a potentially higher portion of disconnected pore-network, hence a more resistive bulk matrix in both R-28d and S-28d, compared to the previously discussed 24h-cured groups (R-24h and S-24h).

Similar to the 24h-cured group, the EIS response for the 28d group depicts a negative effect of the stray current, predominant at the later stages. Although an improvement of the bulk matrix is also observed here (Figure 4.9), the magnitude of $|Z|$ in the LF for specimen S-28d is 2-time lower than that of R-28 at the end of the test. In other words, the effect of curing (group 28d vs group 24h) only results in a delay of the negative effect of stray current, rather than preventing it.

4.3.3 Competitive mechanisms of stray current and Cl^- at early age

In contrast to groups R-24h and S-24h, the EIS responses of groups C-24h and CS-24h (specimens cured for 24h, and then immersed in 5% NaCl solution) show clear evidence of active corrosion (see Figure 4.10). As already mentioned, the recorded R_p (derived from LPR) for C-24h is higher than that of R-24 at early age (period of 3-28 days, see Figure 4.4). This is also reflected by the EIS as shown in Figure 4.11: the LF $|Z|$ of C-24 (at intervals of 3d and 7d) is higher than R-24.

On the one hand the arrival of Cl^- at the steel surface needs time, as the penetration of Cl^- in mortar cover is hysteretic. In this penetration process of Cl^- , the acceleration of cement hydration is triggered in the meanwhile, resulting in a denser bulk matrix (chloride additions in ordinary Portland-cement materials increase the volume of finer pores, and decrease the fraction of coarse pores [405, 406, 417-419]). This denser bulk matrix in turn hinders further penetration of Cl^- . The denser bulk matrix of C-24h compared to R-24h can be verified by the HF response in Figure 4.11: the $|Z|$ values of C-24h of HF are higher than R-24 before 28 days, and an additional time constant (a depressed semi-circle) in the range of 1.05k-49 Hz can be observed in the EIS responses of C-24h-3d and C-24h-7d. This response is typical for a reinforced cement-based system in the presence of Cl^- , and signifies the effect of Cl^- on bulk matrix properties (densification in this case).

An additional effect related to specimen C-24h is the potentially lower $[Cl^-]/[OH^-]$ ratio at steel surface. At very early age in a fresh cement matrix, the OH^- concentration is relatively high, hence together with the low concentration of Cl^- at initial time intervals, a more stable product layer will form on the steel surface at early age. After 28 days, however, the passive layer breakdown of C-24h is already evident. This is reflected by the low R_p values derived from LPR (see Figure 4.4), and by the EIS response for group C-24h, where a semi-circle inclined to the real axis and a decreasing magnitude of $|Z|$ towards 215 days are recorded. The shape of this EIS response had been largely reported to be due to the presence of Cl^- on the steel surface and increasingly active corrosion state [420].

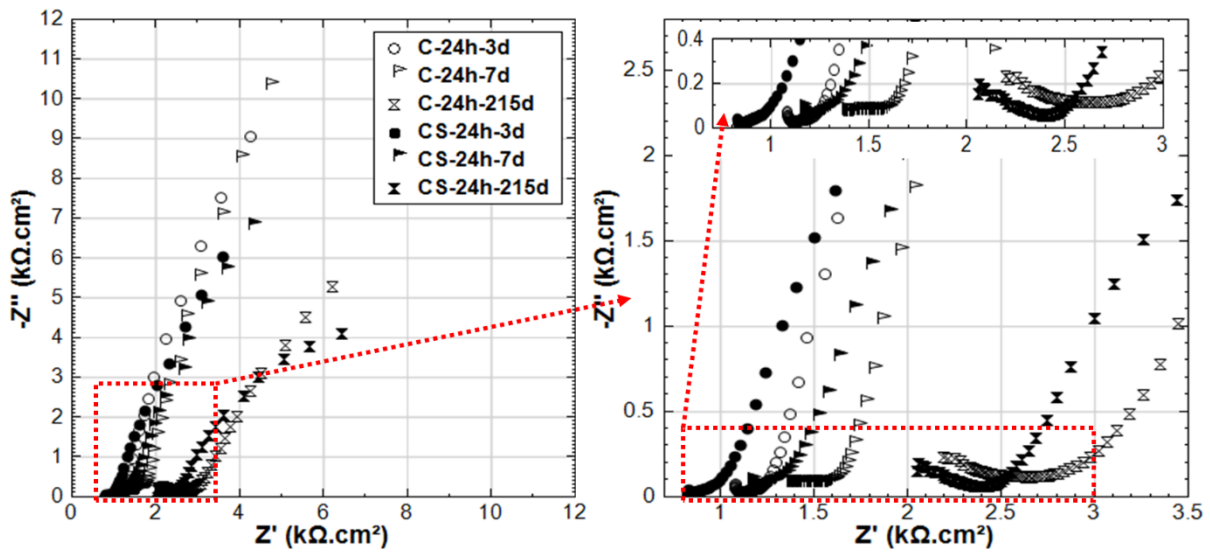


Figure 4.10: EIS responses overlay in Nyquist format of C-24h and CS-24h (C-24h: NaCl medium, CS-24h: NaCl + Stray Current, 24h-cured specimens treated in 5% NaCl).

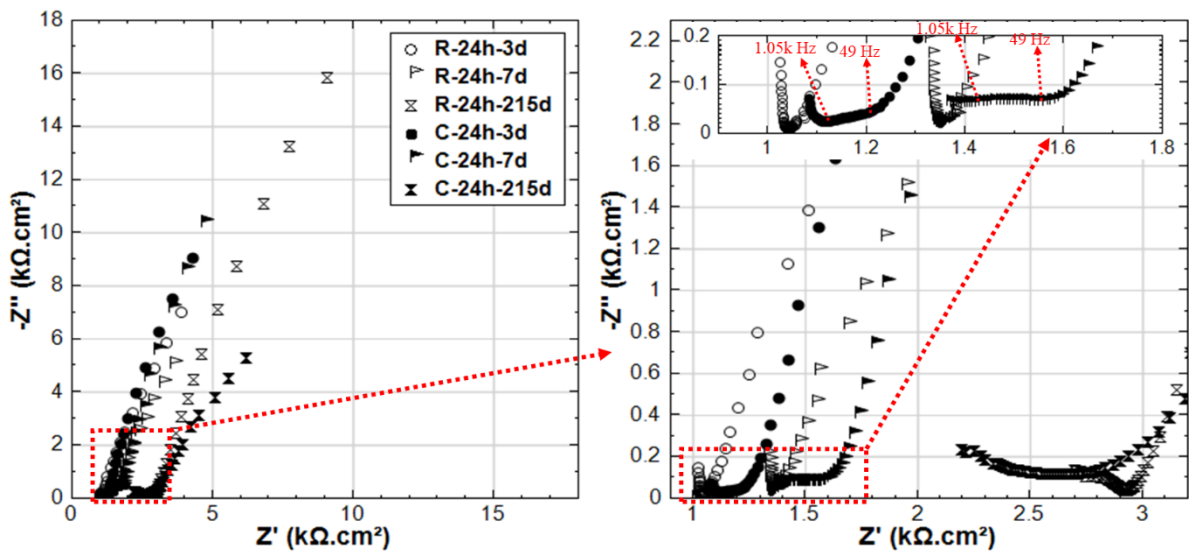


Figure 4.11: EIS responses overlay in Nyquist format of R-24h and C-24h (R-24h: Reference, 24h-cured specimens treated in water; C-24h: NaCl medium, 24h-cured specimens treated in 5% NaCl).

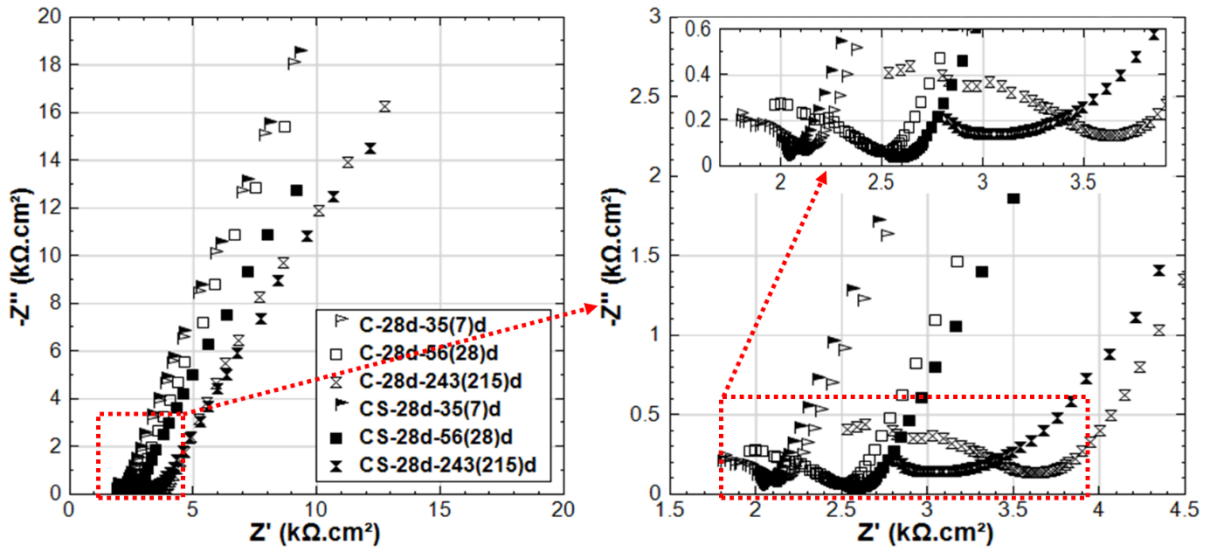


Figure 4.12: EIS responses overlay in Nyquist format of C-28d and CS-28d (C-28d: NaCl medium, CS-28d: NaCl + Stray Current, 28d-cured specimens treated in 5% NaCl).

Comparing the EIS response of C-24h and CS-24h (see Figure 4.10), and also in line with the LPR results, a more active state is recorded for CS-24h, reflected by the LF of EIS response at the end of conditioning. This is because of the synergetic effect of stray current and Cl^- , i.e., after prolonged conditioning of stray current, the more anodic zones are produced where the current leaves the steel surface. This, together with the Cl^- , leads to the lower corrosion resistance of CS-24h at the end of conditioning.

The more active state in CS-24h is accompanied by lower $|Z|$ values in the HF domain for CS-24h, compared to C-24h at all time intervals (Figure 4.10), meaning a lower resistance of the mortar bulk matrix for CS-24h. As already discussed, NaCl leads to acceleration of the hydration process, results in matrix densification (higher resistance). Cl^- and Na^+ ion migration is also accelerated by the potential gradient induced by stray current (as in CS-24h), hence, ions will migrate more easily, and the distribution of ions in the bulk matrix of CS-24h will be more uniform than the case without stray current (C-24h). Consequently the Cl^- ions will more easily reach the steel surface when stray current is involved, especially for the “fresh” bulk matrix with high porosity and more connected pore networks at early age.

As for C-28d and CS-28d (see Figure 4.12), much higher corrosion resistance compared to C-24h and CS-24h are observed. This reflects the curing effect: sufficient curing and hydration of the bulk matrix lead to a more resistive steel surface. At the age of 35 days (after 7 days of stray current supply), the EIS responses of C-28d and CS-28d are similar. In other words, the stray current effect is not significant yet at this stage. Even after 28 days of current supply, although the steel surface of CS-28d shows a slightly enhanced corrosion activity, the HF EIS responses of C-28d and CS-28d are still similar and in the same range of $|Z|$ values. This is in contrast to the previously discussed CS-24h, where only after 3-7 days of stray current supply, the stray current already played roles in both affecting the “fresh” bulk matrix and steel surface (Figure 4.10). At the end of test duration, the EIS response of CS-28d-243(215)d shows lower $|Z|$ and a more inclined to real axis response, compared to that of C-28d-243(215)d. This

indicates a higher corrosion activity in CS-28d after a prolonged supply of stray current, if compared to C-28d specimen, where only Cl⁻-induced corrosion plays a role.

According to above observations, a hypothesis about the stray current effect at early age can be proposed: the competitive mechanisms act in specimens CS-24h, where on the one hand the stray current has positive effects on bulk matrix properties, similar to specimen S-24h, at early stages. On the other hand, stray current accelerates Cl⁻ ion migration towards the steel surface, leading to Cl⁻-induced corrosion and active state of steel. It is also reported that stray current can accelerate the decomposition of the C-S-H gel, and a subsequent desorption of the physically adsorbed Cl⁻ by the C-S-H gel [49].

In the case of CS-24h, when the stray current was supplied at the age of 24h (1d) on the specimen immersed in 5% NaCl, stray current would immediately flow through the bulk matrix and polarize the steel (since steel is the low resistive path in the system). In contrast, Cl⁻ need to firstly penetrate into the mortar cover, before they reach the steel surface. This means that the effects of stray current are immediate, influencing both the steel surface and the bulk matrix (i.e., accelerating cement hydration). Both of these lead to product layer formation on the steel surface (compounds as $\text{Fe}_3\text{O}_4\cdot\text{FeO} + \text{Fe}_2\text{O}_3$, $\gamma\text{-FeOOH}$ or $\gamma\text{-Fe}_2\text{O}_3$ would form). This would be a positive effect of the stray current on steel-mortar interface at early age, which is in line with the OCP and LPR (R_p) results as already discussed in Section 4.3.3.1. The product layer would remain stable before Cl⁻ ions arrive at the steel surface and exceed the threshold value of Cl⁻ concentration towards de-passivation (a transformation from passive layer to $3\text{Fe}(\text{OH})_2\cdot\text{FeCl}_2$ due to Cl⁻).

For specimen CS-28d, the penetration of Cl⁻ into the bulk matrix will be delayed due to the well cured mortar cover (higher resistance, lower porosity, and lower connectivity of pore network of bulk matrix). The denser matrix in CS-28d is evident from the higher HF |Z| (Figure 4.12), compared to that of CS-24h (Figure 4.10) at all time intervals. After curing of 28 days, a more resistive product layer (compared to CS-24h) has also been formed on steel surface of CS-28d (seen by the LF response of EIS, where the LF |Z| values of CS-28d are higher than CS-24h). In this situation (CS-28d) the stray current effect is less significant on both the bulk matrix and the steel surface. Yet, after prolonged conditioning, the stray current still takes effect on the well cured bulk matrix. As can be seen in Figure 4.12, the HF |Z| of CS-28d is lower than C-28d at age of 243 days. Compared to C-28d, the steel surface of CS-28d is more active at 243 days (see Figure 4.12, the LF response of EIS reflect this), indicating that stray current accelerates steel corrosion after prolonged conditioning.

4.3.4 EIS response indicating difference between stray current and anodic polarization

The aim of this section is to clarify the different effects of stray current and anodic polarization, on specimens after 24h curing (fresh bulk matrix) or 28d curing (already hardened bulk matrix), in Cl-free or Cl-containing environment. To illustrate the different behavior of the rebar (by the EIS LF response) and mortar cover (by the EIS HF range) induced by stray current and anodic polarization, the overlays of relevant EIS response are shown in Figures 4.13-4.18.

The comparison of EIS responses of S-24h and A-24h is shown in Figure 4.13. For the response of specimen A-24h, an actively corroding steel surface is already seen at 7 days of age. This behavior is in line with the cathodic OCP values for group A-24h (Figure 4.3) at the initial stage of the test (approx. -590 mV at 3 days, -320 mV at 7 days), as well as with the LPR-derived R_p values (Figure 4.4) of A-24h.

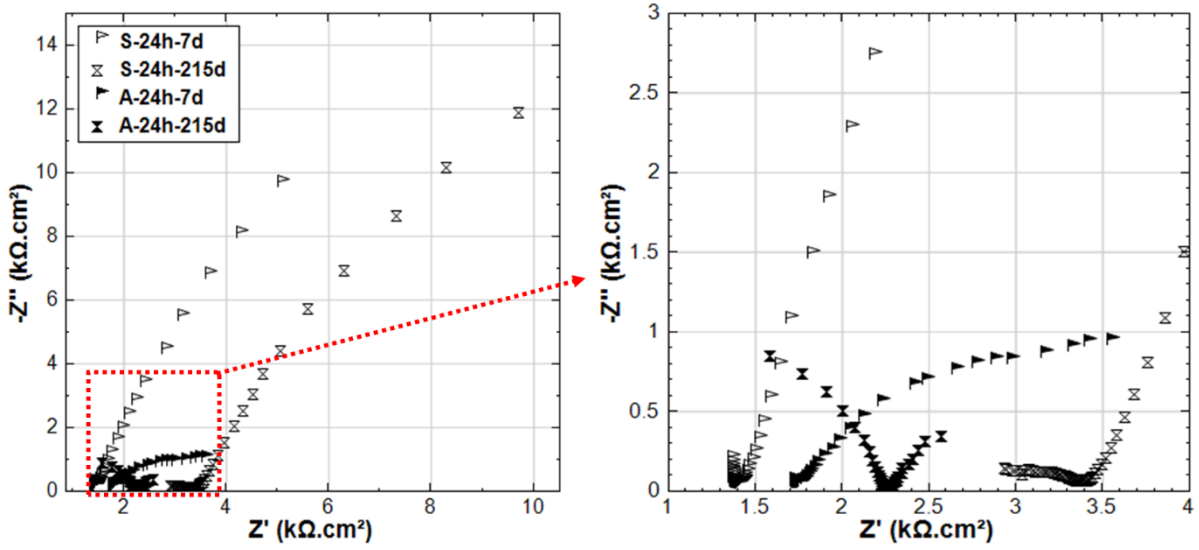


Figure 4.13: EIS responses overlay in Nyquist format of S-24h and A-24h (S-24h: Stray Current, A-24h: Anodic Polarization, 24h-cured specimens treated in water) at age of 7d and 215d.

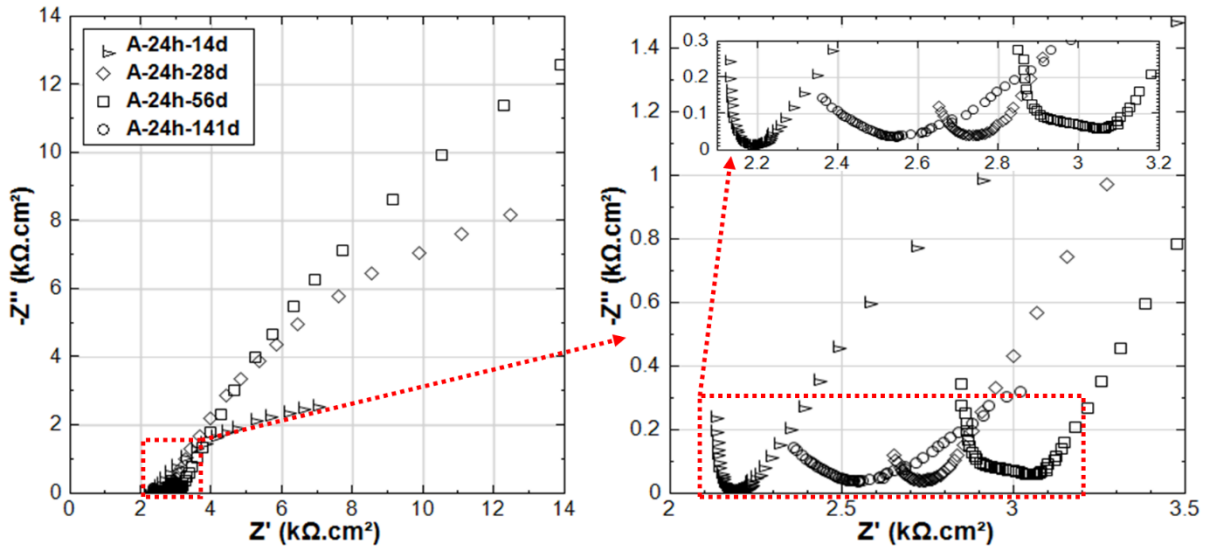


Figure 4.14: Overlay of EIS responses of A-24h in Nyquist format, at age of 14, 28, 56 and 141 days.

The more noble OCP values (Figure 4.3) recorded for A-24h before 56 days of age, together with the increased R_p before 141 days (Figure 4.4), are probably due to the specific product layer formation and compaction in conditions of anodic polarization [421, 422]. This is also supported by the EIS response of A-24h (see Figure 4.14): after active state at 14 days, seen from the LF response, an enhanced corrosion resistance is observed at the stages of 28 and 56 days (increasing of $|Z|$ with prolonged conditioning). Well known is that with anodic polarization, in the absence of corrosives (as Cl^-) and in alkaline medium (pH of 12.5-12.9, for concrete pore solution), a product layer will be forced to form (according to thermodynamical principles as reflected by the Pourbaix diagram of Fe- H_2O system [421]), i.e., with constant anodic current the electrode potential will gradually rise towards a stable value [423-425]. A

transformation to a more active state, together with a drop in bulk matrix resistance is recorded later on after the stage of 141 days. This is ascribed to the anodic polarization-induced crack, by expansion of corrosion product layer on steel surface of A-24h (see Figure B.5 in Appendix B). The reduction of R_p for A-24h (see Figure 4.4), together with a significant cathodic drop of OCP (Figure 4.3), account for an active state of A-24h at the end of the test. In contrast, such a significant corrosion activity is not observed for S-24h.

The above behavior is more significant for 24h curing situation, i.e., A-24h, compared to A-28d (see Figure 4.15). As shown in Figure 4.15a, a clear difference in HF and LF of A-24h and A-28d can be observed in all time intervals. This can be attributed to the sufficient and timely OH^- supply of A-24h, because of hydration process of cement at early age. In the “fresh” matrix, the migration of OH^- (towards steel surface) affected by the electrical field is enhanced. In the meanwhile, the Fe^{2+} is continuously produced by the supplied anodic current, consequently more corrosion products are formed at the steel-mortar interface. The above processes are not significant for the already hardened bulk matrix of A-28d at later age.

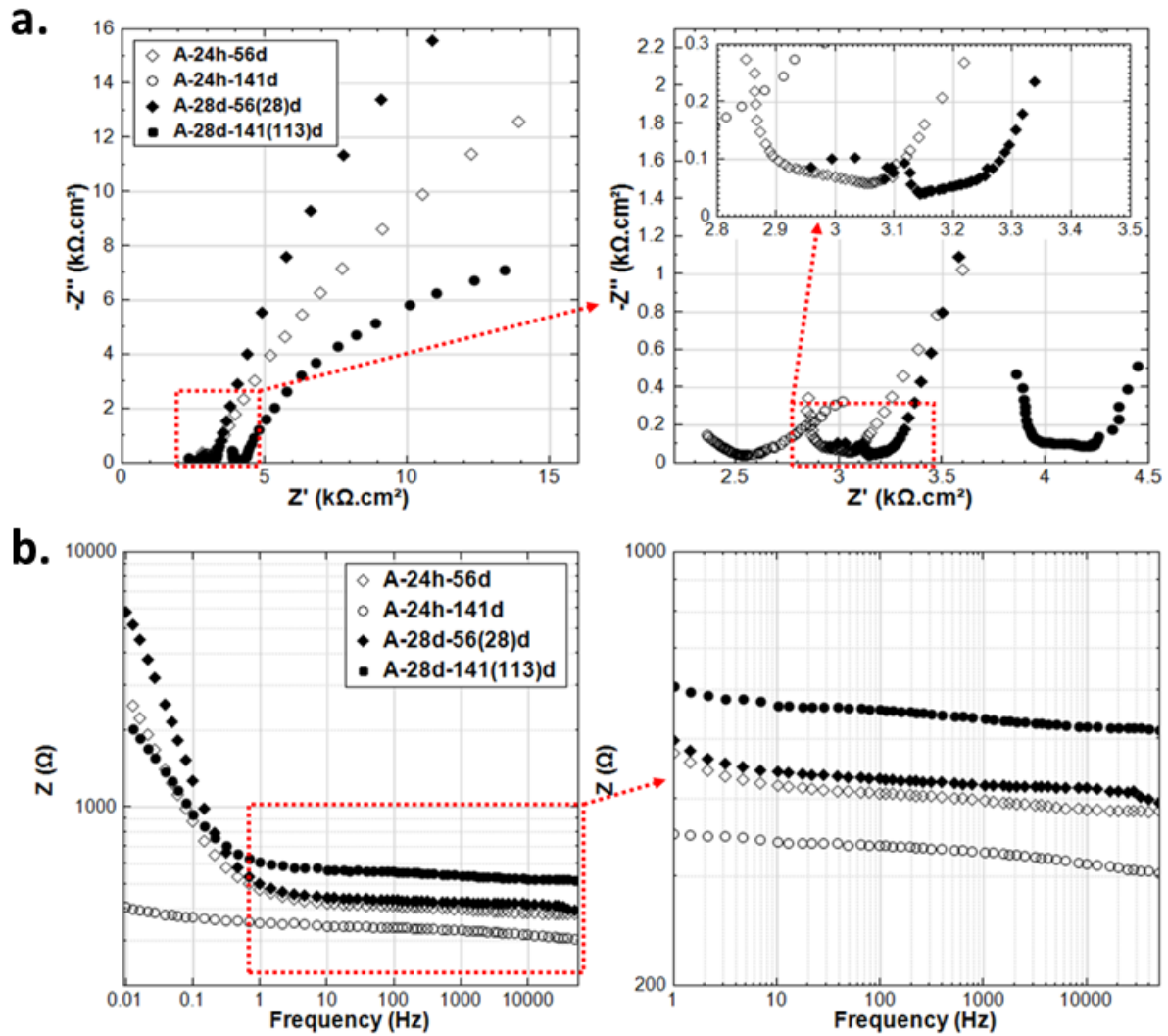


Figure 4.15: Overlay of EIS response of A-24h and A-28d in: a). Nyquist format; and b). Bode format; at age of 56 and 141 days.

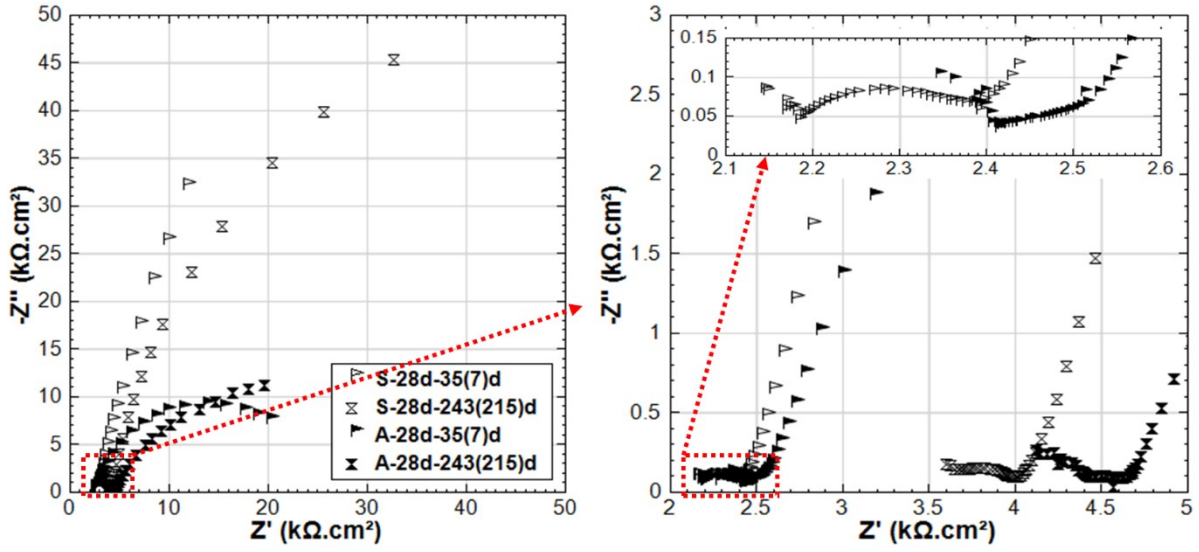


Figure 4.16: EIS responses overlay in Nyquist format of S-28d and A-28d (S-28d: Stray Current, A-28d: Anodic Polarization, 28d-cured specimens treated in water) at age of 35(7)d and 243(215)d.

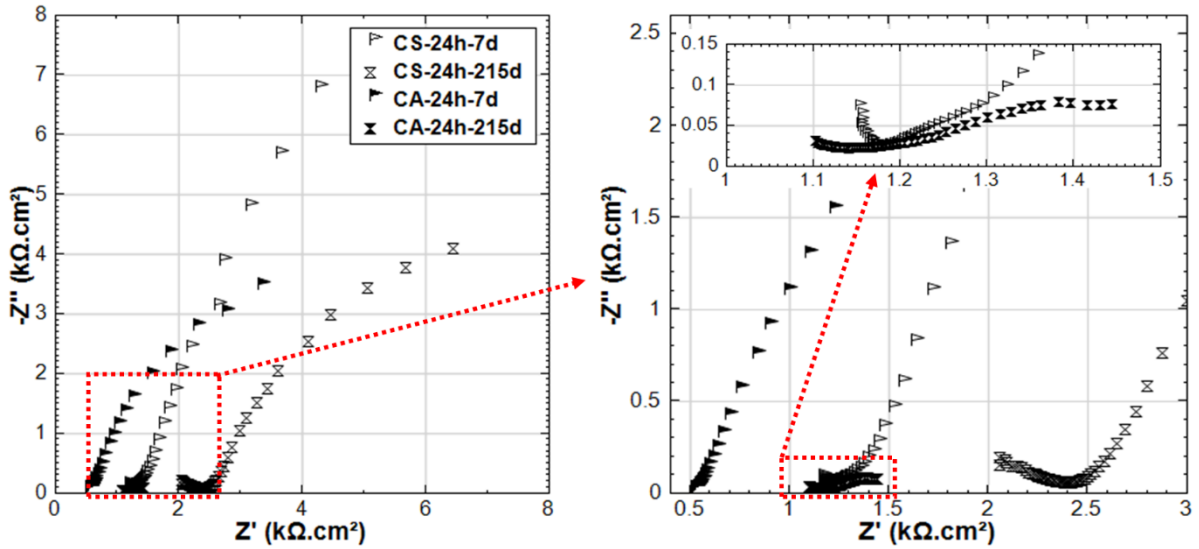


Figure 4.17: EIS responses overlay in Nyquist format of CS-24h and CA-24h (CS-24h: NaCl + Stray Current, CA-24h: NaCl + Anodic Polarization, 24h-cured specimens treated in 5% NaCl) at age of 7d and 215d.

As for A-28d, the evident semi-circle of EIS plots (Figure 4.16) is already recorded at 35 days of age (after 7 days conditioning). The EIS response in the LF domain inclines to the x-axis, indicates an active steel surface. This response again confirms that anodic polarization induces corrosion for reinforcing steel. Comparing the EIS response of S-28d and A-28d (standard curing for 28 days), a more significant corrosion behavior is recorded for A-28d. This is supported by the OCP and R_p (from LPR) values, as shown in Figure 4.5 and 4.6. A capacitive arc (in MF range) is observed for A-28d at 215 days, meaning a potentially improved resistance of the interface, which can also be reflected by the higher $|Z|$ of A-28d at 215d. This may be

attributed to the expansion of corrosion product at steel-mortar interface, and altered steel-mortar interface of A-28d. More details will be further discussed together with potential decay recording in Section 4.3.5.

For the response of the CA groups (NaCl + anodic polarization), CA-24h shows a more significant corrosion activity than CS-24h (NaCl + stray current). At 215 days, a significant drop of impedance and phase angle is recorded for CA-24h (Figure 4.17). This response indicates the synergetic action of two degradation factors, i.e. anodic polarization and Cl^- in the environment, resulting in significantly low corrosion resistance. For this CA-24h case, the EIS response is well supported by the recorded cathodic OCP values and extremely low R_p values (Figure 4.3 and 4.4).

A more active behavior is recorded for group CA-24h, compared to CA-28d. At the end of conditioning, the EIS response of CA-28d shows a more significant corrosion of steel than A-28d and CS-28d. This again, implies the coupling effects of anodic polarization and Cl^- on accelerating corrosion of steel.

For both 24h curing and 28d curing conditions, a more pronounced corrosion is observed for the CA groups (NaCl + anodic polarization, specimens CA-24h and CA-28d), compared to the stray current groups (NaCl + stray current, CS-24h and CS-28d). Visible/macro cracks induced by corrosion are observed for both CA-24h and CA-28d (see Figure B.6, Appendix B). Once cracks are induced, the bulk matrix resistance (in 5% NaCl solution) will decrease, as the water and ions will penetrate into the bulk matrix via cracks. In Cl-containing alkaline environment, a stable passive layer cannot form on the steel surface, although the anodic current was applied continuously. In this situation, Cl-containing iron oxides and hydroxides form on steel surface, because of Cl^- ingress [420]. In addition, the anodic current applied to the steel rebar accelerates Cl^- ion migration towards the steel-mortar interface (Figure 4.1a). This synergy of anodic polarization and Cl^- significantly accelerates the corrosion propagation.

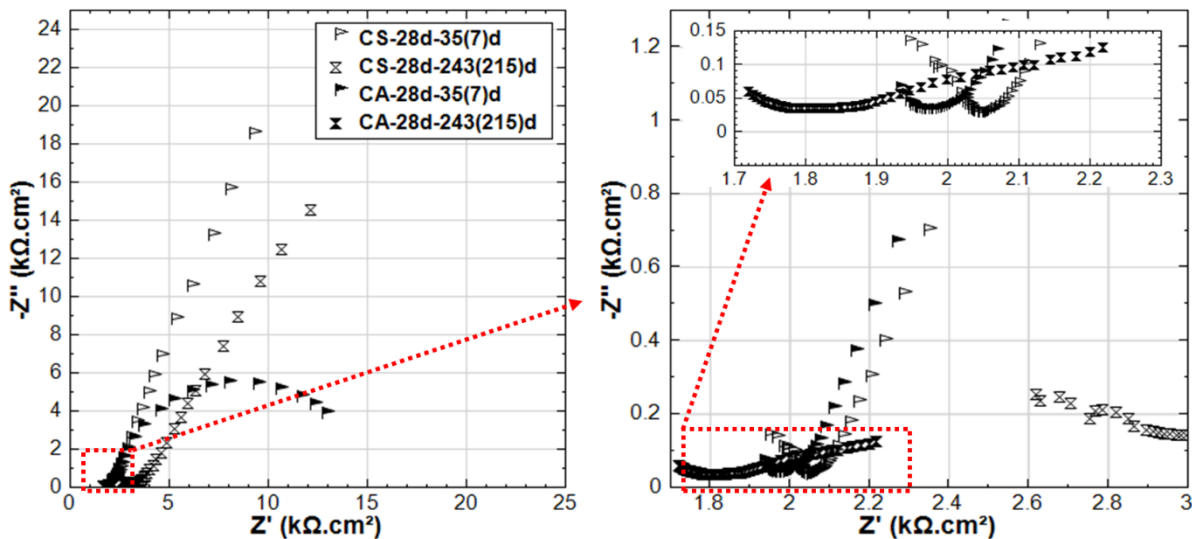


Figure 4.18: EIS responses overlay in Nyquist format of CS-28d and CA-28d (CS-28d: NaCl + Stray Current, CA-28d: NaCl + Anodic Polarization, 28d-cured specimens treated in 5% NaCl) at age of 35(7)d and 243(215)d.

In contrast, the synergy of stray current and Cl^- causes different effects (Figure 4.1b). Stray current leads to the formation of anodic zones (corroding areas) where the current leaves the steel surface. In other words only part of steel surface can be corroded by the stray current, while in conditions of anodic polarization, the whole steel surface acts as an anode.

Overall, stray current and anodic polarization exert significantly different effects on the corrosion behavior of steel and the surrounding mortar matrix, in both 24h-cured and 28d-cured specimens. Regardless of whether there is Cl^- in the external environments, anodic polarization leads to more pronounced effects on corrosion behavior than stray current. Hence anodic polarization cannot reflect the effects of stray current, and should not be adopted to simulate stray current.

4.3.5 Potential decay monitoring over 24 hours

Stray current leads to both cathodic and anodic polarization on the steel surface. The shift of the overall (mixed) potential, induced by stray current flow, can be adopted as an indicator of the presence of stray current [16, 426].

As aforementioned, for the specimens undergoing stray current or anodic polarization, a 24-hour potential decay measurement was performed and recorded prior to any further electrochemical tests. The reason for the decay tests is to verify:

- (1) if the steel rebars were indeed affected by stray current (or anodic polarization, respectively); in other words, a change of potential in “ON” and “OFF” conditions, compared to rest conditions, will indicate polarization of the reinforcement due to current application;
- (2) if an OCP stability would be achieved in rest conditions (when no external electrical field was applied), in the required time for the polarized system. This waiting time reflects the limitation of ion transport, diffusion, or limitation of electron transport along the steel surface, which are also related to the amount/thickness, heterogeneity and composition of the product layer on steel surface.

Figure 4.19 depicts the 24h potential decay results at the hydration age of 95 days. The very first recorded values (at the start of the curves and in the range of first 100 seconds) are the “ON-potentials”, as adopted due to anodic polarization or stray current, respectively (Figure 4.19c). At the moment of switching off the current supply, the potential drop reflects the contribution of the so-called “IR drop”. After a certain decay and towards the 24h time interval, the potentials of all specimens are stable (see Figure 4.19a).

The IR drop is the product of current (I) passing through resistance (with value of R) between the working electrode (the steel rebar) and the reference electrode (SCE). The “R” value is governed by the resistivity of the mortar matrix and the electrolyte (water or 5% NaCl in this case) surrounding the working electrode. The former is more significant and will depend on bulk matrix properties, hence will be different for the 24h and 28d-cured specimens. The latter (electrolyte resistance) is negligible in this set-up. After the IR drop, the potential decay reflects the relaxation of the system, from the previous state of being under stray current or anodic polarization (“ON” conditions) towards the stability in “rest” conditions (“OFF” conditions).

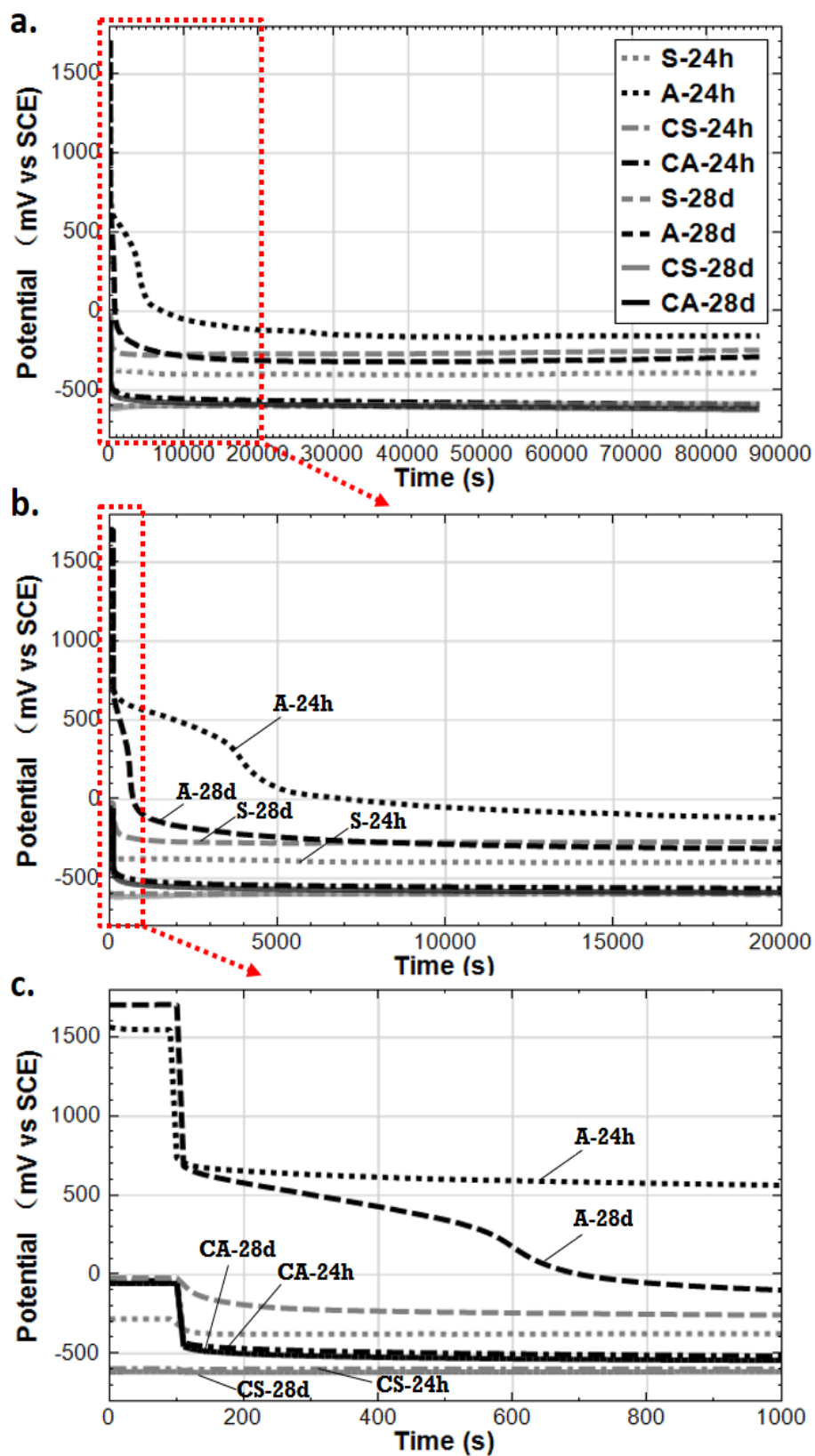


Figure 4.19: Potential decay monitoring over 24h de-polarization process.

As can be seen in Figure 4.19c, the IR drop for the anodic polarization cases (A-24h and A-28d) are the most pronounced. A higher IR drop is recorded for A-28d, if compared to A-24h (the IR drops for A-24h and A-28d are about 800mV and 1000 mV, respectively). The higher IR drop for A-28d reflects the higher resistance of the bulk matrix than A-24h. The higher resistivity of cement-based matrix partly indicates the higher hydration degree (maturity of concrete matrix) and denser bulk, which is as expected for specimen A-28d. This is in accordance with the EIS response at HF domain of A-24h and A-28d. As shown in Figure 4.15, the real component of impedance Z' in the HF range, reflecting the resistance of the bulk matrix, is lower for A-24h compared to that of A-28d, at both 56 and 141 days.

For A-24h and A-28d, it is clear that longer time is needed for establishing an equilibrium condition at the steel-mortar interface of A-24h and A-28d (Figure 4.19b). This reflects limitations of ion transport at the steel-mortar interface. In other words, at age of 95 days a stable steel surface in this environment (mortar pore solution without Cl^- , alkaline medium, pH of 12.5-12.9) was formed, due to the anodic polarization. It can be seen that the “instant-off potentials” of A-24h and A-28d are about 700 mV (vs SCE). These “instant-off potentials” are the potential of steel after the disappearance of IR drop (i.e., instantaneously after the cutting-off of the current). In an alkaline environment and at anodic potentials higher than +300 mV (vs SCE), a passive film formed at the steel surface [422]. By anodic polarization of iron, Fe(III) may be formed directly on the electrode surface as Fe_2O_3 , as mixed iron oxide Fe_3O_4 or as FeOOH [427-432].

A longer time is needed for establishing an equilibrium condition at the steel-mortar interface of A-24h, compared to A-28d. This means that a thicker corrosion product layer was formed in A-24h. As aforementioned, this is attributed to the enrichment of Fe^{2+} produced by anodic polarization at very early age (just at age of 1 day) at steel-mortar interface. In the meanwhile, sufficient and timely OH^- supply in a “fresh” matrix at early age, enhances the migration of OH^- to the steel surface in condition of the present electrical field. After this, the continuous supply of anodic polarization leads to the higher $\text{Fe}^{3+}/\text{Fe}^{2+}$ ratio in the passive film, further enhances the stability of the product layer on the steel surface in A-24h [427-435], until age of 95 days when the potential decay was performed. This is in line with the OCP values and R_p (derived from LPR) of A-24h: noble OCP values are recorded for A-24h before 56 days of age, together with the increasing trend of R_p before 141 days, showing the product layer formation and stabilization process.

For S-24h and S-28d undergoing stray current interference, “instant-off potential” values are much lower (-300 mV for S-24h, 0 mV for S-28d) than those of A-24h and A-28d. Only around 100 mV of IR drop is monitored for S-24h and S-28d. Considering that the resistance (R component of IR) between steel (working electrode) and reference electrode (SCE) is similar, the IR drop difference is mainly attributed to the difference of “I” (current flowing from steel surface to reference electrode). The much lower IR drop of S-24h and S-28d denotes the significantly lower current level flowing into the steel, comparing to the anodic polarization cases (A-24h and A-28d).

Higher than 400 mV of IR drop is recorded for CA-24h and CA-28d. However for CS-24h and CA-28d, no evident IR drop can be identified. It can also be found that the IR drop in Cl^- -containing cases is much lower than that of Cl^- -free specimens. This is due to the reduced resistance, in the external environment of 5% NaCl solution. All these results again denote the

different effects of stray current and anodic polarization, in both Cl-free and Cl-containing environments.

4.4 Conclusions

In this chapter, the effects of stray current on corrosion of reinforcing steel embedded in mortar are studied, in view of electrochemical behavior, in both 24h-curing and 28d-curing regimes. The comparison between stray current and anodic polarization is conducted in Cl-free and Cl-containing conditions. From the experimental results, the following conclusions can be drawn:

1. Stray current and anodic polarization exert significantly different effects on corrosion behavior of steel embedded in mortar, in both 24h curing (the samples are cured in fog room for only 24 hours) and 28d curing (samples are cured in fog room for 28 days) regimes. Anodic polarization simulating stray current means the absence of cathodic polarization, and different corrosion mechanisms. Consequently, anodic polarization cannot reflect the effects of stray current, and therefore it has limited significance for simulating stray current.
2. The curing regimes and starting time of stray current (i.e., the stray current supply starts at age of 24h or 28d) play significant roles in the formation of a corrosion product layer on the steel surface. At very early age, water transport, leaching-out effects, ion migration governed by electrical field are more evident, because of high porosity and pore network connectivity of a fresh bulk. The hydration process and pore network characteristics are influenced by the foregoing factors, and further affect the stability of the corrosion product layer.
3. In Cl-free (conditioned in water) situation, stray current flowing through the fresh (non-mature) bulk matrix, may lead to enhanced migration of water and ions. In this case the cement hydration and steel surface passivation can be enhanced. However, this phenomenon is not evident for the condition of sufficiently cured bulk matrix, as the bulk matrix is already hardened when the stray current is supplied. This also means that the properties of the cementitious material in reinforced cement-based system are of significant importance, and largely determine the electrochemical state of the steel rebar.
4. At early age, competitive mechanisms act in specimen CS-24h (Cl^- + stray current, cured in fog room for only 24 hours). On the one hand the stray current has positive effects: stray current flow through a fresh (non-mature) cement matrix leads to enhanced water and ion transport due to migration. The results are enhanced cement hydration, and consequently a more rapid stabilization of pore solution and steel-mortar interface. On the other hand, stray current enhances Cl^- ion migration, and accelerates Cl-induced corrosion.

Chapter 5

Bond of steel-mortar interface interfered by stray current and anodic polarization

5.1 Introduction

Corrosion of reinforcing steel does not only lead to poor appearance of reinforced concrete (possible cracking, spalling or delamination), but also compromises structural integrity and serviceability [436]. For buried metallic structures (pipelines, underground reinforced concrete structures, etc.), stray current-induced corrosion is one of the most severe forms of damage [437-441]. This is because the matrix (soil and concrete cover) surrounding the metal can offer a conductive path for the stray current.

Once corrosion of reinforcement starts, corrosion products form, (re)precipitate and gradually increase in volume, hence, occupy a larger volume than the parent metal. The volume expansion of corrosion products may firstly induce higher radial pressure (normal stress) between the steel surface and the concrete (mortar) cover. This leads to an initially higher bond strength and induces splitting stress on the concrete (mortar) cover. Once the splitting stress exceeds the concrete (mortar) tensile strength, the cracks appear gradually on the concrete (mortar) cover. The ultimate consequence of corrosion is the loss of bond between the steel and the surrounding concrete [442, 443].

The bond strength of the steel-concrete interface is an important structural property for reinforced concrete structures. The stress transfer between the steel surface and the concrete cover via this bond “combines” the concrete and the reinforcement [444, 445]. The bond between ribbed bars and concrete is made up of three components: (1) chemical adhesion; (2) friction; and (3) mechanical interlocking between ribs of bars [388, 389, 398, 445-459]. The adhesion, friction and interlocking components of transferred forces for a deformed (ribbed) rebar are illustrated in Figure 5.1.

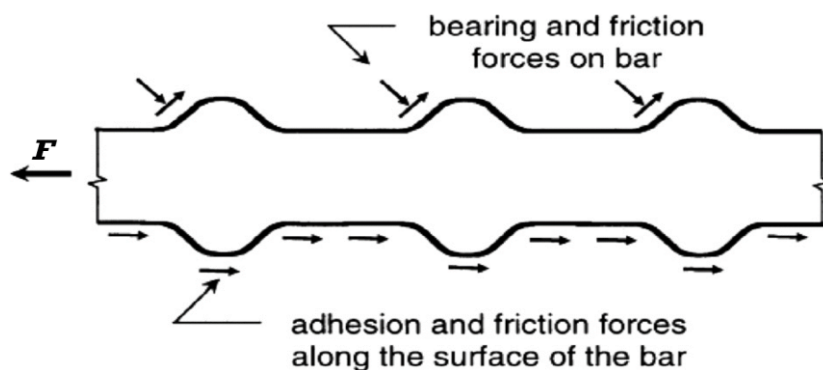


Figure 5.1: Bond force transfer mechanism [460].

The bond determines the crack width and crack spacing of a reinforced concrete elements bearing loads (beams burdening moments for instance). In other words, it determines the load bearing capacity of these elements. Bond degradation induced by corrosion leads to wider crack width and enhances the penetration of corrosive substances, in turn accelerates the corrosion of the embedded steel. This cycle significantly reduces the durability and service life of reinforced concrete structures.

The bond behavior of steel-concrete/mortar interface, affected by steel corrosion, has been extensively studied in the past, where various studies report different aspects [28, 58-65, 183, 461]. Very few investigations, however, report on the influence of stray current on bond of steel-concrete/mortar interface. Furthermore, the current state-of-the-art generally adopts anodic polarization to simulate stray current [28, 58, 59], rather than stray current application.

As already discussed in Chapters 2 and 4, stray current induces both anodic polarization and cathodic polarization on the steel surface, hence, the distribution and effect of stray current are more complex than only anodic polarization. Moreover, Chapter 4 presented the variation in both corrosion state of the steel rebar, as well as alterations in the electrical properties (impedance) of the bulk matrix and interfaces, due to (separately evaluated) stray current and anodic polarization, justifying that anodic polarization cannot be considered as stray current and vice versa.

This chapter presents test results on the bond strength of reinforced mortar undergoing stray current and anodic polarization, conditioned in Cl-free (in water) and Cl-containing (in 5% NaCl solution) medium. The bond behavior of the steel-mortar interface, derived by pull-out tests, is correlated to the electrochemical response of the reinforcing steel and the bulk matrix properties evaluated by Electrochemical Impedance Spectroscopy (EIS). The effect of stray current on bond strength is discussed versus the effect of anodic polarization. The effects of the curing regimes (in terms of duration of curing) and starting point of stray currents (e.g. stray current applied at 24h or 28d) are also considered, by testing both 24h and 28d-cured specimens of identical geometry and environmental conditions. It was found that stray current (level of 0.3 mA/cm^2) exerts bond strength degradation in all cases, irrespective of the presence or absence of a corroder (Cl^-) in the external medium.

5.2 Experimental

5.2.1 Materials and specimen preparation

A presentation of the test specimens (reinforced mortar prisms of $40 \times 40 \times 160 \text{ mm}^3$) and the setup for current supply (stray current or anodic polarization) were previously presented and can be seen in Figure 4.2. The mortar mixture and embedded steel rebar are identical to those discussed in Chapter 4. The alignment of the bars was carefully fixed prior to the casting. The fabrication procedure of moulds and specimens is illustrated in Figure 5.2. In order to produce non-contact areas between the bar and the mortar at each end of the specimen, the two ends of the bar were covered by a heat-shrinkable tube (blue parts in Figure 4.2) and 60-mm-long bond breakers (i.e., PVC tubes, see Figure 5.2). These de-bonding zones were used to protect the reinforcement from the confining pressure of mortar at the supports, and to reduce the arching effects and end restraints [457, 462] during the pull-out tests. The specimens were prepared with a relatively short embedded length (40 mm) of steel rebar, to achieve a relatively uniform bond stress distribution during the pull-out test [456, 463].

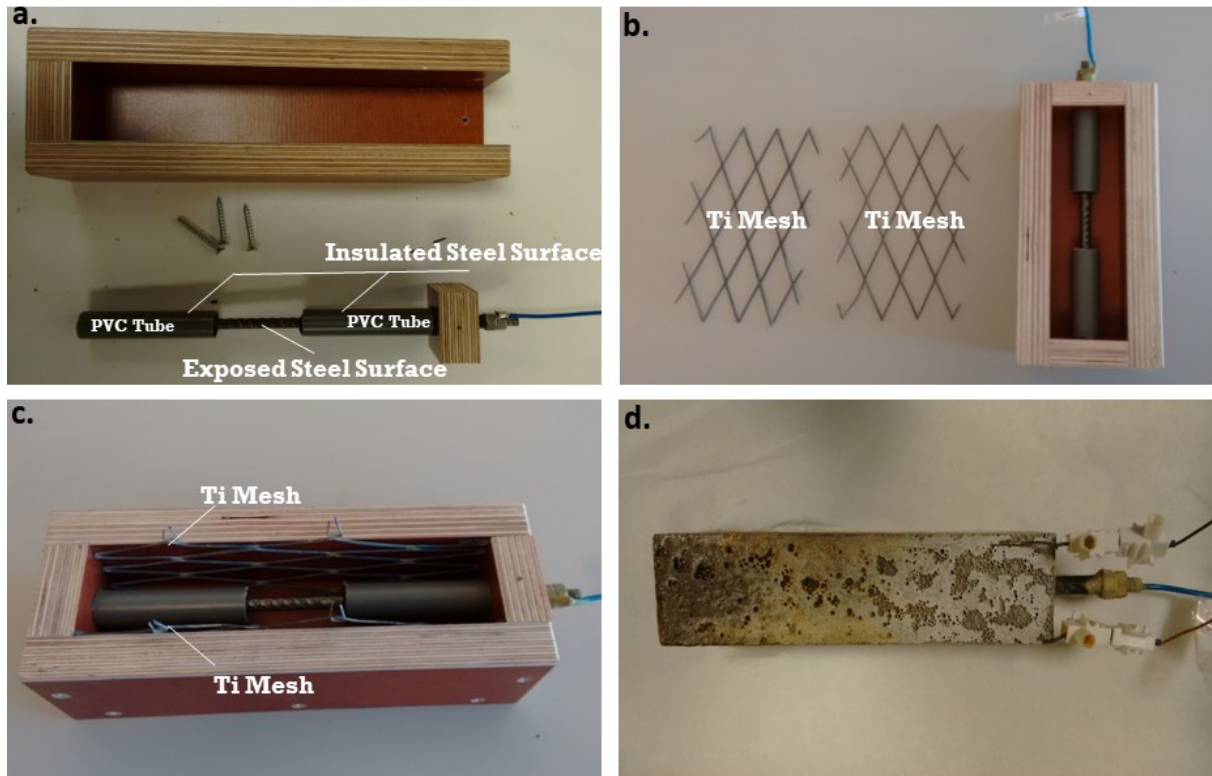


Figure 5.2: Pictures of moulds and specimens fabrication.

5.2.2 Curing and conditioning

The curing (in a fog room with 98% RH, 20 °C) and conditioning regimes, and designations for all specimens are summarized in Table 5.1 and Table 5.2. The treatment of the specimens (after curing) and the set-ups for current supply in this chapter include 2 phases:

Table 5.1*: Summary of curing and conditioning regimes for 24h-cured specimens.

Group \ Age	0-1 d	1-215 d				215-490 d	
	Curing	Immersion (2/3 rd)		Electrical Field		Immersion (full)	
		Water	5% NaCl	Stray Current (0.3 mA/cm ²)	Anodic Polarization (0.3 mA/cm ²)	Water	5% NaCl
R-24h	24h	✓				✓	
C-24h			✓				✓
S-24h		✓		✓		✓	
CS-24h			✓	✓			✓
A-24h		✓			✓	✓	
CA-24h			✓		✓		✓

* R-24h: Reference; C-24h: Corroding (NaCl medium); S-24h: Stray Current; CS-24h: Corroding (NaCl) + Stray Current; A-24h: Anodic Polarization; CA-24h: Corroding (NaCl) + Anodic Polarization – after 24h curing in fog room.

Table 5.2*: Summary of curing and conditioning regimes for 28d-cured specimens.

Age Group	0-28 d	28-243 d				243-490 d	
	Curing	Immersion (2/3 rd)		Electrical Field		Immersion (full)	
		Water	5% NaCl	Stray Current (0.3 mA/cm ²)	Anodic Polarization (0.3 mA/cm ²)	Water	5% NaCl
R-28d	28d	✓				✓	
C-28d			✓				✓
S-28d		✓		✓		✓	
CS-28d			✓	✓			✓
A-28d		✓			✓	✓	
CA-28d			✓		✓		✓

* R-28d: Reference; C-28d: Corroding (NaCl medium); S-28d: Stray Current; CS-28d: Corroding (NaCl) + Stray Current; A-28d: Anodic Polarization; CA-28d: Corroding (NaCl) + Anodic Polarization – after 28d curing in fog room.

Phase 1 - 2/3rd of the specimens' height immersion in water or 5% NaCl for 215 days for the 24h group (243 days for the 28d group). The details and schematic for the conditions in Phase 1 can be seen in Chapter 4.

Phase 2 - Full immersion of the specimens in the same medium as Phase 1, but prolonged after 215 days onwards and until the end of the test of 490 days.

5.2.3 Testing Methods

5.2.3.1 Electrochemical measurements

Electrochemical tests, including Linear Polarization Resistance (LPR), Electrochemical Impedance Spectroscopy (EIS) and Potentio-Dynamic Polarization (PDP) were conducted at Open Circuit Potential (OCP) for all specimens at 490 days of age. An external Saturated Calomel Electrode (SCE) was used as reference electrode. The counter electrode was the initially embedded MMO Ti mesh (Figure 5.2c). Prior to and during the electrochemical tests the specimens were immersed fully in the relevant aqueous medium for 24h. The procedures for LPR tests are identical to those described in Chapter 4, whereas a different EIS protocol was applied in this Chapter 5. In order to account for a more accurate assessment of the bulk matrix characteristics, the EIS tests here were conducted in the maximum frequency range (i.e., 1MHz-10mHz) can be supported by the instrument, by superimposing an AC voltage of 10mV (rms).

The bond strength of steel-concrete interface depends on the: diameter of steel rebar, reinforcement shape, geometry of ribbed bar and the position of the rebar during casting, etc [444, 446, 447, 449-452]. These factors are the same for all specimens in this work. In addition to the steel corrosion state, another variable related to bond behavior is the mortar cover properties (modified porosity, pore interconnectivity, or micromechanics of the bulk matrix). The mortar cover (as depth) was also identical for the tested specimens. Consequently, the factor that could affect the bond strength differently per case and condition, would be the variation in bulk matrix properties. In this chapter EIS was performed in the full (instrument-determining) frequency range (as abovementioned - of 1 MHz to 10 mHz), to offer information for both the property of the bulk matrix and the electrochemical response of the embedded steel.

In order to collect additional information of the electrochemical state of the steel surface, PDP was finally performed in the range of -0.15 V to +0.90 V (vs OCP) at a scan rate of 0.5 mV/s. The properties of both bulk matrix and steel surface obtained by electrochemical measurements will be correlated to the bond behavior.

5.2.3.2 Pull-out test

After the electrochemical tests, pull-out tests were performed on all specimens. The pull-out test set-up followed the specification of ASTM C-234-91a [464] and was performed with a stiff test frame (647 Hydraulic Wedge Grip, MTS Systems Corporation) at loading rate of 0.01 mm/s under displacement control. A steel frame connected to the testing machine was designed and fabricated, to accommodate the specimens on the top of a bearing plate. The test machine and setup for pull-out tests are illustrated in Figure 5.3.

The load-slip curve (relationship) was recorded. The applied load (F) was measured with the help of a force sensor, whose signal was fed to an automatic data acquisition system. The loaded-end slip was measured with the help of 2 LVDTs, output of which is an average value of these 2 LVDTs. Bond stress (τ) was obtained according to: $\tau = F / \pi dl$ ($d = 6$ mm of diameter of rebar, $l = 40$ mm of exposed length of rebar, $F =$ recorded pull-out force), i.e., the pull-out force was divided by the corresponding embedded area of steel to obtain the bond stress.

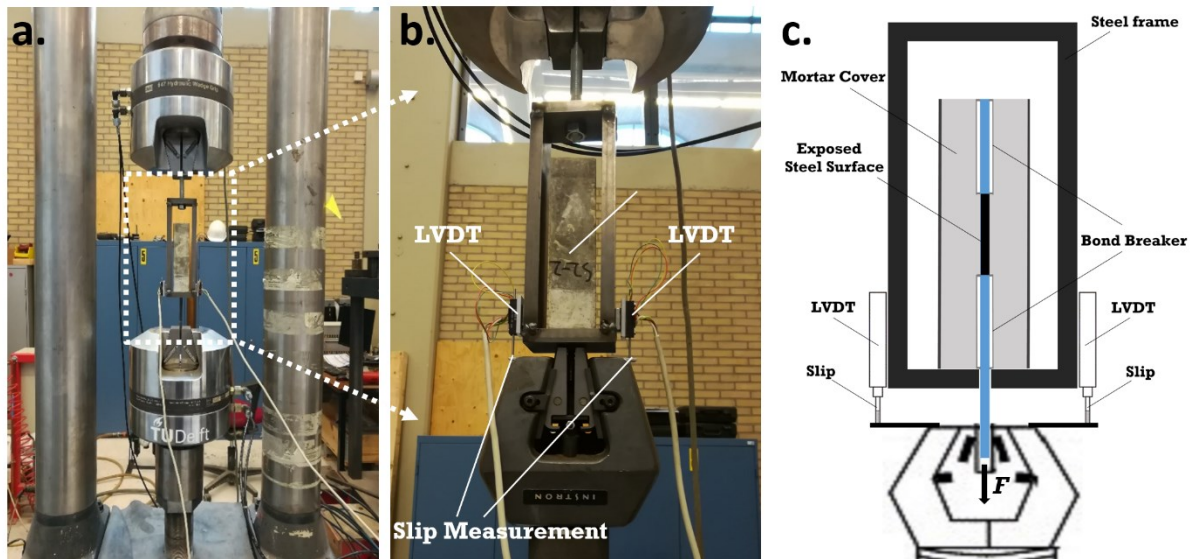


Figure 5.3: Pull-out measurement setup.

5.3 Results and discussion

This chapter focuses on the steel-mortar interface in view of both bond strength and electrochemical properties. The parameters derived from LPR will be presented first, followed by the bond behavior of reinforced specimens. The main points, i.e., (1) the different effects of stray current and anodic polarization in perspective of bond strength of steel-mortar interface, and (2) the recorded bond strength to corrosion state relationship will be further clarified

through the PDP response and qualitative/quantitative information obtained from the EIS response.

5.3.1 OCP and R_p

The OCP and R_p values recorded via LPR measurements at the conditioning stage of 490 days are depicted in Figure 5.4 for Cl-free specimens, and in Figure 5.5 for Cl-containing cases.

The impact of curing on the electrochemical properties of steel embedded in the mortar specimens, is evident from the recorded differences in OCP and R_p values between specimens designated 24h and those with 28d designation. For instance, as expected the R-28d specimens show more noble OCP values (around -240 mV vs SCE) and higher R_p (ca. 230 k Ω /cm²) than R-24h (Figure 5.4), reflecting the higher corrosion resistance of R-28d. This implies the importance of sufficient curing on passive layer formation, for reinforcing steel embedded in mortar (as also discussed in Chapter 4 for the period prior to 490 days). Anodic polarization, also as expected, induces the formation of corrosion products on the steel surface (anodic polarization leads to steel dissolution). Hence, an enhanced corrosion state of the steel surface is relevant for specimens with designation “A”, compared to those in stray current conditions for both 24h-cured and 28d-cured situations: the R_p of A-24h/A-28d are lower than those of S-24h/S-28d. This is especially the case for the 28d-cured group, where a significantly lower R_p is recorded for specimen A-28d if compared to specimens S-28d (Figure 5.4).

If a comparison is made between R-24h (control, cured for 24h) and S-24h (cured for 24h + stray current), a more active state is related to S-24h (a more cathodic OCP and a lower R_p than R-24h). However this is not observed for the 28d-cured cases, where similar R_p values for S-28d and R-28d are recorded at the age of 490d. This means that the stray current effect in sufficiently cured specimens is not as obvious as this would be in a non-mature matrix, as for instance in the case of the only 24h-cured cases (Figure 5.4).

At age of 490 days, the OCP and R_p values of A-24h and A-28 are in the same range. This means that the electrochemical state of the steel surface in A-24h and A-28d specimens is similar at the end of conditioning. However, macro-cracks are observed on the mortar cover of A-24h, but such are not found for A-28d.

The OCP values for the Cl-containing specimens remain at very negative (cathodic) levels (see Figure 5.5, in the range between -620 mV and -760mV, vs SCE). This, together with the recorded low R_p values, reflect the accelerated corrosion state of the steel rebar affected by Cl⁻. For the C-24h and C-28d, higher OCP and R_p are observed for C-28d, showing the more active state of the former, C-24h case, and the highest corrosion resistance among all “C” cases in the latter, C-28d case. This indicates again the significance of sufficient curing/hydration of bulk matrix.

For cases CS-24h and CS-28d (stray current + Cl⁻), CS-24h is more corrosion resistant compared to CS-28d (more anodic OCP and higher R_p of CS-24h, than CS-28d). This is related to the application of stray current at very early age (24h) for the group of specimens CS-24h. At this very early age the stray current played roles in affecting both “fresh” bulk matrix and the steel surface. As discussed in Chapter 4, the stray current has positive effects on “fresh” bulk matrix because of accelerated hydration, induced by ion migration and water transport at early age. In contrast, ion and water transport due to migration are relatively impeded in CS-28d specimens, where the stray current was supplied at the age of 28 days and, the mortar bulk was already hardened. In this case the positive effect of stray current on the bulk matrix is not

significant. This is because of the lower porosity and lower pore interconnectivity in CS-28d, hence, impeded stray current flow.

CA-24h and CA-28d (NaCl + anodic polarization) show a much more severe corrosion state than CS-24h and CS-28d (NaCl + stray current), which is well supported by the recorded significantly lower R_p values of CA-24h and CA-28d. In Cl-containing specimens, anodic polarization does not only dissolve the steel, but also accelerates Cl^- ion migration towards the steel-mortar interface (as already presented and discussed in Chapter 4).

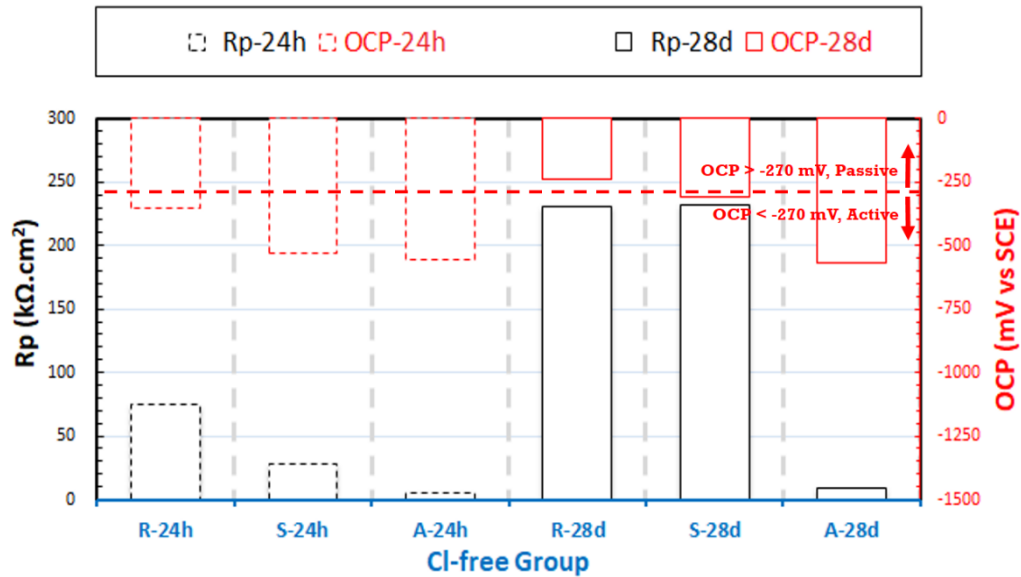


Figure 5.4: OCP and R_p values (derived from LPR) of specimens in water (as summarized in Table 5.1 and 5.2), at 490 days.

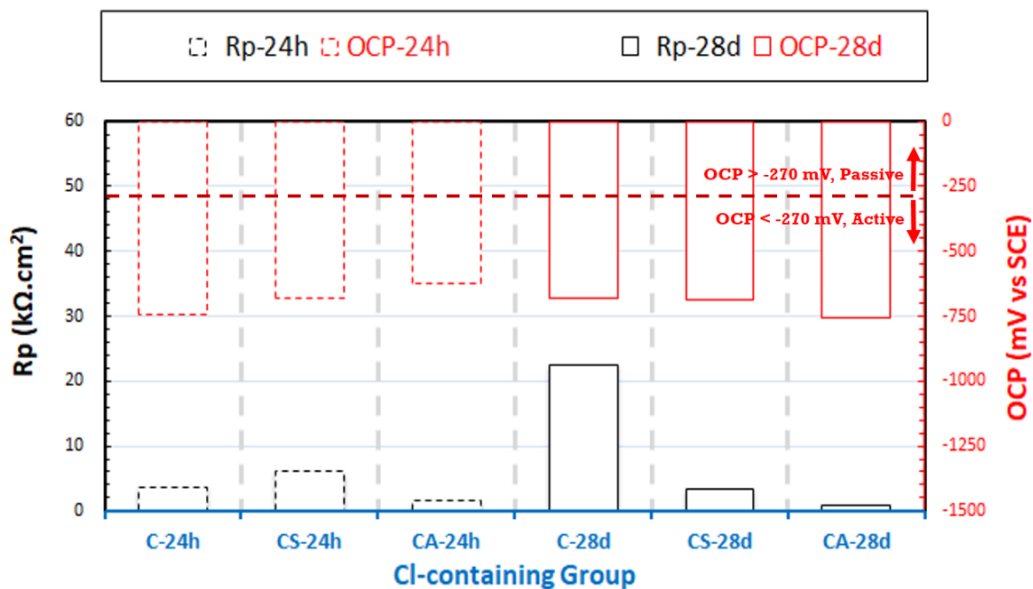


Figure 5.5: OCP and R_p values (derived from LPR) of specimens in 5% NaCl (as summarized in Table 5.1 and 5.2), at 490 days.

The OCP and R_p values derived from LPR only provide global corrosion resistance, but cannot reflect the charge transfer processes, product layer properties and transformations, which are related to the steel surface characteristics and bond property. Hence, more detailed information of steel surface properties under different conditions will be further discussed based on the observations of PDP and EIS response in Sections 5.3.3 and 5.3.4, together with the correlation of electrochemical response and bond behavior, as derived from pull-out test. The pull-out test results will be shown and discussed in next Section 5.3.2.

5.3.2 Pull-out test results

5.3.2.1 Typical bond-slip relationship curves

As a fundamental property of reinforced concrete structures/elements, the bond stress-slip relationship derived from pull-out tests is usually adopted to describe the bond behavior of steel-concrete (mortar) interface. The typical bond-slip curves for steel-concrete (mortar) interface are illustrated in Figure 5.6.

As can be observed, ascending and descending branches exist [446, 465]. Initially, the bond between a bar and surrounding matrix depends on adhesion, as can be seen in Part A of the curve. When the pull-out force increases with increasing slip, the adhesion will undergo damage (Part B). In this stage mechanical interlocking between ribs of rebar and surrounding concrete will be the major mechanism in bonding. On further loading (Point C) a longitudinal splitting crack may occur. The propagation of a longitudinal splitting crack during the pull-out process depends on the confinement state, which is determined by the concrete/mortar cover [446, 466].

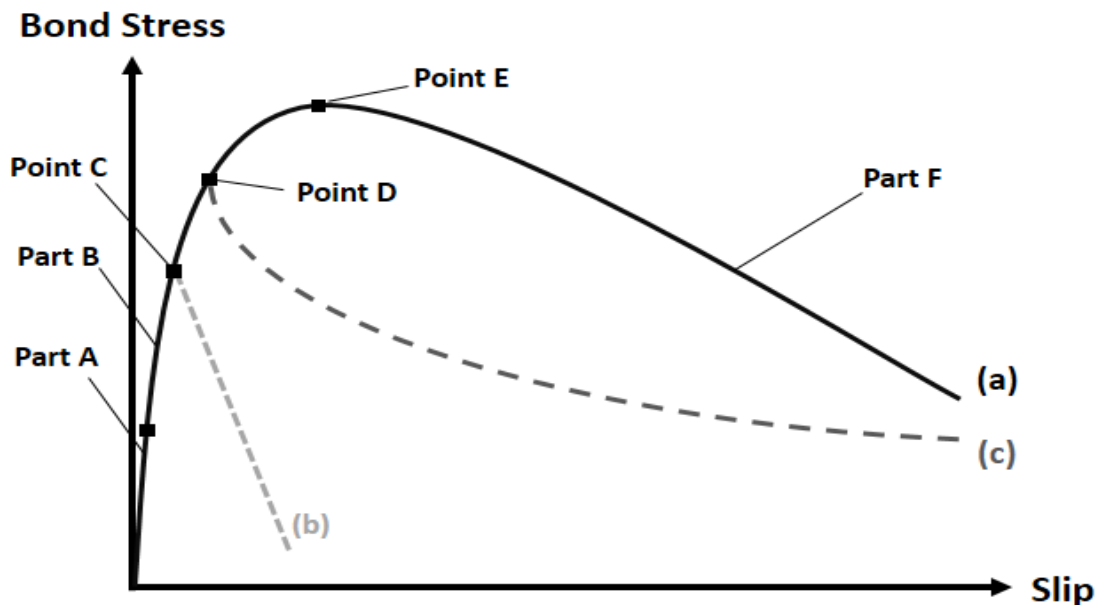


Figure 5.6: Curve of bond stress-slip for: a). well-confined concrete: pull-out failure; b). unconfined concrete: splitting failure; c). confined concrete: splitting induced pull-out failure. Reproduced on the basis of [467].

Once the surrounding material is unable to balance the splitting stress (induced by bearing stresses in front of the rib [468]), the bond stress will abruptly decline (at Point C of the dashed curve (b), and Point D of the dashed curve (c) in Figure 5.6). When a sound confinement is provided, the longitudinal splitting crack will be postponed (curve (a) in Figure 5.6). After the peak, the concrete between two adjacent ribs is already sheared completely (part F), the stress transfer is provided by friction between surrounding concrete (mortar) and reinforcement. Taking this concept in account, the specific bond property of individual specimen will be discussed below.

5.3.2.2 Bond behavior

Figures 5.7-5.10 depict the bond stress-slip relationships for all specimens. A comparison of the bond strength (as reflected by the peak of the pull-out curves in Figures 5.7-5.10) for all specimens can be seen in Figure 5.11. It can be noted that stray current leads to bond degradation of the steel-mortar interface, regardless of the presence or absence of Cl^- in the external environment. The actual specimens after pull-out are shown in Figures 5.12-5.16.

For the 24h-cured Cl^- -free cases (Figure 5.7), the maximum bond strength (19.6 MPa) is observed for the control specimen (R-24h). The sharp drop of bond stress after the peak occurs earlier for S-24h, corresponding to a 9.1% reduction of bond strength for S-24h, 17.8 MPa, compared to R-24h. A remarkable decrease (60.6%) of bond strength (7.7 MPa) is found for A-24h. The bond stress of A-24h is abruptly lost by the split of mortar along the crack (the longitudinal cracks can be seen in Figure 5.13), which is because of the reduced confinement of mortar cover.

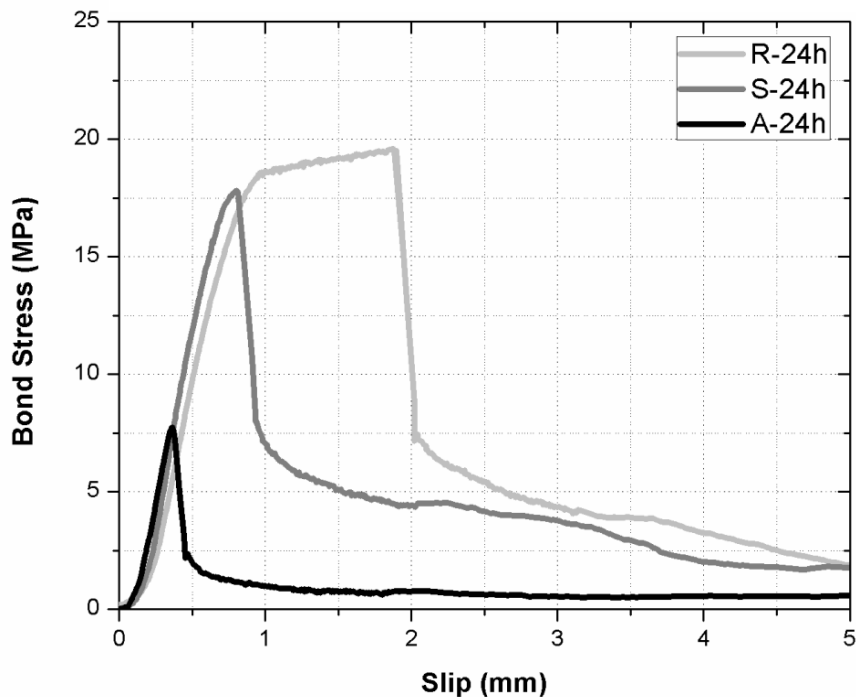


Figure 5.7: Bond stress-slip relationship of 24h-cured specimens (treated in water). R-24h: Reference; S-24h: Stray Current; A-24h: Anodic Polarization – after 24h curing in fog room.

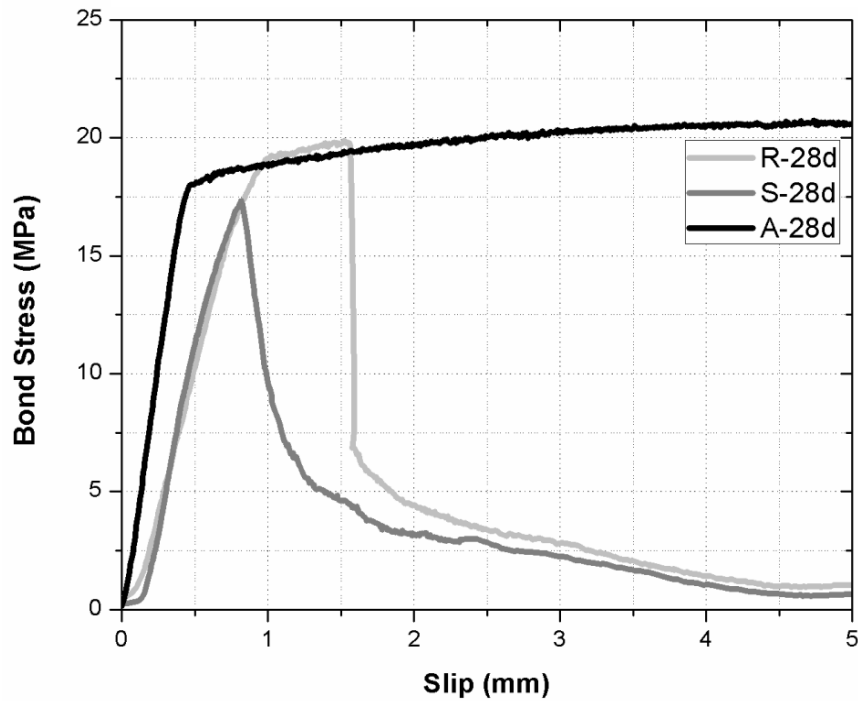


Figure 5.8: Bond stress-slip relationship of 28d-cured specimens (treated in water). R-28d: Reference; S-28d: Stray Current; A-28d: Anodic Polarization – after 28d curing in fog room.

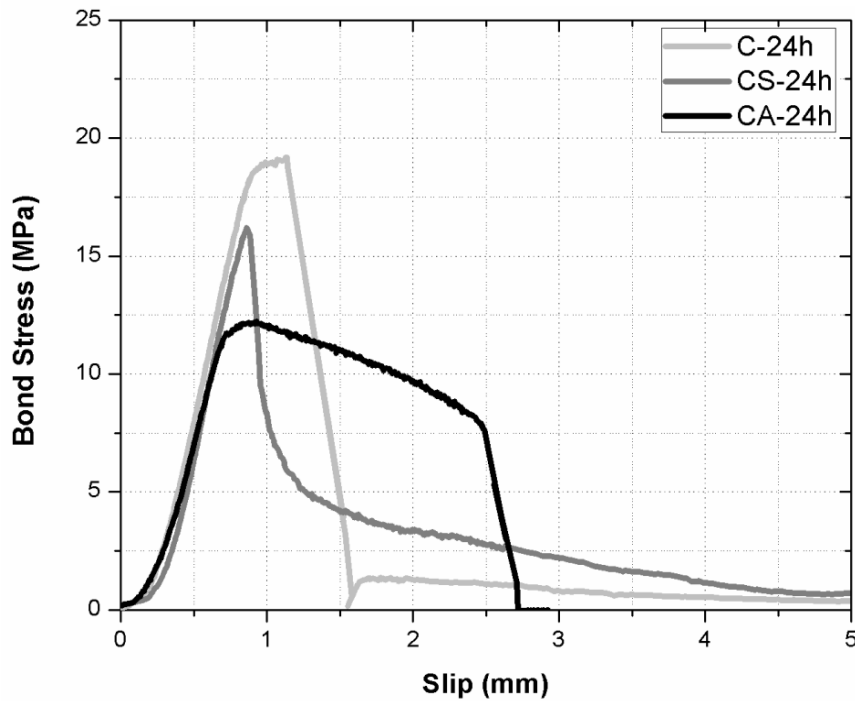


Figure 5.9: Bond stress-slip relationship of 24h-cured specimens (treated in 5% NaCl). C-24h: Corroding (NaCl medium); CS-24h: Corroding (NaCl) + Stray Current; CA-24h: Corroding (NaCl) + Anodic Polarization – after 24h curing in fog room.

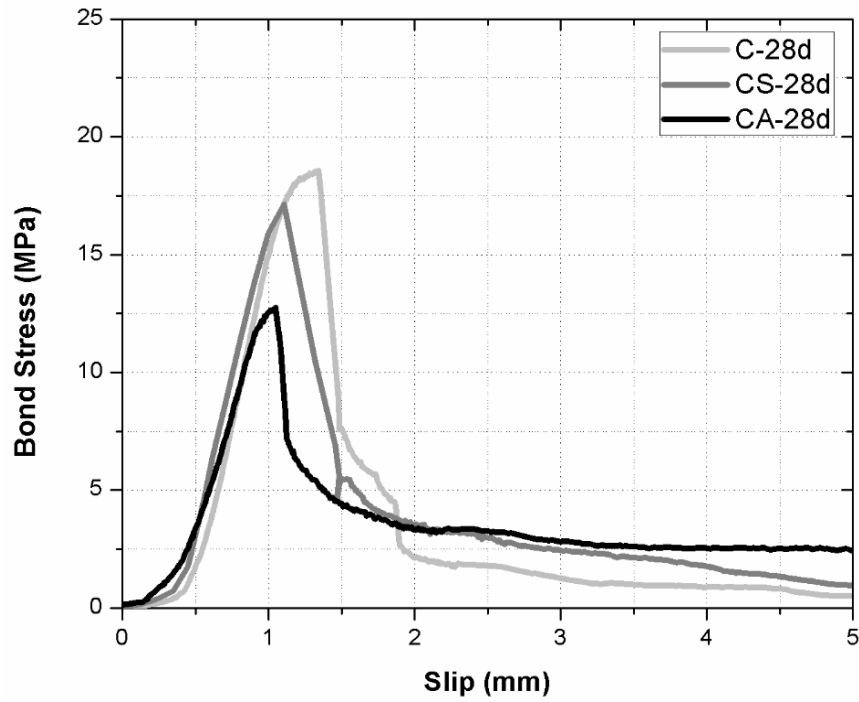


Figure 5.10: Bond stress-slip relationship of 28d-cured specimens (treated in 5% NaCl). C-28d: Corroding (NaCl medium); CS-28d: Corroding (NaCl) + Stray Current; CA-28d: Corroding (NaCl) + Anodic Polarization – after 28d curing in fog room.

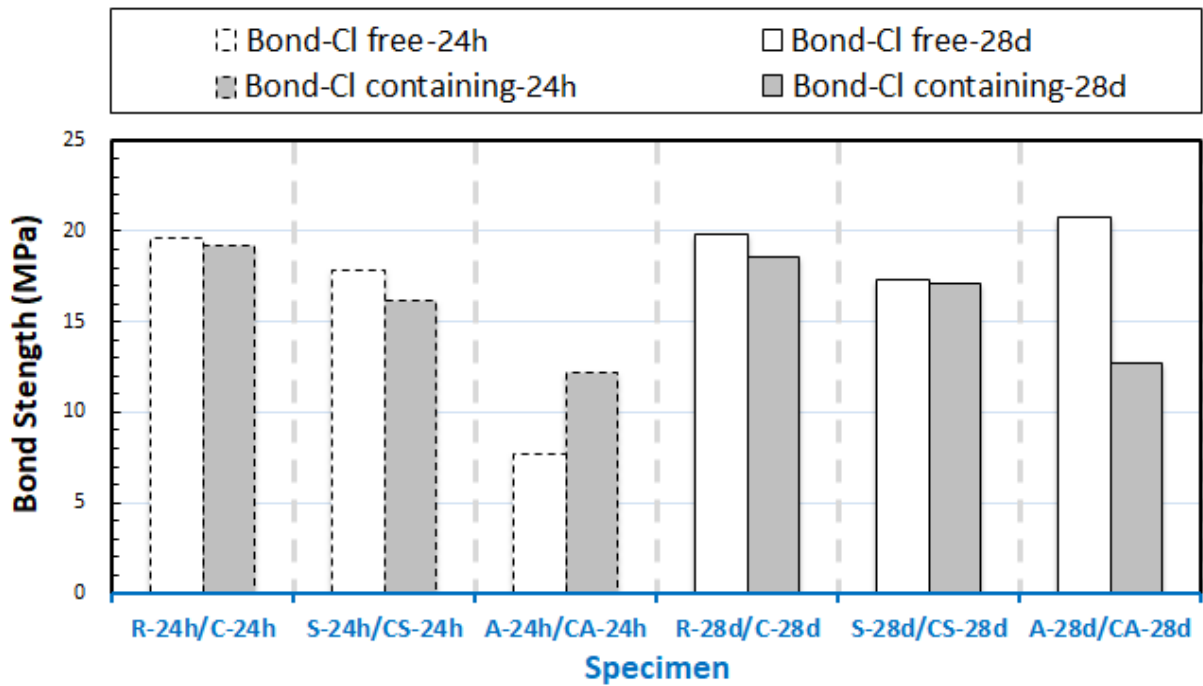


Figure 5.11: Comparison of bond strength of all specimens.

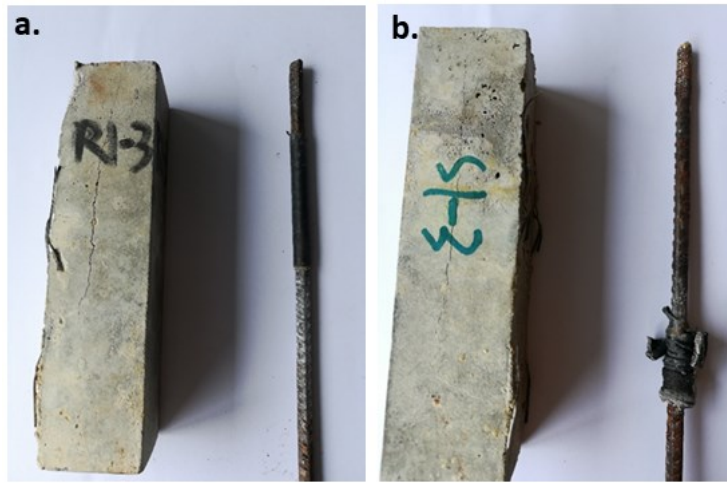


Figure 5.12: Specimens after pull-out: a). R-24h; b). S-24h.

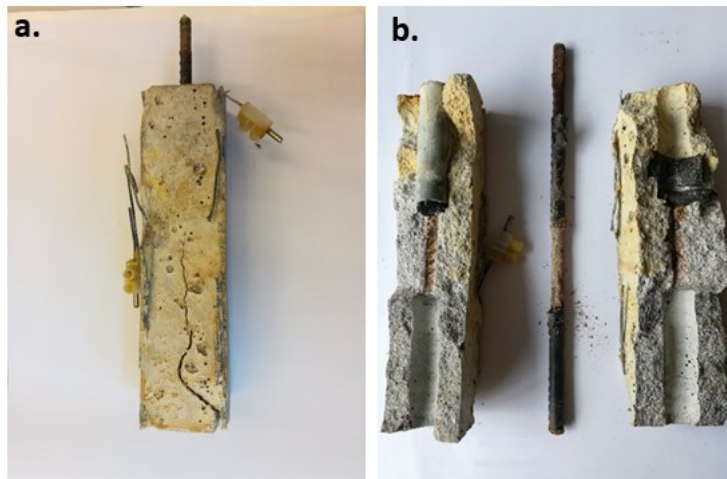


Figure 5.13: Specimen A-24h: a). before pull-out; b). after pull-out.

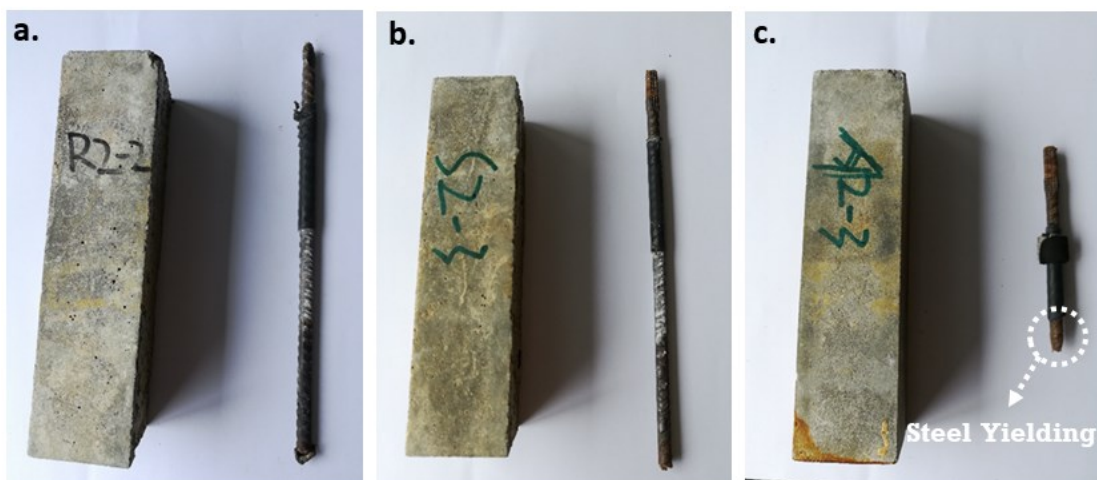


Figure 5.14: Specimens after pull-out: a). R-28d; b). S-28d; c). A-28d.

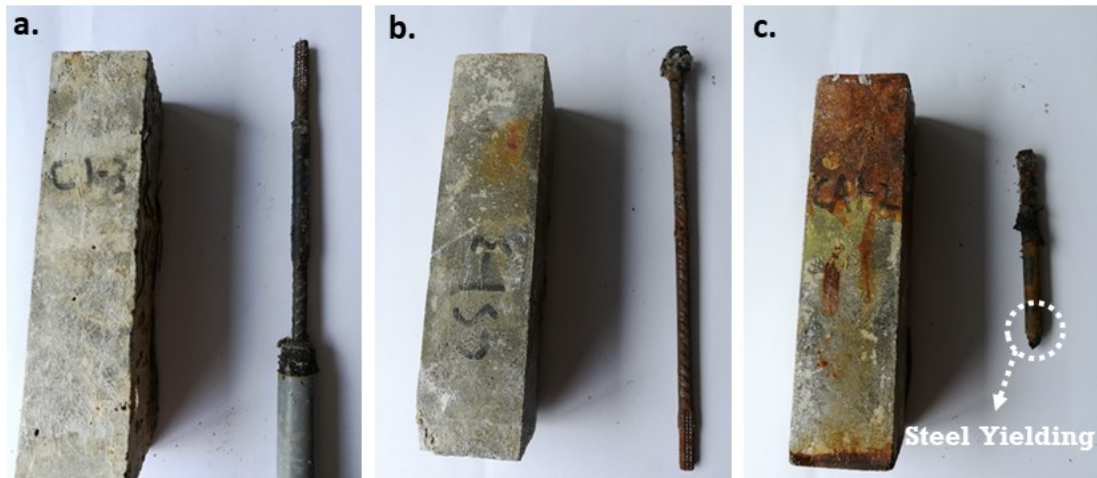


Figure 5.15: Specimens after pull-out: a). C-24h; b). CS-24h; c). CA-24h.

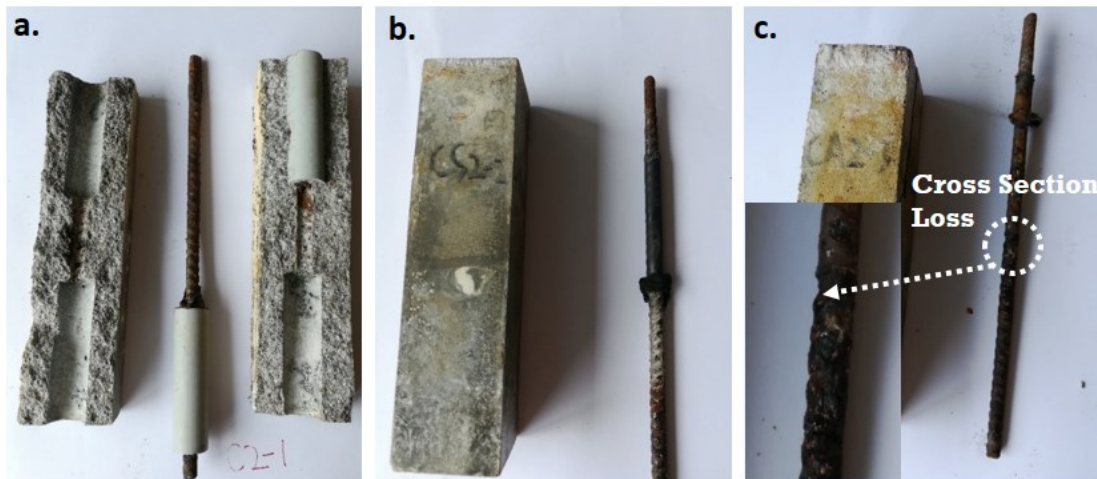


Figure 5.16: Specimens after pull-out: a). C-28d; b). CS-28d; c). CA-28d.

As can be seen in Figure 5.8, the reduction of bond strength is observed for S-28d compared to R-28d (12.7% decrease, from 19.9 to 17.3 MPa). Similar to the 24h-cured situation, a premature drop of bond stress occurs for S-28d. For A-28d, although a pronounced reduction in corrosion resistance is recorded (as shown in Figure 5.4, low R_p and cathodic OCP value of A-28d), a bond loss for A-28d specimen is not found. As shown in Figure 5.14c, the failure mode of A-28d is yielding/rupture of the rebar. This means that the bond capacity of this steel-mortar interface is higher than the tensile strength of the rebar (higher than 20.8 MPa). The high bond strength is attributed to the increase in normal stress at steel-mortar interface, caused by the formation and expansion of corrosion product at the steel-mortar interface. To be noted here is also the fact, that for a relatively mature matrix, as the case of A-28d, the initial corrosion products confinement would be more significant if compared to A-24h (presented in Figure 5.11). For the 24h-cured specimen A-24h, a more open and porous matrix would determine formation, accumulation, dissolution and re-precipitation of corrosion products within the bulk matrix overall, rather than confinement at the steel-mortar interface, as in A-28d. For A-28d a

visible crack is not induced, although the expansion of corrosion product develops mechanical pressure on the surrounding mortar [457, 469]. In contrast, for A-24h, macro-cracks are observed, together with a reduced bond strength. More details related to this will be discussed together with PDP and EIS, in the next sections.

For the effects of Cl^- induced corrosion on bond: compare C-24h to R-24h (C-28d to R-28d), a decreased bond strength is recorded for the Cl^- -containing specimens, as shown in Figure 5.11. For CS-24 and CS-28d (stray current + Cl^- specimens), a decrease of bond strength induced by stray current can again be observed in both 24h and 28d-cured situations, i.e., reduction of 15.5% (from 19.2 MPa to 16.2 MPa) for C-24h and CS-24h, 7.7% (from 18.6 MPa to 17.1 MPa) for C-28d and CS-28d. The most remarkable bond loss is related to the “ Cl^- + anodic polarization” cases. For CA-24h, a rupture of the steel bar is observed, as shown in Figure 5.15. This is because of the reduced cross-section of steel for CA-24h. A significantly low bond strength (only 12.7 MPa) is recorded for CA-28d. After pull-out, loss of cross-section of the steel rebar is observed on specimen CA-28d, as shown in Figure 5.16c.

5.3.3 PDP

5.3.3.1 PDP response of Cl^- -free specimens

PDP curves are presented in Figure 5.17 for the specimens treated in water. For these Cl^- -free cases, the most noble corrosion potential (approx. -220 mV) and lowest corrosion current are recorded for the specimen R-28d (the control specimen cured for 28d) - as expected and in line with the OCP and LPR results in Figure 5.4. In accordance with the much lower R_p values derived from LPR, high anodic current and cathodic corrosion potential (approx. -550 mV) are recorded for A-24h and A-28d.

It can also be noted that limitations within the anodic polarization are observed for A-28d (although the anodic currents remain high if compared to those of specimens R-28d and S-28d, Figure 5.17). Additionally an anodic peak around -210 mV (vs SCE) is observed for the case of A-28d (with current density peak of $11.43 \mu\text{A}/\text{cm}^2$). This is related to the dissolution of iron oxide/hydroxide layer previously formed on the steel surface.

Both of above observations mean that a relatively stable and compact product layer exist on the steel surface of A-28d, and cause limitations to the dissolution process within anodic polarization. In an alkaline environment the main corrosion product of iron is $\text{Fe}(\text{OH})_2$ [422]. By anodic polarization of iron, $\text{Fe}(\text{III})$ may be formed directly on the electrode surface as Fe_2O_3 , as mixed iron oxide (including Fe_3O_4) or as FeOOH [427, 429]. These corrosion products have higher volume than the original steel itself, and occupy a greater volume at the steel-mortar interface. Since the bulk matrix of A-28d is sufficiently cured, hence a less porous matrix (with less water) is present at steel-mortar interface. This means that the corrosion product cannot easily penetrate into the surrounding bulk matrix, and a more confined product layer is at hand, which is also reflected by the anodic limitation of PDP response. In this situation the corrosion product growth, dissolution and (re)precipitation are restricted (the mortar cover is sufficiently cured and hardened, cracks are not induced for A-28d at the end of conditioning). This further leads to the compacted product layer and limitations to a steel dissolution process. This supports the bond behavior derived from the pull-out test (Figure 5.8): the highest bond strength is recorded for A-28d.

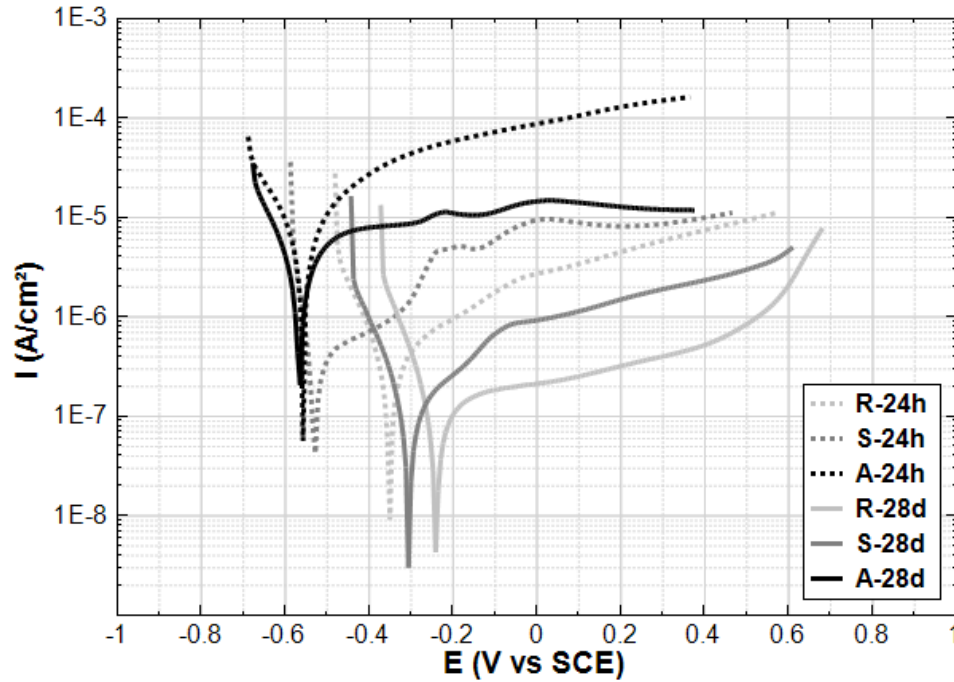


Figure 5.17: Overlay of PDP curves for specimens in water at 490 days.

For specimen A-24h (Figure 5.17), anodic currents limitation after ca. -210 mV are not pronounced (for A-24h only 24h curing was relevant, after which anodic polarization was applied). The anodic current of A-24h is almost one order higher than that of A-28d. The PDP response of A-24h reflects a presumably unstable and porous corrosion product layer. This is attributed to the crack induced by the continuous product layer growth starting at very early age (as actually recorded and discussed based on the EIS response evolution, in Section 4.3.4, Chapter 4). For A-24h, at early age the bulk matrix surrounding steel surface is porous (also with a higher water content, compared to A-28d). In this situation the corrosion products disperse into the matrix more easily. In other words, the corrosion product layer is more porous and less homogeneous (i.e., compromised ITZ properties), compared to A-28d. Additionally, the mortar cover was cured in fog room for only 24h (i.e., not cured sufficiently, not fully hydrated), the strength of mortar is also lower than that of A-28d. The consequence of this is crack propagation. Once macro-cracks are induced, the environmental condition in the vicinity of steel surface will be changed (H_2O and oxygen penetrate to the vicinity of the steel surface via cracks). This will allow an ongoing process of corrosion product formation, (re)precipitation and transport towards voids and cracks in the bulk matrix. The ultimate consequence is the loss of steel-mortar bond (reduced bond strength of A-24h is recorded in Figure 5.7). These properties and behavior can also be reflected by the EIS response, and will be further discussed in the next section.

For the 24h-cured control specimen (R-24h), a more active state (compared to R-28d specimen) is recorded (more cathodic potential and higher anodic current than R-28d). The recorded corrosion current of S-24h (cured for 24h, followed by supply of stray current) is one order higher than that of specimen R-24h, accompanied by a more cathodic potential (about -520 mV). Different from R-24h, anodic limitation is observed after the OCP for S-24h. After

this, the first current density peak of $5.16 \mu\text{A}/\text{cm}^2$ is observed at around -210 mV (vs SCE), and the second current density peak of $10 \mu\text{A}/\text{cm}^2$ is observed at around 10 mV (vs SCE). These peaks are related to the dissolution of $\text{Fe}_2\text{O}_3 \cdot n\text{H}_2\text{O}$ and/or a mixture of oxide and hydroxide [470, 471].

These phenomena (the peaks and anodic limitation after corrosion potential) however are not significant for S-28d, reflecting that in the case of S-24h specimen, a product layer of different composition and/or distribution on the steel surface was formed. This is also in accordance with the pull-out result: the bond strength of S-24h is higher than S-28d (Figure 5.11), although higher anodic current density is recorded for S-24h (see the PDP response in Figure 5.17). This recorded difference between S-24h and S-28d is again related to the curing regimes, and illustrates the importance of the starting time of stray current supply, as aforementioned in Chapter 4: at very early age (24h in present work), the stray current induced a more significant interference than the case of later age (after 28 days).

5.3.3.2 PDP response of Cl-containing specimens

Figure 5.18 depicts the PDP response of the specimens treated in 5% NaCl. As can be observed in Figure 5.18, a cathodic corrosion potential is evident for the Cl-containing specimens (more cathodic than -600 mV). Additionally, the corrosion current densities for these specimens are significantly higher, compared to the cases treated in water. The most pronounced corroding state is related to specimens, subjected to both anodic polarization and Cl-containing medium (CA-24h and CA-28d). If a comparison is made between specimens C-24h and CS-24h, the pronounced effect of the stray current in group CS-24h towards enhanced corrosion is not observed: the corrosion current density of CS-24h is even lower than that of specimens C-24h. This relatively higher corrosion resistance in specimen CS-24h reflects the potentially positive effect of the stray current at very early age, because of enhanced cement hydration. This will result in a faster development of pore network, and lead to a more rapid stabilization of the pore solution and hydration products.

Based on this, competitive mechanisms would be relevant for specimen CS-24h. On one hand, the stray current has positive effects on the bulk matrix properties at early age (in a fresh matrix). On the other hand stray current accelerates Cl^- ion migration, and enhances steel corrosion, finally results in a corrosion products build-up on the steel surface. The recorded lower bond strength of CS-24h (compared to C-24h, where only Cl-induced corrosion plays a role) is in line with this. Again, the different electrochemical state of CS-24h, compared to C-24h, can be reflected by the EIS, and will be discussed later on in Section 5.3.4.3.

In contrast to the above sketched different performance of C-24h and CS-24h, this difference is not obvious in the 28d-cured specimens (C-28d and CS-28d). It can be observed via PDP (Figure 5.18) that the steel surface of CS-28d shows more corrosion than C-28d. In other words, the stray current effect for 28d-cured specimen leads to accelerated steel corrosion. For CS-24h, at the age of 1-28 days, the stray current already played roles (positive and negative) in both affecting the “fresh” bulk matrix and the steel surface. For the 28d-cured specimen CS-28d, the stray current exerts mainly negative effects, predominantly affects the steel. Some of these details were discussed in Chapter 4 for the relevant duration of treatment, and will be clarified again for the full test duration relevant to this chapter, by the EIS response in Section 5.3.4.2.

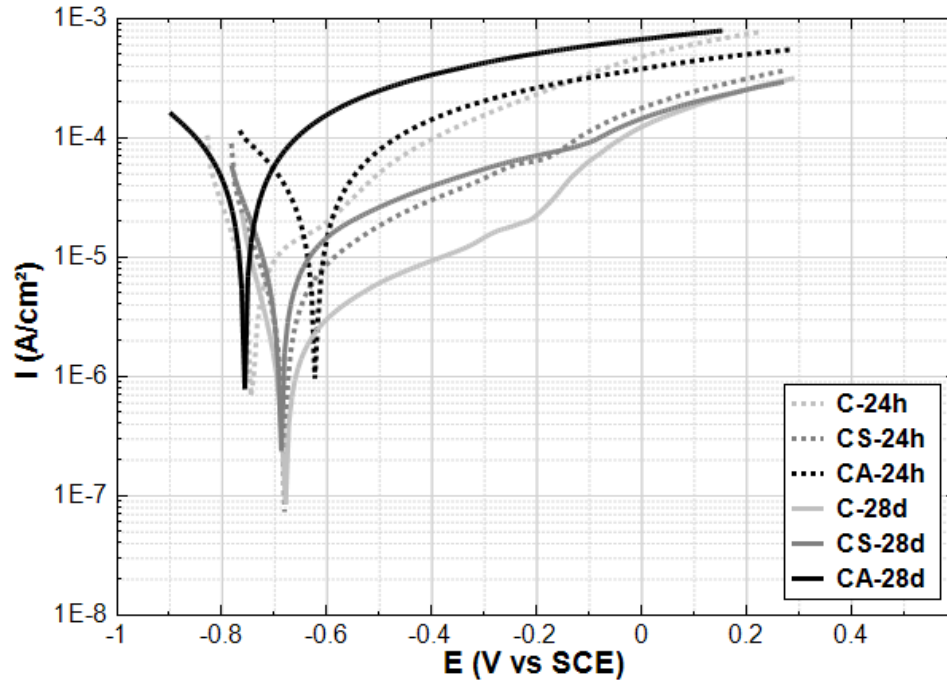


Figure 5.18: Overlay of PDP curves for specimens in 5% NaCl at 490 days.

According to the PDP responses, it is clear that anodic polarization (A or CA groups) leads to a more active status of the steel surface than stray current (S or CS groups), in all conditions investigated in the present work. The different effects of stray current and anodic polarization on bond of steel-mortar interface will be further discussed, together with EIS response in the next section.

5.3.4 EIS

5.3.4.1 General consideration for EIS fitting

The EIS experimental results for all investigated specimens are shown in Figures 5.19-5.22, in Nyquist formats. All impedance plots present values in Ω , since the geometries of the cells and the steel surface are identical. The equivalent electrical circuit used for fitting the EIS response can be seen in Figure 5.23: R_0 represents the electrolyte resistance; R_1 is the resistance of the solid phase of mortar cover, the capacitance C_1 represents the dielectric capacitance of solid phase of mortar cover; C_2 and R_2 are related to double layer effects and ionic motion in pore network; R_3 and Q_3 are related to the bulk matrix in the vicinity of steel-mortar interface; $R_4(R_p)$ and Q_4 correspond to the charge/mass transfer processes, linked to the electrochemical reaction on the steel surface [472-474], i.e., the R_{ct} and $R_{red/ox}$ make up R_p . For deriving R_p from EIS measurements in reinforced concrete/mortar, the low frequency limit of the impedance spectra is generally considered for calculations, as reported in Ref. [386, 475-478] and used in the present study as well. The replacement of pure capacitance (C) with constant phase element (CPE or Q) in the equivalent circuits is widely accepted for systems as in this study, denoted to in-homogeneities at different levels, hereby being mainly relevant to the heterogeneity of

hydration/corrosion products, that form on the steel surface in different conditions [415, 477, 479-481].

Quantification of the cases of interests is presented and discussed. The interests here are to clarify the different effects of stray current and anodic polarization, in perspective of bond strength of steel-mortar interface; and to correlate the bond behavior of steel-mortar interface with the electrochemical response of reinforced mortar specimens, affected by stray current and anodic polarization. Hence in order to intensively illustrate the above points, only the results from EIS fitting for groups S-24h, A-24h, S-28d and A-28d (cases only related to stray current and anodic polarization) are shown in Figure 5.24 and 5.25. An example (specimen S-28d, 28d-cured in fog room, then treated by supplying stray current in water) of the EIS fitting process is shown in Appendix C.

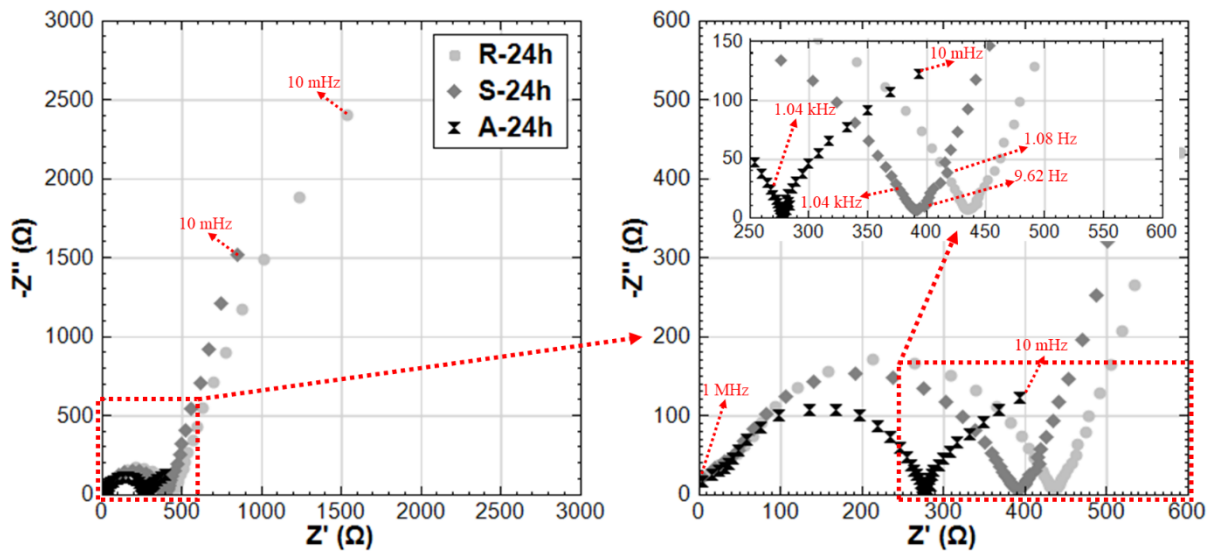


Figure 5.19: EIS responses in Nyquist format of 24h-cured specimens (treated in water).

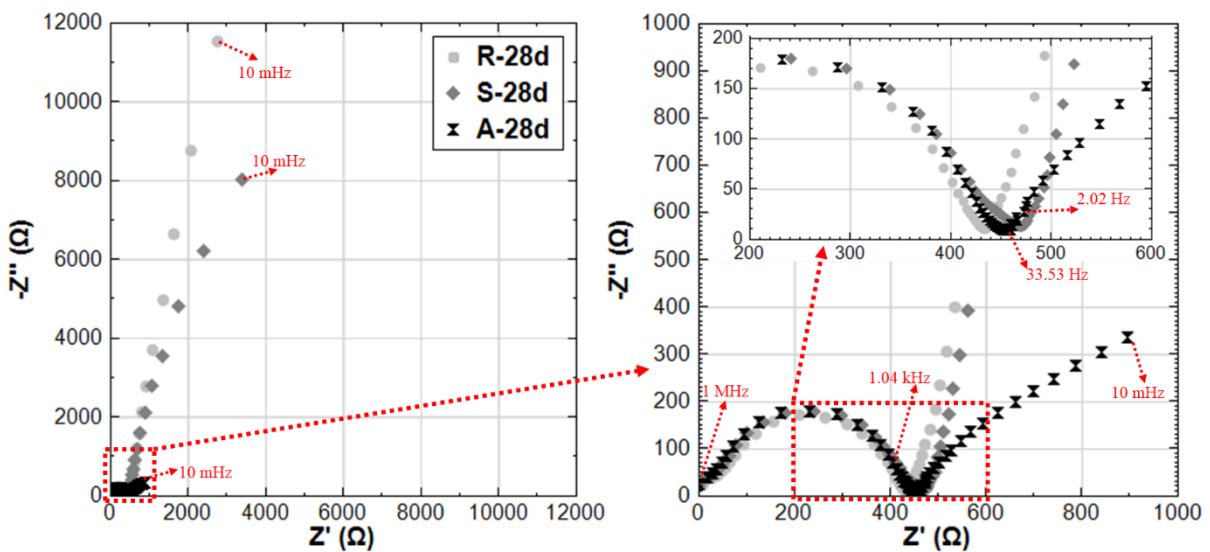


Figure 5.20: EIS responses in Nyquist format of 28d-cured specimens (treated in water).

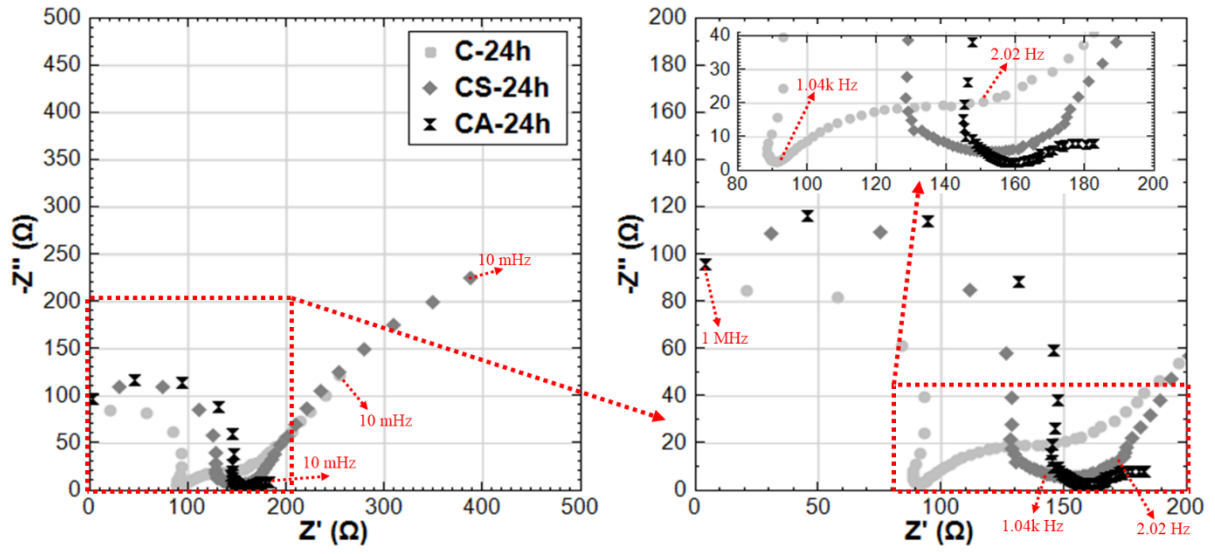


Figure 5.21: EIS responses in Nyquist format of 24h-cured specimens (treated in 5% NaCl).

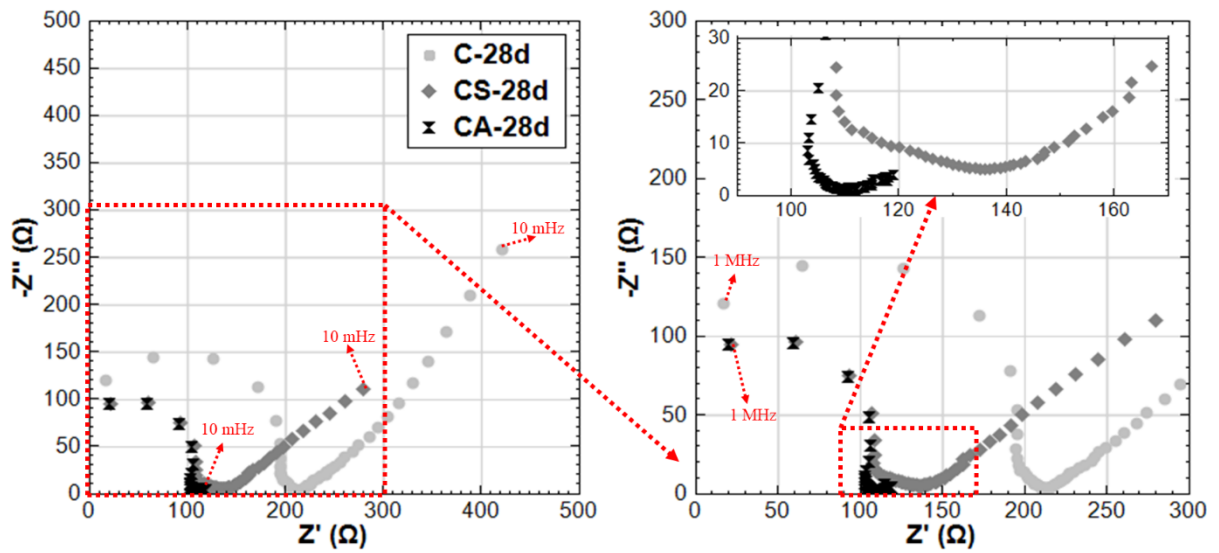


Figure 5.22: EIS responses in Nyquist format of 28d-cured specimens (treated in 5% NaCl).

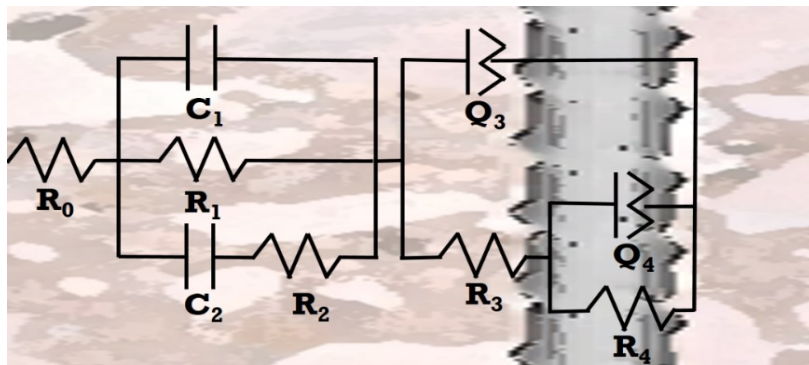
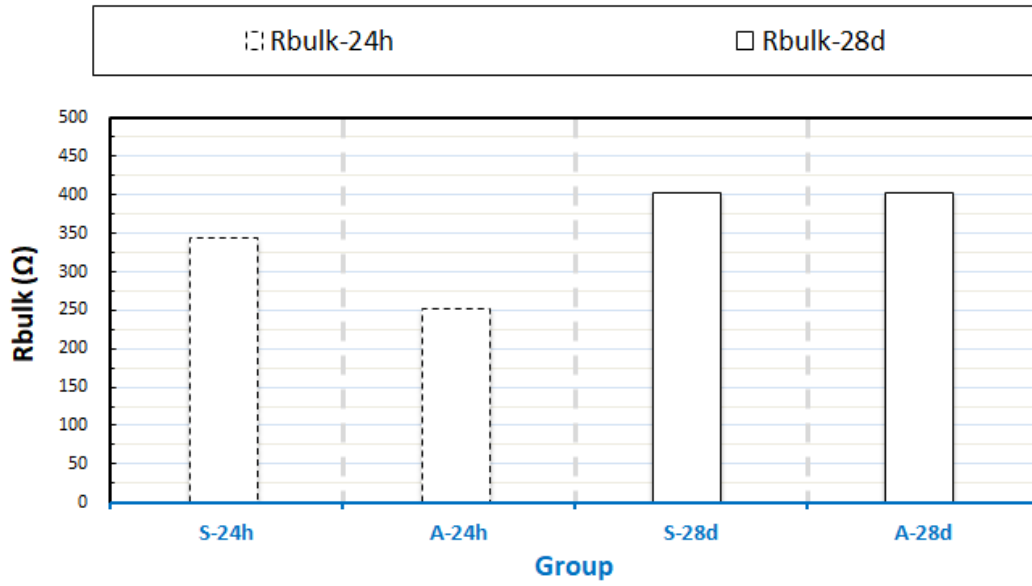
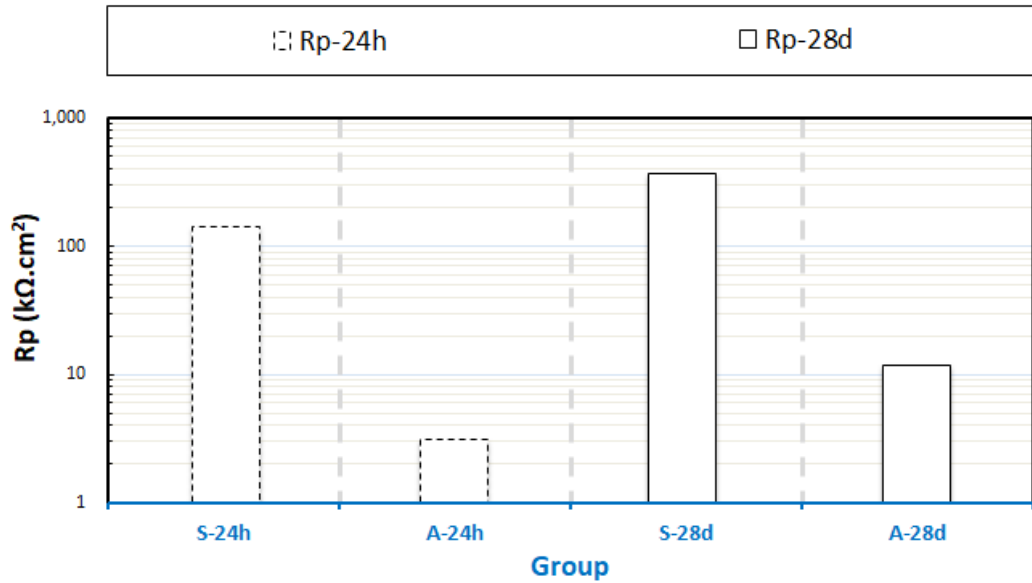


Figure 5.23: Equivalent electrical circuit used for fitting EIS response.

Figure 5.24: R_{bulk} values calculated from EIS.Figure 5.25: R_p values calculated from EIS of selected specimens, at 490 days.

As can be seen in Figures 5.19-5.22, the HF domain (higher than 1 kHz) of all specimens depicts the semi-circle capacitive arcs, attributed to the properties of the mortar bulk matrix [482]. The first time constant (R_1C_1) is related to the properties of the mortar bulk matrix. The matrix resistance R_{bulk} (R_1) values of mortar cover are adopted as indicators for bulk matrix properties. The higher resistance of cement-based matrix R_{bulk} (R_1) partly reflects a denser matrix, a lower permeability, and consequently higher strength. The C_{bulk} of mortar/concrete solid phase is in the order of nF [413], and is normally detected in the high frequency range (i.e., approx. 50 kHz to MHz). The R_{bulk} (R_1) values derived from EIS tests are included in Figure 5.24. The derived values of R_p are normalized and given in Figure 5.25.

5.3.4.2 EIS response of Cl-free specimens

Evidently R-24h and R-28d have similar HF EIS response (Figure 5.19 and 5.20), which is well in line with the almost identical bond strength of R-24h and R-28d (see Figure 5.11). Additionally, the higher corrosion resistance of R-28d compared to R-24h is reflected by the LF EIS response, and completely in line with the higher R_p from LPR and lower anodic currents from PDP of R-28d. The higher corrosion resistance of R-28d leads to a higher bond strength, compared to R-24h, as illustrated in Figure 5.11.

The bond strength at the interface between a steel bar and concrete (mortar) is affected by the corrosion of the steel bar. Corrosion products can alter the steel-mortar interface and influence the development of bond stresses. Research on bond degradation due to reinforcement corrosion has produced a variety of results. Although the results show remarkable scatter, they indicate that the bond strength decreases with the increase of steel corrosion [443].

This, however, is not always a straightforward scenario. For the EIS response of S-24h and S-28d, the lower corrosion resistance of S-24h can be reflected by LF EIS response (lower R_p of S-24h, as shown in Figure 5.25). This is in accordance with the lower anodic current density of S-28d recorded by PDP. However, a higher bond strength is recorded for S-24h compared to S-28d. This is attributed to the altered corrosion product layer (a product layer of different composition and/or distribution) formed on steel surface of S-24h, together with an obviously different microstructural property at the steel-mortar interface, where initially positive effects of the stray current on cement hydration could have been relevant (as already discussed in Chapter 4).

The stray current effect in S-24h obviously leads to alterations of both product layer (on steel surface) and matrix. The significant accumulation of a product layer in the case of S-24h is reflected by the PDP response (the plateau region after E_{corr}). Compared to S-28d, an intermediate (MF to LF) additional time constant is recorded for S-24h (as marked in inlet of Figure 5.19, in the frequency range of 9.62-1.08 Hz). This is linked to the anodic peaks in the PDP of S-24h, indicating again the altered steel-mortar interface in the sense of a well adhering product layer on the steel surface (evident from the several anodic current limitations in the PDP response). A lower bulk matrix resistance at the stage of 490 days for S-24h is reflected by the HF EIS, compared to S-28d. This implies a more porous bulk and steel-mortar interface of S-24h, facilitating corrosion products penetration into the bulk matrix, and possibly a more uniform distribution of corrosion products. The consequences of all above are alterations towards a more uniform stress distribution in the system, including the steel-mortar interface and higher bond strength of S-24h.

For A-24h and A-28d, as already shown in the above sections, a similar global corrosion resistance is recorded by LPR and PDP. However, a bond increase is recorded for A-28d, while a bond reduction is recorded for A-24h (Figure 5.11). These different bond properties are related to the properties of the mortar matrix, the steel-mortar interface and the product layer. It is clear that the similar shape of the HF semicircle of EIS (a similar semi-circle capacitive arc for the HF time constant) are recorded for both A-24h and A-28d (Figure 5.19 and 5.20), where 150 Ω higher R_{bulk} for A-28d is recorded (see Figure 5.24), which is normal in view of the more mature A-28d mortar matrix, compared to A-24h. This again implies a less porous bulk matrix around the steel surface of A-28d (compared to A-24h), and hence a good confinement of the interface (because the corrosion product cannot penetrate into mortar bulk easily). This leads to a higher

interaction force between steel surface and mortar cover. The consequence of this is the higher normal stress at steel-mortar interface [457, 469].

This is in line with the anodic limitation of PDP response, as discussed in Section 5.3.3.1. This can also be reflected by EIS response: an intermediate MF to LF response (in the range of 35.53-2.02 Hz) is recorded for A-28d. This, together with the two anodic peaks of PDP response of A-28d, reflect the mixed charge transfer and diffusion processes, which is also indicated by the depressed semi-circular EIS response in the LF (see Figure 5.20). Diffusion accounts for mass transport within the product layer on the steel surface, i.e., it is a proof for a layer that limits anodic dissolution with external polarization, as actually recorded by PDP of A-28d.

However for A-24h, the well expressed intermediate time constant is not recorded. On the contrary, an overlap of two constants into a second semi-circular response is observed, which is related to (although limited) charge transfer mainly, i.e., dissolution of corrosion product on the steel surface. This is well supported by anodic dissolution in PDP response (Figure 5.17). This is also in line with the lower R_p derived from EIS (compare with A-28d), which implies the pronounced corroding status and a thick, porous and non-homogeneous corrosion product layer in A-24h [483, 484]. The consequence of the above property, is the corresponding reduction of bond strength for A-24h. It can be summarized that a more porous and volume expanding hydroxide layer will form in conditions of “more water present” in the system (as in A-24). A more open bulk matrix would also result in conditions for corrosion products dissolution and precipitation. In contrast, for A-28d, Fe oxides-based and/or Ca-substitutes are formed on steel surface (a less porous and volume expanding layer). This together with the mature matrix in A-28d leads to a confinement of the corrosion products, and maintains structural property at the steel-mortar interface over the duration of these tests.

5.3.4.3 EIS response of Cl-containing specimens

For EIS of specimens C-24h and CS-24h (Figure 5.21), a higher corrosion status is relevant for specimen C-24h (LF EIS response of C-24h denotes for a more active state of C-24h, compared to CS-24h). This conforms to previous results from PDP. This is due to the more significant formation of non-protective and non-adherent corrosion product layer on the steel surface of C-24h. This again indicates the possible positive effect of stray current on steel surface properties, at early age for CS-24h, as also discussed in Chapter 4. However, the bond strength of C-24h is higher than that of CS-24h, irrespective of the lower bulk matrix resistance for C-24h, compared to CS-24h (Figure 5.21).

Obviously, different properties of the bulk matrix at the steel-mortar interface are relevant for C-24h, where an additional and very well pronounced time constant can be observed (in the range of 1.04 kHz-2.02 Hz, as marked in Figure 5.21). This is in line with the PDP response of C-24h, where a limitation after E_{corr} is recorded (Figure 5.18). For C-24h both EIS and PDP results indicate a larger contribution of a mass transfer control process on the steel surface (evident by the anodic current limitation immediately after E_{corr} in the PDP response and the LF EIS response) and at the steel-mortar interface (evident by the HF EIS response). The limitations are linked to a thick and non-uniform, non-adhering product layer on the steel surface of C-24h. In contrast, well pronounced additional time constant (HF in EIS response) and anodic limitation after E_{corr} (of PDP) are not observed for CS-24h. For CS-24h, though the stray current at early age had positive effect on accelerating cement hydration, stray current also induces mortar softening by substantially increasing the solubility of the C-S-H and CH

[263, 388-398]. The result will be a coarser pore network structure at the steel-mortar interface, which consequently leads to a decrease of bond strength.

Comparing C-28d and CS-28d (Figure 5.22), a lower bond strength is again recorded for the stray current case (CS-28d). This is in line with the more corrosion resistance of C-28d, compared to CS-28d, which is also evidenced by both PDP and EIS. In this situation, the stray current adds-up to the “negative” effect of Cl^- and enhances corrosion. It means that for hardened mortar/concrete in aggressive medium, stray current can only enhance damage, rather than exert possible positive effects. This again indicates the importance of the stray current start time (the moment of stray current start), which is already discussed in detail in Section 4.3.3 of Chapter 4.

For CA-24h and CA-28d specimens (Cl^- + anodic polarization), a significant bond reduction is recorded. This is in line with the extreme corrosion status confirmed by electrochemical tests. Loss of steel cross-section because of severe corrosion is observed, which subsequently destroys the steel-mortar interface. The pull-out failure modes of CA-24h and CA-28d are different: yielding/rupture of steel for CA-24h, but a complete pull-out of the rebar for CA-28d. On one hand, a more severe corroding state is observed for CA-28d. On the other hand, the HF $|Z|$ values of CA-24h are higher than CA-28d (see Figure 5.21 and 5.22), indicating the denser mortar cover of CA-24h. The consequence is that the bond strength of steel-mortar interface is higher than the tensile strength of the steel for CA-24h. Thus the steel rebar is broken before the complete loss of bond. However, for CA-28d the significantly reduced steel cross-section and lower strength of the mortar cover lead to the smooth process of rebar pull-out.

In summary, the correlation between the electrochemical response (corrosion state of the reinforcing steel and the bulk matrix properties) obtained by the electrochemical measurements (PDP and EIS), and bond properties of steel-mortar interface derived from pull-out tests, is found and established. Although limited range of stray current level is investigated in this research, both PDP and EIS provide valuable insights into the bond strength development and/or degradation of the steel-mortar/concrete interface, as affected by stray current or anodic polarization.

5.3.5 Summary of mechanisms for stray current inducing bond loss

Regardless of whether there is corrodent in the external environment (with or without Cl^- in the present work), anodic polarization leads to more pronounced effects on steel-mortar interface than stray current, in views of both bond behavior and electrochemical response. Though the stray current effect is moderate compared to anodic polarization, the pull-out results show that stray current (at level of 0.3 mA/cm^2) still leads to bond degradation of the steel-mortar interface.

First of all, according to the electrochemical tests, it is clear that the stray current induces steel corrosion (lower corrosion resistance) in all conditions investigated in the present work, compared to the control cases. The stray current induced-steel corrosion is one of the reasons for bond reduction of steel-mortar interface. The corrosion of steel is attributed to the anodic polarization induced by stray current (where stray current flows out from steel surface).

Besides, as already discussed in Chapter 4, it is reported that hydration products previously occupying the pore space, would dissolve due to electrical current flow. This will result in vacancies, and coarsening of the pore network [400, 485]. The transport of sodium and potassium is faster than that for calcium ions [399, 400]. In the stray current electrical field, the sodium (Na^+) or potassium ions (K^+) accumulate more easily, and displace the calcium ion

(Ca^{2+}), i.e., reacts with the calcium-silicate-hydrate (C-S-H) phase and $\text{Ca}(\text{OH})_2$ (CH) previously formed on steel surface. This initiates mortar dissolution by substantially increasing the solubility of the C-S-H and CH [263, 388-398], and leads to bond loss of steel-mortar interface.

5.4 Conclusions

The effects of stray current on the steel-mortar interface are clarified, in views of both electrochemical properties of steel and bond strength of steel-mortar interface. Correlating the electrochemical property and bond behavior, the following conclusions can be drawn:

1. Stray current (at level of 0.3 mA/cm^2) leads to bond degradation of the steel-mortar interface in all cases (specimens cured in fog room for 24h or 28d, then conditioned by supplying stray current in water or 5% NaCl) investigated in this work.
2. The correlation between the electrochemical response (corrosion state of the reinforcing steel), the bulk matrix properties (derived by EIS), and bond properties of steel-mortar interface (derived from pull-out tests), is established.
3. Regardless of whether there is Cl^- in the external environment, anodic polarization leads to more pronounced effects on the steel-mortar interface, compared to stray current. The anodic polarization produces more corrosion product, the subsequent corrosion product expansion leads to two extremes: the evidently increased bond strength because of more significant confinement at steel-mortar interface; and the significantly reduced bond strength due to the cracking or spalling of the cover. The two effects are bulk matrix properties-dependent. This again indicates the difference between stray current and anodic polarization, in view of affecting bond property of steel-mortar interface.

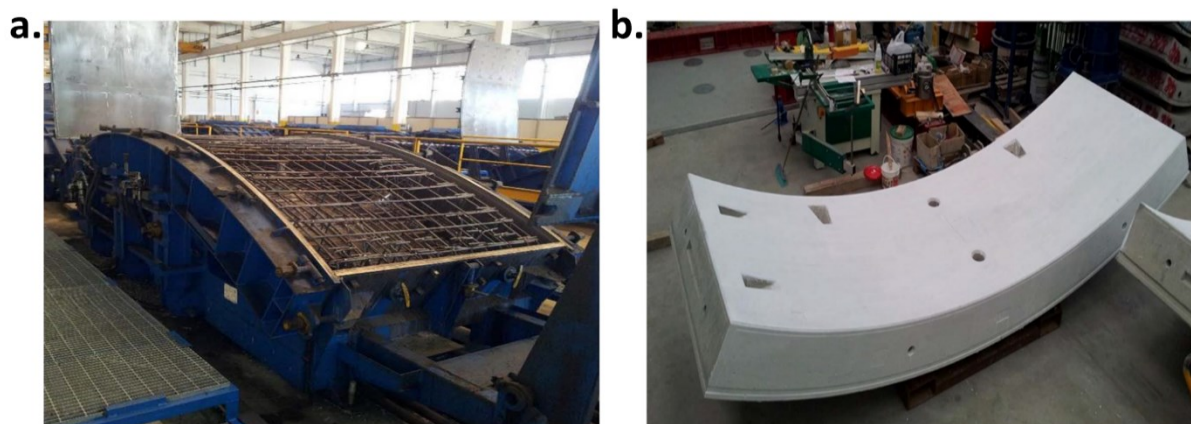
Chapter 6

Stray current corrosion as determined by geometrical orientation of steel rebar

6.1 Introduction

As is well-known in construction engineering, the layout of reinforcing steel embedded in concrete elements is usually a steel rebar cage [486-490]. An example (a metro segment) for this is shown in Figure 6.1 [491]. In this case, the stray current flowing in the tunnel segments can be parallel or orthogonal to the steel rebar. To study the stray current-induced corrosion for steel in concrete, although various works report different aspects [61, 81, 492-499], the effects of the steel rebar orientation on the amount and distribution of stray current corrosion product are still not investigated sufficiently. This aspect is of significance in view of the levels of corrosion damage, and geometrical location of corrosion product accumulation on the steel rebar surface.

This chapter presents the effects of different steel orientation, in identical specimens' geometry, on the levels of stray current-induced corrosion on the steel surface. For this reason, two geometrical positions of the reinforcement embedded in mortar are tested - the steel bar placed parallel or orthogonal to the direction (or flow) of the stray current. The level of stray current is set at 3 mA/cm^2 (through the application of external DC electrical field). The supplied stray current level is increased (from 0.3 mA/cm^2 of previous tests to 3 mA/cm^2 in this chapter), to investigate the multiple stray current levels and induce more significant corrosion on steel surface. The stray current conditions are simulated in both Cl-free (in water) and Cl-containing medium (in 5% NaCl solution).



6.1a: Reinforcing steel cage before casting.

6.1b: Metro segment after casting.

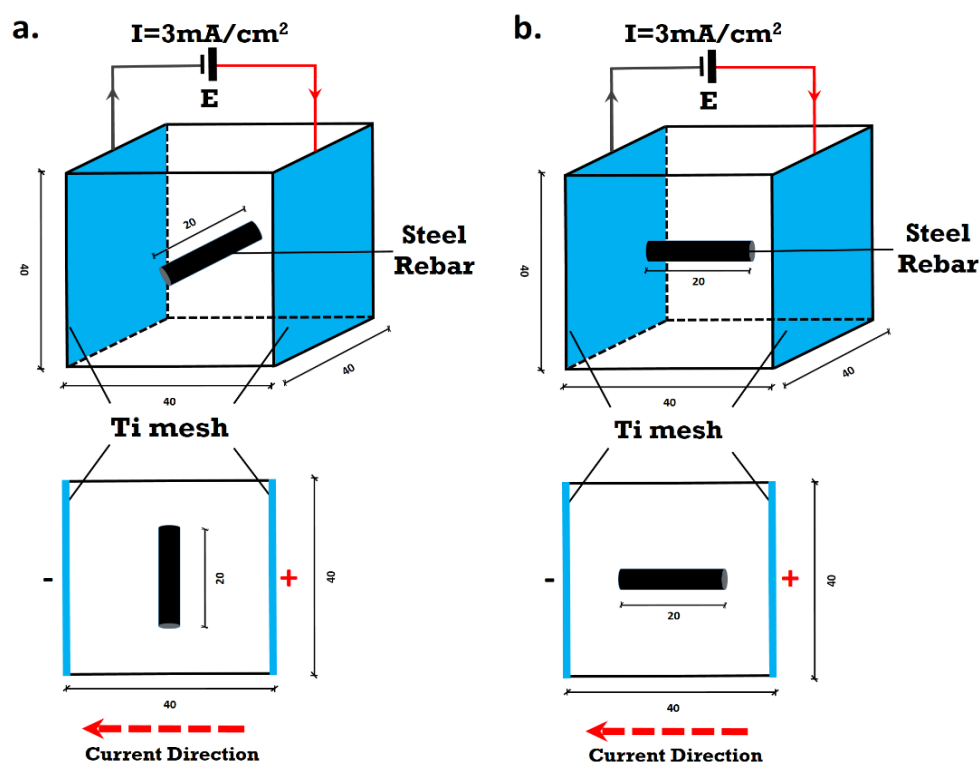
Figure 6.1: Metro segment: a). reinforcing steel cage before casting; b). after casting [491].

A more corrosive state is observed when the steel bar is parallel to the current direction, compared to the situation of a rebar orthogonal to the current. This phenomenon is further clarified via additional series of tests, where the picked-up stray current level and potential shift of the rebar undergoing stray current are monitored. Another aim of this series of tests is to better understand the time-dependent process of stray current interference on the steel, in the period of stray current supply as well as after stray current cut-off. The time-dependent response of a steel rebar undergoing stray current is rarely studied before. It is found that, though the supplying stray current is constant, the level of current picked-up by the steel rebar is decreasing. At the instant when the stray current supply is just turned off, an opposite current flow (back flow) is monitored.

6.2 Experimental

6.2.1 Materials and Specimens

Reinforced mortar cubes of $40 \times 40 \times 40 \text{ mm}^3$ were cast from Ordinary Portland cement CEM I 42.5 N and normed sand. The water-to-cement (W/C) ratio was 0.5; the cement-to-sand (C/S) ratio was 1:3. Construction steel (rebar) FeB500HKN ($d=6\text{mm}$), with a length of 20 mm, was centrally and fully embedded in the mortar cubes in two different geometrical arrangements - steel rebar placed parallel or orthogonal to the current direction (Figure 6.2).



6.2a: Steel bar orthogonal to stray current.

6.2b: Steel bar parallel to stray current.

Figure 6.2: Schematic and top-view of test specimen and setup for stray current supply and position of electrodes: a). Steel bar orthogonal to the stray current direction; b). Steel bar parallel to stray current direction.

Table 6.1: Specimens' designations and relevant conditions summary.

Groups	Specimen designations	Immersion (1/2 nd)	Rebar Layout
S(O)	S(O)-1	Water	Orthogonal
	S(O)-2	Water	Orthogonal
S(P)	S(P)-1	Water	Parallel
	S(P)-2	Water	Parallel
CS(O)	CS(O)-1	5% NaCl	Orthogonal
	CS(O)-2	5% NaCl	Orthogonal
CS(P)	CS(P)-1	5% NaCl	Parallel
	CS(P)-2	5% NaCl	Parallel

After casting and prior to demoulding/conditioning, all specimens were cured in a fog room (98% RH, 20 °C) for 24 hours. After demoulding at age of 24 hours (24h), the specimens were lab-conditioned (lab air). All specimens were immersed with 1/2nd (50%) of their height in water or 5% NaCl solution. The relevant conditions and specimen designations are summarized in Table 6.1. Each group (with the same steel layout and conditioning) had 2 replicate specimens.

Supply of stray current (at the level of 3 mA/cm²) started at 24h of age in the relevant conditions (the current density was calculated according to the exposed steel surface area). The experimental set-up and the electrodes' configuration for supplying stray current are also presented in Figure 6.2: two cast-in Ti electrodes (MMO Ti mesh, 40×40 mm²) served as terminals for stray current application. The conditioning of these specimens, specifically with respect to the stray current application, was performed in two phases: Phase 1 - 24h (1 day) to 28 days; Phase 2 - 72 days to 123 days. Between 28 days to 72 days, the stray current supply was cut off, the specimens were placed only in water or 5% NaCl solution. In this period, at 34 days of age, additional tests were performed, with the aim to monitor the potential changes of steel rebar due to stray current application (and/or interruption).

6.2.2 Testing Methods

6.2.2.1 Electrochemical tests

Linear Polarization Resistance (LPR) was performed at intervals of 14, 102 and 123 days. Electrochemical Impedance Spectroscopy (EIS) and Potentio-Dynamic Polarization (PDP) tests were performed at the end of conditioning (123 days). The two Ti-mesh electrodes (connected with each other) served as a counter electrode in a 3-electrode system, where the rebar was the working electrode and an external Saturated Calomel Electrode (SCE) served as a reference electrode. The details of electrochemical measurements can be seen in the previous Chapters 4 and 5.

6.2.2.2 Potential change monitoring on individual specimens

At the age of 34 days (between Phase 1 and Phase 2, when the continuous stray current supply was off), stray current was supplied on selected samples for about 1500 s, to monitor the potential change of the embedded steel undergoing stray current. This monitoring test was conducted on S(O)-1 and S(O)-2 specimens. The schematic and top-view of the specimens and

the reference electrode arrangement for potential shift monitoring on individual specimens are depicted in Figure 6.3.

As already discussed on a few foregoing occasions in this work, stray current leads to both cathodic and anodic polarization on the steel surface. The shift of the overall (mixed) potential induced by stray current flow reflects the intensity of stray current interference. The aim of this test was to monitor the potential shifts (ON and OFF potentials) of the rebar undergoing stray current, and the potential decay after stray current supply. The IR drop involved in the potential shift of rebar was also recorded and will be discussed.

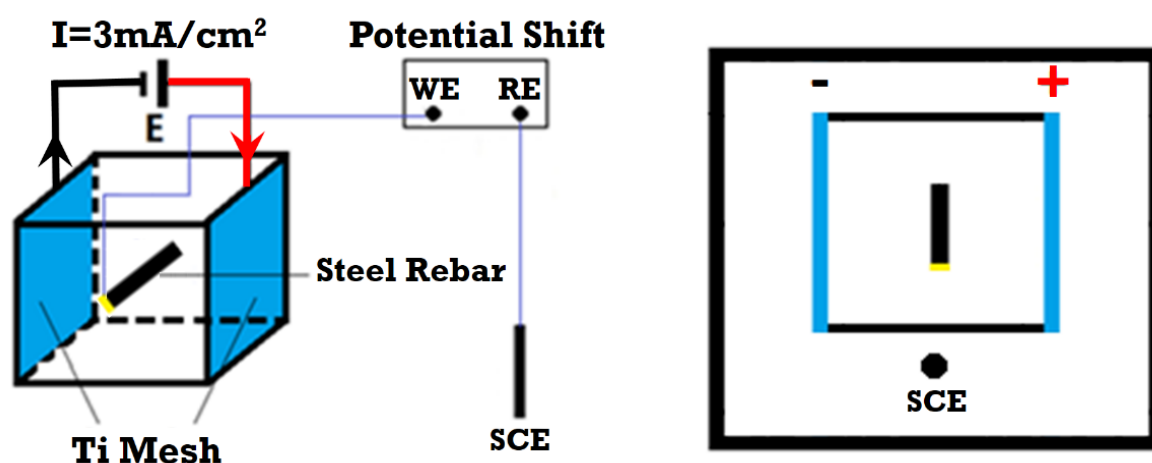


Figure 6.3: Schematic and top-view of specimen and reference electrode arrangement for potential shift monitoring on individual specimens.

6.2.2.3 Picked-up current levels in a stray current electrical field

In practice, only part of the stray current can flow into a reinforced concrete element. To simulate the situation where part of the stray current flows in the external medium, while the other part flows into the reinforced structure, the specific set-up was adopted and presented in Figure 6.4. Two external electrodes (Ti meshes) were used as terminals for current supply, and to produce a stray current electrical field. Two reinforced mortar cubes were placed in this stray current electrical field. These tests were performed at the end of test period (after 123 days of conditioning). This series of the testing procedures were conducted on specimens CS(P)-1 and CS(P)-2 in 5% NaCl solution (fully immersed).

As shown in Figure 6.4, two pieces of steel rebars were coupled to each other, as anode and cathode according to the direction of stray current supply. The aim of this arrangement is to identify the behavior of anodic/cathodic polarization during stray current supply. The electrode potential change of the rebar undergoing stray current electrical field was recorded. The current level picked-up by steel (the stray current flowing into the two pieces of steel rebars) was also obtained, by recording the potential difference via $100\ \Omega$ resistor R_0 . The potential shifts were collected and recorded by a data collector - “Ultra low input current/Instrumentation amplifier/Analog to digital convertor, Demo 2011 CvB”.

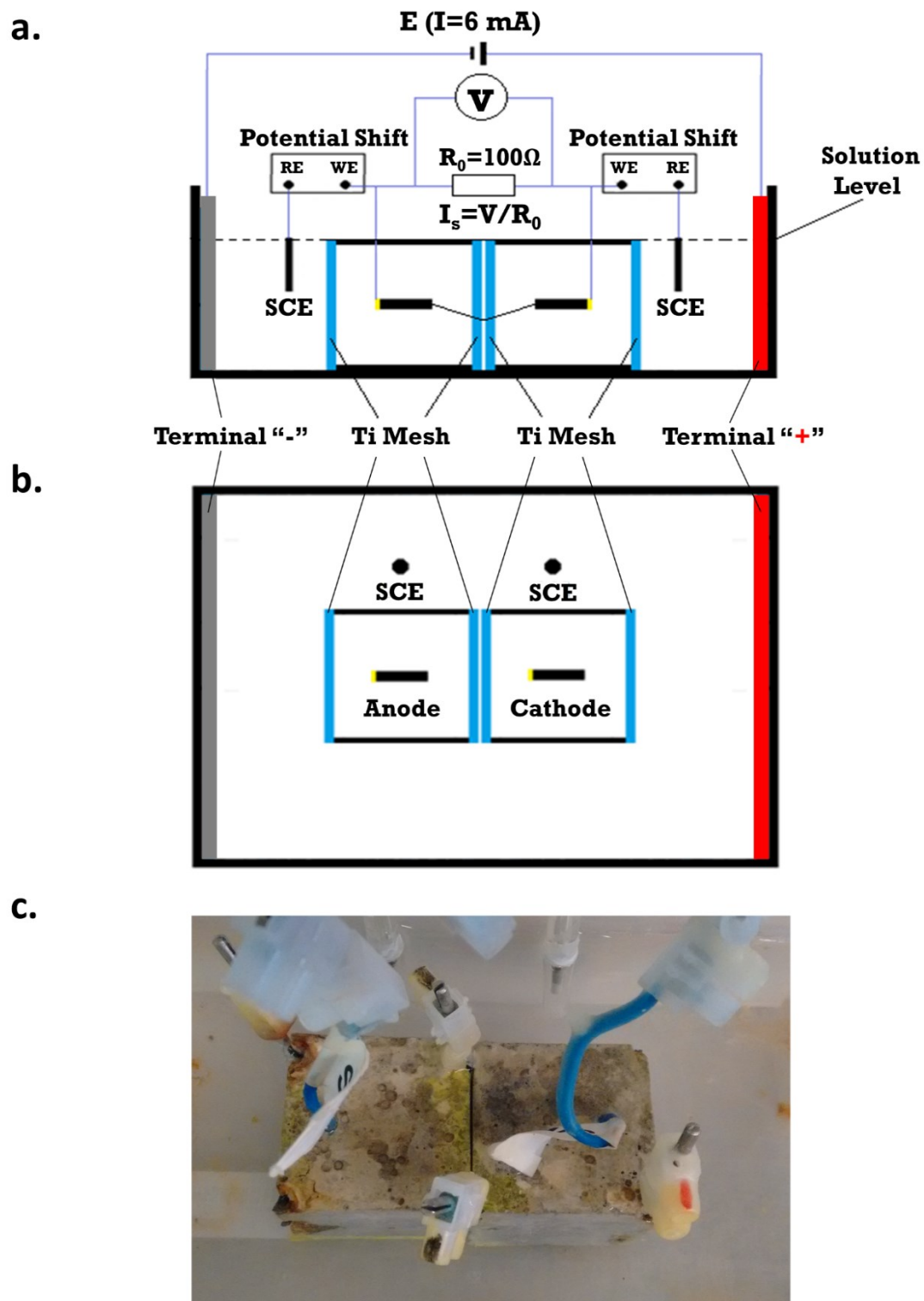


Figure 6.4: Basic testing arrangement for simulation of practical stray current electric field: a). Cross-section; b). Top-view; c). Actual testing setup.

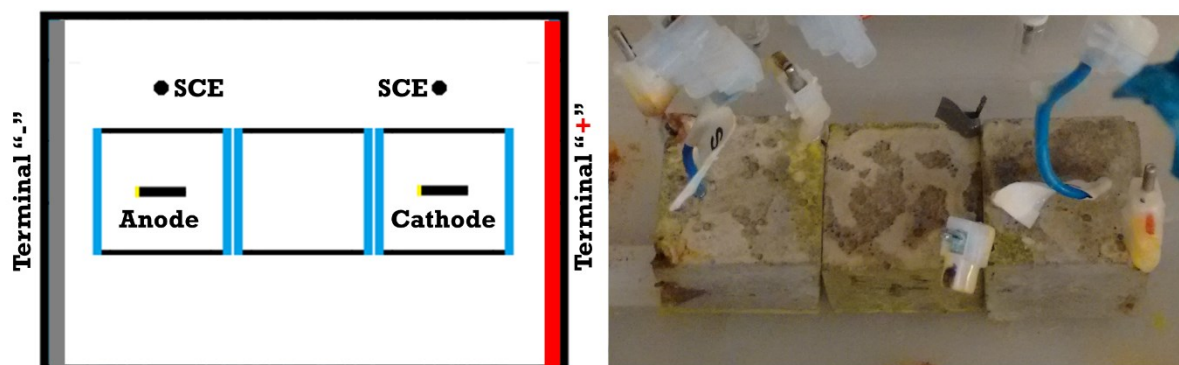


Figure 6.5: Advanced testing arrangement for simulation of practical stray current electric field: longer length of steel undergoing stray current interference.

By these tests, the better understanding of the time-dependent process of stray current interference on steel (in stray current supplying period and after stray current supply period) can be obtained. These results will also be the supporting evidence of the corrosion product distribution (e.g., the relevance of the recorded back flow to the corrosion product nearby the cathode), observed by Environmental Scanning Electron Microscope (ESEM).

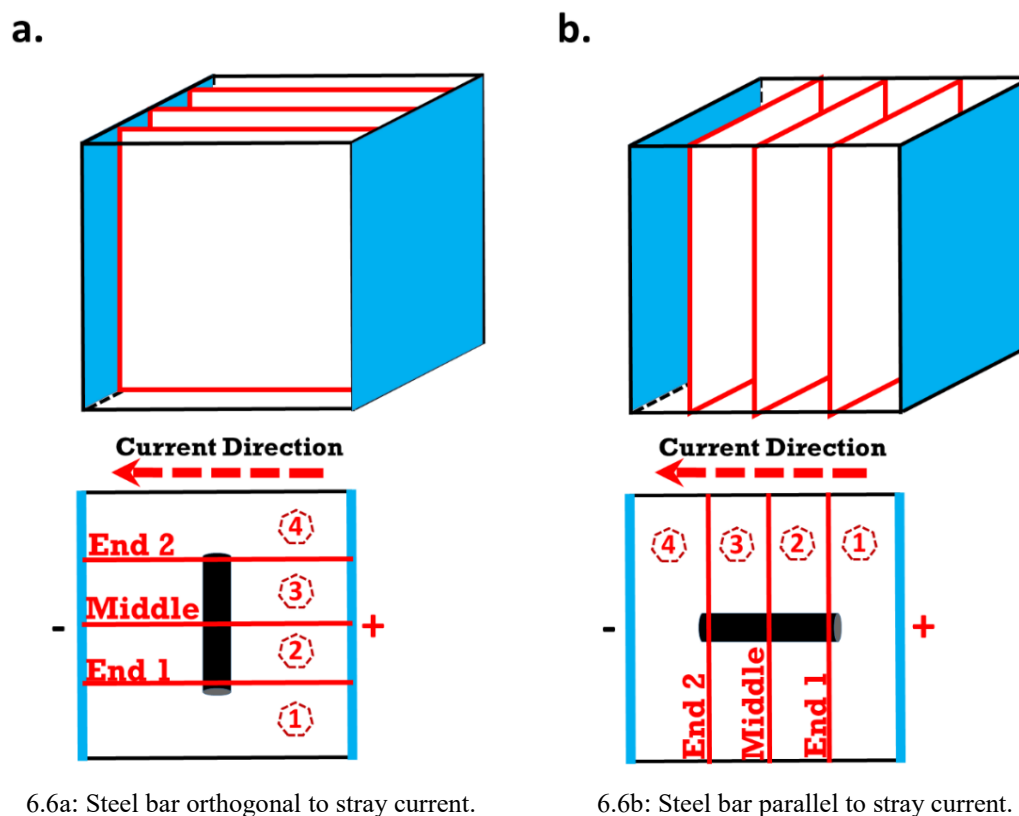
The measurement steps were as below:

- Step 1 - Stray current supply stayed off, the OCPs of the specimens were recorded;
- Step 2 - Turning on the external stray current supply for 250-300 s;
- Step 3 - Cut-off of the stray current supply, then monitor the response after cut-off for 100-150 s.

Moreover, to investigate the effect of steel length on the level of stray current-induced corrosion, an additional layout was investigated as well: adding a third plain mortar cube between two specimens, to simulate longer length reinforced element undergoing stray current (i.e., a longer distance and additional resistance between anode and cathode). The schematics for this additional testing arrangement are shown in Figure 6.5. In these tests the level of external stray current supply was 6 mA.

6.2.2.4 Microstructural observation on corrosion product distribution

At the end of test period (after all above tests), the distribution and morphology of the corrosion products formed at the steel-mortar interface were investigated using ESEM (the used equipment is ESEM Philips XL30), in a backscattered electrons (BSE) mode. The image analysis was performed at magnification 125x. The cross-sections of the steel-mortar interfaces for ESEM analysis were taken from identical geometrical locations of the cubes. Figure 6.6 depicts the sampling strategy for ESEM analysis. For each specimen, 3 cross-sections were chosen: the cross-section at middle (namely “Middle”) and 2 ends of the fully embedded steel piece (namely “End 1” and “End 2”, respectively).



6.6a: Steel bar orthogonal to stray current.

6.6b: Steel bar parallel to stray current.

Figure 6.6: Schematic and top-view of cross-sections for ESEM: a). Steel bar orthogonal to the stray current direction; b). Steel bar parallel to the stray current direction.

The cube was cut into 4 slices (Slices ①②③④), as shown in Figure 6.6). Slice ② was used for cross-section “End 1”, Slice ③ for “Middle”, and Slice ④ for “End 2”. These series of tests aimed to visually clarify the importance of steel orientation on the level of stray current-induced corrosion, i.e., positioning and distribution of corrosion products on the steel surface, as influenced by the two different manners of rebar embedment in the cubes (see Figure 6.2 and 6.6).

6.3 Results and discussion

6.3.1 OCP and R_p evolution

The average OCP/ R_p values of 2 replicates per group are shown in Figure 6.7. The OCP values for all specimens at 14 days of age are cathodic and far beyond the passivity threshold. This is due to the “fresh” mortar matrix (only 24h fog room curing). After 102 days a more passive state is recorded for Cl-free cases. Additionally and with respect to positioning of the steel rebar in control (Cl-free) conditions, the following can be noted: specimens S(O) exhibit more anodic potentials (more noble). This is accompanied by higher R_p values. In contrast, specimens S(P) present the relatively active state, judged from both OCP and R_p values.

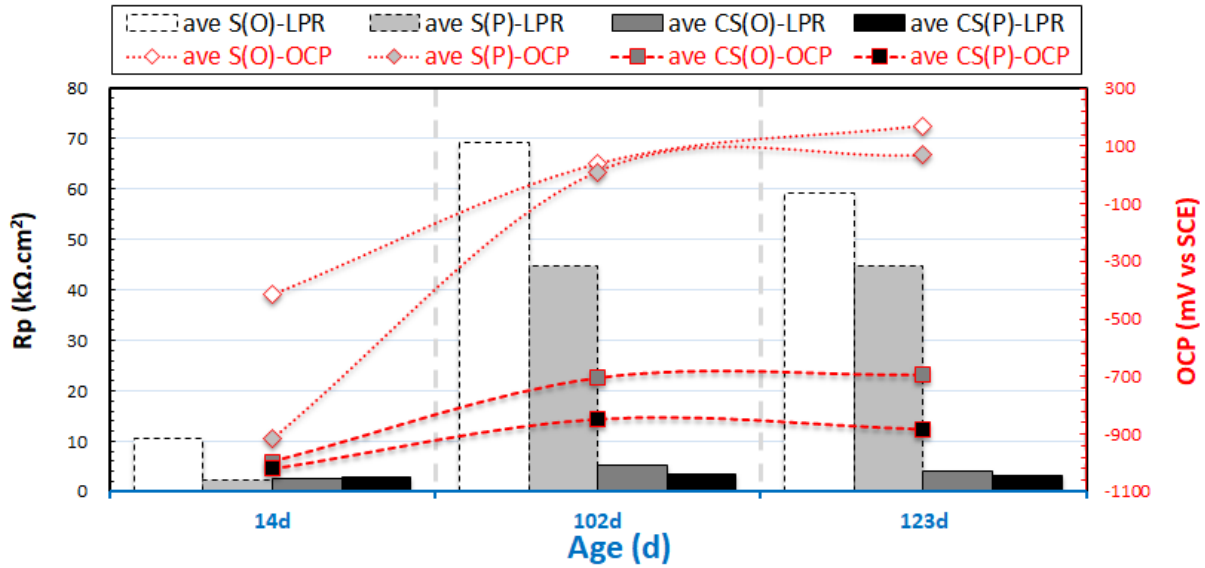


Figure 6.7: Comparison of average OCP/ R_p values of Cl-free groups: S(O) and S(P); and Cl-containing groups: CS(O) and CS(P).

For the Cl-containing medium, as expected, the OCP values of Cl-containing specimens always remained negative. This, together with the recorded low R_p values (compared to the Cl-free situations), indicate an accelerated corrosion state of the steel rebar. In these cases, the coupling effect of stray current and Cl^- is relevant. At the end of conditioning (123 days), the most corrosive state is recorded for CS (P) specimens, exhibiting lower R_p values and more cathodic OCP values than CS (O) specimens.

It can be noted that the geometrical position of the steel affects the electrochemical response. The stray current interference is more significant for a steel bar parallel to the current direction, compared to the case of steel bar orthogonal to the current direction. This is in the sense of minimal polarization for the orthogonal cases - S(O) and CS(O), or significant polarization for the parallel groups - S(P) and CS(P)) due to stray current flow. In the former case, the effect of stray current is limited to the cross section of the bar only. Consequently, specimens S(O) and CS(O) present higher corrosion resistance. In the latter case, the effect of stray current is significant, since the full length of the bar is exposed to the field of stray current flow. Therefore, specimens S(P) and CS(P) are in a more active state, irrespective of the presence or not of Cl^- in the medium.

6.3.2 PDP and EIS

PDP and EIS were performed to further clarify the corrosion performance of the tested specimens. PDP results (at 123 days) are presented in Figure 6.8 for the S-specimens (treated in water), and in Figure 6.9 for the CS-specimens (treated in 5% NaCl). The experimental impedance responses in Nyquist format for all samples at the end of conditioning (at 123 days) are presented in Figure 6.10 and 6.11.

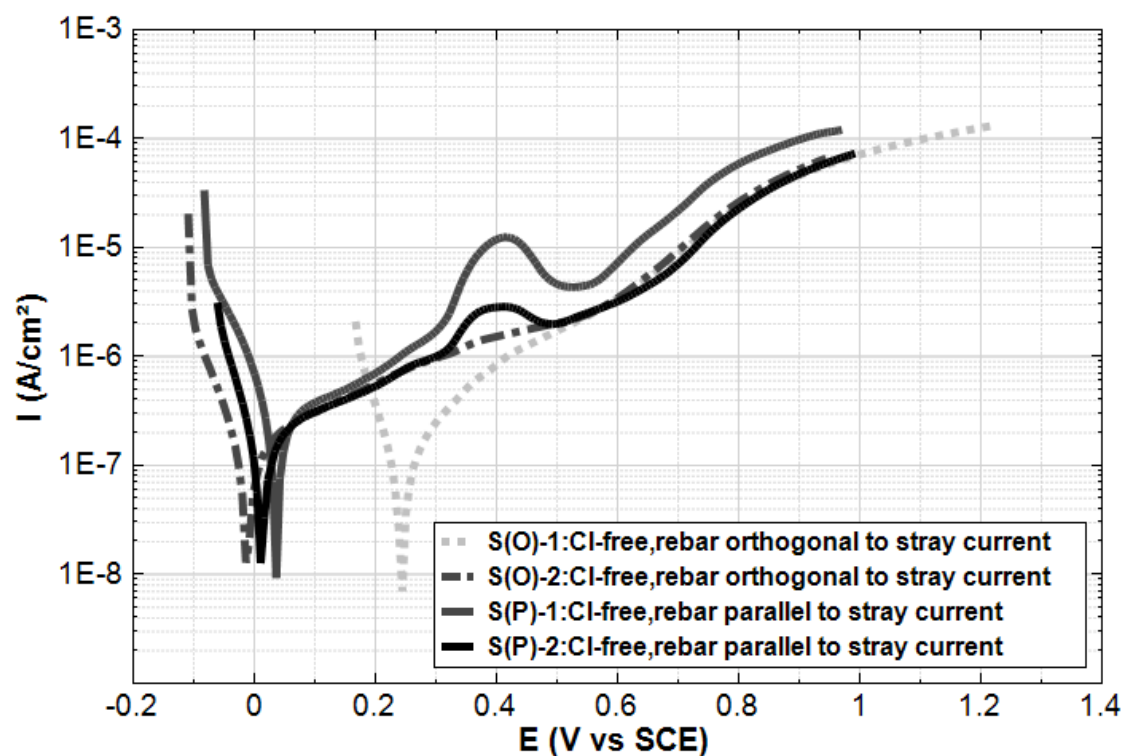


Figure 6.8: Overlays of PDP response for Cl-free specimens at 123 days.

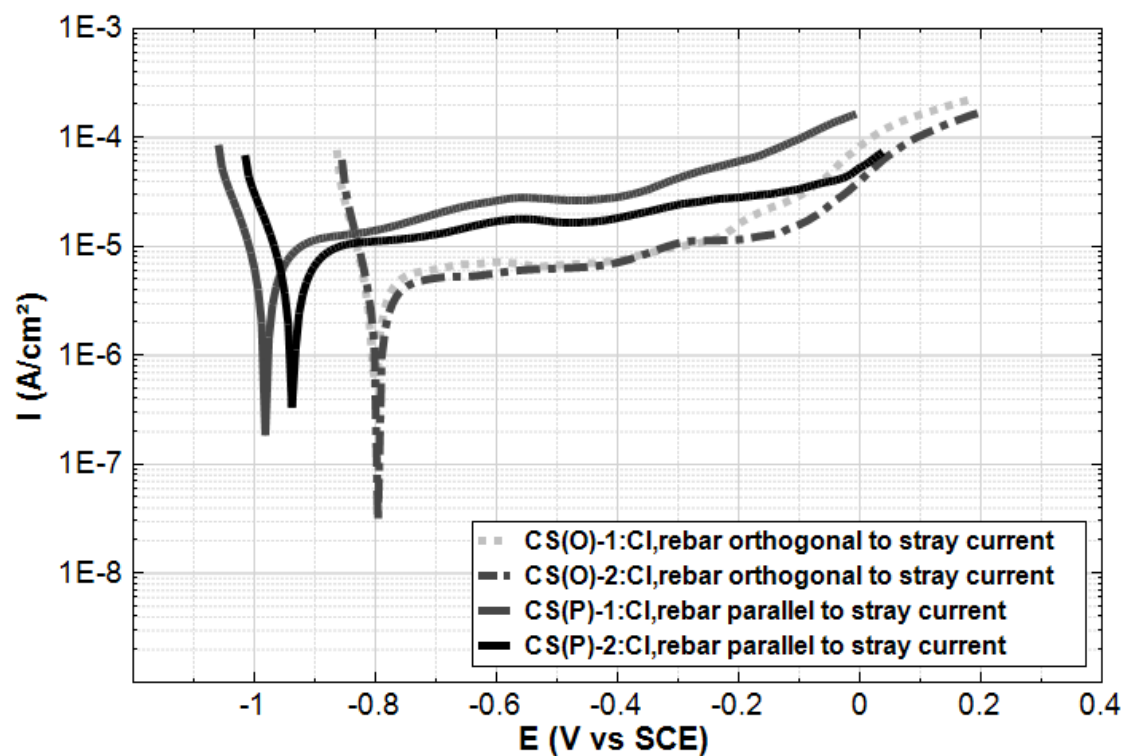


Figure 6.9: Overlays of PDP response for Cl-containing specimens at 123 days.

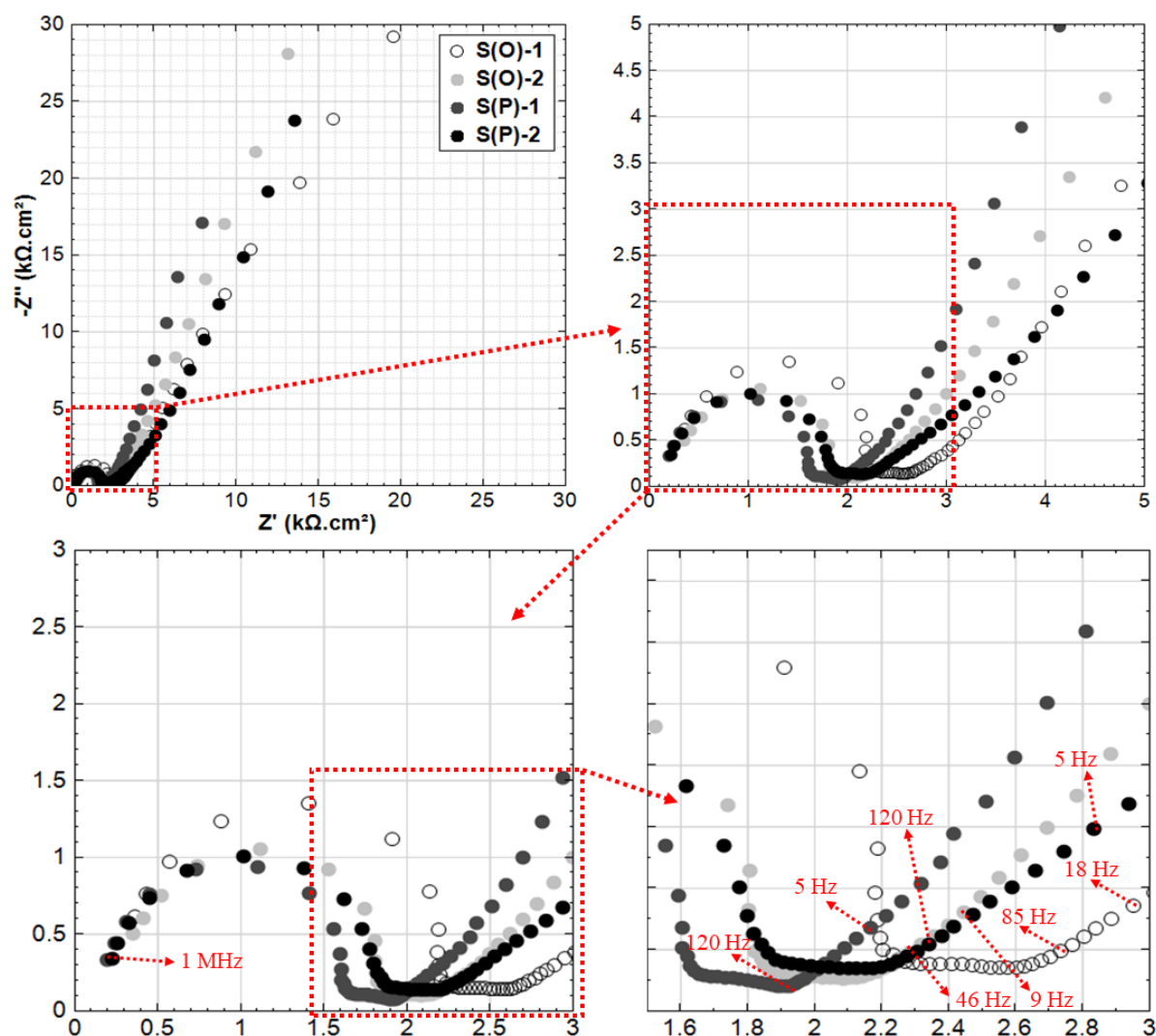


Figure 6.10: Overlays of EIS response for Cl-free specimens at 123 days.

According to the corrosion potential and anodic current density in Figure 6.8, the corrosion resistance of the S(O) groups is higher than that for the S(P) groups. The highest anodic current density is recorded for S(P)-1 specimen. At about +420 mV (vs SCE) a current maximum (ca. $15.92 \mu\text{A}/\text{cm}^2$) is observed for the S(P)-1 specimen, which is related to the dissolution of iron oxide/hydroxide layer previously formed on the steel surface [500-502]. Similar behavior with an anodic current peak at +400 mV (vs SCE) is found for S(P)-2 specimen. An indication for dissolution of product layer (anodic current peak) is not observed for S(O)-1 and S(O)-2. This implies the lack of or a minimum amount of product layer on the steel surface of the S(O) cases.

The PDP responses of S(P)-1 and S(P)-2 specimens are in line with the EIS. A time constant at MF (middle frequency, between 120 Hz and 5 Hz) can be observed for S(P) cases - the $|Z|$ value in MF of S(P)-1 is 3.6Ω , which is higher than 2.2Ω of S(P)-2. While this time constant is much less pronounced for the S(O) specimens and shifted in frequency - see Figure 6.10. This, together with the anodic peaks of PDP, imply the more significant deposition and potential variations in the product layer properties/performance for S(P) cases.

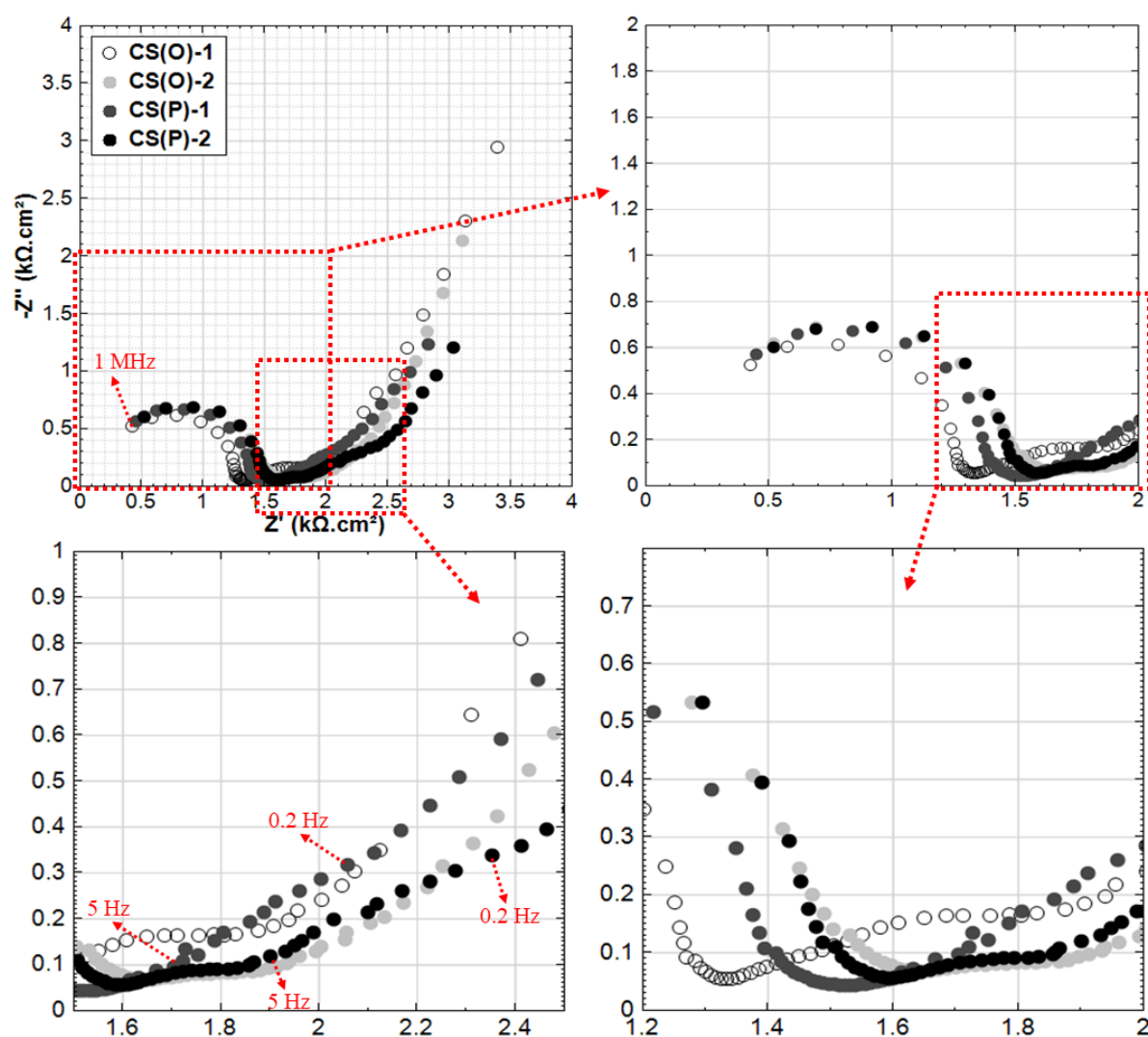


Figure 6.11: Overlays of EIS response for Cl-containing specimens at 123 days.

Judging from thermodynamic principles, the E/pH region i.e. +420 mV (vs SCE)/pH~13 (conditions relevant to specimens S(P)-1 and S(P)-2), the layer is most likely Ca-substituted $\text{Fe}_2\text{O}_3 \cdot n\text{H}_2\text{O}$ and/or a mixture of oxide and hydroxide [471]. Ca-containing product layer stabilizes the passive layer on the steel surface and further leads to a more uniform attraction and adherence of Ca^{2+} , resulting in a product layer with higher stability of S(P) groups [471]. Based on the PDP and EIS, it can be hypothesized that in the case of S(P) specimens a product layer of different amount, and/or distribution on the steel surface was formed. This is an indication of the more significant effect of stray current in S(P) groups, if compared to the S(O) groups (orthogonal direction of the steel).

The anodic current of PDP response for the Cl-containing CS specimens (Figure 6.9) is one order higher than S groups (Cl-free), indicating the much more active status of CS specimens. This can also be reflected by the EIS LF responses of groups CS(O) and CS(P) (specimens immersed in 5% NaCl). The slope of the anodic curves (PDP) in the potential range after +30 mV (vs E_{corr}) in anodic direction, accounts for limitations of the anodic dissolution (although

the anodic currents remain significantly higher if compared to those for specimens S). This means that in CS groups a corrosion products layer exists on the steel surface and causes limitations to the dissolution process within anodic polarization.

The CS(P) specimens show higher anodic current compared to CS(O) cases. It can be judged from PDP, that the effect of stray current is more pronounced in the CS (P) group. Additionally, the small peaks in the CS(P) cases are recorded after -0.6 V (vs SCE) in the PDP (Figure 6.9). This points to a more significant accumulation of corrosion products on the steel surface of the specimens CS(P), compared to other cases.

Besides, there is also another observable difference between the CS(O) and CS(P) groups, judged from EIS tests. If the HF to MF response is compared in Figure 6.11, we observe an additional time constant appears (between 5 and 0.2 Hz), especially pronounced for the CS(P) specimens. This time constant is linked to the abovementioned more pronounced accumulation of corrosion product over a larger surface of specimens CS(P). This time constant (between 5 and 0.2 Hz) is already in different frequency window compared to the control cases. These outcomes, together with the indication of PDP of the CS(P), again illustrate the larger stray current effects in the CS(P) groups, compared to CS(O) specimens. The above electrochemical behavior is well supported and visualised by ESEM observations at the steel-mortar interface, which will be discussed in Section 6.3.5.

6.3.3 Potential change monitoring on individual reinforced mortar specimens

At the age of 34 days, stray current was supplied on selected specimens, for about 1500 s, to monitor the potential change of the embedded steel undergoing stray current. These tests, as introduced in Section 6.2.2.2, were performed on orthogonal specimens S(O)-1 and S(O)-2. The test results in this section aim to justify the importance of the bulk matrix properties, on the level of current picked-up by the reinforcement. These specimens are meant to illustrate the stray current flowing paths, since the most significantly different performance is observed for S(O)-1 and S(O)-2, in both PDP tests (E_{corr} values) and HF EIS (bulk matrix resistance), irrespective of the fact that S(O)-1 and S(O)-2 are replicates.

As can be seen in Figure 6.12, an anodic potential shift of S(O)-1 is recorded at the instant once the current supply is on - the potential increased immediately after the stray current application, from $E_{\text{off2}} = -140\text{ mV}$, to the stable value of $E_{\text{on}} = 178\text{ mV}$. This E_{on} potential of 178 mV reflects the stray current-induced anodic polarization on the rebar. When the current is interrupted, a potential decay is recorded, reaching the value of -150 mV (E_{off2}). This value (E_{off2}) is similar to the initial E_{off} of -140 mV , however, with 10 mV more cathodic. The anodic potential shift from E_{off1} to E_{on} , together with the adopted more cathodic value of E_{off2} , compared to E_{off1} , imply a process of steel dissolution. Fundamentally, the driving force for steel corrosion is anodic polarization (the potential change from E_{off1} to E_{on} is an anodic shift) - this is the primary kinetic effect in steel corrosion.

Upon stray current interruption and prior to E_{off2} stabilization (Figure 6.12), the potential-time curve includes the so-called ohmic drop (IR drop) component, equal to 271 mV for the S(O)-1 case. From this point forward (i.e. after the so-called instant-off potential $E_{\text{ins.off}} = -93\text{ mV}$) a decay of 57 mV is observed. The IR drop contribution disappears in a very short time, normally in the order of 10^{-6} s [62, 503, 504]. The potential decay (57 mV) means that indeed, the steel bar is polarized by the applied stray current, inducing an overall positive potential shift under current conditions. This means that in this situation, anodic polarization induced by stray

current is a predominant phenomenon i.e. the stray current causes positive polarization, hence, enhances the driving force of steel corrosion following the principles of fundamental electrochemical kinetics.

A similar trend can be found for S(O)-2 (Figure 6.13): the IR drop of 217 mV and a potential decay of 125 mV can be observed after the shut-down of current supply. The lower IR drop of S(O)-2 (compared to S(O)-1) reflects the lower resistance of mortar bulk matrix of S(O)-2. The higher potential decay of S(O)-2 implies the more efficient polarization of this rebar, undergoing the identical to S(O)-1 stray current supply. This again reflects the lower resistance of the mortar bulk matrix of S(O)-2, because if the lower resistance of bulk matrix (compared to S(O)-1) was at hand, the stray current can flow into the steel more easily. The sequence of this is the more significant corrosion of S(O)-2.

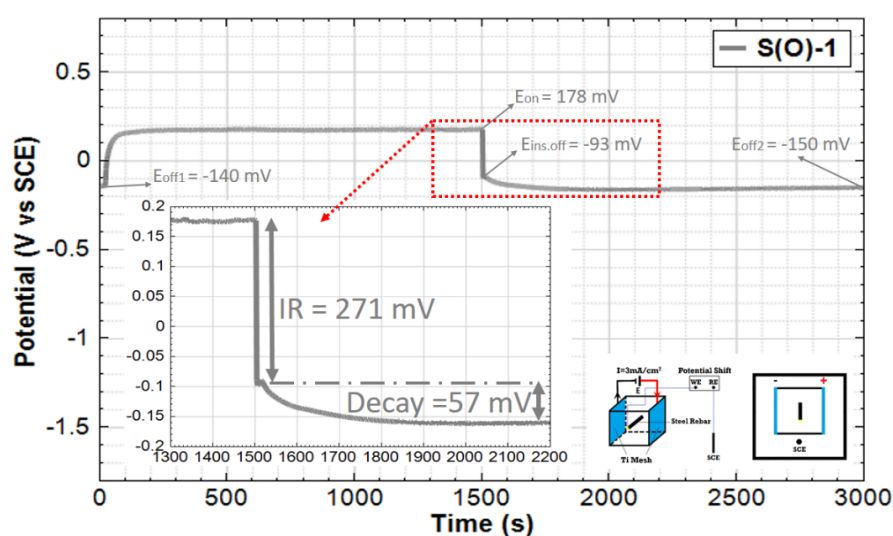


Figure 6.12: Monitoring of potential shift undergoing stray current: S(O)-1. (specimen and reference electrode arrangement for potential shift monitoring in Figure 6.3).

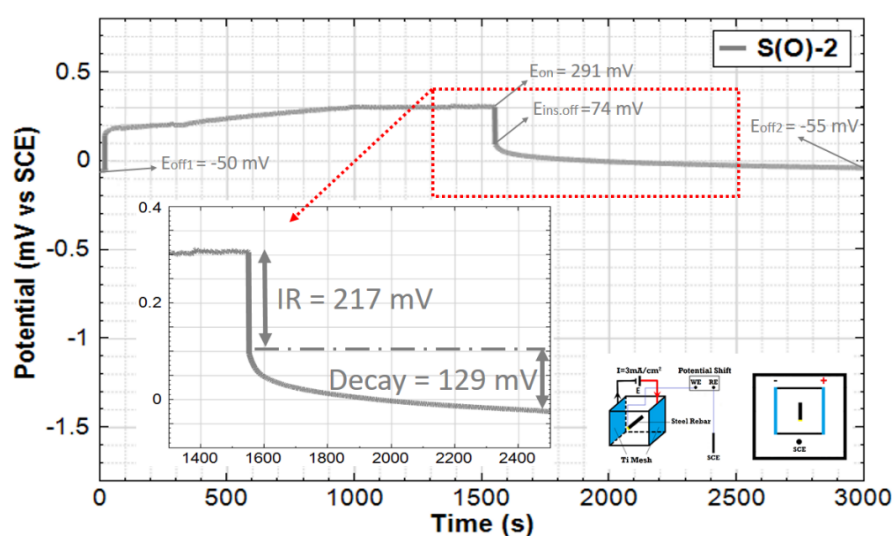


Figure 6.13: Monitoring of potential shift undergoing stray current: S(O)-2. (specimen and reference electrode arrangement for potential shift monitoring in Figure 6.3).

The lower bulk matrix resistance of S(O)-2 is in accordance with the lower $|Z|$ of EIS HF response (Figure 6.10), as already discussed in Section 6.3.2. The lower corrosion resistance of S(O)-2 can also be verified by the PDP (Figure 6.8): the corrosion potential of S(O)-1 is 200 mV more noble than S(O)-2, corrosion current for S(O)-2 is higher. A gradual increase of anodic current with PDP polarization after corrosion potential is recorded for S(O)-1, while there is anodic limitation for S(O)-2. This means that a less significant corrosion product accumulation is relevant for S(O)-1, compared to S(O)-2.

6.3.4 Mechanism of stray current-induced corrosion initiation with respect to geometrical orientation of the bar

Based on the above results, it can be concluded firstly that, the stray current interference is more pronounced for a steel bar parallel to the current direction than the case of steel bar orthogonal to the current direction. The schematics of stray current parallel or orthogonal to steel rebar are shown in Figure 6.14 and 6.15, respectively.

In the former case, parallel position, the effect of stray current is significant, since the full length of the bar is exposed to the field of stray current flow, i.e., the portion of stray current “picked-up” by the bar flows through the full length of rebar, since the bar is the least resistive path. However, for the orthogonal case, the effect of stray current is limited to the cross section of the bar only.

As already explained in Chapter 2 (Figure 2.10), once the stray current is picked-up by the steel rebar of a reinforced concrete structure, the cathodic and anodic polarized regions (where ψ_c and ψ_a take place, respectively) are stimulated on the surface of steel. If stray current can be “picked-up” by the steel reinforcement, a driving voltage ($\Delta U = \psi_c + \psi_a$, see Figure 6.14 and 6.15) has to be present.

This driving voltage (ΔU) is the potential difference (produced by supplied stray current surrounding the steel rebar) between the cathodic and anodic polarized regions, equals to $L \cdot \lambda \cdot I$: $\Delta U = L \cdot \lambda \cdot I$, where, L is length of anodic and cathodic sites of steel undergoing stray current; λ is resistance of mortar matrix per unit length; I is stray current flowing in mortar matrix. If stray current can be picked-up by steel, ΔU must be higher than the sum of the cathodic (ψ_c) and anodic (ψ_a) polarizations induced by inflow and outflow of stray current circulating in the steel, i.e., $L \cdot \lambda \cdot I > \psi_c + \psi_a$. The higher L , the higher driving voltage (ΔU) is present and the easier stray current can be picked-up by steel - and vice versa.

Besides inducing corrosion, stray current can also result in the different distribution of corrosion products. Stray current produces the variation of distribution of anodic and cathodic sites (with a distance of L) on steel surface. For the parallel situation (Figure 6.14), the L (length of steel conducting the current) is longer than orthogonal situation (Figure 6.15), i.e., in the parallel situation the distance of anodic and cathodic regions is longer than that in orthogonal situation. In the parallel case, with long distance between the anode and cathode, stray current induces a macrocell-like corrosion. Corrosion products do not accumulate at the exact anodes where current flows out, but nearby the anodic sites. For the orthogonal case with shorter distance between the anode and cathode, a microcell-like corrosion mechanism is relevant, where many microcells will finally result in a corrosion damage at this particular cross section. In both situations and as a next step, the accumulated corrosion products occupy the steel-bulk matrix interface (as discussed in Chapter 5) and further can penetrate into the bulk matrix. The

propagation of corrosion product into the mortar matrix is observed by ESEM, and will be discussed in the next section.

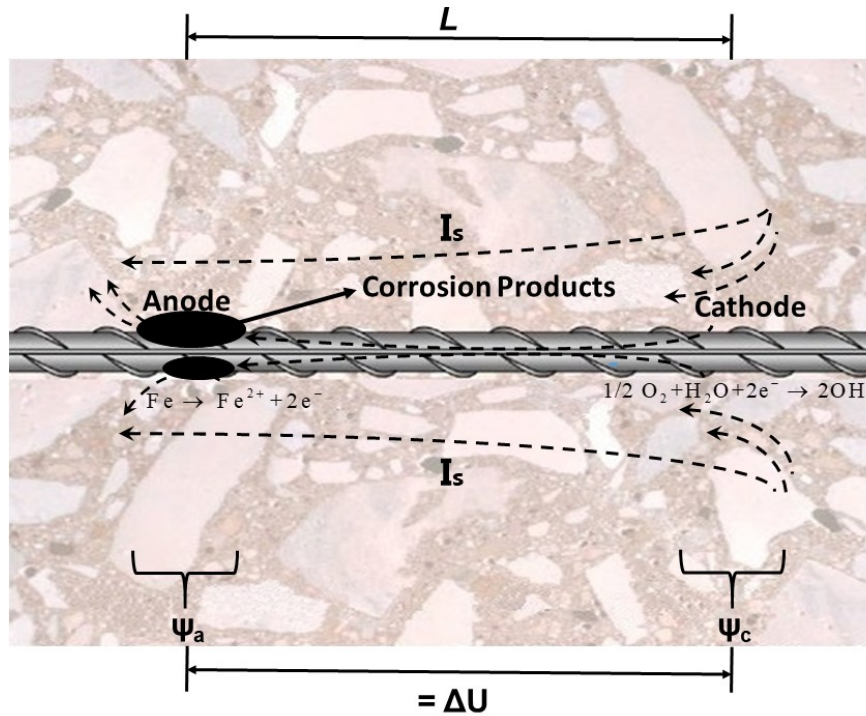


Figure 6.14: Schematic of stray current parallel to steel rebar: Macrocell-like, tends to induce localized corrosion.

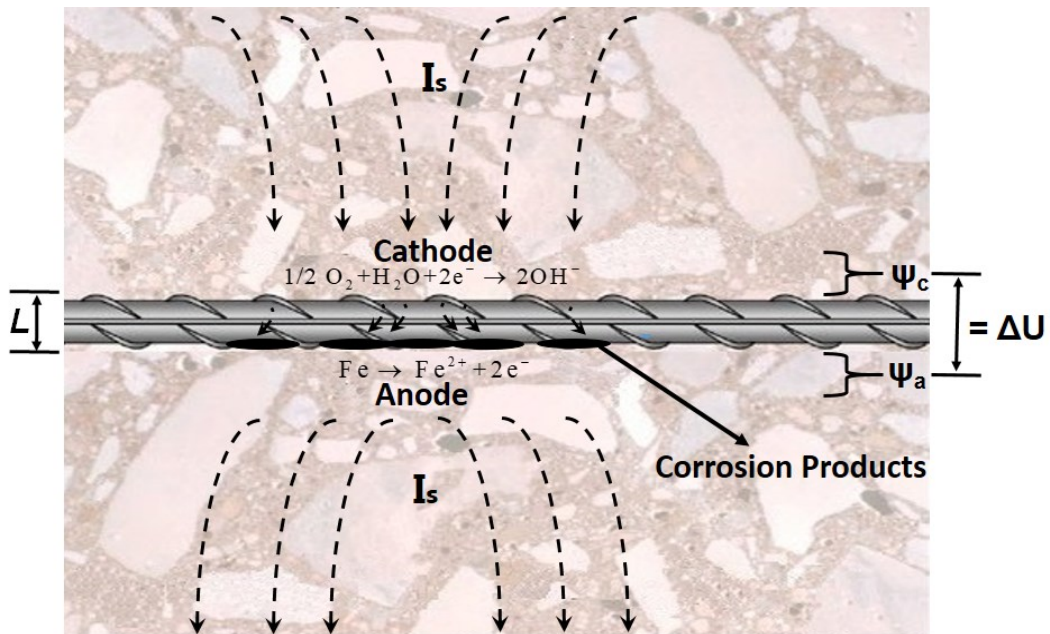


Figure 6.15: Schematic of stray current orthogonal to steel rebar: Microcell-like, tends to induce general/uniform corrosion.

6.3.5 ESEM observation

The combination of ESEM observations and the obtained electrochemical parameters reflect the distribution of corrosion product on the steel surface. Hence a better insight into the mechanisms of stray current corrosion can be achieved. To this aim, the ESEM observations were performed on only corroding cases, where the corrosion products are more pronounced and visible than in the control cases.

The ESEM images taken at different locations of “End 1” and “Middle” cross-sections of CS(O)-1 are shown in Figures 6.16 and 6.17. The images of “End 1” and “End 2” cross-sections of CS(P)-2 are shown in Figures 6.18 and 6.19. The location of each cross-section of specimen is also illustrated in the inlet of according figures.

These series of images aim to visualise the effects of rebar orientation, on distribution of corrosion product along radial direction: CS(O)-1 for steel rebar orthogonal to stray current, and longitudinal direction: CS(P)-2 for steel rebar parallel to stray current. For instance, the anode is expected to be mostly corroded (because of current outflow), the corrosion product may be localized at the anodic site, which is determined by the direction of stray current.

As can be seen in Figures 6.16 and 6.17, the “anode” and “cathode” coexist in both cross-sections of CS(O)-1 according to the direction of stray current flow. In this situation the anode and cathode are close by (distance between them is just the rebar diameter 6 mm). For CS(P)-2 as indicated in Figures 6.18 and 6.19, the “anode” is the whole “End 2” cross-section, “cathode” is the whole “End 1” cross-section. The distance between anode and cathode is the length of rebar (2 cm).

As can be seen in Figure 6.16, more corrosion product is accumulated on the “anode” side (see Plot 4, 5, 6 in Figure 6.16) of the “End 1” cross-section of CS(O)-1. Similar trend is observed in Figure 6.17 - the most severe corrosion is observed at the “anode” side (see Plot 5, 6, 7 in Figure 6.16) of the “Middle” cross-section of CS(O)-1. This is obviously attributed to the stray current direction.

It can be noted that the corrosion product is also formed at the “cathode” location (Plot 2 in Figure 6.16 and 6.17) in both cross-sections of CS(O)-1. However, the corrosion damage at the “cathode” side is visually much less than that at the “anode” side. The corrosion at “cathode” here is attributed to Cl^- in the vicinity of steel surface. Another cause for the corrosion at “cathode” is the back flow of current once the stray current is switched off. The back flow is induced by the potential difference between anode and cathode when the stray current supply is on. Once the stray current is cut off, a reversed current will flow from “anode” to “cathode”. This back flow is actually recorded and will be discussed in the next Section 6.3.6.

As for the cross-sections of CS(P)-2, much more corrosion product is observed at the “anode” location (Figure 6.18), i.e., “End 2” cross-section (compare to “cathode” - “End 1” cross-section in Figure 6.17). It is obvious that the corrosion accumulation at the “anode” of CS(P)-2 is more intensive than the “anode” of CS(O)-1. As can be observed in Figure 6.18 in some locations of “anode” of CS(P)-2 (“End 2” cross-section), the corrosion product even penetrates into the surrounding mortar matrix (Plots 1, 3, 6, 7 in Figure 6.18). This verifies the hypothesis proposed in section 6.3.4: stray current parallel to steel rebar leads to localized corrosion more easily.

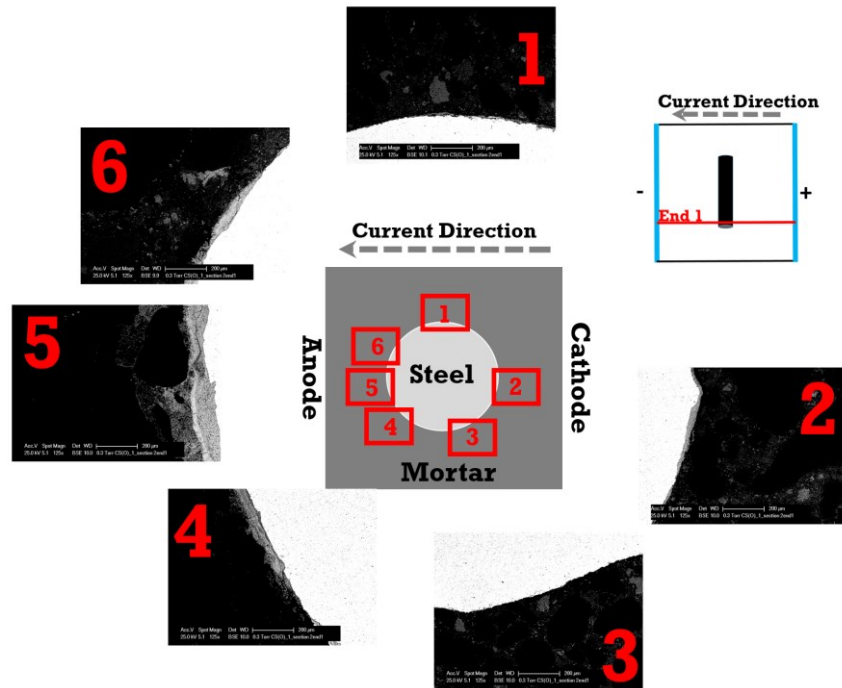


Figure 6.16: ESEM images (BSE mode) at different locations of the steel-mortar interface, the “End 1” cross-section of CS(O)-1.

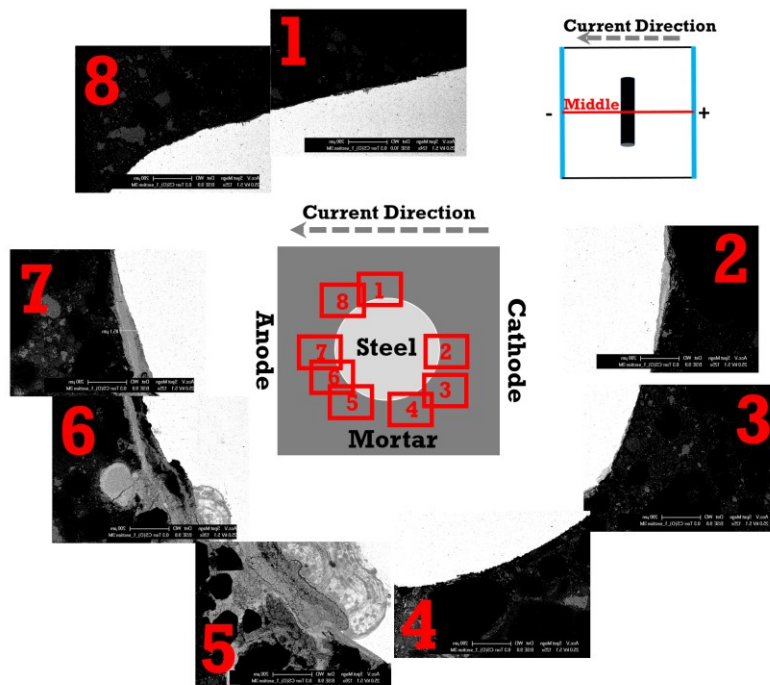


Figure 6.17: ESEM images (BSE mode) at different locations of the steel-mortar interface, the “Middle” cross-section of CS(O)-1.

For the “cathode” of CS(P)-2 (“End 1” cross-section), the corrosion product is only observed at Plots 1, 2, 5, 6 (see Figure 6.19). The substantial penetration of corrosion product into the mortar matrix is not observed in “cathode” cross-section. This may be because the cathode is far away from the anode. Hence there is more resistance to the back flow towards the cathode in this situation. All these observations again indicate the effect of steel rebar orientation on distribution of corrosion product induced by stray current: the rebar parallel to stray current leads to more significant corrosion than rebar orthogonal to stray current.

6.3.6 Picked-up current monitoring

As aforementioned, the aim of these tests (as introduced in Section 6.2.2.3) was to monitor the picked-up stray current level. The stray current electrical field was simulated in 5% NaCl medium (as external environment). The obtained test results are the supporting evidence of the corrosion product distribution (for example, due to the recorded back flow), observed by ESEM.

As shown in Figure 6.20, the current level picked-up by steel is around 0.01 mA of the peak value. In this simulated stray current electrical field, it is clear that only small part of the supplied stray current can flow into the steel rebar. The IR drops are clearly recorded instantaneously after application and cutting off of the current. At the instant the stray current is applied, it is clear that CS(P)-1 is the cathode and CS(P)-2 the anode, according to the negative potential shift for steel piece CS(P)-1 and positive for CS(P)-2. This trend can also be judged by the constant direction of current flowing within the steel pieces (i.e., the negative sign of current): the current flows into CS(P)-1 firstly (cathodic current), flows through the shunt resistor R_0 , and finally flows out (anodic current) at the steel piece of CS(P)-2. In the present work, the sign of the current is defined as the current direction: the negative sign means the current flowing from CS(P)-1 to CS(P)-2, while the positive values of current show the opposite direction of current flow.

What can clearly be observed is that the stray current flowing into the steel rebar is decreasing. As can be seen in Figure 6.20, after the current is just supplied (i.e., after the “ON” point), the measured current level sharply changes from zero to around -0.01 mA, thereafter decreases. This observation can be attributed to the coexistence of polarization resistance and double layer capacitance on the steel-mortar interface (i.e., a typical Randles circuit). The transient response of steel surface induced by a given electrical interference is governed by the property of this Randles circuit [504].

Upon applying the stray current electrical field, part of current is picked-up by the steel. The picked-up current flowing in steel contains two components in parallel: part of it is “Non-faradic current”, which can only play role on charging the double layer capacitance (for CS(P)-1 is charging, while for CS(P)-2 is discharging when current is just “ON” as shown in Figure 6.20); simultaneously the other part of current takes part in the redox reactions (CS(P)-1 is reduction due to cathodic current, while CS(P)-2 is oxidation because of anodic current), which is the so-called “Faradic current” [505-512]. Once the double layer capacitor is fully charged, only the “Faradic current” can circulate within the steel. This is the reason why the picked-up current is decreasing.

At the instant of $t = 300$ s (see Figure 6.20), when the stray current supply is turned off, a sudden positive increase of current flowing within steel pieces is monitored (i.e., back flow), again followed by the decrease of current level. This abrupt alternation of negative to positive sign of the picked-up current, implies a direction change of the current flowing within the steel

pieces. This is attributed to the potential difference between cathode and anode, previously induced by inflow and outflow of stray current. This recorded back flow is the supporting evidence of the corrosion product distribution, i.e., the relevance of back flow to corrosion product nearby the cathode.

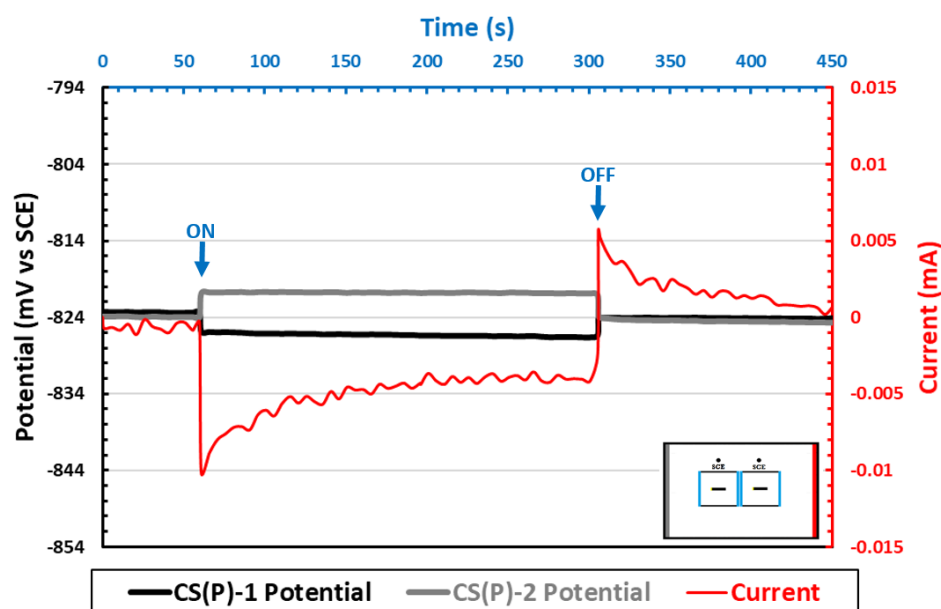


Figure 6.20: Response of CS(P)-1/CS(P)-2 (basic arrangement) undergoing simulated practical stray current electric field (6 mA) in Cl^- containing environment. (test arrangement in Figure 6.4, performed after 123d).

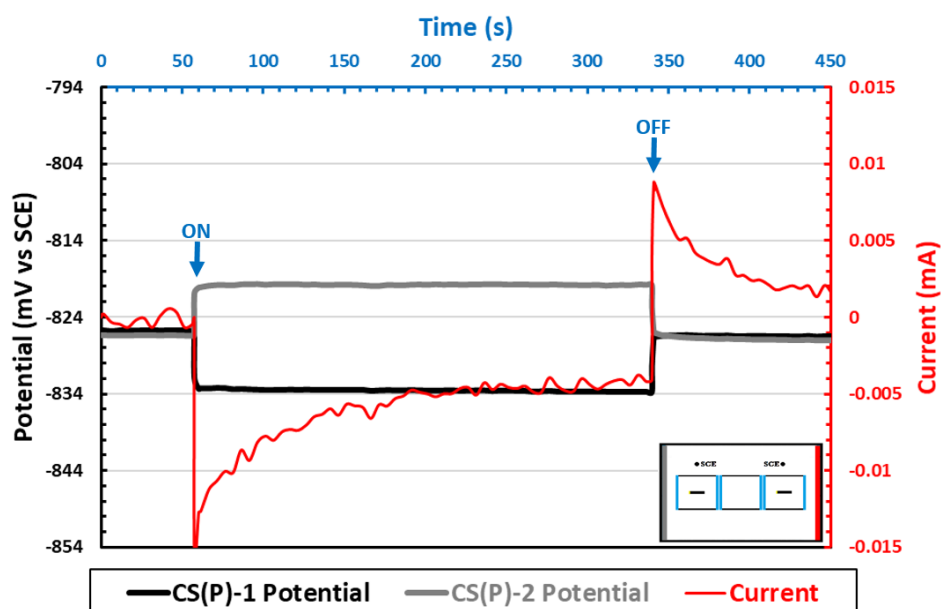


Figure 6.21: Response of CS(P)-1/CS(P)-2 (advanced arrangement, longer length of steel undergoing stray current) undergoing simulated practical stray current electric field (6 mA) in Cl^- containing environment. (test arrangement in Figure 6.5, performed after 123d).

As already introduced, the longer distance between 2 pieces of steel bars (i.e., anode and cathode) was produced (another non-reinforced cube was placed between CS(P)-1 and CS(P)-2, see Figure 6.5). It can be observed in Figure 6.21 that similar trends/shapes of time-dependent response are recorded. However, this “3 cubes case” shows the higher values for the level of picked-up current and higher potential shift. In other words, the response of “3 cubes case” is more intensive than the “basic arrangement”. In the “3 cubes case”, the resistance of the bulk matrix between anode and cathode is higher. This case shows more significant “Macrocell-like” behavior, and undergoes more intensive polarization (resistance polarization). The consequence of the above is the higher stray current interference on steel surface. This implies that, for practical reinforced concrete structure, once the contacts of steel bars (between main reinforcement and stirrup) are loose, the stray current corrosion will be more severe at the anodic locations. In this situation the resistance between steel bars is higher, and the macrocell is more easily to be produced by stray current, hence the polarization effects induced by stray current are more significant.

As can be observed in Figure 6.21, a potential difference between the 2 steel bars has been established at the time interval of 50-340 s, which is due to the stray current interference: CS(P)-1 is cathode, and cathodically polarized because of current inflow; however CS(P)-2 is anode, anodically polarized due to the current outflow. At the instant when the stray current is just absent, the induced potential difference between anode and cathode still exists (at 340s). This induced potential difference leads to an opposite current flow from the previous anode to the previous cathode.

In other words, the spontaneous interconversion between anode and cathode occurs just after the instant as the stray current is cut off. This means that in case of stray current-induced corrosion, corrosion (anodic reaction, i.e., the steel dissolution) can not only occur at the location (the anode) where picked-up current flows out when stray current is present, but also on the position where stray current flows into the steel (previous cathode, but transformed to anode) when stray current is just off. This is actually observed by ESEM. If insulation on reinforced elements is adopted (a coating for example) to mitigate the stray current corrosion, not only the area of the anode portion induced by stray current should be insulated, but also the location nearby the anode, to prevent the back flow around the anode portion after the stray current attack. In fact, a best case scenario would be to insulate the full length of the conductive path (both anode and cathode). This aims to absolutely cut off the stray current picking-up and leaving paths.

6.3.7 Summary of effects of steel rebar orientation on stray current-induced corrosion

In summary, compared to the situation of a steel bar orthogonal to the current direction, the more significant corrosion states are recorded when the steel bar is parallel to current direction. Stray current parallel to steel rebar tends to induce localized corrosion, in contrast the orthogonal situation leads to relatively uniform corrosion on the affected area. At the instant that the stray current supply is turned off, an opposite current flow (back flow) from the previous anode to the previous cathode is recorded. According to these results, some recommendations for the related challenges in civil engineering practice are as below:

To evaluate the stray current corrosion possibility, the reinforced concrete element parallel to stray current should be firstly inspected. Sectionalization of reinforced concrete structures (similar to the principle of general expansion joint in civil engineering) is a possible solution

for reducing the stray current effect, as it is found that the longer length of steel rebar leads to more severe corrosion damage. The sectionalized structure means shorter length of reinforced elements undergoing stray current.

For modeling or predicting the bond properties of steel-concrete interface undergoing stray current, the corrosion product distribution should be considered as well. In this aspect the post-stray current effect, for instance the back flow, should be involved, as the back flow re-distributes the corrosion product after the stray current interference.

6.4 Conclusions

The main objective of this chapter is to investigate the role of the rebar orientation in conditions when stray current induces corrosion damage. The rebar orientation was hypothesized to significantly affect the stray current corrosion damage degree and distribution of stray current corrosion product. The orthogonal and parallel directions (to stray current) of the cast-in steel are investigated in different conditions. Additionally, for clarifying the time-dependent response of steel rebar undergoing stray current, the potential shift and current level of stray current picked-up by steel are studied in a variety of layouts. The recorded time-dependent response can be the foundation for interpreting the data obtained from practical stray current monitoring. Besides an expansion of the database for monitoring stray current interference on reinforced concrete structures, the recorded results can be the basis for better understanding the process of stray current interference.

Based on the experimental results, the following conclusions can be drawn:

1. The geometrical position of the steel bar undergoing stray current affects the electrochemical response and polarization intensity of steel rebar induced by stray current. Compared to the situation of a steel bar orthogonal to the current direction, a more significant corrosion state is recorded when the steel bar is parallel to current direction.
2. The “anode” and “cathode” areas are distinguished in each cross-section of the steel-mortar interface underwent stray current. Stray current parallel to the steel rebar tends to induce localized corrosion, in contrast the orthogonal situation, where a relatively uniform corrosion of the relevant section is at hand. A more significant corrosion product accumulation and deeper corrosion penetration are observed on a steel rebar parallel to stray current, nearby the locations where the current leaves the steel rebar.
3. Though the supplying stray current is constant, the level of current picked-up by the steel rebar is decreasing. This observation can be attributed to the coexistence of polarization resistance and double layer capacitance on the steel-mortar interface.
4. At the instant when the stray current supply is turned off, an opposite current flow (back flow) from the previous anode to the previous cathode is monitored. It is attributed to the stray current-induced potential difference between the anode and cathode. This implies the spontaneous interconversion between anode and cathode induced by stray current, i.e., post-stray current effect. Thus not only the anodic part of steel, but also the temporary cathodic portion should be carefully considered and treated.

Chapter 7

Retrospection, Conclusions and Prospects

7.1 Retrospection

Various types of reinforced concrete structures (such as viaducts, bridges and tunnels) in the neighborhoods of railways may be subjected to stray current leaking from the rails. In these cases the concrete pore solution acts as an electrolyte, and the reinforcing rebar (or any other metallic parts, e.g. pre-stressed steel wires) embedded in concrete can “pick up” the stray current.

Compared with stray current-induced corrosion of pipelines, reinforced concrete has some typical problems to deal with: the volume of corrosion product gradually increases, the induced normal stress around the embedded steel can lead to cracking, spalling or delamination of the concrete cover. This may finally lead to the failure of the whole structure. Stray current can also affect the microstructural properties of the concrete matrix. As it is difficult to rebuild or repair structures under or near rail transits, this kind of corrosion of reinforced concrete structures is urgently in need of more in-depth investigation and understanding.

For understanding, evaluating, and eliminating stray current corrosion of reinforcing steel in concrete structures, factors that should be considered/investigated are recommended and summarized in Table 7.1. Table 7.1 includes previously studied and reported factors, as well as factors investigated in this thesis.

The clarified main points with regard to the stray current-induced corrosion of steel rebar, are listed as follows:

1. Different effects of stray current and anodic polarization on corrosion performance (corrosion resistance) of embedded steel rebar.
2. Bond behavior of steel-mortar interface affected by stray current.
3. The importance of the geometric orientation (with respect to the electrical field) of steel rebar in view of stray current-induced corrosion damage.
4. The time-dependent behavior of steel rebar response, in the sense of potential shift and current actually picked-up by steel rebar, in condition of stray current.

The conditions for steel rebar (concrete culvert under railway line as a practical case) to pick up stray current were analyzed in Chapter 3. The existing means for reducing stray current-induced corrosion of infrastructure in practice were discussed. On the basis of literature review and practical cases, the remaining scientific challenges related with stray current-induced corrosion of steel in reinforced concrete structures were summarized.

In Chapter 4, the effects of stray current on the corrosion behavior of reinforcing steel, embedded in fresh (24h-cured) and hardened (28d-cured) mortar specimens, conditioned in Cl-

free and Cl-containing environment, were investigated. The electrochemical responses of the reinforcing steel in stray current conditions were compared to that of steel rebar in conditions of anodic polarization.

Chapter 5 correlates the corrosion state and bond strength of steel-mortar interface affected by stray current and anodic polarization, conditioned in Cl-free and Cl-containing medium. Additionally, the effect of stray current starting time was considered, by testing 24h and 28d-cured specimens of otherwise identical geometry and conditions.

Chapter 6 aimed to investigate the stray current corrosion of the steel rebar positions in different orientations, in relation to the direction of the imposed current. For this reason, two geometrical positions of the reinforcement embedded in mortar were tested: steel bars placed parallel or orthogonal to the stray current direction. The response (potential shift and stray current level picked-up by steel) of steel embedded in mortar undergoing stray current was studied. The time-dependent behavior of steel response undergoing stray current was recorded and discussed.

Table 7.1: Summary of factors about stray current corrosion of reinforcing steel in concrete.

Categories	Factors	Studied before	Studied in this work	Summarized conclusions of this thesis
Sources of stray current	AC Level/Density	✓		
	AC Frequency	✓		
	Continuity or not			
	DC level/Density	✓		
	Fluctuation/Dynamic	✓		
	Continuity or not			
Measures for reducing stray current on stray current source		✓		Summarized in Section 3.4.1.
Ambient conditions	Resistivity of surrounding media (soil, groundwater, sea water)	✓		
	Distance between power source and interfered structure			
	Potential gradient in soil	✓		
Measures for reducing stray current on ambient conditions		✓		Summarized in Section 3.4.2.
Interfered reinforced concrete	Different mixtures/additives			
	Effects on fatigue/deflection/ductility			
	Anode/Cathode ratio			
	Starting point of stray current	Bulk matrix	✓	The curing regim and starting point of stray current play the significant role in the formation of a corrosion product layer on the steel surface.
		Steel-concrete interface	✓	
	Couple with other erosive substance		✓	At early age, competitive mechanisms act in situation of Cl^- + stray current, cured in fog room for only 24 hours.
	Reinforce-ment type	Steel fibre	✓	
		Pre-stressed wire/bar		
		Steel rebar	✓	

Monitoring	Time-dependent behavior of steel		✓	Though the supplying stray current is constant, the level of current picked-up by the steel rebar is decreasing; At the instant when the stray current supply is just turned off, an opposite current flow (back flow) was monitored.
	Post-stray current effect		✓	
	Stray current level flowing in steel rebar		✓	
	Potential distribution in steel	✓	✓	
	IR drop	✓	✓	
Bond degradation of steel-mortar/concrete interface			✓	Stray current (at level of 0.3 mA/cm ²) leads to bond degradation of the steel-mortar interface, regardless of whether there are Cl ⁻ in external environment.
Corrosion product composition/distribution			✓	Stray current direction and back flow determine corrosion location.
Rebar direction to stray current			✓	Rebar parallel to stray current is more dangerous than orthogonal.
Rebar length undergoing stray current			✓	Longer rebar length undergoing stray current leads to higher picked-up current level.
Judge stray current effects on steel-mortar interface via electrochemical response			✓	It is possible to use either PDP, EIS or combination of them, to gain insights into the bond of steel-mortar/concrete interface.
Stray current effects V.S. Anodic polarization			✓	Stray current and anodic polarization exert significantly different effects on both corrosion behavior and bond property of steel-mortar interface.
Measures for reducing stray current on reinforced concrete structures		✓ (Very few)		Summarized in Section 3.4.3, and recommended in Section 7.3.
Modelling/Predicting methods for stray current corrosion risk on reinforced concrete structures		✓ (Few)		Summarized in Section 2.5.

7.2 Conclusions

This thesis highlights a few aspects about stray current-induced corrosion of steel rebar. With this research a better insight is gained into the behavior of steel rebar (embedded in cement-based materials) affected by stray current. On the basis of experimental studies, the main conclusions of this research are:

1. As introduced, some investigations actually applied anodic polarization on samples to simulate stray current corrosion on steel in reinforced specimens. However, the stray current induces both anodic polarization and cathodic polarization. In this study it is found that stray current and anodic polarization exert significantly different effects on the corrosion behavior of steel embedded in mortar. Hence, anodic polarization cannot reflect all the effects of stray current, and therefore it has limited significance for simulating stray current.
2. The curing regime and starting time of stray current play significant roles in the formation of a corrosion product layer on the steel surface. At very early age, water transport, leaching-out effects and ion migration governed by electrical field are more evident, because of high porosity and pore network connectivity of a fresh bulk. However, this phenomenon is not

evident for the condition of sufficiently cured bulk matrix, as the bulk matrix is already hardened when the stray current is supplied.

3. Significantly different states of corrosion were recorded in Cl-free and Cl-rich external medium, as expected. However, in conditions of both stray current and anodic polarization, competitive mechanisms were recorded, i.e., positive in view of enhanced cement hydration and negative in terms of accelerating Cl-induced corrosion. On the one hand the current has positive effects: current flow through a fresh (non-mature) cement matrix led to enhanced water and ion transport due to migration. The result was enhanced cement hydration, consequently environment, assisting a more rapid stabilization of pore solution and steel-cement paste interface. On the other hand, stray current enhances Cl^- ion migration, leading to Cl-induced corrosion.
4. Though corrosion induced by stray current was considered and studied previously, the effect of stray current on bond property of steel-concrete/mortar interface is not generally investigated yet. This research clarified the bond degradation of steel-mortar interface due to stray current. It was found that stray current (at level of 0.3 mA/cm^2) exerts bond strength degradation, irrespective of the presence or absence of a corrodent (Cl^- as an example). Anodic polarization leads to more pronounced effects on bond of the steel-mortar interface than stray current.
5. This work clarified the effects of rebar orientation on the stray current-induced corrosion of reinforcement. Compared to the situation of a steel bar orthogonal to the current direction, a more significant corrosion state was recorded when the steel bar is parallel to current direction. The “anode” and “cathode” areas were distinguished in cross-section of the steel-mortar interface underwent stray current. Stray current parallel to the steel rebar tends to induce localized corrosion, in contrast the orthogonal situation, a relatively uniform corrosion of the relevant section is at hand. A more significant corrosion product accumulation and deeper corrosion penetration are observed on a steel rebar parallel to stray current.
6. In this study the time-dependent response (potential shift and current level picked-up by steel) of steel interfered by stray current was recorded and interpreted. At the moment that the stray current supply is just turned off, an opposite current flow (back flow) from the previous anode to the previous cathode was monitored. It is caused by the stray current-induced potential difference between anode and cathode. This implies the spontaneous interconversion between anode and cathode induced by stray current. It implies that stray current-induced corrosion (anodic reaction, i.e., the steel dissolution) occurs not only on positions where the current flows out, but also on points where stray current previously flows into steel (previous cathode, but transformed to an anode when stray current is absent). In other words, the cathodic locations, or the entry points of stray current, do not always remain cathodes only.

7.3 Contributions to science and recommendations to engineering

The understanding of stray current-induced corrosion of reinforcing steel in concrete still remains unclear, as it is difficult to inspect the steel rebar embedded in the concrete. Most of

previous understanding and prevention measures for stray current corrosion rely on the investigations or field tests on pipelines. This thesis aims to expand the current body of knowledge of stray current corrosion for reinforcing steel embedded in cement-based materials.

Based on the experimental studies in this thesis, deeper insights are gained into the behavior of reinforcing steel embedded in cement-based materials undergoing stray current, in views of both electrochemical (fundamental) and civil (practical) engineering. The test results can be the basis of the further understanding of stray current corrosion mechanism and process, more reliable methods for monitoring stray current interference, and feasible prevention measures for reducing stray current-induced corrosion risk of reinforced concrete structures.

According to the test results, the recommendations to test, predict and model stray current effects, to monitor stray current interference, to design of reinforced concrete structures for reducing stray current corrosion risk, are proposed as a finalization of this thesis:

1. Stray current induces both anodic polarization and cathodic polarization on reinforcing steel embedded in cement-based materials. Only testing anodic polarization is not sufficient to judge stray current effects on steel-concrete interface.
2. The correlation between the electrochemical response and bond properties of steel-mortar interface affected by stray current was established. It is possible to use either PDP, EIS or combination of them, to gain insights into the bond of the steel-concrete interface. For judging the effect of stray current corrosion on the bond properties of the steel-concrete interface by electrochemical tests, not only the steel corrosion, but also the properties of mortar cover (e.g., porosity, pore structures, strength, confinement effect, etc.) affected by current flow should be evaluated.
3. The above Item 2 also holds for the prediction and modeling of stray current corrosion of the steel rebar. The more comprehensive approaches are still necessary to thoroughly evaluate the process of stray current corrosion. The evaluation of both electrochemical phenomena (of steel rebar) and micromechanical properties (of concrete matrix in the vicinity of steel-concrete interface) will allow a more accurate appraisal of stray current corrosion probability. The starting time of stray current should be considered, as it is found that at early age the stray current even has positive effect on steel-concrete interface.
4. For modelling or simulating the stray current effects on bond of steel-concrete interface, not only the corrosion of steel induced by anodic polarization (stimulated by stray current), but also the cathodic polarization at steel-concrete interface, should be considered. The ion migration governed by a stray current electrical field is another factor that should be involved in modeling, because the concentrated Na^+ and K^+ lead to softening of CH and C-S-H at steel-concrete interface. For modeling or predicting the bond properties of steel-concrete interface undergoing stray current, the corrosion product distribution should be considered as well. In this aspect the post-stray current effect, for instance the back flow, should be involved, as the back flow re-distributes the corrosion product after the stray current interference.
5. Assessments of stray current corrosion impacts can be made as qualitative assessments using a mix of engineering judgment and applications of Faraday's law. However, the application of Faraday's law requires density of current flows. The most common indicators

for monitoring stray current are potential shifts of metallic structures. The discovered time-dependent behavior of monitored potential shift and picked-up current level of steel rebar, can be further used as basis for analysing the monitoring data about stray current interference. The ohmic drop (IR component) can always be involved during potential shift measurement in practice, especially in reinforcing concrete due to the relatively higher resistivity of the concrete matrix surrounding the steel rebar. In this case the IR drop should be considered carefully. Besides, the back flow induced by stray current is of importance in stray current corrosion monitoring and evaluation. Not only the anodic part of steel, but also the temporary cathodic portion should be carefully considered and treated.

6. Measures for diminishing stray current disturbance to nearby constructions or infrastructure should be provided at the initial stage of design. Infrastructures should be located as far as possible from stray currents sources. Once the location of structure is fixed and stray current is expected to be a problem, the removal of the stray current source or reduction in its output current should be considered. If measures taken on the stray current sources are impractical or ineffective, the attention should be focused on the interfered structure itself and surrounding external environment. Sectionalization of reinforced concrete structures (similar to the principle of general expansion joint in civil engineering) is a possible solution for reducing the stray current effect, as it is found that the longer length of steel rebar leads to more severe corrosion damage. The sectionalized structure means shorter length of reinforced elements undergoing stray current.

7.4 Prospects for further investigations

Following this study, several aspects are further proposed for further investigations related to stray current:

1. Although stray AC is much “safer” than stray DC flow, AC can also affect the corrosion behavior of steel. The relationship between AC density, frequency, and corrosion rate has been studied and reported. However, the case when both stray AC and DC are present has not been studied sufficiently so far. Attention should be further paid to the possible synergistic effects of stray AC and DC. The possible thermal activation (the temperature rise within the test cells) created by currents should also be considered in this situation.
2. Stray current effects on reinforced concrete structures with different mixtures/additives should be studied, because the different mixtures/additives lead to different properties of bulk matrix surrounding steel, and influence the stray current effects on steel-concrete interface.
3. Stray current effects on the fatigue, deflections and ductility of reinforced concrete elements (for instance, beams) are worthy to be investigated. This is because stray current leads to the degradation of steel-concrete interface, which determines the above properties of reinforced concrete elements.
4. Steel fibre reinforced segmental (or steel fibre reinforced shotcrete) tunnels may encounter stray current corrosion risk. Stray current-induced corrosion of steel fibre reinforced concrete structures is another issue to be studied.

5. In engineering the environments or conditions surrounding reinforced concrete structures are more complex. The wet-dry cycles, temperature or humidity variations, carbonization of concrete cover, other erosion factors, etc, may coexist with stray current. The possible coupled effects of these factors and stray current should also be considered and investigated in further studies.
6. The A/C ratio (i.e., the ratio of surface area of anode and cathode) is vital in view of the corrosion process. The ratio of anode part/cathode part of steel surface undergoing stray current should be further investigated.
7. The stray current effect on pre-stressed concrete structures need to be studied, as cathodic polarization induced by stray current may leads to hydrogen evolution, which is dangerous for pre-stressed wires (due to hydrogen embrittlement).
8. The post-stray current effect addressed in this research should be further considered. This is related to the interruptions of stray current, which should be taken into account in some particular situations. In this case the back flow following stray current will be more frequent, as the stray current turn-off occurs frequently.

Appendix

A EIS response evolution of specimens in various conditions as involved in Chapter 4

A.1 EIS response of 24h-cured groups

The experimental impedance responses, in Nyquist and Bode format, for all 24h-cured groups are presented in Figures A.1-A.6.

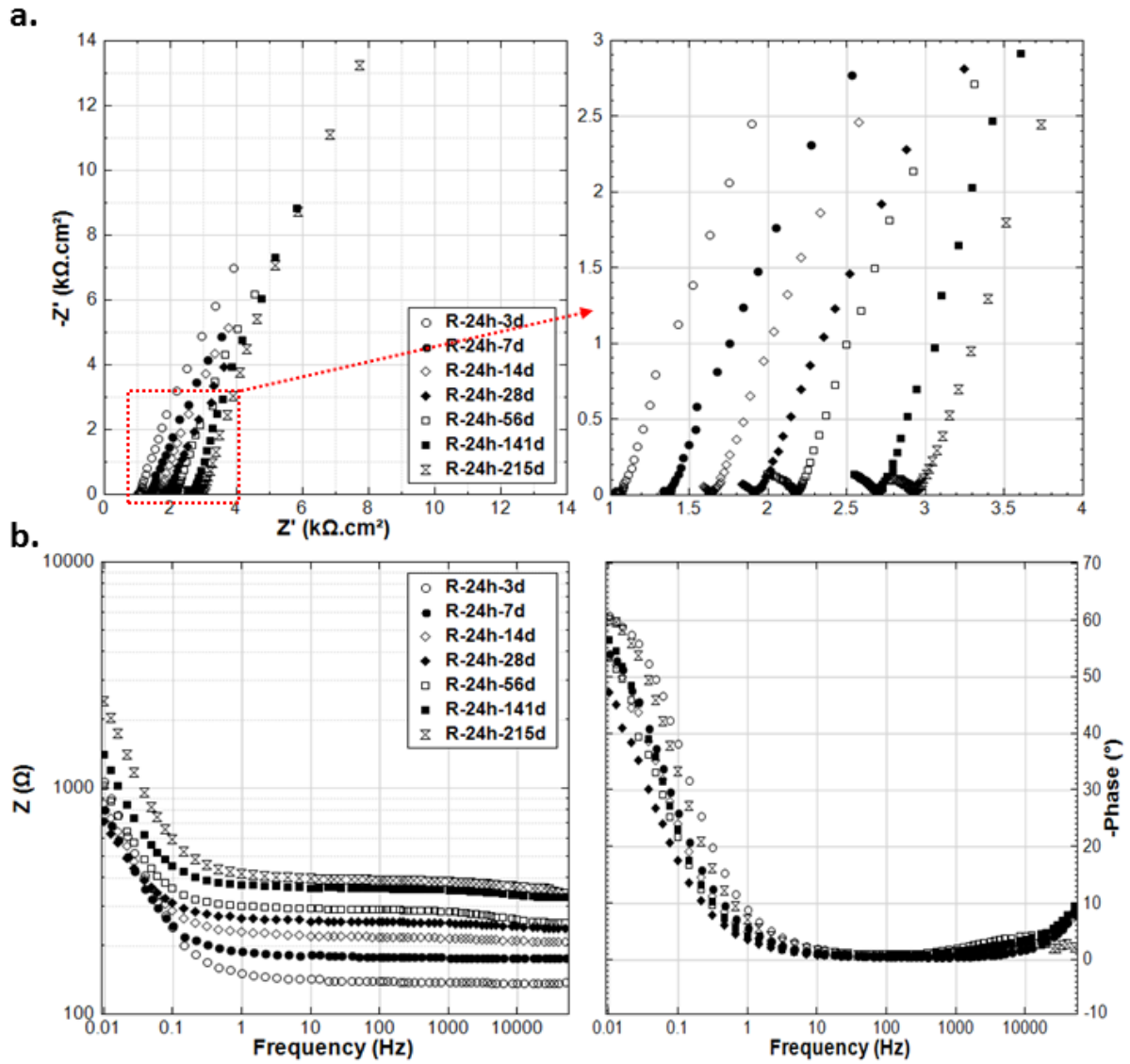


Figure A.1: EIS responses in a). Nyquist and b). Bode format, for specimen R-24h at different intervals.

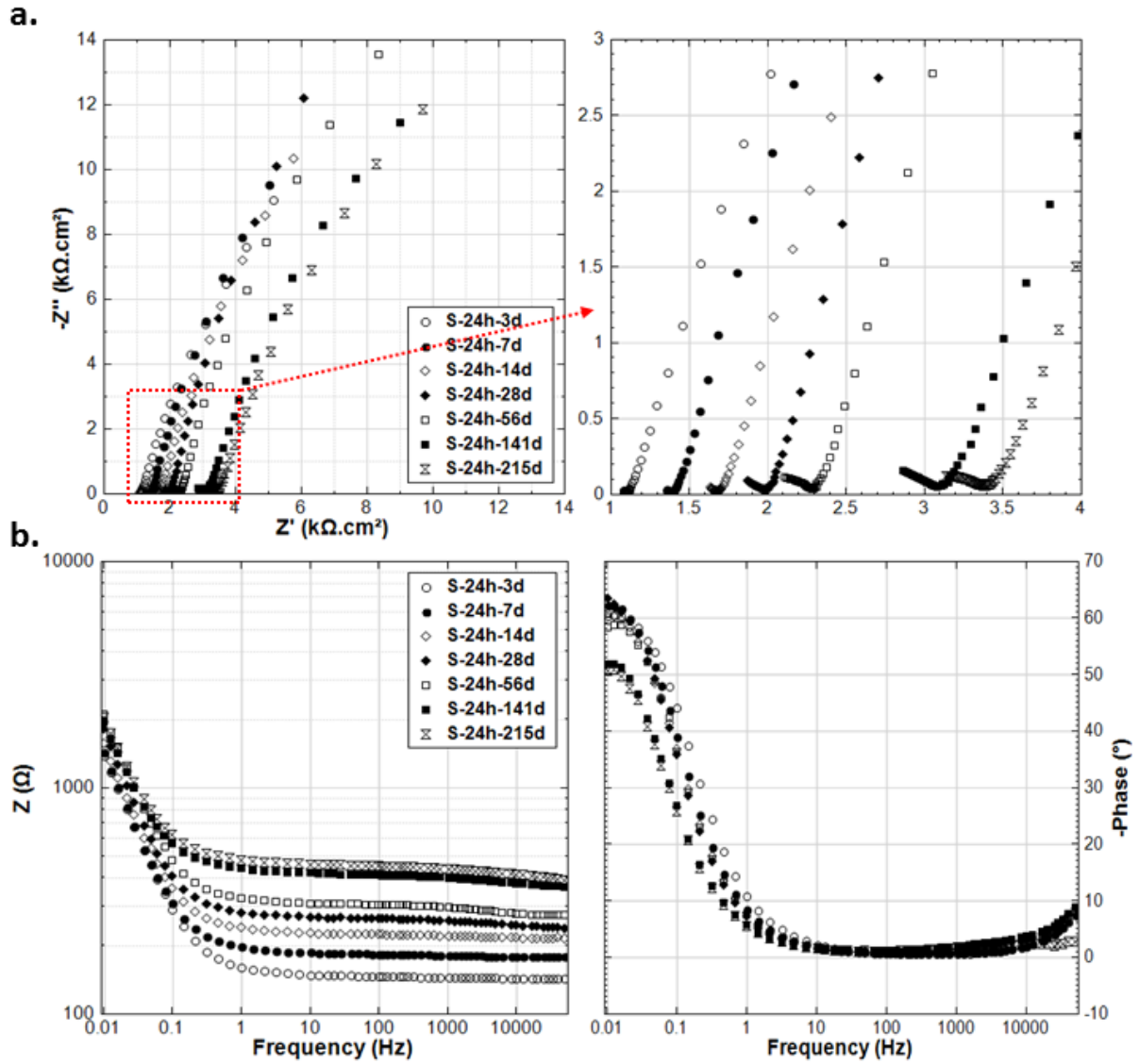


Figure A.2: EIS responses in a). Nyquist and b). Bode format, for specimen S-24h at different intervals.

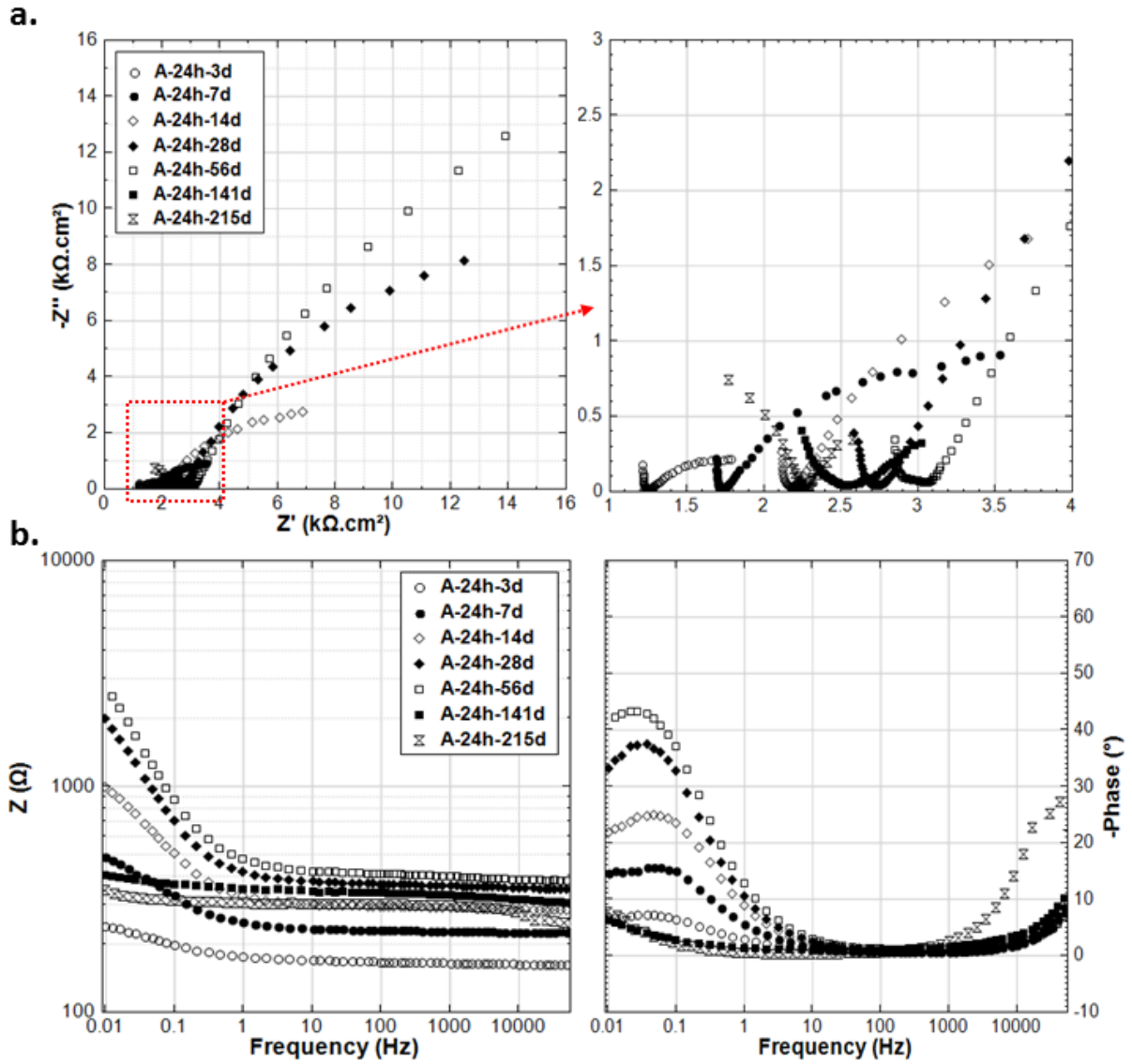


Figure A.3: EIS responses in a). Nyquist and b). Bode format, for specimen A-24h at different intervals.

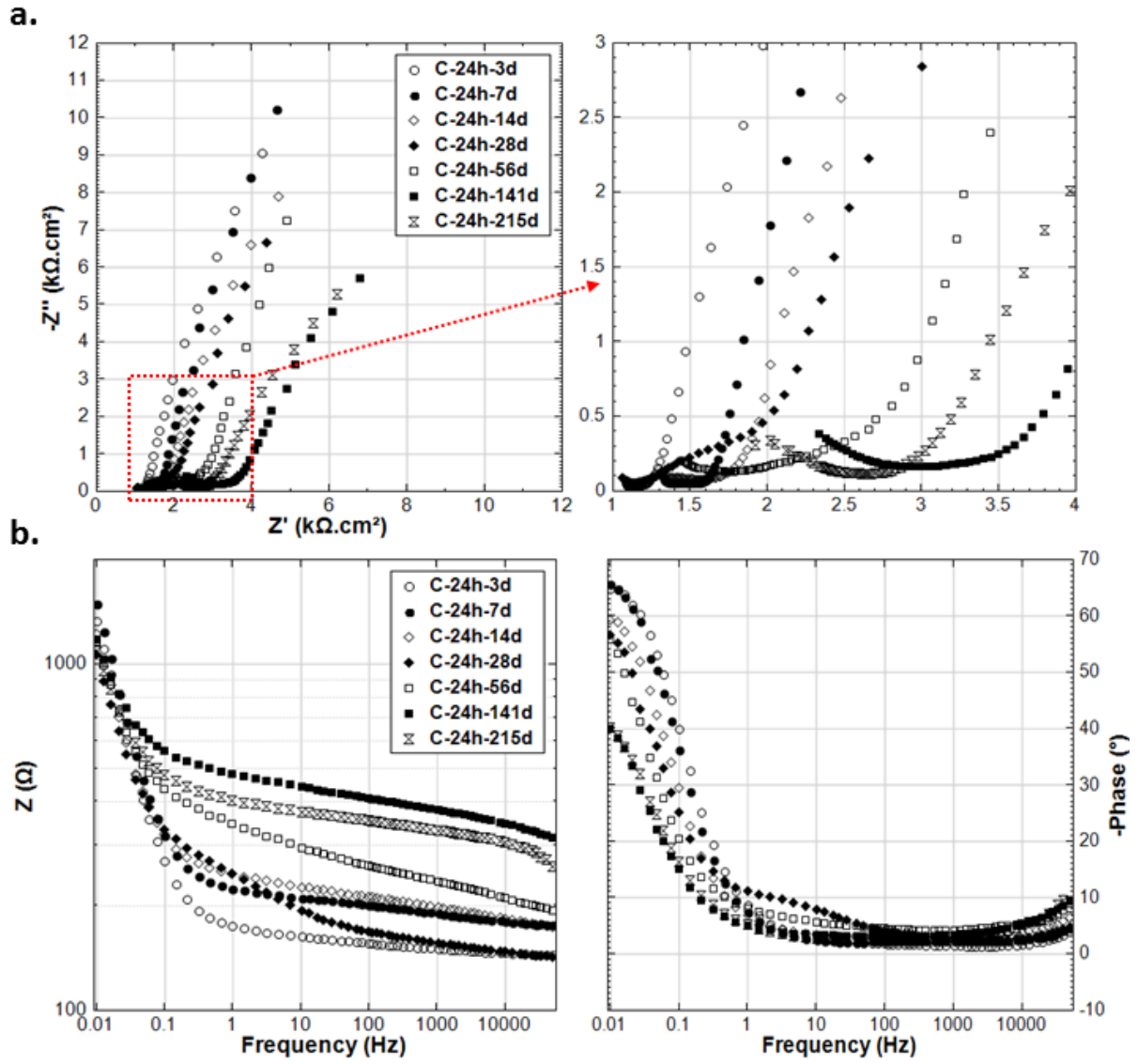


Figure A.4: EIS responses in a). Nyquist and b). Bode format, for specimen C-24h at different intervals.

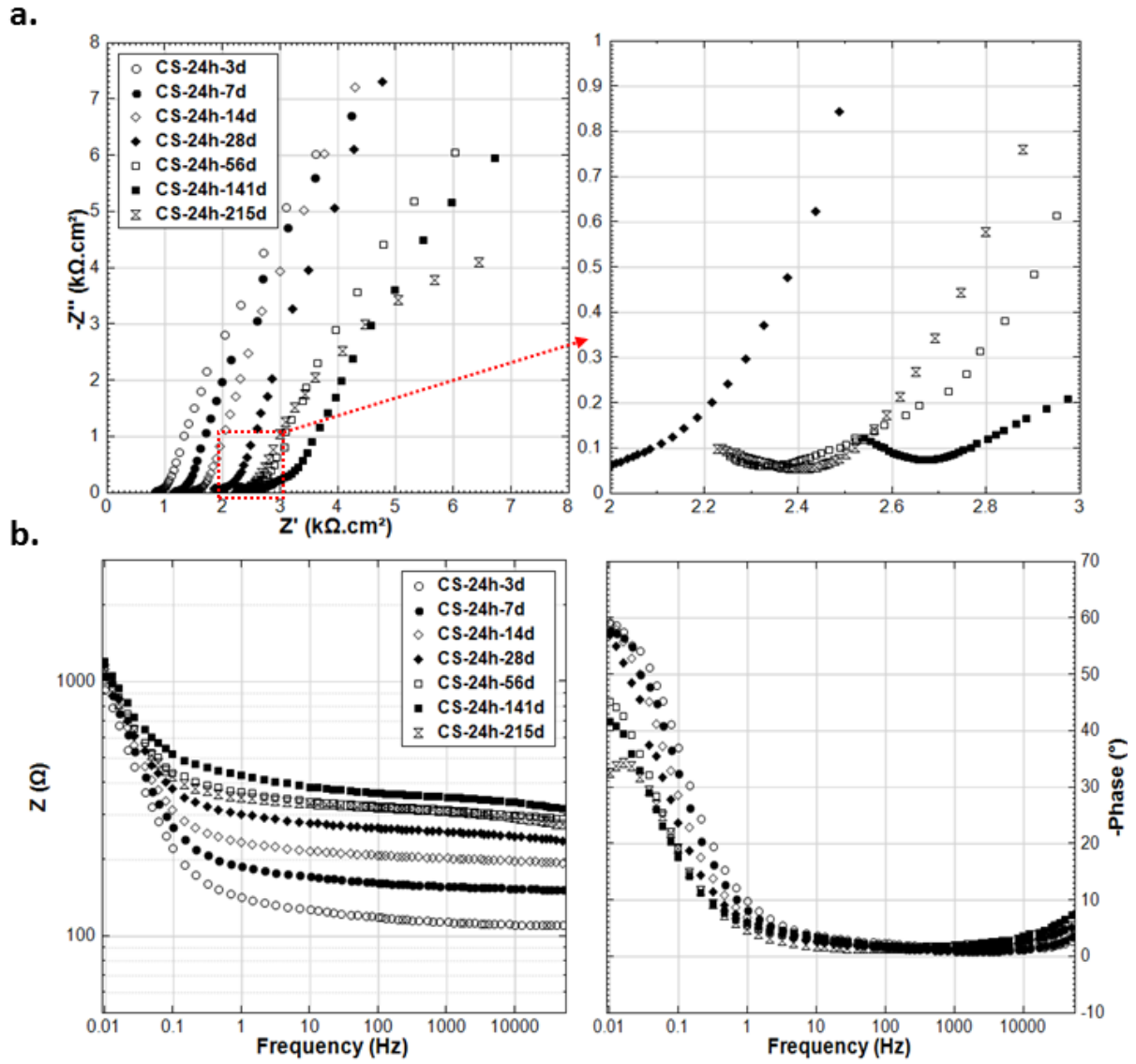


Figure A.5: EIS responses in a). Nyquist and b). Bode format, for specimen CS-24h at different intervals.

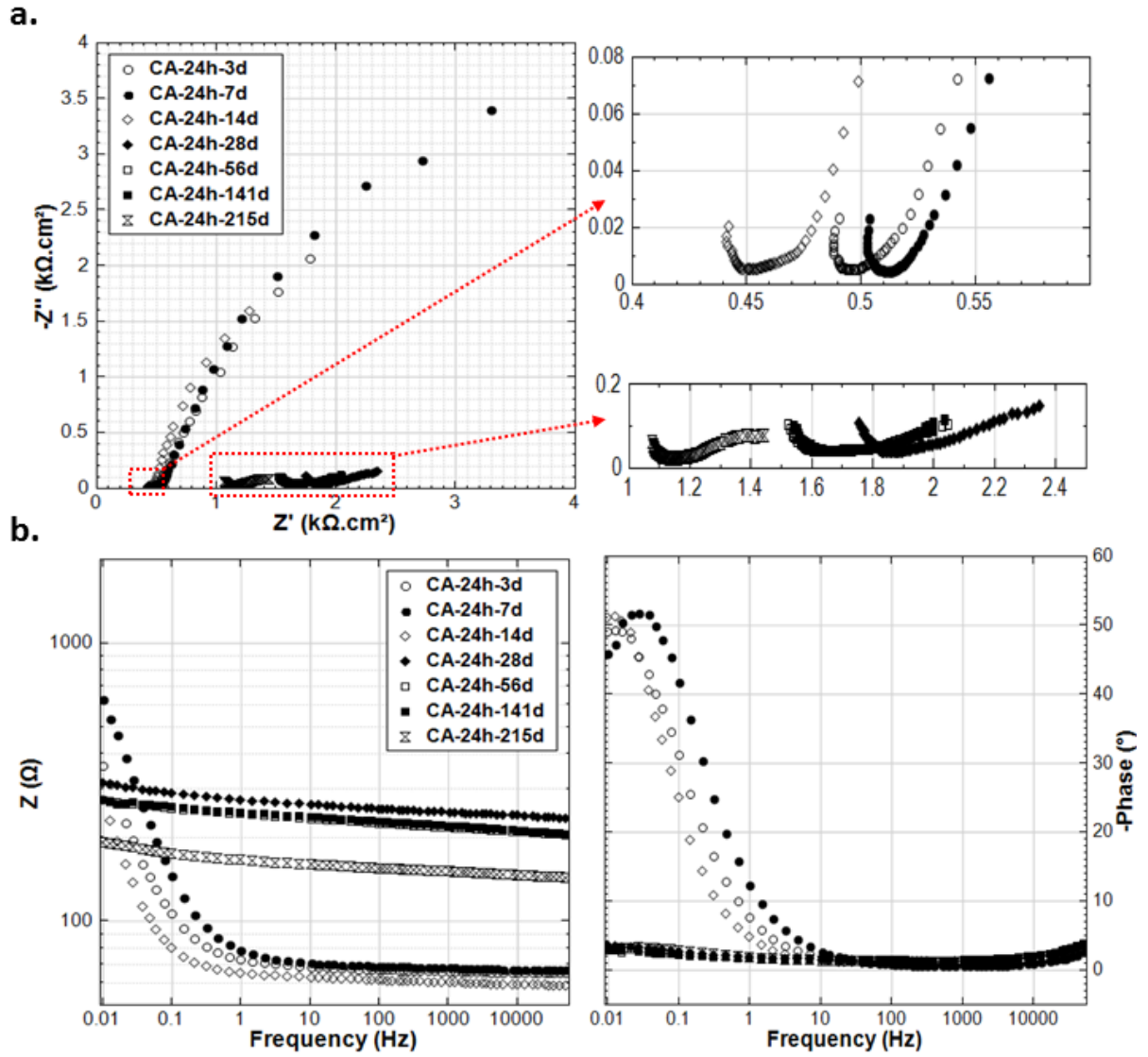


Figure A.6: EIS responses in a). Nyquist and b). Bode format, for specimen CA-24h at different intervals.

A.2 EIS response of 28-cured groups

The experimental impedance responses, in Nyquist and Bode format, for all 28d-cured groups are presented in Figures A.7-A.12.

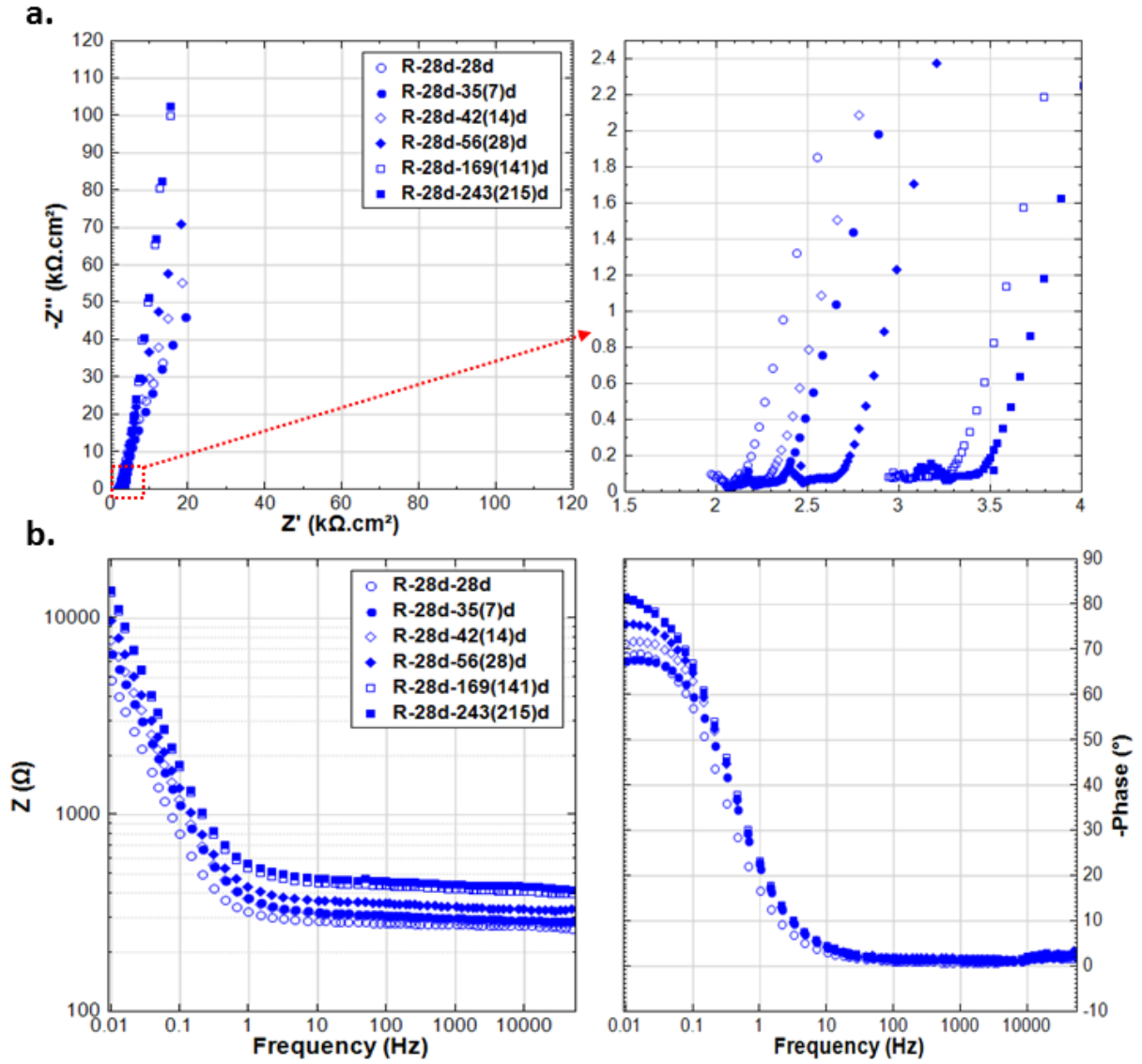


Figure A.7: EIS responses in a). Nyquist and b). Bode format, for specimen R-28d at different intervals.

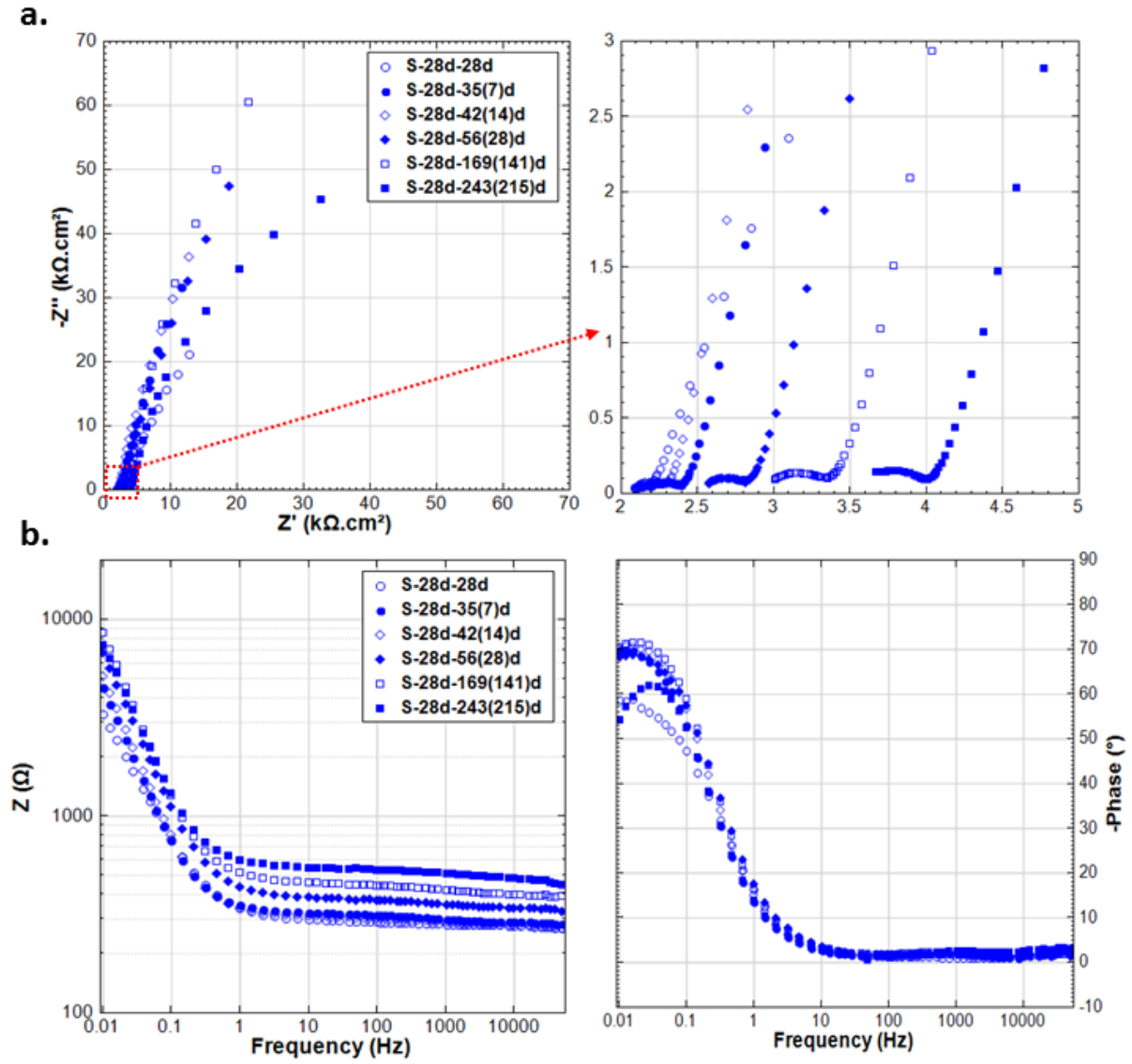


Figure A.8: EIS responses in a). Nyquist and b). Bode format, for specimen S-28d at different intervals.

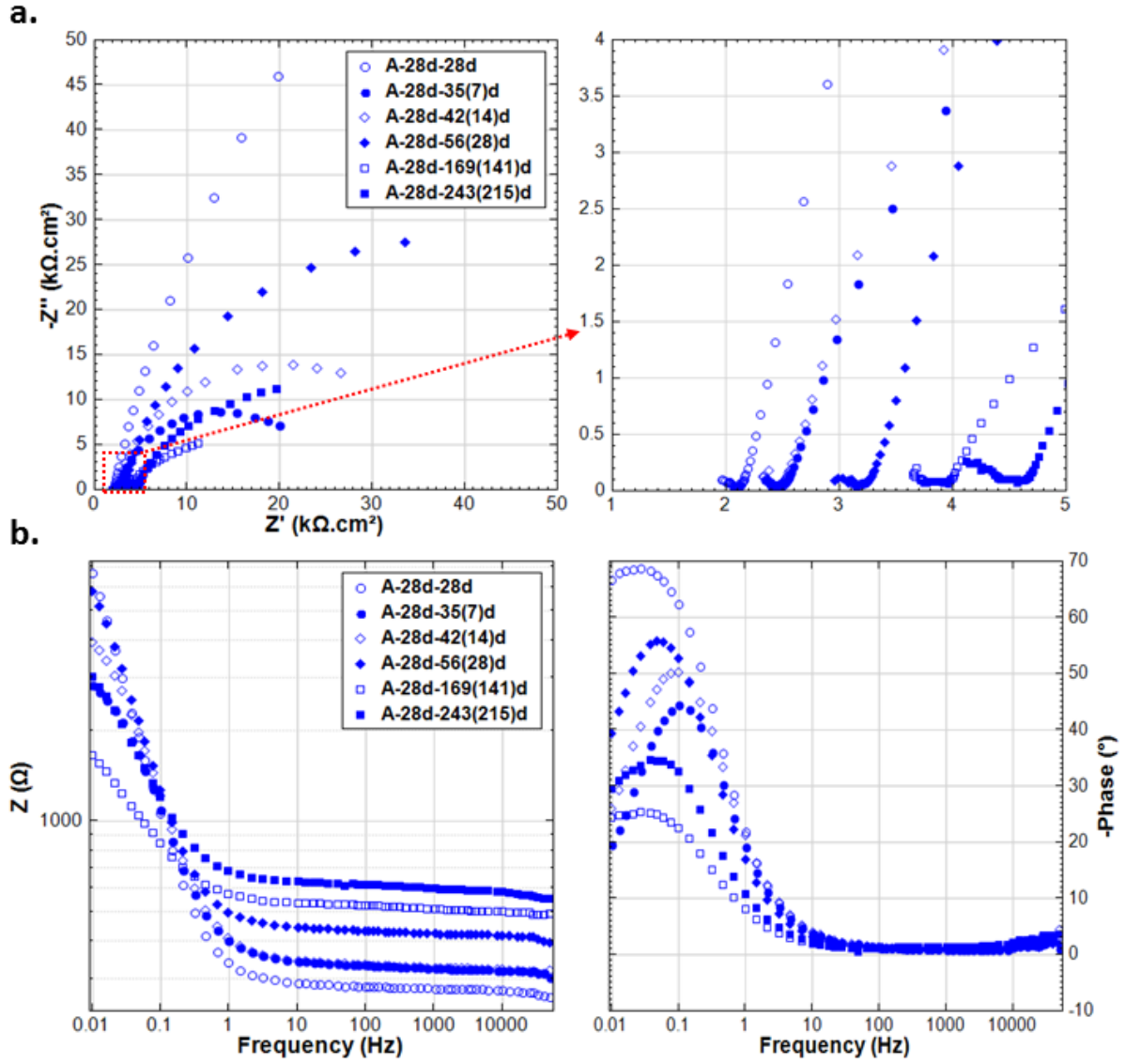


Figure A.9: EIS responses in a). Nyquist and b). Bode format, for specimen A-28d at different intervals.

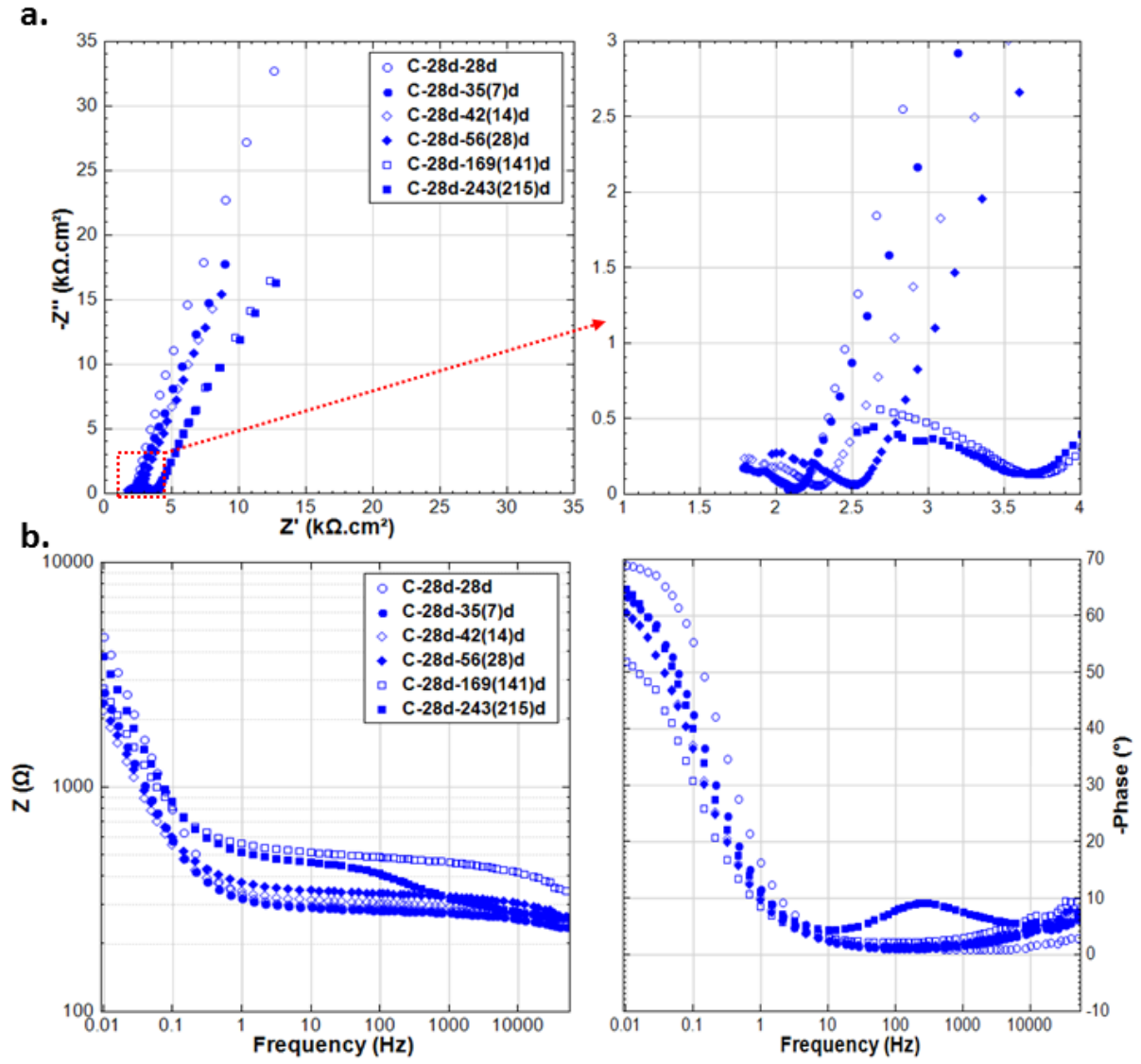


Figure A.10: EIS responses in a). Nyquist and b). Bode format, for specimen C-28d at different intervals.

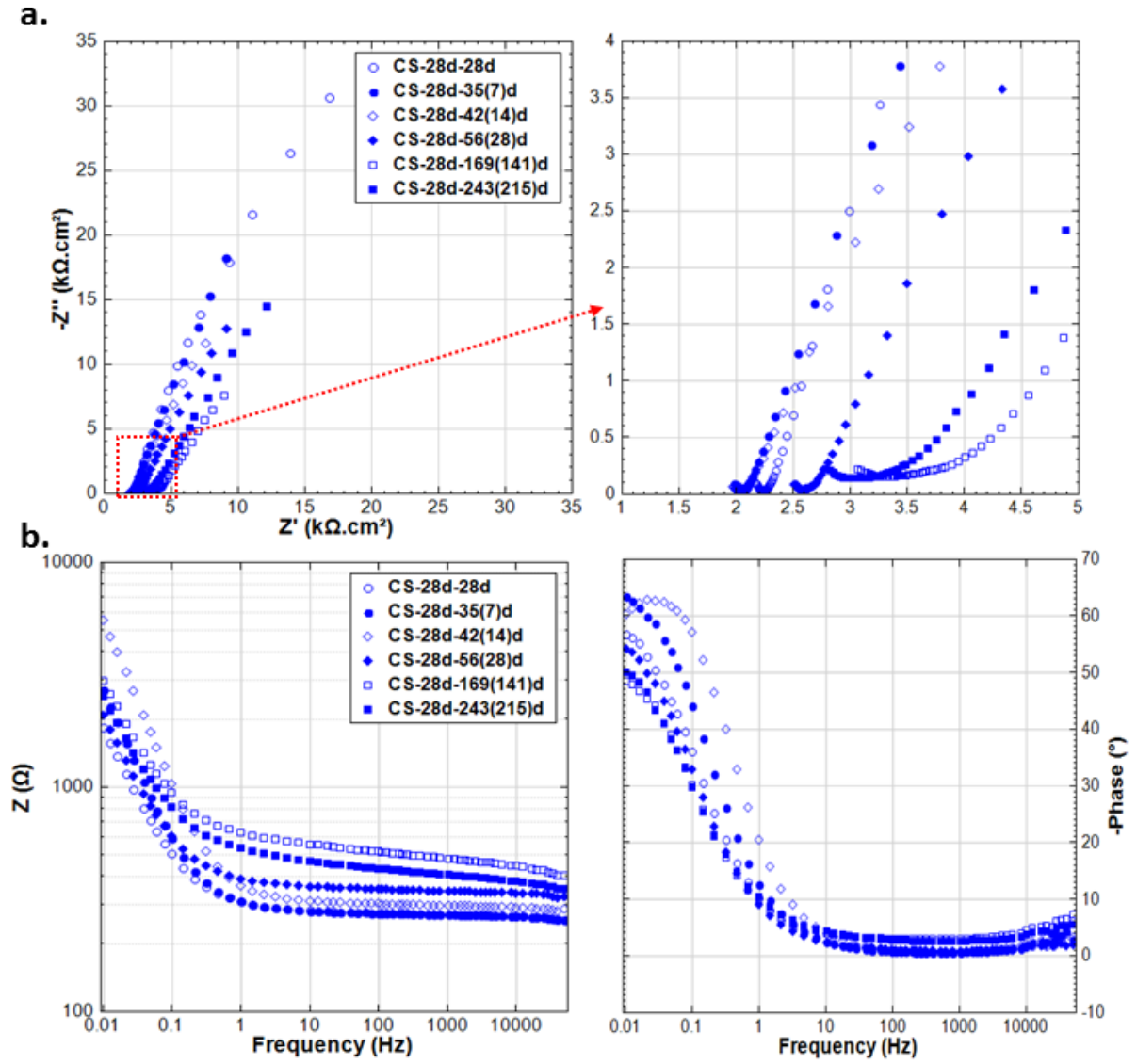


Figure A.11: EIS responses in a). Nyquist and b). Bode format, for specimen CS-28d at different intervals.

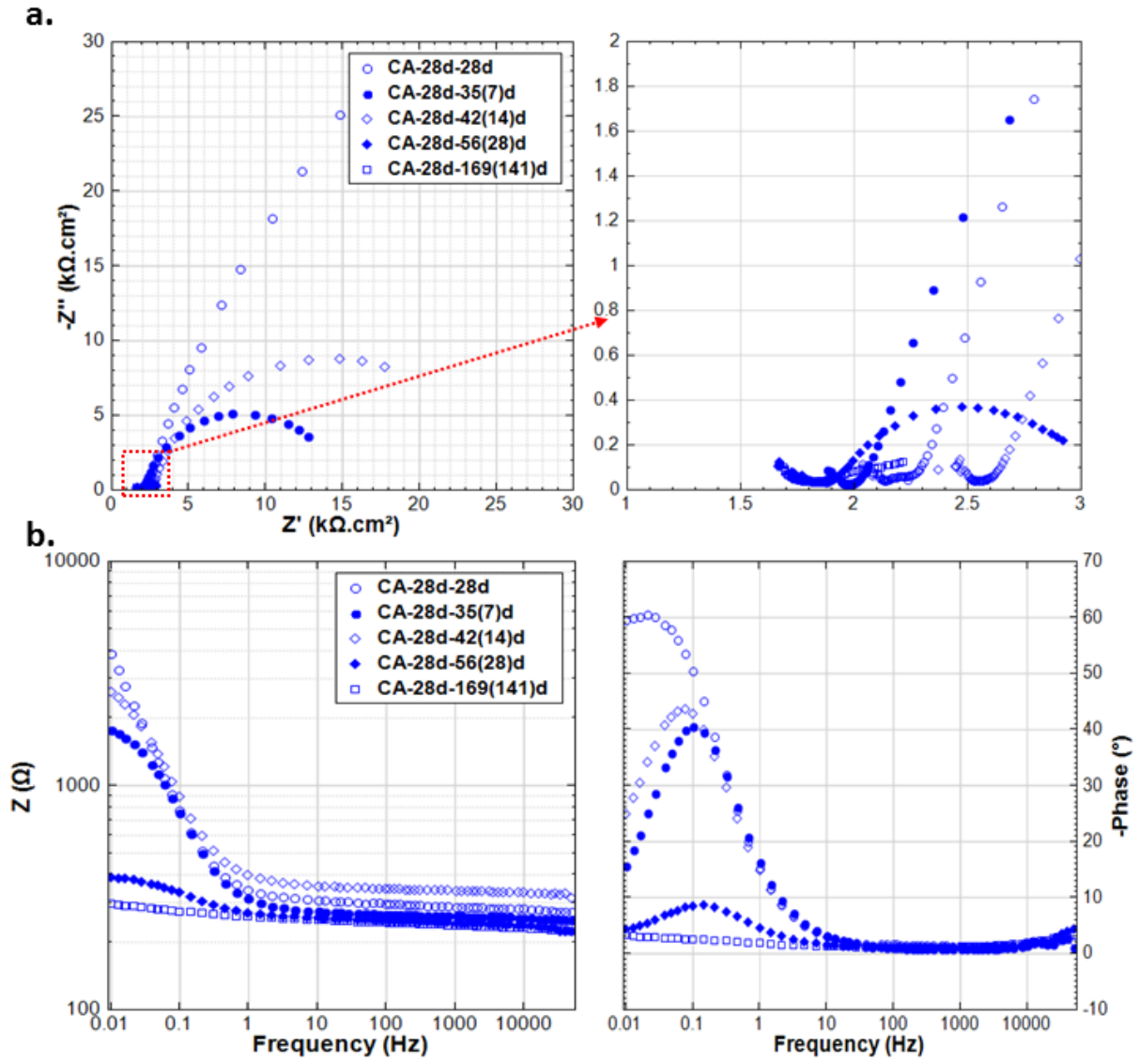


Figure A.12: EIS responses in a). Nyquist and b). Bode format, for specimen CA-28d at different intervals.

B Schematics of different effects of stray current and anodic polarization at early and later age

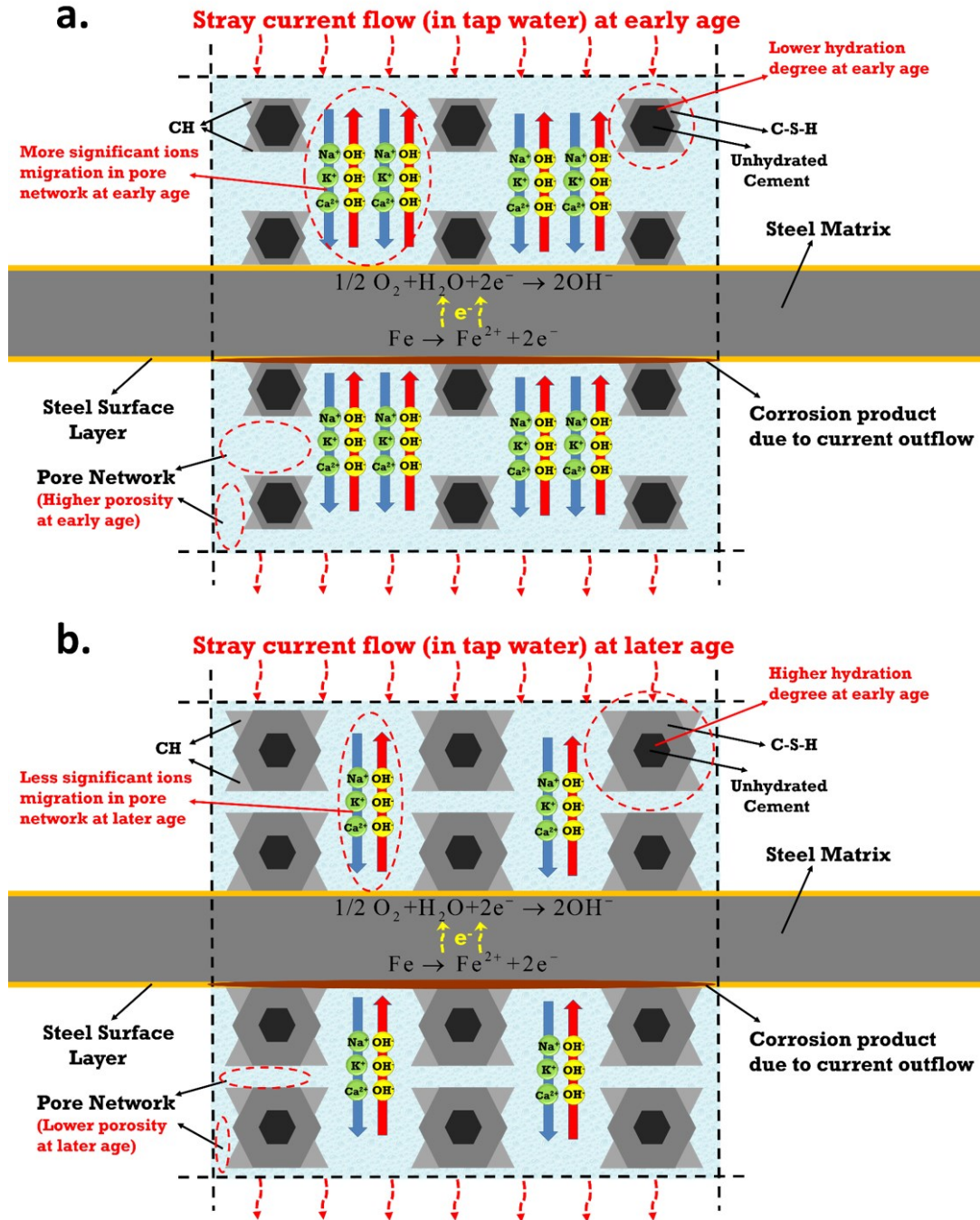


Figure B.1: Schematic of stray current effect in CI-free matrix: a). Stray current supply started at early age (24h, when bulk matrix was still young); b). Stray current supply started at later age (28d, bulk matrix was already hardened).

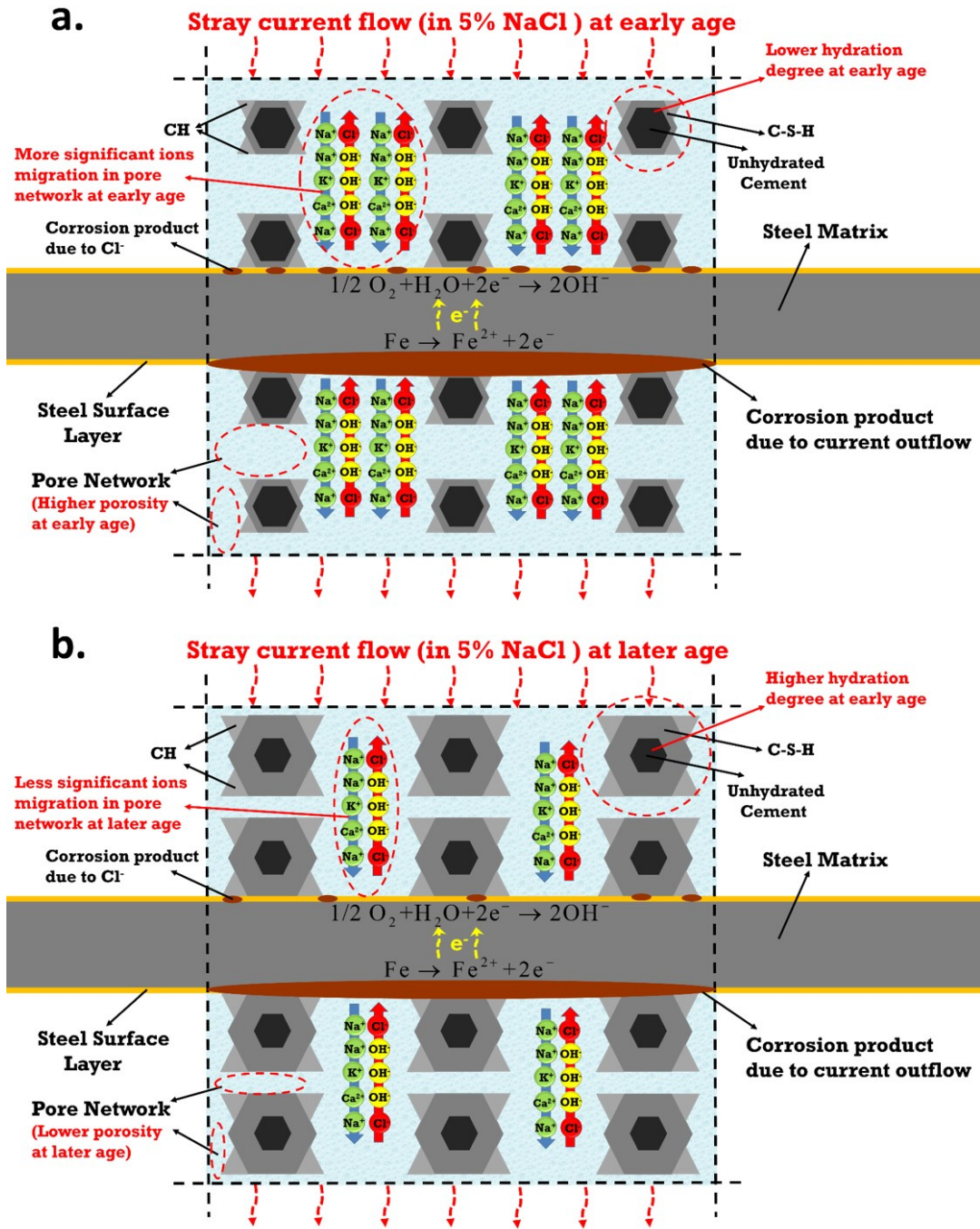


Figure B.2: Schematic of stray current effect in Cl-containing matrix: a). Stray current supply started at early age (24h, when bulk matrix was still young); b). Stray current supply started at later age (28d, bulk matrix was already hardened).

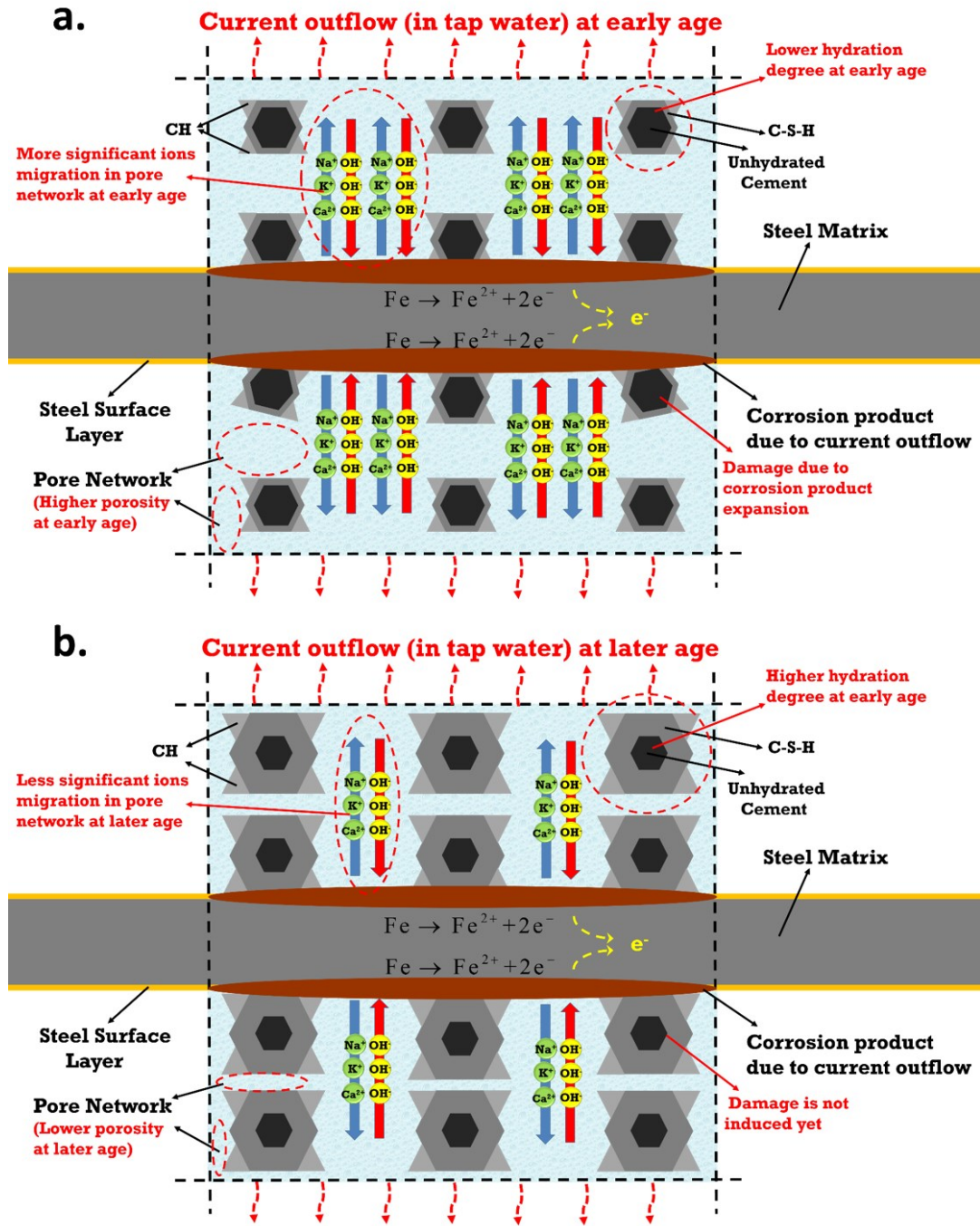


Figure B.3: Schematic of anodic polarization effect in Cl-free matrix: a). Anodic polarization started at early age (24h, when bulk matrix was still young); b). Anodic polarization started at later age (28d, bulk matrix was already hardened).

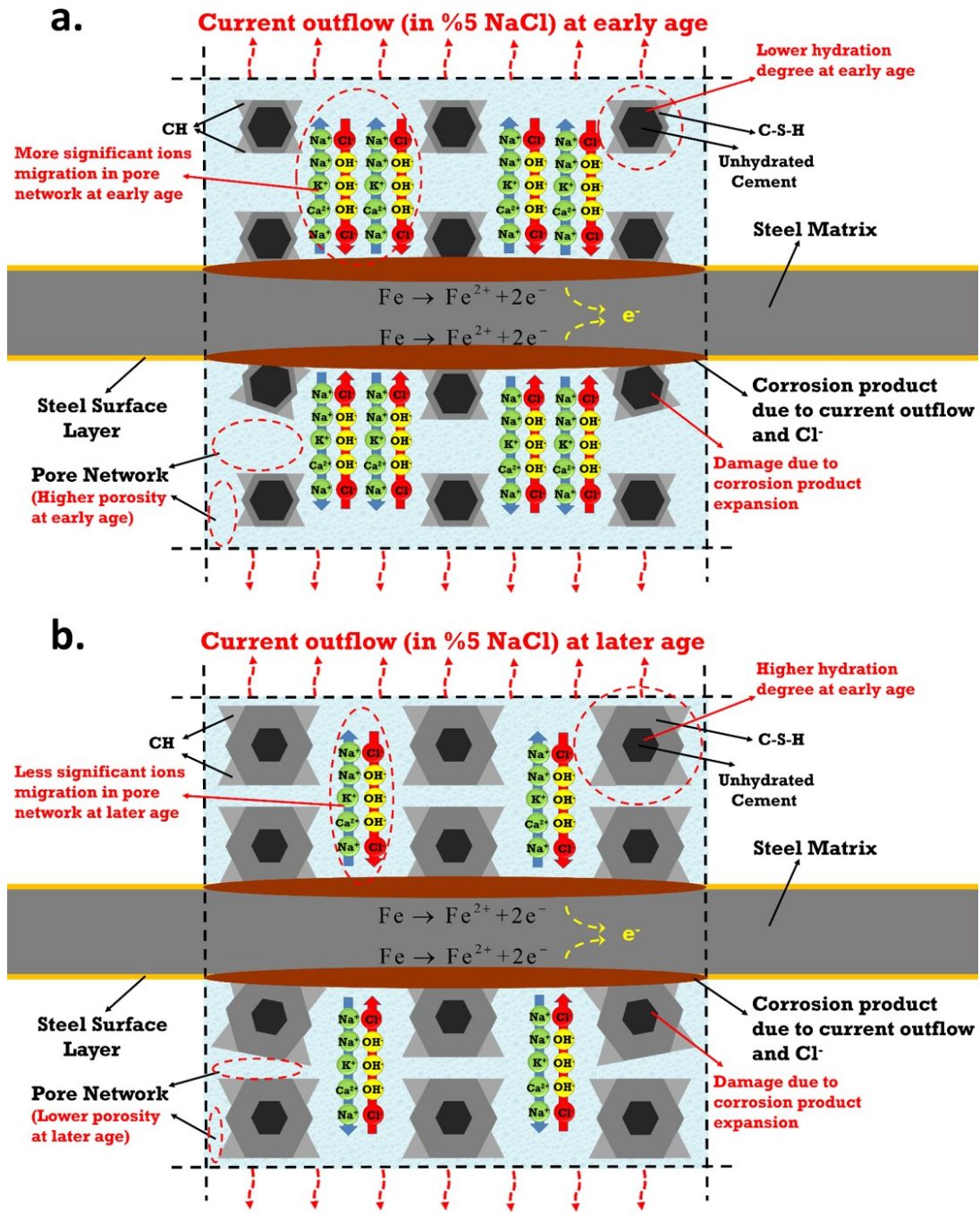
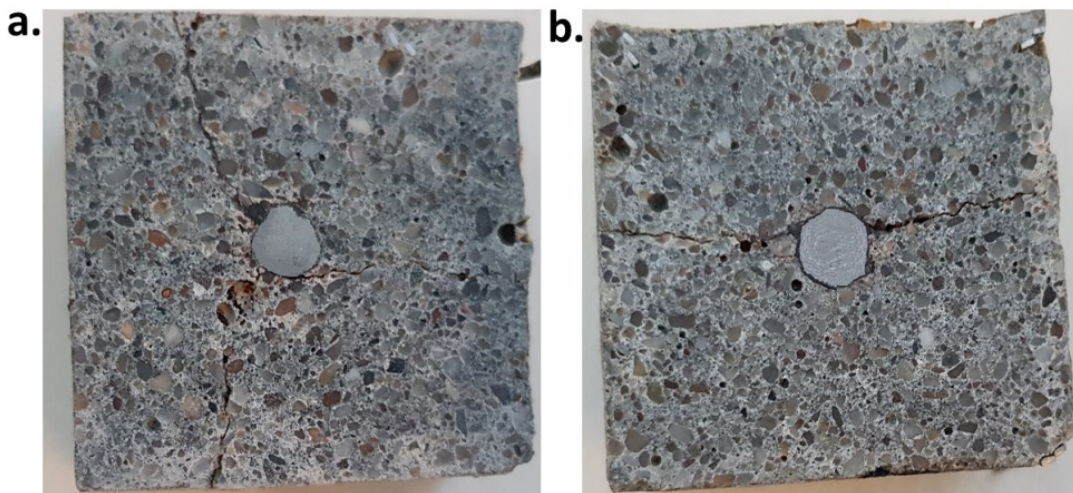


Figure B.4: Schematic of anodic polarization effect in Cl-containing matrix: a). Anodic polarization started at early age (24h, when bulk matrix was still young); b). Anodic polarization started at later age (28d, bulk matrix was already hardened).



Figure B.5: Cross section of A-24h at the end of conditioning.



B.6a: Cross section of: CA-24h.

B.6b: Cross section of: CA-28d.

Figure B.6: Cross section of: a). CA-24h; b). CA-28d at the end of conditioning.

C An example of EIS fitting procedure involved in Chapter 5

Electrochemical impedance spectroscopy (EIS) in Chapter 5 was conducted in the wider frequency range of 1MHz-10mHz, by superimposing an AC voltage of 10mV (rms). One of the main points of this chapter is to clarify the different effects of stray current and anodic polarization, in perspective of bond strength of steel-mortar interface; another point is to correlate the bond behavior of steel-mortar interface with the electrochemical response of reinforced mortar specimens underwent stray current and anodic polarization.

The bond strength can be affected by the diameter of steel, reinforcement shape, geometry of ribbed bar and the position of the reinforcement during casting, etc. These factors are the same for all specimens in this work. In addition to the corrosion state of the steel surface, another variable related to bond behavior is the mortar cover. The mortar cover (as depth) was also identical for the tested specimens.

Consequently, the factor that could affect the bond strength would be a variation in bulk matrix properties. This variation would be expected due to the corrosion process itself on one hand, but also modified porosity, pore interconnectivity or micromechanics of the bulk matrix, on the other hand. Hence the aim of the widened frequency range of 1 MHz to 10 mHz is to offer a more detailed information for both the contribution of the bulk matrix and the electrochemical response of the embedded steel.

The used equipment for electrochemical tests in this work was Metrohm Autolab (Potentiostat PGSTAT302N), combined with a FRA2 module and NOVA software package (Version 1.11). The EIS fitting process was performed by NOVA software package (Version 1.11). An example (EIS response of S-28d at age of 490 days; S-28d: 28d-cured in fog room, then treated by supplying stray current in water) for experimental response and fit for the studied specimens in this thesis is presented in Figure C.1 in both Nyquist and Bode format. It can be seen that the proposed circuit - $[R(CR[CR])(Q[R(QR)])]$ gives generally good fitting results. The best-fit parameters for S-28d are presented in Figure C.2. The errors per element for S-28d and R-24h are summarized in Table C.1 and C.2, respectively.

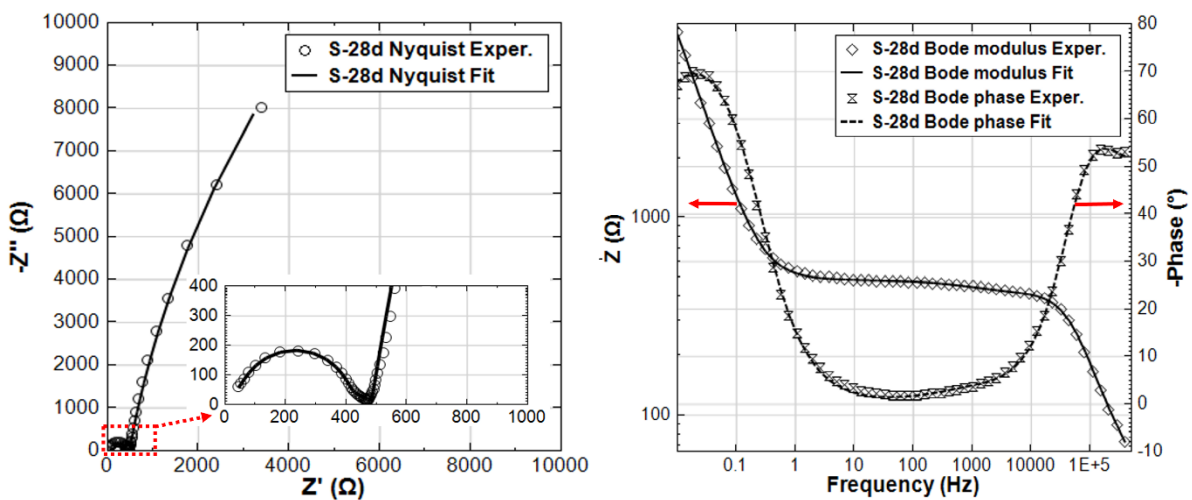


Figure C.1: EIS experimental response (symbols) and fit (lines) of S-28d at age of 490 days, in Nyquist and Bode format. (S-28d: 28d-cured in fog room, then treated by supplying stray current in water).

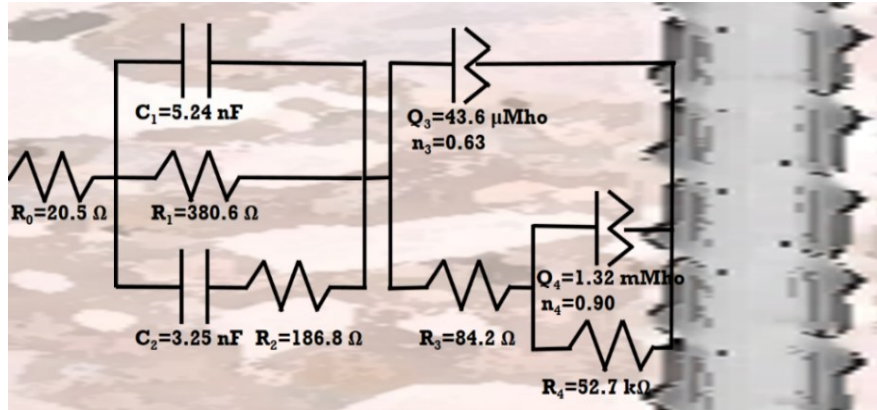


Figure C.2: The best-fit parameters, derived on basis of the experimental EIS response of S-28d at age of 490 days.

Table C.1: Summary of errors per element for S-28d.

Element	Parameter	Value	Estimated Error (%)
R ₀	R ₀	20.483	21.067
C ₁	C ₁	5.24E-09	14.154
R ₁	R ₁	380.61	2.369
C ₂	C ₂	3.25E-09	17.266
R ₂	R ₂	186.76	29.835
Q ₃	Y ₀	4.36E-05	30.416
	n ₃	0.63209	14.524
R ₃	R ₃	84.198	14.299
Q ₄	Y ₀	0.0013192	2.091
	n ₄	0.90397	1.024
R ₄	R ₄	52666	15.687
	χ ²	0.012188	

Table C.2: Summary of errors per element for R-24h.

Element	Parameter	Value	Estimated Error (%)
R ₀	R ₀	16.863	21.878
C ₁	C ₁	5.23E-09	16.117
R ₁	R ₁	342.52	6.802
C ₂	C ₂	5.59E-09	16.379
R ₂	R ₂	114.8	22.262
Q ₃	Y ₀	3.08E-05	26.758
	n ₃	0.55043	17.218
R ₃	R ₃	83.025	35.933
Q ₄	Y ₀	0.0033458	0.838
	n ₄	0.79762	0.685
R ₄	R ₄	28843	16.170
	χ ²	0.0064078	

References

- [1] K. van Breugel, Urgency and challenges of ageing in science and engineering, *The Ageing of Materials and Structures: Towards Scientific Solutions for the Ageing of Our Assets* 2017, pp. 3-13.
- [2] D. Landolt, *Corrosion and surface chemistry of metals*, CRC Press 2007.
- [3] L. Bertolini, M. Carsana, P. Pedferri, Corrosion behaviour of steel in concrete in the presence of stray current, *Corros. Sci.*, 49 (2007) 1056-1068.
- [4] S. Nikolakakos, *Stray Currents-Generation, Interference Effects and Control*, CORROSION 98, NACE International, San Diego, California, 1998, pp. 10.
- [5] E.L. Kirkpatrick, *Stray Current Interference From a Light Rail Traction System*, CORROSION 2011, NACE International, Houston, Texas, 2011, pp. 5.
- [6] D.K. Kim, T.H. Ha, Y.C. Ha, J.H. Bae, H.G. Lee, D. Gopi, J.D. Scantlebury, Alternating current induced corrosion, *Corros. Eng., Sci. Technol.*, 39 (2004) 117-123.
- [7] K. Miskiewicz, A. Wojaczek, S. Fraczek, F. Krasucki, *Electromagnetic compatibility in underground mining: selected problems*, Elsevier 2012.
- [8] R. Dodds, DC traction stray current control - A case study from a utility, *IEE Colloquium (Digest)*, (1999) 49-52.
- [9] Z. Chen, D.A. Koleva, K. van Breugel, Electrochemical Tests in Reinforced Mortar Undergoing Stray Current-Induced Corrosion, in: L.E. Rendon Diaz Miron, D.A. Koleva (Eds.) *Concrete Durability: Cementitious Materials and Reinforced Concrete Properties, Behavior and Corrosion Resistance*, Springer International Publishing, Cham, 2017, pp. 83-108.
- [10] L.J. Mackay, *Steps towards the universal direct current distribution system*, 2018.
- [11] A. Demetriou, D. Buxton, C.A. Charalambous, Stray Current DC Corrosion Blind Spots Inherent to Large PV Systems Fault Detection Mechanisms: Elaboration of a Novel Concept, *ITPD*, 33 (2018) 3-11.
- [12] Y. Jiang, L. Yuan, Z. Zhao, H. Zhang, R. Yi, Y. Ding, W. Gu, An experimental method for extracting stray inductance of bus bars without high bandwidth current measurement, *2017 IEEE Energy Conversion Congress and Exposition, ECCE 2017*, 2017, pp. 1446-1450.
- [13] J.H. Fitzgerald, J. Beggs, *Preparing Gas Distribution Piping for the Construction of Light Rail Transit System*, CORROSION 2003, NACE International, San Diego, California, 2003, pp. 9.
- [14] C. Charalambous, I. Cotton, P. Aylott, *The Influence Of Soil Characteristics On Coupling Between Dc Traction Systems And Buried Utilities*, CORROSION 2007, NACE International, Nashville, Tennessee, 2007, pp. 18.
- [15] Z. Chen, C. Qin, J. Tang, Y. Zhou, Experiment research of dynamic stray current interference on buried gas pipeline from urban rail transit, *Journal of Natural Gas Science and Engineering*, 15 (2013) 76-81.
- [16] J. Riskin, *Electrocorrosion and Protection of Metals: General approach with particular consideration to electrochemical plants*, Elsevier Science 2008.
- [17] I. Lingvay, A. Voina, C. Lingvay, C. Mateescu, The impact of the electromagnetic pollution of the environment on the complex build-up media, *Rev. Roum. Sci. Techn. Series Electrotech. Energ*, 53 (2008) 95-112.
- [18] Z. Jiang, Y. Du, M. Lu, Y. Zhang, D. Tang, L. Dong, New findings on the factors accelerating AC corrosion of buried pipeline, *Corros. Sci.*, 81 (2014) 1-10.
- [19] R.W. Bonds, *Stray current effects on ductile iron pipe*, Alabama, USA: Ductile Iron Pipe Research Association, (1997).
- [20] Y.T. Li, X. Li, G.W. Cai, L.H. Yang, Influence of AC interference to corrosion of Q235 carbon steel, *Corros. Eng., Sci. Technol.*, 48 (2013) 322-326.
- [21] X. Wang, X. Tang, L. Wang, C. Wang, Z. Guo, Corrosion behavior of X80 pipeline steel under coupling effect of stress and stray current, *Int. J. Electrochem. Sci.*, 9 (2014) 4574-4588.
- [22] Q.J. Zhu, A.L. Cao, Z.F. Wang, J.W. Song, S.L. Chen, *Fundamental Aspects of Stray Current Corrosion on Buried Pipeline*, *Advanced Materials Research*, 146-147 (2010) 70-74.
- [23] *Pipelines and Light Rail Transit: A Pipeline Owner's Guide to Stray Current*, Pipelines 2008, pp. 1-7.
- [24] Q. Zhu, A. Cao, W. Zaifeng, J. Song, C. Shengli, Stray current corrosion in buried pipeline, *Anti-Corrosion Methods and Materials*, 58 (2011) 234-237.
- [25] V.S. Sastri, 5 - Corrosion processes and the use of corrosion inhibitors in managing corrosion in underground pipelines, in: M.E. Orazem (Ed.) *Underground Pipeline Corrosion*, Woodhead Publishing 2014, pp. 127-165.
- [26] P. Ferenc, Do we determine the corrosion aggressivity correctly?, *Koroze a Ochrana Materialu*, 36 (1992) 81.
- [27] A.O.S. Solgaard, M. Carsana, M.R. Geiker, A. Küter, L. Bertolini, Experimental observations of stray current effects on steel fibres embedded in mortar, *Corros. Sci.*, 74 (2013) 1-12.
- [28] S.J. Duranceau, W.J. Johnson, R.J. Pfeiffer-Wilder, A Study Examining the Effect of Stray Current on the Integrity of Continuous and Discontinuous Reinforcing Bars, *ExT*, 35 (2011) 53-58.

- [29] L. Carmen, C. Anca, V. Teodor, L. Losif, DEGRADATIONS OF REINFORCED CONCRETE STRUCTURES DUE TO D.C. AND A.C. STRAY CURRENTS, U.P.B. Sci. Bull., Series B, 7 (2011) 143-152.
- [30] L. Bertolini, B. Elsener, P. Pedferri, R. Polder, Corrosion of Steel in Concrete: Prevention, Diagnosis, Repair, (2004).
- [31] A.C. Carmen LINGVAY, Teodor VIŞAN, Iosif LINGVAY, DEGRADATIONS OF REINFORCED CONCRETE STRUCTURES DUE TO D.C. AND A.C. STRAY CURRENTS, U.P.B. Sci. Bull., Series B, 7 (2011) 143-152.
- [32] M.M. Alamuti, H. Nouri, S. Jamali, Effects of earthing systems on stray current for corrosion and safety behaviour in practical metro systems, IET Electrical Systems in Transportation, 1 (2011) 69-79.
- [33] C. Charalambous, I. Cotton, Influence of soil structures on corrosion performance of floating-DC transit systems, IET Electric Power Applications, 1 (2007) 9.
- [34] S. Jamali, M.M. Alamuti, M. Savaghebi, Effects of different earthing schemes on the stray R current in rail transit systems, Padova, 2008.
- [35] E.B. Rosa, B. McCollum, O.S. Peters, Electrolysis in concrete, Govt. Print. Off. 1913.
- [36] A.A. Knudson, Electrolytic corrosion of iron and steel in concrete, Proceedings of the American Institute of Electrical Engineers, 26 (1907) 133-148.
- [37] B. McCollum, K.H. Logan, Leakage of Currents from Electric Railways, (1916).
- [38] G.M. Magee, Electrolytic Corrosion of Steel in Concrete, 한국정밀공학회지 Vol.31 No.2, 31 (2014) 143-143.
- [39] T.W. Ni, T.T. Bi, Z.G. Yang, Failure analysis on abnormal perforation of super large diameter buried gas pipeline nearby metro, Eng. Failure Anal., 103 (2019) 32-43.
- [40] Y. Wang, X. Sun, A. Ren, Investigations of rock anchor corrosion and its influence factors by exhumations in four typical field sites, Eng. Failure Anal., 101 (2019) 357-382.
- [41] J. Chen, S. Ai, J. Liu, H. Yang, L. Wang, M. Zhu, D. Fu, S. Yang, X. Ai, Y. Ai, The life span and influencing factors of metal mesh in artificial soil on railway rock-cut slopes in humid areas, ScTen, 671 (2019) 41-51.
- [42] G. Santi, L. Sandrolini, Stray current interference on high-speed rail transit systems and surrounding buried metallic structures, Proc. 6th Int. Congress CECOR, 2003, pp. 1-12.
- [43] L. Sandrolini, Analysis of the insulation resistances of a high-speed rail transit system viaduct for the assessment of stray current interference. Part 1: Measurement, Electric Power Systems Research, 103 (2013) 241-247.
- [44] S.L. Chen, S.C. Hsu, C.T. Tseng, K.H. Yan, H.Y. Chou, T.M. Too, Analysis of rail potential and stray current for Taipei Metro, ITVT, 55 (2006) 67-75.
- [45] Y.-C. Ha, J.-H. Bae, D.K. Kim, T.-H. Ha, H.-G. Lee, Investigation of Stray Current from DC Subway System in Korea, CORROSION 2005, NACE International, Houston, Texas, 2005, pp. 8.
- [46] C.T. Wang, W. Li, G.F. Xin, Y.Q. Wang, X.F. Yang, Z.A. Guo, Experimental Research Examining the Stray Current Corrosion of Rock Bolts in the DC Transit System, ExT, (2019).
- [47] A. Susanto, D.A. Koleva, O. Copuroglu, K. van Beek, K. van Breugel, Mechanical, Electrical and Microstructural Properties of Cement-Based Materials in Conditions of Stray Current Flow, Journal of Advanced Concrete Technology, 11 (2013) 119-134.
- [48] A. Aghajani, M. Urgan, L. Bertolini, Effects of DC stray current on concrete permeability, J. Mater. Civ. Eng., 28 (2016).
- [49] H. Chu, T. Wang, M.-Z. Guo, Z. Zhu, L. Jiang, C. Pan, T. Liu, Effect of stray current on stability of bound chlorides in chloride and sulfate coexistence environment, Construction and Building Materials, 194 (2019) 247-256.
- [50] C. Pan, J. Geng, Q. Ding, Stray current affects the release of bound chloride ions in hydrated cement paste, Int. J. Electrochem. Sci., 13 (2018) 6098-6111.
- [51] C. Wang, W. Li, Y. Wang, S. Xu, K. Li, Evaluation Model for the Scope of DC Interference Generated by Stray Currents in Light Rail Systems, 12 (2019) 746.
- [52] B. Wang, G.J.J.o.T. Li, Evaluation, The Deterioration of Cement Mortar under the Coupled Conditions of Stray Current and Sulfate, 49 (2019).
- [53] Y.H. Zhu, Y.S. Zou, J. Geng, F.Z. Wang, Influence of stray current on chloride ion migrates in concrete, Wuhan Ligong Daxue Xuebao/Journal of Wuhan University of Technology, 34 (2012) 32-36.
- [54] R. Radeka, D. Zorovic, D. Barisin, Influence of frequency of alternating current on corrosion of steel in seawater, ANTI-CORROS. METHODS & MATER., 27 (1980) 13-15+19.
- [55] R.W. Revie, Corrosion and corrosion control, John Wiley & Sons 2008.
- [56] V. Kolar, R. Hrbac, Measurement of ground currents leaking from DC electric traction, Electric Power Engineering (EPE), Proceedings of the 2014 15th International Scientific Conference on, IEEE, 2014, pp. 613-617.
- [57] M. Ormellese, S. Goidanich, L. Lazzari, M. Pedferri, F. Bolzoni, Laboratory Testing on the Influence of Alternated Current on Steel Corrosion, CORROSION 2004, NACE International, New Orleans, Louisiana, 2004, pp. 11.

- [58] C. Lingvay, A. Cojocaru, T. Vişan, I. Lingvay, Degradations of reinforced concrete structures due to d.c. and a.c. stray currents, *UPB Scientific Bulletin, Series B: Chemistry and Materials Science*, 73 (2011) 143-152.
- [59] H.W. Teng, S.M. Yang, Z.C. Shu, Y. Huang, D. Huo, Simulation experiment of loading influence to reinforcement corrosion affected by stray current and salt solution, *Wuhan Ligong Daxue Xuebao/Journal of Wuhan University of Technology*, 32 (2010) 147-151.
- [60] Z.J. Dong, X.Y. Li, P. Yan, F. Xing, Distribution of the stray current of rebar in the ballast bed, *Applied Mechanics and Materials*, 2012, pp. 2147-2153.
- [61] Y. Luo, C. Wang, C. Luo, Q. Huang, S. Wang, X. Peng, Effect of electrical field on TSA failure of cement-based materials, *Cem. Concr. Res.*, 90 (2016) 19-26.
- [62] A. Brenna, L. Lazzari, M. Ormellese, Stray current control by a new approach based on current monitoring on a potential probe, *Corrosion Engineering Science and Technology*, 52 (2017) 359-364.
- [63] K. Tang, Stray current induced corrosion of steel fibre reinforced concrete, *Cem. Concr. Res.*, 100 (2017) 445-456.
- [64] J. Tinnea, R. Tinnea, D. Burke, L. Nelson, S. Cochran, E. Anderson, L. Pham, Evaluating Concrete Resistivity: Reducing Stray Current From Dc Streetcars, *NACE International*.
- [65] M. Narozny, K. Zakowski, K. Darowicki, Method of sacrificial anode dual transistor-driving in stray current field, *Corros. Sci.*, 98 (2015) 605-609.
- [66] C. Wang, W. Li, Y. Wang, S. Xu, X. Yang, Chloride-induced stray current corrosion of Q235A steel and prediction model, *Construction and Building Materials*, 219 (2019) 164-175.
- [67] M. Chen, K. Wang, Q. Wu, Z. Qin, An Experimental Corrosion Investigation of Coupling Chloride Ions with Stray Current for Reinforced Concrete, *Applied Mechanics and Materials*, 166-169 (2012) 1987-1993.
- [68] K. Wang, Q.S. Wu, M.C. Chen, L. Xie, Corrosion fatigue of reinforced concrete in the presence of stray current, 2011 International Conference on Electric Technology and Civil Engineering, ICETCE 2011 Lushan, 2011, pp. 1133-1136.
- [69] X. Wang, X. Song, Y. Chen, Z. Wang, L. Zhang, Study on corrosion and delamination behavior of X70 steel under the coupling action of AC-DC interference and Stress, *Int. J. Electrochem. Sci.*, 14 (2019) 1968-1985.
- [70] C. Wen, J. Li, S. Wang, Y. Yang, Experimental study on stray current corrosion of coated pipeline steel, *Journal of Natural Gas Science and Engineering*, 27 (2015) 1555-1561.
- [71] F.E. Sloan, J.B. Talbot, Corrosion of Graphite-Fiber-Reinforced Composites II Anodic Polarization Damage, *Corrosion*, 48 (1992) 7.
- [72] C. Wang, W. Li, G. Xin, Y. Wang, S. Xu, Prediction Model of Corrosion Current Density Induced by Stray Current Based on QPSO-Driven Neural Network, *Complexity*, 2019 (2019).
- [73] G. Cui, Z.L. Li, C. Yang, M. Wang, The influence of DC stray current on pipeline corrosion, *Petroleum Science*, 13 (2016) 135-145.
- [74] G. Xu, H.F. Fei, Y.M. Wang, Q. Wang, Research on Corrosion Characteristics of Stainless Steel Bar in Stray Current and Chloride Ion Coexisted Environment, *Advanced Materials Research*, 261-263 (2011) 56-60.
- [75] I. Cotton, C. Charalambous, P. Aylott, P. Ernst, Stray current control in DC mass transit systems, *ITVT*, 54 (2005) 722-730.
- [76] E. Wetzel, Track-to-Earth Resistance, What Does it Mean?, *CORROSION 2005*, NACE International, Houston, Texas, 2005, pp. 22.
- [77] L. Sandrolini, Analysis of the insulation resistances of a high-speed rail transit system viaduct for the assessment of stray current interference. Part 2: Modelling, *Electric Power Systems Research*, 103 (2013) 248-254.
- [78] P.D. Simon, P.O. Ford, Lessons Learned During the Startup of the Phoenix Valley Light Rail System, *CORROSION 2011*, NACE International, Houston, Texas, 2011, pp. 12.
- [79] J.L. Didas, Interference Testing And Case Histories, *CORROSION 2003*, NACE International, San Diego, California, 2003, pp. 9.
- [80] K.T. Solheim, J.K. Lervik, M. Hoeyer-Hansen, Direct Electrical Heating Closer to Subsea Structures, The 26th International Ocean and Polar Engineering Conference, International Society of Offshore and Polar Engineers, Rhodes, Greece, 2016, pp. 4.
- [81] Z. Chen, D. Koleva, E. Koenders, K. van Breugel, Stray Current Induced Corrosion Control in Reinforced Concrete by Addition of Carbon Fiber and Silica Fume, *MRS Proceedings*, Cambridge Univ Press, 2015, pp. imrc2014-2016d-2007.
- [82] C.A. Charalambous, P. Aylott, Dynamic stray current evaluations on cut-and-cover sections of DC metro systems, *ITVT*, 63 (2014) 3530-3538.
- [83] F.C. Robles Hernández, G. Plascencia, K. Koch, Rail base corrosion problem for North American transit systems, *Engineering Failure Analysis*, 16 (2009) 281-294.
- [84] M. Berman, Q.P. Williams, Corrosion control of modern light rail transit (LRT) systems, 2017 Joint Rail Conference, JRC 2017, 2017.
- [85] A.W. Peabody, Peabody's control of pipeline corrosion, *NACE international* 2001.
- [86] C.Y. Ma, D.L. Zhang, Z. Wang, G.X. Li, J.J. Tang, Study on ANFIS application in coal mining stray current security prediction, 3rd International Conference on Engineering and Technologies and Ceeuro, ICETC2009 Changzhou, Jiangsu, 2010, pp. 216-219.

- [87] D.R. Hardman, D.P. Creedy, H.R. Phillips, Strategies to monitor non-homogeneous atmospheres in sealed off panels in coal mines, Jun-2001, (2001).
- [88] K.K. Francisco C. Robles Hernandez, Gabriel Plascencia Barrera, Rail Base Corrosion Detection and Prevention, 2007.
- [89] S. Qian, Y.F. Cheng, Accelerated corrosion of pipeline steel and reduced cathodic protection effectiveness under direct current interference, *Construction and Building Materials*, 148 (2017) 675-685.
- [90] Q. Ding, T. Shen, Y. Cui, J. Xue, Study on the Electrochemical Performance of Sacrificial Anode Interfered by DC Stray Current, *International Journal of Corrosion*, 2018 (2018).
- [91] T.H. Ha, J.H. Bae, H.G. Lee, Y.C. Ha, D.K. Kim, Rapid potential-controlled rectifier for securing the underground pipeline under electrolytic interference, 2004 International Conference on Power System Technology, POWERCON 2004, 2004, pp. 537-541.
- [92] M.Y. Tan, F. Varela, Y. Huo, F. Mahdavi, M. Forsyth, B. Hinton, Monitoring Dynamic Corrosion and Coating Failure on Buried Steel Using an Multi-Electrode Array, CORROSION 2017, NACE International, New Orleans, Louisiana, USA, 2017, pp. 8.
- [93] J.L. Didas, Cathodic Protection Interference - Interference Testing and Mitigation of Interference Issues, CORROSION 2018, NACE International, Phoenix, Arizona, USA, 2018, pp. 8.
- [94] C. Baeté, L. Bortels, K. De Gussemé, G. Schevernels, Investigating Railway Corrosion Caused by Cathodic Protection Systems, CORROSION 2015, NACE International, Dallas, Texas, 2015, pp. 12.
- [95] M. Cadle, T. Whited, Cathodic Protection of Underground Storage Tank Systems with Directionally Drilled Groundbeds below the Tanks, CORROSION 2002, NACE International, Denver, Colorado, 2002, pp. 9.
- [96] E.W. Klechka, G.H. Koch, A.R. Kowalski, A.W. Al-Mithin, E.E. Al-Nasser, Interference Testing in Seawater Injection Treatment Facility, CORROSION 2006, NACE International, San Diego, California, 2006, pp. 13.
- [97] M.A. Klunk, A.A. De Oliveira, G.G. Furtado, G. Knörnschild, L.F.P. Dick, Study of the corrosion of buried steel grids of electrical power transmission towers, 18th Biannual Brazilian Meeting on Electrochemistry and Electroanalytical, SIBEE 2011Bento, Goncalves, 2012, pp. 23-27.
- [98] C. Fu, J. Hu, D. Yang, B. Yang, K. Shuang, J. Zhao, E.H. Han, W. Ke, Survey on soil corrosion of grounding grid of power substations in Hainan Island, *Corrosion Science and Protection Technology*, 29 (2017) 97-102.
- [99] X.M. Lopez-Fernandez, L.A. Alvarez-Gomez, Calculation of stray losses in continuously transposed conductor cable transformer windings by multi-slice methodology, *International Journal of Electrical Power and Energy Systems*, 111 (2019) 25-33.
- [100] R. Qin, Y. Du, G. Peng, M. Lu, Z. Jiang, High Voltage Direct Current Interference on Buried Pipelines: Case Study and Mitigation Design, CORROSION 2017, NACE International, New Orleans, Louisiana, USA, 2017, pp. 11.
- [101] I. Ragault, AC Corrosion Induced by V.H.V. Electrical Lines on Polyethylene Coated Steel Gas Pipelines, CORROSION 98, NACE International, San Diego, California, 1998, pp. 14.
- [102] F.R. Wojcicki, M.E.M. Negrisoni, C.V. Franco, Stray current induced corrosion in lightning rod cables of 525 kV power lines towers: A case study, *Revista de Metalurgia (Madrid)*, (2003) 124-128.
- [103] Y. Li, X. Yan, C. Wang, Q. Yang, C. Zhang, Eddy Current Loss Effect in Foil Winding of Transformer Based on Magneto-Fluid-Thermal Simulation, *ITM*, 55 (2019).
- [104] Z. Panossian, S.E. Filho, N.L. de Almeida, M.L. Pereira Filho, D. de L.Silva, E.W. Laurino, J.H. L.Oliver, G. de S.Pimenta, J.A. C.Albertini, Effect Of Alternating Current By High Power Lines Voltage And Electric Transmission Systems In Pipelines Corrosion, CORROSION 2009, NACE International, Atlanta, Georgia, 2009, pp. 41.
- [105] S.P. Beton, Onderzoek en vervolg (Report), Structon Prefab Beton, Netherlands, 2012.
- [106] P.R. Roberge, Handbook of corrosion engineering, 2nd ed., McGraw-Hill Education, Columbus, 2012
- [107] L. Trichtchenko, Telluric and ocean current effects on buried pipelines and their cathodic protection systems, (2002).
- [108] P. Nicholson, Correcting CIPS Surveys for Stray and Telluric Current Interference, CORROSION 2007, NACE International, Nashville, Tennessee, 2007, pp. 9.
- [109] D.H. Boteler, Telluric Currents And Their Effect On Cathodic Protection Of Pipelines, CORROSION 2004, NACE International, New Orleans, Louisiana, 2004, pp. 12.
- [110] D.R. Lenard, J.G. Moores, Initiation of crevice corrosion by stray current on stainless steel propeller shafts, *Corrosion*, 49 (1993) 769-775.
- [111] G.D. Sump, M.D. Schrantz, Stray Current Corrosion During Platform Welding Operations Offshore, Offshore Technology Conference, Offshore Technology Conference, Houston, Texas, 1977, pp. 8.
- [112] M. Islam, J. Ellor, Analysis of Corrosion Damage on Propulsion Shafts of Marine Vessels, CORROSION 2015, NACE International, Dallas, Texas, 2015, pp. 9.
- [113] S. Muralidharan, D.-K. Kim, T.-H. Ha, J.-H. Bae, Y.-C. Ha, H.-G. Lee, J.D. Scantlebury, Influence of alternating, direct and superimposed alternating and direct current on the corrosion of mild steel in marine environments, *Desalination*, 216 (2007) 103-115.
- [114] S.J. Sutton, P.L. Lewin, S.G. Swingle, Review of global HVDC subsea cable projects and the application of sea electrodes, *International Journal of Electrical Power and Energy Systems*, 87 (2017) 121-135.

- [115] A. Drach, I. Tsukrov, Low Cost Real-Time Stray Current Monitoring System for Seawater Field Studies, CORROSION 2013, NACE International, Orlando, Florida, 2013, pp. 12.
- [116] I. Cornet, D. Pirtz, M. Polivka, Y. Gau, A. Shimizu, Effect Of Stray Electric Current On The Corrosion Of Prestressed Concrete In Sea Water, Offshore Technology Conference, Offshore Technology Conference, Houston, Texas, 1978, pp. 6.
- [117] P. Nicholson, High Voltage Direct Current Interference With Underground/Underwater Pipelines, CORROSION 2010, NACE International, San Antonio, Texas, 2010, pp. 13.
- [118] A.L. Cao, L. Guo, J.J. Li, Stray Current Corrosion of Aluminum Electrolysis System, IOP Conference Series: Materials Science and Engineering, 2018.
- [119] G. Schick, F.N. Speller Award Lecture: Corrosion and Corrosion Control in the Telecommunications Outside Plant, Corrosion, 57 (2001) 7.
- [120] A. Dimitriou, C.A. Charalambous, DC Interference Modeling for Assessing the Impact of Sustained DC Ground Faults of Photovoltaic Systems on Third-Party Infrastructure, ITIE, 66 (2019) 2935-2945.
- [121] S. Al Mahrooqi, M.K. Azim, Solving a Mysterious Casings Failure Problem in ESP Fitted Production Field, SPE Middle East Oil & Gas Show and Conference, Society of Petroleum Engineers, Manama, Bahrain, 2015, pp. 30.
- [122] K. Żakowski, K. Darowicki, Detection of Stray Current Field Interference on Metal Constructions Using STFT, Key Eng. Mater., 293-294 (2005) 785-780.
- [123] K. Żakowski, K. Darowicki, Methods of Evaluation of the Corrosion Hazard Caused by Stray Currents to Metal Structures Containing Aggressive Media, Pol J Environ Stud, 9 (2000) 237-241.
- [124] K. Zakowski, K. Darowicki, Some aspects of potential measurements in a stray current field, Corros. Rev., 19 (2001) 55-67.
- [125] K. Zakowski, K. Darowicki, Potential changes in an electric field and electrolytic corrosion, Anti-Corrosion Methods and Materials, 50 (2003) 25-33.
- [126] K. Darowicki, K. Zakowski, A new time-frequency detection method of stray current field interference on metal structures, Corros. Sci., 46 (2004) 1061-1070.
- [127] M. Narozny, K. Zakowski, K. Darowicki, Method of sacrificial anode transistor-driving in cathodic protection system, Corros. Sci., 88 (2014) 275-279.
- [128] K. Zakowski, K. Darowicki, J. Orlikowski, A. Jazdzewska, S. Krakowiak, M. Gruszka, J. Banas, Electrolytic corrosion of water pipeline system in the remote distance from stray currents-Case study, Case Studies in Construction Materials, 4 (2016) 116-124.
- [129] Y. Li, C. Xu, R. Zhang, Q. Liu, X. Wang, Y. Chen, Effects of stray AC interference on corrosion behavior of X70 pipeline steel in a simulated marine soil solution, Int. J. Electrochem. Sci., 12 (2017) 1829-1845.
- [130] H. Wang, C. Du, Z. Liu, L. Wang, D. Ding, Effect of Alternating Current on the Cathodic Protection and Interface Structure of X80 Steel, Materials, 10 (2017) 851.
- [131] X. Wang, C. Xu, Q. Liu, C. Tu, Y. Chen, Y. Li, Effects of stray AC on delamination of epoxy coatings with defects in 3.5% NaCl solution, Int. J. Electrochem. Sci., 12 (2017) 6520-6534.
- [132] X. Wang, C. Xu, Y. Chen, C. Tu, Z. Wang, X. Song, Effects of stray AC on corrosion of 3-layer polyethylene coated X70 pipeline steel and cathodic delamination of coating with defects in 3.5 wt-% NaCl solution, Corrosion Engineering Science and Technology, 53 (2018) 214-225.
- [133] X. Wang, Q. Liu, Y. Chun, Y. Li, Z. Wang, Evaluation of Delamination of X80 Pipeline Steel Coating Under Alternating Stray Current Via Scanning Electrochemical Microscopy, J. Mater. Eng. Perform., 27 (2018) 3060-3071.
- [134] X. Wang, X. Song, Y. Chen, Z. Wang, Effect of alternating stray current and stress on the corrosion behavior of X80 pipeline steel in soil simulated solution, Int. J. Electrochem. Sci., 13 (2018) 5654-5666.
- [135] E. Ghanbari, S. Lillard, M. Iannuzzi, M.R. Ortiz, Corrosion Behavior of Buried Pipeline in Presence of AC Stray Current in Controlled Environment, CORROSION 2015, NACE International, Dallas, Texas, 2015, pp. 10.
- [136] T. Reyes, D.L. Olson, S. Bhola, B. Mishra, Study Of Corrosion Of Super Martensitic Stainless Steel Under Alternating Current In Artificial Sea Water, CORROSION 2011, NACE International, Houston, Texas, 2011, pp. 12.
- [137] J. George, Alternating Current Interference on Cathodically Protected Pipeline From Railway Electrification Systems, CORROSION 2018, NACE International, Phoenix, Arizona, USA, 2018, pp. 7.
- [138] J. Land, T. Yahner, S. Finneran, Transformer Use for Mitigating Induced Alternating Current Effects on Pipelines, CORROSION 2018, NACE International, Phoenix, Arizona, USA, 2018, pp. 10.
- [139] K. Tang, S. Wilkinson, Corrosion resistance of electrified railway tunnels made of steel fibre reinforced concrete, Construction and Building Materials, 230 (2020).
- [140] Q. Ding, Z. Li, T. Shen, G. Cui, Corrosion behavior of X80 steel under disbond coating interfered with AC, Anti-Corrosion Methods and Materials, 66 (2019) 704-718.
- [141] K. Tang, Corrosion of discontinuous reinforcement in concrete subject to railway stray alternating current, Cem. Concr. Compos., 109 (2020) 103552.

- [142] C. Wang, W. Li, Y. Wang, X. Yang, S. Xu, Study of electrochemical corrosion on Q235A steel under stray current excitation using combined analysis by electrochemical impedance spectroscopy and artificial neural network, *Construction and Building Materials*, 247 (2020) 118562.
- [143] E. Smulders, *Zwerfstromen: Al een eeuw een uitdaging*, Movares.
- [144] D. Seimbille, Design of power supply system in DC electrified transit railways-Influence of the high voltage network, 2014.
- [145] G. Van Alphen, V.W.M. Van Rens, H.W.M. Smulders, Analysis of AC traction power supplies using the SIMSPOG® simulation tool, *Advances in Transport*, 2000, pp. 555-565.
- [146] A. Zoeteman, F. Ten Harve, T. Ploeg, Analysing the business case for introducing a 3 kV traction power supply in Dutch railways, *WIT Transactions on the Built Environment*, 2014, pp. 745-755.
- [147] J.-M. Allenbach, P. Chapas, M. Comte, R. Kaller, *Traction électrique*, PPUR presses polytechniques 2008.
- [148] R. Kaller, J.M. Allenbach, *Traction électrique*, Presses polytechniques et universitaires romandes 1995.
- [149] D. Hetherington, G. White, Understanding power supply from a railway operating company's perspective, (2007).
- [150] D. Faugt, AC/DC interference corrosion in pipelines, Summary Report, MetriCorr, (2006).
- [151] E.H.W.M. Smulders, G.G.C. Van Der Hoeven, When D.C. Traction Systems Meet HF Disturbances: The Best of Both Worlds?, *IEEE International Symposium on Electromagnetic Compatibility*, 2018, pp. 255-259.
- [152] V. Kustova, D. Lindemuth, C. Kuykendall, DC transit stray current corrosion control: Everyone wins when you work together, *NACE - International Corrosion Conference Series*, 2018.
- [153] A. Mujezinović, S. Martinez, K. Kekez, Estimating harmful effect of dynamic stray currents on pipeline by simultaneous multiparametric field measurements, continuous wavelet cross-correlation analysis, and frequency plots, *Mater. Corros.*, (2018).
- [154] M. Liu, S. Lin, L. Zhao, X. Lin, L. Chen, Study on Dynamic Characteristics of Metro Stray Current Based on CDEGS, *Lecture Notes in Electrical Engineering*, 2018, pp. 571-578.
- [155] H. Qin, Y. Du, J. Liu, Z. Liu, X. He, Corrosion behavior of buried pipeline under dynamic DC stray current interference, *NACE - International Corrosion Conference Series*, 2018.
- [156] R. De Las Casas, Dynamic Stray Current Interference Mitigation Commissioning Testing For a 90-inch (2.28 M) Water Main, *CORROSION 2011*, NACE International, Houston, Texas, 2011, pp. 12.
- [157] Y. Du, D. Tang, H. Qin, M. Lu, Research on Parameter Fluctuation Characteristics and Effects on Corrosion Rates Under Dynamic DC Stray Current From Metro System, *CORROSION 2019*, NACE International, Nashville, Tennessee, USA, 2019, pp. 13.
- [158] Y. Zhang, L. Xing, M. Lu, Y. Du, Z. Jiang, Study on Dynamic AC Interference of High-Speed Railway on Pipelines, *CORROSION 2019*, NACE International, Nashville, Tennessee, USA, 2019, pp. 14.
- [159] K.J. Moody, Dynamic Stray Current Analysis for New DC Powered Transit Systems, *CORROSION 2005*, NACE International, Houston, Texas, 2005, pp. 10.
- [160] A.Q. Fu, Y.F. Cheng, Effects of alternating current on corrosion of a coated pipeline steel in a chloride-containing carbonate/bicarbonate solution, *Corros. Sci.*, 52 (2010) 612-619.
- [161] M. Zhu, C. Du, X. Li, Z. Liu, H. Li, D. Zhang, Effect of AC on stress corrosion cracking behavior and mechanism of X80 pipeline steel in carbonate/bicarbonate solution, *Corros. Sci.*, 87 (2014) 224-232.
- [162] M. Zhu, C. Du, X. Li, Z. Liu, S. Wang, J. Li, D. Zhang, Effect of AC current density on stress corrosion cracking behavior of X80 pipeline steel in high pH carbonate/bicarbonate solution, *Electrochim. Acta*, 117 (2014) 351-359.
- [163] M.A. Pagano, S.B. Lalvani, Corrosion of mild steel subjected to alternating voltages in seawater, *Corros. Sci.*, 36 (1994) 127-140.
- [164] M. Zhu, C.W. Du, X.G. Li, Z.Y. Liu, L.Y. Wang, Effects of alternating current (AC) frequency on corrosion behavior of X80 pipeline steel in a simulated acid soil solution, *Journal of the Chinese Society of Corrosion and Protection*, 34 (2014) 225-230.
- [165] L. Lazzari, P. Pedferri, *Cathodic Protection*, (2006).
- [166] D.A. Jones, Effect of Alternating Current on Corrosion of Low Alloy and Carbon Steels, *Corrosion (Houston)*, 34 (1978) 428-433.
- [167] H.-S. Song, Y.-T. Kho, Y.-G. Kim, S.-M. Lee, Y.S. Park, Competition of AC and DC Current in AC Corrosion Under Cathodic Protection, *NACE International*, 2002.
- [168] M. Büchler, Alternating current corrosion of cathodically protected pipelines: Discussion of the involved processes and their consequences on the critical interference values, *Mater. Corros.*, 63 (2012) 1181-1187.
- [169] M. Zhu, C.W. Du, X.G. Li, Z.Y. Liu, X.G. Wu, Effect of AC on corrosion behavior of X80 pipeline steel in high pH solution, *Mater. Corros.*, (2014) n/a-n/a.
- [170] A. Junker, L.V. Nielsen, C. Heinrich, P. Møller, Laboratory and field investigation of the effect of the chemical environment on AC corrosion, *NACE - International Corrosion Conference Series*, 2018.
- [171] H.R. Hanson, J. Smart, AC corrosion on a pipeline located in an HVAC utility corridor, *NACE Meeting Papers*, 2004.
- [172] S. Goidanich, L. Lazzari, M. Ormellese, AC corrosion. Part 2: Parameters influencing corrosion rate, *Corros. Sci.*, 52 (2010) 916-922.

- [173] X. Wang, Z. Wang, Y. Chen, X. Song, C. Xu, Research on the Corrosion Behavior of X70 Pipeline Steel Under Coupling Effect of AC + DC and Stress, *J. Mater. Eng. Perform.*, (2019).
- [174] M. Zamanzadeh, P. Taheri, G.T. Bayer, J. Hristov, K. Groll, AC Interference Corrosion, Corrosive Soil, Design Issues, Zinc Ribbon and Corrosion Mitigation, *CORROSION 2019*, NACE International, Nashville, Tennessee, USA, 2019, pp. 15.
- [175] F. Bolzoni, S. Goidanich, L. Lazzari, M. Ormellese, Laboratory test results of AC interference on polarized steel, *Proc. Int. Conf. CORROSION/03*, (2003).
- [176] S. Goidanich, L. Lazzari, M. Ormellese, M.P. Pedferri, Effect of AC interference on CP monitoring, *Proc. Int. Conf. EUROCORR/04*, (2004).
- [177] S. Goidanich, L. Lazzari, M. Ormellese, M.P. Pedferri, Effect of AC on CP of carbon steel in soil simulated conditions, *Proc. Int. Conf. EUROCORR/06*, (2006).
- [178] M. Ormellese, L. Lazzari, A. Brenna, Ac-induced corrosion on passive metals, *Corrosion 2010* San Antonio, TX, 2010.
- [179] K. Tang, Stray alternating current (AC) induced corrosion of steel fibre reinforced concrete, *Corros. Sci.*, (2019).
- [180] M. Ormellese, L. Lazzari, S. Goidanich, V. Sesia, Cp Criteria Assessment In The Presence Of Ac Interference, *CORROSION 2008*, NACE International, New Orleans, Louisiana, 2008, pp. 10.
- [181] L. Lazzari, S. Goidanich, M. Ormellese, F. Bolzoni, Laboratory Test Results of AC Interference on Polarized Steel, *CORROSION 2003*, NACE International, San Diego, California, 2003, pp. 13.
- [182] R.A. Gummow, R.G. Wakelin, S.M. Segall, AC Corrosion - A New Challenge to Pipeline Integrity, NACE International, 1998.
- [183] Z. Chen, D. Koleva, K. van Breugel, A review on stray current-induced steel corrosion in infrastructure, *Corros. Rev.*, 35 (2017) 397-423.
- [184] P. Vernon, STRAY-CURRENT CORROSION CONTROL IN METROS, *Proceedings of the Institution of Civil Engineers (London)*, 80 (1986) 641-650.
- [185] Y. Du, J. Wang, L. Wang, M. Lu, Researches on mitigation methods of interference caused by cathodic protection system, *NACE - International Corrosion Conference Series*, 2015.
- [186] G.C. Liu, W. Sun, L. Wang, Y. Li, Modeling cathodic shielding of sacrificial anode cathodic protection systems in seawater, *Mater. Corros.*, 64 (2013) 472-477.
- [187] H. Cheng, Z. Xiao, X. Wang, N. Sun, Study on Protection from Stray Current in the Metro System, in: L. Jia, Y. Qin, J. Suo, J. Feng, L. Diao, M. An (Eds.) *Proceedings of the 3rd International Conference on Electrical and Information Technologies for Rail Transportation (EITRT) 2017*, Springer Singapore, Singapore, 2018, pp. 709-716.
- [188] X. Wang, N. Qu, X. Fang, Reducing stray corrosion in jet electrochemical milling by adjusting the jet shape, *J. Mater. Process. Technol.*, 264 (2019) 240-248.
- [189] Z. Yu, L. Liu, Z. Wang, M. Li, X. Wang, Evaluation of the interference effects of HVDC grounding current on a buried pipeline, *ITAS*, 29 (2019).
- [190] L. Liu, Z. Yu, Z. Wang, M. Li, X. Wang, Analysis of the Monitoring Data of UHVDC Grounding Current Interference in a Buried Pipeline, *ITAS*, 29 (2019).
- [191] S. Memon, P. Fromme, Stray current simulation models for direct current transit system - An industry perspective, *2015 Joint Rail Conference, JRC 2015*, 2015.
- [192] T. Chuchit, T.J.E.E. Kulworawanichpong, Stray current assessment for DC transit systems based on modelling of earthing and bonding, (2019).
- [193] L. Liu, Z. Yu, Z. Jiang, J. Hao, W. Liu, Observation research on the effect of UHVDC grounding current on buried pipelines, *Energies*, 12 (2019).
- [194] X. Liu, C. Wang, N. Liu, X. Jiao, Current-induced corrosion of aluminium heat sinks in water-cooling systems for high-voltage direct-current converters, *Corrosion Engineering Science and Technology*, 54 (2019) 131-142.
- [195] S.A. Memon, E.C. Flounders, Jr., Stray Current Guidebook for Rail Transit and the Lessons Learned, *CORROSION 2019*, NACE International, Nashville, Tennessee, USA, 2019, pp. 6.
- [196] P.D. Simon, Quantifying LRT Stray Current Effects Using Coupons, *CORROSION 2005*, NACE International, Houston, Texas, 2005, pp. 17.
- [197] K. Zakowski, The determination and identification of stray current source influences on buried pipelines using time/frequency analysis, *Anti-Corrosion Methods and Materials*, 56 (2009) 330-333.
- [198] M.C. Briglia, B. Bazzoni, G. Cavallero, D. Melodia, F. Panaro, Monitoring of Stray Current Interference in the Reinforced Concrete Structures of the Turin Underground Railway Loop, NACE International, 1999.
- [199] K. Zakowski, W. Sokólski, 24-hour characteristic of interaction on pipelines of stray currents leaking from tram tractions, *Corros. Sci.*, 41 (1999) 2099-2111.
- [200] A. Ogunsola, A. Mariscotti, L. Sandrolini, Estimation of stray current from a DC-electrified railway and impressed potential on a buried pipe, *ITPD*, 27 (2012) 2238-2246.
- [201] G. Lucca, Estimating stray current interference from DC traction lines on buried pipelines by means of a Monte Carlo algorithm, *Electrical Engineering*, 97 (2015) 277-286.

- [202] W. Machczynski, K. Budnik, J. Szymenderski, Assessment of d.c. traction stray currents effects on nearby pipelines, *COMPEL - The International Journal for Computation and Mathematics in Electrical and Electronic Engineering*, 35 (2016) 1468-1477.
- [203] A. Zaboli, B. Vahidi, S. Yousefi, M.M. Hosseini-Biyouki, Evaluation and Control of Stray Current in DC-Electrified Railway Systems, *ITVT*, 66 (2017) 974-980.
- [204] A. Ogunsola, L. Sandrolini, A. Mariscotti, Evaluation of stray current from a DC-electrified railway with integrated electric-electromechanical modeling and traffic simulation, *ITIA*, 51 (2015) 5431-5441.
- [205] G. Du, C. Wang, J. Liu, G. Li, D. Zhang, Effect of over zone feeding on rail potential and stray current in DC mass transit system, *Mathematical Problems in Engineering*, 2016 (2016).
- [206] G. Cui, Z. Li, L. Zhao, X. Wei, Local cathodic protection design based on numerical simulation, *Anti-Corrosion Methods and Materials*, 62 (2015) 407-415.
- [207] F. Brichau, J. Deconinck, T. Driesens, Modeling of Underground Cathodic Protection Stray Currents, *Corrosion (Houston)*, 52 (1996) 480-488.
- [208] L. Bortels, J. Parlongue, P.J. Stehouwer, K. Dijkstra, Methods, Simulations And Experiences On Dc-Traction Interference On Pipeline Networks, *NACE International*.
- [209] C. Baeté, L. Bortels, K. De Gussemé, G. Schevernels, Investigating Railway Corrosion Caused by Cathodic Protection Systems, *NACE International*.
- [210] A.L. Cao, Q.J. Zhu, S.T. Zhang, B.R. Hou, BP neural network predictive model for stray current density of a buried metallic pipeline, *Anti-Corrosion Methods and Materials*, 57 (2010) 234-237.
- [211] M. Brenna, A. Dolara, S. Leva, D. Zaninelli, Effects of the DC stray currents on subway tunnel structures evaluated by FEM Analysis, (2010).
- [212] F. Fichera, A. Mariscotti, A. Ogunsola, Evaluating stray current from DC electrified transit systems with lumped parameter and multi-layer soil models, *IEEE EuroCon 2013 Zagreb*, 2013, pp. 1187-1192.
- [213] S. Li, Y.G. Kim, Numerical modeling of stray current corrosion of ductile iron pipe induced by foreign cathodic protection system, *Metals and Materials International*, 19 (2013) 717-729.
- [214] C.A. Charalambous, I. Cotton, P. Aylott, N.D. Kokkinos, A holistic stray current assessment of bored tunnel sections of DC transit systems, *ITPD*, 28 (2013) 1048-1056.
- [215] A. Dolara, F. Foiadelli, S. Leva, Stray current effects mitigation in subway tunnels, *ITPD*, 27 (2012) 2304-2311.
- [216] C.A. Charalambous, I. Cotton, P. Aylott, Modeling for preliminary stray current design assessments: The effect of crosstrack regeneration supply, *ITPD*, 28 (2013) 1899-1908.
- [217] Y.Q. Wang, W. Li, S.Y. Xu, X.F. Yang, Prediction for corrosion status of the metro metal materials in the stray current interference, *Int. J. Electrochem. Sci.*, 8 (2013) 5314-5329.
- [218] D. Tang, Y. Du, J. Liu, M. Lu, S. Chen, Some considerations on the use of coupon under stray direct traction current interference, *NACE - International Corrosion Conference Series*, 2018.
- [219] E.S. Langelund, Pipeline stray current (DC) interference, *NACE - International Corrosion Conference Series*, 2018.
- [220] E. Llewellyn, Z. Sharon, Long-term monitoring of influence from dc transit stray currents on underground pipelines, *NACE - International Corrosion Conference Series*, 2018.
- [221] K. Yu, F. Zhu, J. Yan, R.J.H.-s.R.T. QIU, Testing of DC stray current along highspeed railway, 5 (2014) 14.
- [222] S.L. Greenberger, Parametric Stray Current Monitoring and Mitigation for Electric Rail Stray Current, *CORROSION 2005*, NACE International, Houston, Texas, 2005, pp. 37.
- [223] S. Martinez, A. Ivanković, K. Kekez, Stray current detection on hazardous liquid buried pipelines as a part of pipeline integrity management, *CEOCOR 2014*, 2014.
- [224] M.Y.J. Tan, F. Varela, K. Wang, Field Experiences of Using Electrochemically Integrated Electrode Arrays as Corrosion Monitoring Probes for Visualizing Buried Pipeline Corrosion, *CORROSION 2019*, NACE International, Nashville, Tennessee, USA, 2019, pp. 15.
- [225] A. Rezaie, A. Char, A. Chikkam, T. Wockenfuss, P. Taheri, M. Zamanzadeh, Corrosion Risk Assessment at Anchor Shafts of Telecommunication Towers, *CORROSION 2019*, NACE International, Nashville, Tennessee, USA, 2019, pp. 10.
- [226] V.r. Gangula, K. Bera, Electrical Interference-Emerging Threat to Pipeline, *SPE Oil and Gas India Conference and Exhibition*, Society of Petroleum Engineers, Mumbai, India, 2019, pp. 8.
- [227] D. Lindemuth, D. Crabtree, AC And DC Stray Current Mitigation And Corrosion Control For a New Urban Pipeline, *CORROSION 2012*, NACE International, Salt Lake City, Utah, 2012, pp. 15.
- [228] K.J. Moody, Maintenance Testing of Stray Current Control Equipment on DC Transit Systems - Present and Future, *CORROSION 2003*, NACE International, San Diego, California, 2003, pp. 14.
- [229] J.F. Jenkins, Use of Reference Electrodes for Galvanic Corrosion and Stray Current Detection and Assessment, *CORROSION 2001*, NACE International, Houston, Texas, 2001, pp. 14.
- [230] C. Wu, L. Liu, H. Chen, Study On Pipeline Interference From Stray Current Of Dc Light Railway, *CORROSION 2008*, NACE International, New Orleans, Louisiana, 2008, pp. 5.
- [231] J. Ivaschenko, Y.A. Tabib, J.H. Fitzgerald, Alternative to Resolving Third Party Stray Currents on the Electric and Gas Utilities, *CORROSION 2000*, NACE International, Orlando, Florida, 2000, pp. 17.

- [232] S.M. Hesjevik, Isolation Joint Stray Currents Experimental Testing And Modelling, CORROSION 2009, NACE International, Atlanta, Georgia, 2009, pp. 20.
- [233] J. Zhao, Y. Teng, F. Zhang, H. Chen, An Application of ECDA to a Buried Pipeline Affected by Stray Current Interference, CORROSION 2014, NACE International, San Antonio, Texas, USA, 2014, pp. 7.
- [234] M. Yunovich, Ecda Indirect Assessment Methods - Limitations And Resolution In Presence Of Dynamic Stray Currents, CORROSION 2008, NACE International, New Orleans, Louisiana, 2008, pp. 12.
- [235] B. Bazzoni, L. Lazzari, L. Bertolini, P. Peddeferri, Potential Measurements And Monitoring In Reinforced Concrete Structures In Presence Of Stray Currents, Corrosion97, NACE International, New Orleans, Louisiana, 1997, pp. 15.
- [236] A. Brenna, L. Lazzari, M. Ormellese, Effects of Intermittent DC Stray Current on Carbon Steel Under Cathodic Protection, CORROSION 2015, NACE International, Dallas, Texas, 2015, pp. 11.
- [237] B. Bazzoni, L. Lazzari, The Lateral Gradient Technique for Potential Measurements in Presence of Stray Current, CORROSION 96, NACE International, Denver, Colorado, 1996, pp. 11.
- [238] L. Dong, M. Lu, Y. Du, Z. Jiang, Analysis of Metro Stray Current Interference On Underground Pipelines With a SACP System By Field Tests And Numerical Simulation, CORROSION 2012, NACE International, Salt Lake City, Utah, 2012, pp. 11.
- [239] J.H. Fitzgerald, J. Beggs, Stray Current Testing on a Gas Distribution Piping Following Start-up of a New Light Rail Transit Line, CORROSION 2005, NACE International, Houston, Texas, 2005, pp. 11.
- [240] Y. Liu, Z. Liang, H. Chen, P. Luo, Use Fft Method For The Detection And Characterization Of Pipeline's Ac Stray Current Interference, CORROSION 2011, NACE International, Houston, Texas, 2011, pp. 12.
- [241] P.S. Rothman, S. Nikolakakos, M. Szeliga, Innovative Approach to Stray Current Monitoring at the Site of the World Trade Center in New York City, CORROSION 2006, NACE International, San Diego, California, 2006, pp. 14.
- [242] M. Yunovich, N.G. Thompson, Coupon Monitoring for Cathodic Protection Optimization: Real Time Automated Remote Control of Dynamic Stray Current on Pipe Type Cables, CORROSION 2002, NACE International, Denver, Colorado, 2002, pp. 18.
- [243] T. Gooderham, D.G. John, S. Viles, B. Stipac, Design and Supply of a Condition Monitoring System for Corrosion and Stray Current Monitoring on the Cityringen Metro Project in Copenhagen, CORROSION 2016, NACE International, Vancouver, British Columbia, Canada, 2016, pp. 10.
- [244] L. Lazzari, P. Galimberti, F. Gaddi, M. Alberizzi, Corrosion Monitoring System for Reinforced Concrete Transit Tunnel, CORROSION 98, NACE International, San Diego, California, 1998, pp. 14.
- [245] S. Al-Sulaiman, A. Jaragh, H. Sabri, R. Rahim, DC Interference Testing and Mitigation of New Electrically Isolated Pipelines Installed within Congested Existing Pipeline Network, CORROSION 2013, NACE International, Orlando, Florida, 2013, pp. 14.
- [246] J. Araujo, Electrical Interference Between Buried Pipelines, CORROSION 2013, NACE International, Orlando, Florida, 2013, pp. 8.
- [247] Y. Hosokawa, F. Kajiyama, T. Fukuoka, Alternating Current Corrosion Risk Arising from Alternating Current-Powered Rail Transit Systems on Cathodically Protected Buried Steel Pipelines and Its Measures, Corrosion, 60 (2004) 6.
- [248] Y. Hosokawa, F. Kajiyama, External Corrosion Risk Management For Aged Steel Pipelines Buried In High Consequence Areas, CORROSION 2005, NACE International, Houston, Texas, 2005, pp. 15.
- [249] J.M. Kilpatrick, L.V. Collings, Use of the Casing Potential Profile Test for Well Casing Interference Studies, Drilling and Production Practice, American Petroleum Institute, New York, New York, 1967, pp. 6.
- [250] R. Mishra, S.S. Varadkar, Combined Cathodic and Anodic Critical Interference on a Pipeline - Detection, Analysis and Mitigation of Corrosion Risk, CORROSION 2017, NACE International, New Orleans, Louisiana, USA, 2017, pp. 7.
- [251] T. Sirola, Review of Recent Developments in Induced AC Current Corrosion Mitigation Design, Materials, Installation and Monitoring Technologies, CORROSION 2017, NACE International, New Orleans, Louisiana, USA, 2017, pp. 12.
- [252] N. International, Alternating Current Corrosion on Cathodically Protected Pipelines: Risk Assessment, Mitigation, and Monitoring, NACE International, 2018, pp. 16.
- [253] F. Song, Field Methods For Measuring Off-Potentials On A Buried Pipeline In Challenging Conditions, CORROSION 2011, NACE International, Houston, Texas, 2011, pp. 21.
- [254] P. Nicholson, Is Your Pipeline Corroding?, CORROSION 2008, NACE International, New Orleans, Louisiana, 2008, pp. 15.
- [255] K. Tang, Corrosion of steel fibre reinforced concrete (SFRC) subjected to simulated stray direct (DC) interference, Materials Today Communications, 20 (2019).
- [256] W.H.A. Peelen, E.A.C. Neeft, G. Leegwater, W. van Kanten-Roos, W.M.G. Courage, Monitoring dc stray current corrosion at sheet pile structures, in: O. Buyukozturk (Ed.) RILEM Bookseries, 2012, pp. 921-926.
- [257] W.H.A. Peelen, E.A.C. Neeft, G. Leegwater, W. Van Kanten-Roos, W.M.G. Courage, Monitoring DC stray current interference of steel sheet pile structures in railway environment, Heron, 56 (2011) 107-122.
- [258] L. Guoxin, Z. Dongliang, W. Chonglin, D. Wei, Research on real-time measurement of key parameters of stray current in DC traction system, Proc. of the 2009 IWISA, (2009).

- [259] E. Nicholson, Stray current detection and correction, B. Eng. Cathodic Technology Ltd, Bolton, Ontario, Canada., Jurata, Poland, 2010.
- [260] C. Andrade, I. Martínez, M. Castellote, Feasibility of determining corrosion rates by means of stray current-induced polarisation, *JApEl*, 38 (2008) 1467-1476.
- [261] Y.-H. Yoo, T.-H. Nam, Y.-S. Choi, J.-G. Kim, L. Chung, A galvanic sensor system for detecting the corrosion damage of the steel embedded in concrete structures: Laboratory tests to determine the cathodic protection and stray-current, *Metals and Materials International*, 17 (2011) 623-629.
- [262] S. Xu, W. Li, Y. Wang, F. Xing, Stray current sensor with cylindrical twisted fiber, *ApOpt*, 53 (2014) 5486-5492.
- [263] Y. Hong, Z. Li, G. Qiao, J. Ou, Numerical simulation and experimental investigation of the stray current corrosion of viaducts in the high-speed rail transit system, *Construction and Building Materials*, 157 (2017) 416-423.
- [264] C. Wang, W. Li, Y. Wang, S. Xu, M. Fan, Stray current distributing model in the subway system: A review and outlook, *Int. J. Electrochem. Sci.*, 13 (2018) 1700-1727.
- [265] C.A. Charalambous, Comprehensive modeling to allow informed calculation of DC traction systems' stray current levels, *ITVT*, 66 (2017) 9667-9677.
- [266] S. Zajaczek, J. Ciganek, J. Mohylova, M. Durica, Modelling of stray currents near a railway platform, *Advances in Electrical and Electronic Engineering*, 15 (2017) 763-769.
- [267] Y. Lin, K. Li, M. Su, Y. Meng, Research on stray current distribution of metro based on numerical simulation, 2018 IEEE International Symposium on Electromagnetic Compatibility and 2018 IEEE Asia-Pacific Symposium on Electromagnetic Compatibility, EMC/APEMC 2018, 2018, pp. 36-40.
- [268] J.G. Yu, Effects of earthing strategies on rail potential and stray currents in D.C. transit railways, *IEE Conference Publication*, 1998, pp. 303-309.
- [269] S.Y. Xu, W. Li, Y.Q. Wang, Effects of vehicle running mode on rail potential and stray current in DC mass transit systems, *ITVT*, 62 (2013) 3569-3580.
- [270] J. Wang, Study on Distribution of Metro Stray Current Based on Multi-locomotive Operation, (2012).
- [271] G. Wang, X.X. Pei, Three dimensional finite element modeling and analysis of different subway tunnels stray current fields, *Open Electrical and Electronic Engineering Journal*, 8 (2014) 124-132.
- [272] Y.S. Tzeng, C.H. Lee, Analysis of rail potential and stray currents in a direct-current transit system, *ITPD*, 25 (2010) 1516-1525.
- [273] P. Svoboda, S. Zajaczek, R. Šprlak, J. Mohylova, Simulation of stray currents on single track in Matlab Simulink, *Proceedings of the 2014 15th International Scientific Conference on Electric Power Engineering, EPE 2014*, 2014, pp. 609-612.
- [274] R. Šprlak, P. Svoboda, Analysis of stray currents for traction vehicles, *2014 14th International Conference on Environment and Electrical Engineering, IEEEIC 2014 - Conference Proceedings*, 2014, pp. 265-270.
- [275] J.V. Rodríguez, J.S. Feito, Calculation of remote effects of stray currents on rail voltages in DC railways systems, *IET Electrical Systems in Transportation*, 3 (2013) 31-40.
- [276] K.D. Pham, R.S. Thomas, W.E. Stinger, Analysis of stray current, track-to-earth potentials & substation negative grounding in DC traction electrification system, *Proceedings of the IEEE/ASME Joint Railroad Conference*, 2001, pp. 141-160.
- [277] A. Mariscotti, U. Reggiani, A. Ogunsola, L. Sandrolini, Mitigation of electromagnetic interference generated by stray current from a dc rail traction system, *IEEE International Symposium on Electromagnetic Compatibility*, 2012.
- [278] C.H. Lee, H.M. Wang, Effects of grounding schemes on rail potential and stray currents in Taipei Rail Transit Systems, *IEE Proceedings: Electric Power Applications*, 148 (2001) 148-154.
- [279] C.H. Lee, C.J. Lu, Assessment of grounding schemes on rail potential and stray currents in a DC transit system, *ITPD*, 21 (2006) 1941-1947.
- [280] C.H. Lee, Evaluation of the maximum potential rise in Taipei rail transit systems, *ITPD*, 20 (2005) 1379-1384.
- [281] S. Jamali, M.M. Alamuti, M. Savaghebi, Effects of different earthing schemes on the stray current in rail transit systems, *2008 Universities Power Engineering Conference (Upec 08)*, (2008) 1-5.
- [282] Y. Hu, Z. Zhong, J. Fang, Finite element simulation of subway stray current field, *Zhongguo Tiedao Kexue/China Railway Science*, 32 (2011) 129-133.
- [283] F. Fichera, A. Mariscotti, A. Ogunsola, L. Sandrolini, Comparison of distributed and lumped parameters stray current models, *IEEE AFRICON Conference*, 2013.
- [284] C.A. Charalambous, I. Cotton, P. Aylott, A simulation tool to predict the impact of soil topologies on coupling between a light rail system and buried third-party infrastructure, *ITVT*, 57 (2008) 1404-1416.
- [285] C. Charalambous, I. Cotton, Influence of soil structures on corrosion performance of floating-DC transit systems, *IET Electric Power Applications*, 1 (2007) 9-16.
- [286] A. Cerman, F. Janicek, M. Kubala, Resistive-type network model of stray current distribution in railway DC traction system, *Proceedings of the 2015 16th International Scientific Conference on Electric Power Engineering, EPE 2015*, 2015, pp. 364-368.

- [287] A.L. Cao, Protection Against Stray Current Corrosion of Buried Metals Pipeline, Doctor thesis dissertation, College of Material Science and Engineering, (2010).
- [288] Y. Cai, M.R. Irving, S.H. Case, Iterative techniques for the solution of complex DC-rail-traction systems including regenerative braking, *IEE Proceedings: Generation, Transmission and Distribution*, 142 (1995) 445-452.
- [289] Y. Cai, M.R. Irving, S.H. Case, Modelling and numerical solution of multibranch DC rail traction power systems, *IEE Proceedings: Electric Power Applications*, 142 (1995) 323-328.
- [290] M. Brenna, A. Dolara, S. Leva, D. Zaninelli, Effects of the DC stray currents on subway tunnel structures evaluated by FEM analysis, *IEEE PES General Meeting, PES 2010*, 2010.
- [291] L. Bortels, A. Dorochenko, B. Van den Bossche, G. Weyns, J. Deconinck, Three-dimensional boundary element method and finite element method simulations applied to stray current interference problems. A unique coupling mechanism that takes the best of both methods, *Corrosion*, 63 (2007) 561-576.
- [292] P. Aylott, I. Cotton, C.A. Charalambous, Impact and management of stray current on DC rail systems, *IET Seminar Digest*, 2009, pp. 238-245.
- [293] N. Abdullah, A.M.A. Marican, M. Osman, N.A.A. Rahman, Case study on impact of seasonal variations of soil resistivities on substation grounding systems safety in tropical country, *2011 7th Asia-Pacific International Conference on Lightning, APL2011*, 2011, pp. 150-154.
- [294] Y. Chao, L. Jianliang, L. Zili, Z. Shouxin, D. Long, Z. Chengbin, Study on interference and protection of pipeline due to high-voltage direct current electrode, *Corros. Rev.*, 37 (2019) 273-281.
- [295] D. Liao, L. Zhang, G. Tao, Study on corrosion rate of buried gas steel pipeline in Nanjing based on the GM(1,N) optimization model, *IOP Conference Series: Materials Science and Engineering*, 2019.
- [296] Z. Yang, G. Cui, Z. Li, J. Liu, Study on the interference between parallel pipelines and optimized operation for the cathodic protection systems, *Anti-Corrosion Methods and Materials*, 66 (2019) 195-202.
- [297] L.P. Zhao, J.H. Li, M.J. Liu, Simulation and analysis of metro stray current based on multi-locomotives condition, *Chinese Control Conference, CCC*, 2016, pp. 9252-9258.
- [298] C. Zhichao, H. Cheng, Evaluation of metro stray current corrosion based on finite element model, *The Journal of Engineering*, 2019 (2019) 2261-2265.
- [299] M. Wang, X. Yang, T.Q. Zheng, J. Gu, Power Analysis on DCAT Traction Power Supply System for DC Railways, *Proceedings - 2018 IEEE International Power Electronics and Application Conference and Exposition, PEAC 2018*, 2018.
- [300] M. Wang, X. Yang, L. Wang, T.Q. Zheng, DC Auto-Transformer Traction Power Supply System for DC Railways Application, *Lecture Notes in Electrical Engineering*, 2018, pp. 175-184.
- [301] L. Wang, X. Yang, J. Xu, T.Q. Zheng, DC Traction System Hardware Emulator for Rail Potential Distribution in DCAT Traction Power Supply System, *Proceedings - 2018 IEEE International Power Electronics and Application Conference and Exposition, PEAC 2018*, 2018.
- [302] V.A. Kandaev, K.V. Avdeeva, A.V. Utkina, Determination of Electrical Quantities in the Traction Rail Network and Buried Pipelines Located Under the Influence of Stray Currents from Electrified Railway Transport, *12th International Scientific and Technical Conference "Dynamics of Systems, Mechanisms and Machines"*, Dynamics 2018, 2019.
- [303] A. Peratta, J. Baynham, R. Adey, Mathematical Modeling Applications In Reinforced Concrete Structures, *CORROSION 2010, NACE International*, San Antonio, Texas, 2010, pp. 12.
- [304] J.G. Yu, C.J. Goodman, Modelling of rail potential rise and leakage current in DC rail transit systems, *IEE Colloquium on Stray Current Effects of DC Railways and Tramways*, (1990) 221-226.
- [305] G.W. Parker, J. Walton, Non-contact stray current measurements in a multi-line, multi-crossing pipeline corridor, *NACE - International Corrosion Conference Series*, 2007, pp. 076491-0764918.
- [306] N. International, Detection and Mitigation of Stray-Current Corrosion of Reinforced and Prestressed Concrete Structures, *NACE International*, 2019, pp. 16.
- [307] P.J. Aylott, A. Hassanein, I. Cotton, The Application of Modeling Systems at the Design Stage to the Mitigation of Stray Current Interference, *CORROSION 2003, NACE International*, San Diego, California, 2003, pp. 17.
- [308] B.B. Jensen, P.V. Nielsen, T. Pedersen, K. Schultz, Modeling And Monitoring Stray Currents For Existing Metro Systems As a Result of Using Voltage Limiting Devices, *CORROSION 2012, NACE International*, Salt Lake City, Utah, 2012, pp. 14.
- [309] S. Li, Y.-G. Kim, Numerical modeling of stray current corrosion of ductile iron pipe induced by foreign cathodic protection system, *Metals and Materials International*, 19 (2013) 717-729.
- [310] Y.S. Kim, G.J. Jeong, H.J. Sohn, Mathematical modeling on the corrosion of unprotected structure due to stray current resulting from cathodic protection system, *Metals and Materials International*, 5 (1999) 93-99.
- [311] W.M.G.C. W.H.A. Peelen, An advanced finite element reliability tool for stray current corrosion assessments, *The European COMSOL Multiphysics Conference Grenoble France*, 2007, pp. 23-28.
- [312] Y. Zhang, Q. Feng, L. Yu, C.-M.L. Wu, S.-P. Ng, X.J.J.o.E.S. Tang, Engineering, Numerical modelling of buried pipelines under DC stray current corrosion, 9 (2019) 125-134.
- [313] C. Wang, W. Li, Improved PSO-NN Prediction Model for Corrosion Current Density Under the Stray Current Excitation Based on Data Mining Technique, *Proceedings of the 2019 2nd International Conference on Data Science and Information Technology, ACM*, 2019, pp. 77-84.

- [314] T. Serdiuk, V. Havryliuk, M. Feliziani, K. Serdiuk, Propagation of Harmonics of Return Traction Current in Rail lines, 2019 International Symposium on Electromagnetic Compatibility-EMC EUROPE, IEEE, 2019, pp. 550-555.
- [315] J. Szymenderski, W. Machczyński, K. Budnik, Modeling Effects of Stochastic Stray Currents from D.C. Traction on Corrosion Hazard of Buried Pipelines, 12 (2019).
- [316] T. Eichler, B. Isecke, Stray current-induced corrosion in cathodic protection installations of steel-reinforced concrete structures: FEM study of the critical parameters, Mater. Corros., n/a (2020).
- [317] R. Polder, C. Andrade, B. Elsener, O. Vennesland, J. Gulikers, R. Weidert, M. Raupach, Test methods for on site measurement of resistivity of concrete, Mater. Struct., 33 (2000) 603-611.
- [318] R. Tinnea, J. Tinnea, K. Kuder, High-early-strength, high-resistivity concrete for direct-current light rail, J. Mater. Civ. Eng., 29 (2017).
- [319] A. Wilkinson, Long range inspection and condition monitoring of rails using guided waves, 51st Annual Conference of the British Institute of Non-Destructive Testing 2012, BINDT 2012, British Institute of Non-Destructive Testing, Northamptonshire, 2012, pp. 165-175.
- [320] A.R.T. Corporation, Engineering Practices Manual - Civil Engineering, Inspection of Level Crossings - Procedure, 2006, pp. 1-3.
- [321] M.T. Söylemez, S. Açıkbaş, A. Kaypmaz, Controlling rail potential of DC supplied rail traction systems, Turkish Journal of Electrical Engineering and Computer Sciences, 14 (2006) 475-484.
- [322] L. Lazzari, M. Ormellese, F. Duranti, P. Fabbri, Stray current control by a new approach based on true potential monitoring, Corrosion 2007Nashville, TN, 2007, pp. 070411-070419.
- [323] G. Mole, Electrical Techniques for Combating Underground Corrosion by Stray Electric Current, Anti-Corrosion Methods and Materials, 1 (1954) 280-285.
- [324] D. Lindemuth, D. Kroon, Light rail transit stray current control: How much water line protection is really needed?, Corrosion 2008New Orleans, LO, 2008, pp. 080631-0806318.
- [325] E.D. Kale, M. Sanders, W. Sidoriak, Corrosion control for the Dallas area rapid transit system, Railroad Conference, Proceedings of the ASME/IEEE Joint, (1999) 1-5.
- [326] D. Paul, DC traction power system grounding, ITIA, 38 (2002) 818-824.
- [327] K.S. Bahra, R.E. Catlow, Control of stray currents for DC traction systems, Paper Presented at IEE Int. Conf. on Electric Railways in A United Europe, (1995).
- [328] M.J. Dekker, Stray current control - An overview of options, Paper Presented at IEE Seminar on DC Traction Stray Current Control - Offer A Stray A Good Ohm? (Ref. No. 1999/212), (1999).
- [329] W. Machczyński, Simulation model for drainage protection of earth-return circuits laid in stray currents area, Electrical Engineering, 84 (2002) 165-172.
- [330] S. Jamali, M.M. Alamuti, M. Savaghebi, Effects of different earthing schemes on the stray R current in rail transit systems, 43rd International Universities Power Engineering Conference, UPEC 2008Padova, 2008.
- [331] J.G. Yu, The effects of earthing strategies on rail potential and stray currents in DC transit railways, Developments in Mass Transit Systems, 1998. International Conference on (Conf. Publ. No. 453), 1998, pp. 303-309.
- [332] BSI, Protection against corrosion by stray current from direct current systems, BSI, 2005.
- [333] L. Bertolini, B. Elsener, P. Pedferri, R. Polder, Corrosion of Steel in Concrete: Prevention, Diagnosis, Repair, (2013).
- [334] J.G. Yu, C.J. Goodman, Stray current design parameters for D.C. Railways, Proc. ASME/IEEE Joint Railroad Conf., (1992) 19-28.
- [335] T. Elliott, M.E. Collentine, S.L. Greenberger, Considerations and Criteria for Relocating Utilities in Electric Rail Corridors, CORROSION 2005, NACE International, Houston, Texas, 2005, pp. 18.
- [336] M.F. Báez H, A. Fraile, J. Fernández, L. Hermanns, A vibration prediction model for culvert-type railroad underpasses, Eng. Struct., 172 (2018) 1025-1041.
- [337] K. Nakarai, K. Shitama, S. Nishio, Y. Sakai, H. Ueda, T. Kishi, Long-term permeability measurements on site-cast concrete box culverts, Construction and Building Materials, 198 (2019) 777-785.
- [338] Y. Wang, L. Guan, J. Chen, Y. Kong, Influences on mammals frequency of use of small bridges and culverts along the Qinghai-Tibet railway, China, Ecol. Res., 33 (2018) 879-887.
- [339] G. Yang, G. Wang, W. Lu, X. Zhao, P. Yan, M. Chen, Numerical modeling of surface explosion effects on shallow-buried box culvert behavior during the water diversion, Thin-Walled Structures, 133 (2018) 153-168.
- [340] Z. Wang, Z. Hu, J. Lai, H. Wang, K. Wang, W. Zan, Settlement Characteristics of Jacked Box Tunneling underneath a Highway Embankment, J. Perform. Constr. Facil., 33 (2019).
- [341] J.N. Varandas, P. Hölscher, M.A.G. Silva, Three-dimensional track-ballast interaction model for the study of a culvert transition, Soil Dyn. Earthquake Eng., 89 (2016) 116-127.
- [342] C. Esveld, Modern Railway Track, Modern Railway Track, (2001).
- [343] J.N. Varandas, A. Paixão, E. Fortunato, A study on the dynamic train-track interaction over cut-fill transitions on buried culverts, CoStr, 189 (2017) 49-61.
- [344] J. Oscarson, T. Dahlberg, Dynamic train/track/ballast interaction - Computer models and full-scale experiments, VSD, 29 (1998) 73-84.

- [345] B. Zuada Coelho, J. Priest, P. Hölscher, Dynamic behaviour of transition zones in soft soils during regular train traffic, *Proc. Inst. Mech. Eng. Pt. F: J. Rail Rapid Transit*, 232 (2018) 645-662.
- [346] C. Alves Ribeiro, R. Calçada, R. Delgado, Experimental assessment of the dynamic behaviour of the train-track system at a culvert transition zone, *Eng. Struct.*, 138 (2017) 215-228.
- [347] Y. Shan, S. Zhou, Q. Gong, B. Wang, Y. Shu, Z. Zhao, Soil dynamic stress of a transition zone influenced by the shield tunnel beneath a railroad, *Transportation Research Record*, 2016, pp. 40-47.
- [348] D. Beben, W. Anigacz, Dynamic testing of railway metal culvert using geodetic methods, *MATEC Web of Conferences*, 2017.
- [349] J.N. Varandas, P. Hölscher, M.A.G. Silva, Settlement of ballasted track under traffic loading: Application to transition zones, *Proc. Inst. Mech. Eng. Pt. F: J. Rail Rapid Transit*, 228 (2014) 242-259.
- [350] A. Paixão, Transition zones in railway tracks: an experimental and numerical study on the structural behaviour, (2014).
- [351] Bridge ends – embankment structure transition, (1999).
- [352] B. Coelho, Dynamics of railway transition zones in soft soils, *Dynamics of Railway Transition Zones in Soft Soils*, (2011).
- [353] D. Bowness, A.C. Lock, W. Powrie, J.A. Priest, D.J. Richards, Monitoring the dynamic displacements of railway track, *Proc. Inst. Mech. Eng. Pt. F: J. Rail Rapid Transit*, 221 (2007) 13-22.
- [354] P. Alves Costa, R. Calçada, A. Silva Cardoso, Track-ground vibrations induced by railway traffic: In-situ measurements and validation of a 2.5D FEM-BEM model, *Soil Dyn. Earthquake Eng.*, 32 (2012) 111-128.
- [355] G.H. Willson, Keeping Stray-Current Corrosion At Bay Pipelines and light rail transit: a delicate balance, *PIPELINE AND GAS JOURNAL*, 233 (2006) 51-53.
- [356] K. Zan, V. Mawley, M. Ramos, S. Singh, Recommended maintenance practices for stray current corrosion on DC electrified systems, 2014 Joint Rail Conference, JRC 2014, American Society of Mechanical Engineers (ASME), Colorado Springs, CO, 2014.
- [357] J.G. Rose, Highway-Railway At-Grade Crossing Rehabilitation Practices to Enhance Long-Term Performances: Criteria and Evaluations, in: T.T. Institute (Ed.) 2013 National Highway-Rail Grade Crossing Safety Training Conference, Texas Transportation Institute, Ft. Worth, TX, 2013.
- [358] Manual for Railway Engineering, (2005).
- [359] Railway culvert, Miodowa street, Kazimierz, Krakow, Poland, 2011.
- [360] Concrete box culvert.
- [361] T. Ledbetter, R. Vail, Coordinated Efforts To Sustain Stray Current Mitigation On An Aging Heavy-Rail Dc Transit System, *CORROSION 2010*, NACE International, San Antonio, Texas, 2010, pp. 13.
- [362] K.L. McCaffrey, Cathodic Protection Design Considerations for Waterlines Impacted by Light Rail Construction, *CORROSION 2005*, NACE International, Houston, Texas, 2005, pp. 10.
- [363] K.L. McCaffrey, Stray Current Control for Steel Reinforced Concrete Light Rail Bridges, *CORROSION 2005*, NACE International, Houston, Texas, 2005, pp. 8.
- [364] J.H. Fitzgerald, R.B. Bosma, F. Paladines, Building Stray Current Control into the Rehabilitation of an Old Transit Yard and Shop Facility in a Large Urban Area, *CORROSION 98*, NACE International, San Diego, California, 1998, pp. 13.
- [365] Y.S. Tzeng, C.H. Lee, Assessment of grounding, bonding, and insulation on rail potential and stray currents in a direct current transit system, *Proc. Inst. Mech. Eng. Pt. F: J. Rail Rapid Transit*, 223 (2009) 229-240.
- [366] S. Jabbehdari, A. Mariscotti, Distribution of stray current based on 3-Dimensional earth model, *Electrical Systems for Aircraft, Railway and Ship Propulsion*, ESARS, 2015.
- [367] M. Niasati, A. Gholami, Overview of stray current control in dc railway systems, *IET International Conference on Railway Engineering 2008, ICRE 2008 Hong Kong*, 2008, pp. 237-242.
- [368] V. Kolar, R. Hrbac, T. Mlcak, J. Placek, Design of electrical regulated drainage with energy harvesting, *Lecture Notes in Electrical Engineering*, 2020, pp. 835-843.
- [369] B. Šavija, Experimental and numerical investigation of chloride ingress in cracked concrete, *None (EN)*, 2014.
- [370] W. Elkey, E.J. Sellevold, Electrical resistivity of concrete, *Electrical Resistivity of Concrete*, (1995).
- [371] K. Hornbostel, C.K. Larsen, M.R. Geiker, Relationship between concrete resistivity and corrosion rate – A literature review, *Cem. Concr. Compos.*, 39 (2013) 60-72.
- [372] A. García, D. Castro-Fresno, J.A. Polanco, Evolution of penetration resistance in fresh concrete, *Cem. Concr. Res.*, 38 (2008) 649-659.
- [373] L. Struble, T.Y. Kim, H. Zhang, Setting of cement and concrete, *Cement, Concrete and Aggregates*, 23 (2001) 88-93.
- [374] Standard practice for preparing, cleaning, and evaluating corrosion test specimens, *Annual Book of ASTM Standards*, (2003) 17-25.
- [375] C. Alonso, M. Castellote, C. Andrade, Chloride threshold dependence of pitting potential of reinforcements, *Electrochim. Acta*, 47 (2002) 3469-3481.
- [376] N.S. Rengaswamy, S. Srinivasan, T.M. Balasubramanian, Y.I. Mahadeva, N.U. Nayak, R.H.S. Bapu, Corrosion survey of reinforced and prestressed concrete structures - methodology of approach, *Transactions of the SAEST (Society for Advancement of Electrochemical Science and Technology)*, 23 (1988) 207-212.

- [377] C. Andrade, C. Alonso, Corrosion rate monitoring in the laboratory and on-site, *Construction and Building Materials*, 10 (1996) 315-328.
- [378] J.A. González, A. Molina, M.L. Escudero, C. Andrade, Errors in the electrochemical evaluation of very small corrosion rates—I. polarization resistance method applied to corrosion of steel in concrete, *Corros. Sci.*, 25 (1985) 917-930.
- [379] D.A. Jones, *Principles and prevention of corrosion*, Macmillan 1992.
- [380] M. Stern, A.L. Geary, Electrochemical Polarization: I. A Theoretical Analysis of the Shape of Polarization Curves, *JEIS*, 104 (1957) 56-63.
- [381] J.A. Gonzalez, S. Algaba, C. Andrade, Corrosion: Of reinforcing bars in carbonated concrete, *Br. Corros. J.*, 15 (1980) 135-139.
- [382] C. Andrade, J.A. González, Quantitative measurements of corrosion rate of reinforcing steels embedded in concrete using polarization resistance measurements, *Mater. Corros.*, 29 (1978) 515-519.
- [383] M. Keddah, H. Takenouti, X.R. Nóvoa, C. Andrade, C. Alonso, Impedance measurements on cement paste, *Cem. Concr. Res.*, 27 (1997) 1191-1201.
- [384] C. Andrade, L. Soler, X.R. Novoa, Advances in electrochemical impedance measurements in reinforced concrete, *Mater Sci Forum*, 192-194 (1995) 843-856.
- [385] W. Cui, Z. Shi, G. Song, H. Lin, C.n. Cao, Electrochemical study on the reinforced concrete during curing, *Corrosion Science and Protection Technology*, 10 (1998) 201-207.
- [386] F. Wenger, J. Galland, Analysis of local corrosion of large metallic structures or reinforced concrete structures by electrochemical impedance spectroscopy (EIS), *Electrochim. Acta*, 35 (1990) 1573-1578.
- [387] M.V.A. Florea, H.J.H. Brouwers, Chloride binding related to hydration products: Part I: Ordinary Portland Cement, *Cem. Concr. Res.*, 42 (2012) 282-290.
- [388] J. García, F. Almeraya, C. Barrios, C. Gaona, R. Núñez, I. López, M. Rodríguez, A. Martínez-Villafañe, J.M. Bastidas, Effect of cathodic protection on steel-concrete bond strength using ion migration measurements, *Cem. Concr. Compos.*, 34 (2012) 242-247.
- [389] J.J. Chang, W. Yeih, R. Huang, Degradation of the bond strength between rebar and concrete due to the impressed cathodic current, *J. Mar. Sci. Technol.*, 7 (1999) 89-93.
- [390] E. Garcia-Diaz, J. Riche, D. Bulteel, C. Vernet, Mechanism of damage for the alkali-silica reaction, *Cem. Concr. Res.*, 36 (2006) 395-400.
- [391] M.B. Haha, E. Gallucci, A. Guidoum, K.L. Scrivener, Relation of expansion due to alkali silica reaction to the degree of reaction measured by SEM image analysis, *Cem. Concr. Res.*, 37 (2007) 1206-1214.
- [392] D.W. Hobbs, INFLUENCE OF MIX PROPORTIONS AND CEMENT ALKALI CONTENT UPON EXPANSION DUE TO THE ALKALI-SILICA REACTION, Technical Report - Cement and Concrete Association, (1980).
- [393] A. Leemann, B. Lothenbach, The influence of potassium-sodium ratio in cement on concrete expansion due to alkali-aggregate reaction, *Cem. Concr. Res.*, 38 (2008) 1162-1168.
- [394] J.K. McGowan, H.E. Vivian, Studies in cement-aggregate reaction: Correlation between crack development and expansion of mortars, *Aust. J. Appl. Sci.*, 3 (1952) 228-232.
- [395] R. Narayan Swamy, M.M. Al-Asali, EXPANSION OF CONCRETE DUE TO ALKALI-SILICA REACTION, *ACI Mater. J.*, 85 (1988) 33-40.
- [396] J.M. Ponce, O.R. Batic, Different manifestations of the alkali-silica reaction in concrete according to the reaction kinetics of the reactive aggregate, *Cem. Concr. Res.*, 36 (2006) 1148-1156.
- [397] K. Ishii, H. Seki, T. Fukute, K. Ikawa, Cathodic protection for prestressed concrete structures, *Construction and Building Materials*, 12 (1998) 125-132.
- [398] J.J. Chang, A study of the bond degradation of rebar due to cathodic protection current, *Cem. Concr. Res.*, 32 (2002) 657-663.
- [399] H. Saito, S. Nakane, S. Ikari, A. Fujiwara, Preliminary experimental study on the deterioration of cementitious materials by an acceleration method, *NuEnD*, 138 (1992) 151-155.
- [400] A. Susanto, D.A. Koleva, K. Van Breugel, K. Van Beek, Stray current-induced development of cement-based microstructure in water-submerged, Ca(OH)₂-submerged and sealed conditions, *Journal of Advanced Concrete Technology*, 15 (2017) 244-268.
- [401] F.J. Ulm, J.M. Torrenti, F. Adenot, Chemoporoplasticity of calcium leaching in concrete, *J. Eng. Mech.*, 125 (1999) 1200-1210.
- [402] D. Kuhl, F. Bangert, G. Meschke, Coupled chemo-mechanical deterioration of cementitious materials. Part I: Modeling, *IJSS*, 41 (2004) 15-40.
- [403] D. Kuhl, F. Bangert, G. Meschke, Coupled chemo-mechanical deterioration of cementitious materials Part II: Numerical methods and simulations, *IJSS*, 41 (2004) 41-67.
- [404] D.A. Koleva, J. Hu, A.L.A. Fraaij, K. van Breugel, J.H.W. de Wit, Microstructural analysis of plain and reinforced mortars under chloride-induced deterioration, *Cem. Concr. Res.*, 37 (2007) 604-617.
- [405] M.N. Haque, O.A. Kayyali, Free and water soluble chloride in concrete, *Cem. Concr. Res.*, 25 (1995) 531-542.

- [406] F. Pruckner, O.E. Gjörv, Effect of CaCl₂ and NaCl additions on concrete corrosivity, *Cem. Concr. Res.*, 34 (2004) 1209-1217.
- [407] M. Siegwart, J.F. Lyness, B.J. McFarland, Change of pore size in concrete due to electrochemical chloride extraction and possible implications for the migration of ions, *Cem. Concr. Res.*, 33 (2003) 1211-1221.
- [408] G.E. Monfore, The Electrical Resistivity of Concrete, Portland Cement Association 1968.
- [409] E. Hammond, T.D.J.E. Robson, Comparison of electrical properties of various cements and concretes, 199 (1955) 114-115.
- [410] D.A. Koleva, O. Copuroglu, K. van Breugel, G. Ye, J.H.W. de Wit, Electrical resistivity and microstructural properties of concrete materials in conditions of current flow, *Cem. Concr. Compos.*, 30 (2008) 731-744.
- [411] D.A. Koleva, J.H.W. de Wit, K. van Breugel, L.P. Veleza, E. van Westing, O. Copuroglu, A.L.A. Fraaij, Correlation of microstructure, electrical properties and electrochemical phenomena in reinforced mortar. Breakdown to multi-phase interface structures. Part II: Pore network, electrical properties and electrochemical response, *Mater. Charact.*, 59 (2008) 801-815.
- [412] M. Keddad, X.R. Nóvoa, L. Soler, C. Andrade, H. Takenouti, An equivalent electrical circuit of macrocell activity in facing electrodes embedded in cement mortar, *Corros. Sci.*, 36 (1994) 1155-1166.
- [413] C. Andrade, L. Soler, X.R. Nóvoa, Advances in Electrochemical Impedance Measurements in Reinforced Concrete, *MSF*, 192-194 (1995) 843-856.
- [414] A.A. Sagüés, M.A. Pech-Canul, A.K.M. Shahid Al-Mansur, Corrosion macrocell behavior of reinforcing steel in partially submerged concrete columns, *Corros. Sci.*, 45 (2002) 7-32.
- [415] V. Feliu, J.A. González, S. Feliu, Algorithm for Extracting Corrosion Parameters from the Response of the Steel-Concrete System to a Current Pulse, *JEIS*, 151 (2004) B134-B140.
- [416] D.A. Koleva, K. Van Breugel, W. De, T.U. Delft, E. Civil, Geosciences, D.U.o.T. Tu Delft, Corrosion and protection in reinforced concrete: pulse cathodic protection: an improved cost-effective alternative, 2007.
- [417] A.K. Suryavanshi, J.D. Scantlebury, S.B. Lyon, Pore size distribution of OPC & SRPC mortars in presence of chlorides, *Cem. Concr. Res.*, 25 (1995) 980-988.
- [418] B. Díaz, X.R. Nóvoa, M.C. Pérez, Study of the chloride diffusion in mortar: A new method of determining diffusion coefficients based on impedance measurements, *Cem. Concr. Compos.*, 28 (2006) 237-245.
- [419] H. Brouwers, A hydration model of Portland cement using the work of Powers and Brownnyard, (2011).
- [420] D.A. Koleva, K. van Breugel, J.H.W. de Wit, E. van Westing, N. Boshkov, A.L.A. Fraaij, Electrochemical Behavior, Microstructural Analysis, and Morphological Observations in Reinforced Mortar Subjected to Chloride Ingress, *JEIS*, 154 (2007) E45.
- [421] M. Pourbaix, Atlas of electrochemical equilibria in aqueous solutions, National Association of Corrosion Engineers 1974.
- [422] M. Čekerevac, M. Simić, L.N. Bujanović, N. Popović, The influence of silicate and sulphate anions on the anodic corrosion and the transpassivity of iron and silicon-rich steel in concentrated KOH solution, *Corros. Sci.*, 64 (2012) 204-212.
- [423] K. Takahashi, J.A. Bardwell, B. MacDougall, M.J. Graham, Mechanism of anodic dissolution and passivation of iron—II. Comparison of the behavior in neutral benzoate and acetate buffer solutions, *Electrochim. Acta*, 37 (1992) 489-494.
- [424] K. Takahashi, J.A. Bardwell, B. MacDougall, M.J. Graham, Mechanism of anodic dissolution and passivation of iron—I. Behavior in neutral acetate buffer solutions, *Electrochim. Acta*, 37 (1992) 477-487.
- [425] A. Ejaz, Z. Lu, J. Chen, Q. Xiao, X. Ru, G. Han, T. Shoji, The effects of hydrogen on anodic dissolution and passivation of iron in alkaline solutions, *Corros. Sci.*, 101 (2015) 165-181.
- [426] Protection Against Corrosion by Stray Current from Direct Current Systems, (2004).
- [427] S.T. Amaral, I.L. Müller, A RRDE study of the electrochemical behavior of iron in solutions containing silicate and sulphate at pH 10-13, *Corros. Sci.*, 41 (1999) 759-771.
- [428] R.D. Armstrong, I. Baurhoo, The dissolution of iron in concentrated alkali, *J. Electroanal. Chem.*, 40 (1972) 325-338.
- [429] G.T. Burstein, G.W. Askley, EARLY STEPS IN THE ANODIC OXIDATION OF IRON IN AQUEOUS SOLUTION, *Corrosion*, 39 (1983) 241-247.
- [430] D. Geana, A.A. El Miligy, W.J. Lorenz, Electrochemical behaviour of iron in alkaline sulphate solutions, *JApE*, 4 (1974) 337-345.
- [431] R.S. Schreiber Guzmán, J.R. Vilche, A.J. Arví, The potentiodynamic behaviour of iron in alkaline solutions, *Electrochim. Acta*, 24 (1979) 395-403.
- [432] S. Suzuki, E. Matsubara, T. Komatsu, Y. Okamoto, K. Kanie, A. Muramatsu, H. Konishi, J. Mizuki, Y. Waseda, Ex-situ and in-situ X-ray diffractions of corrosion products freshly formed on the surface of an iron-silicon alloy, *Corros. Sci.*, 49 (2007) 1081-1096.
- [433] L. Kwiatkowski, F.J.J.o.t.E.S. Mansfeld, Surface modification of stainless steel by an alternating voltage process, 140 (1993) L39-L41.
- [434] F. Mansfeld, S. Lin, L.J.C.s. Kwiatkowski, The effects of process parameters on alternating voltage (AV) passivation of 304 stainless steel, 34 (1993) 2045-2058.
- [435] F. Mansfeld, S. Lin, L.J.C. Kwiatkowski, Optimization of the alternating voltage passivation process for stainless steel, 50 (1994) 838-847.

- [436] J.G. Cabrera, Deterioration of concrete due to reinforcement steel corrosion, *Cem. Concr. Compos.*, 18 (1996) 47-59.
- [437] D.H. Boteler, W.H. Seager, Telluric Currents: A Meeting of Theory and Observation, *Corrosion*, 54 (1998) 751-755.
- [438] I.A. Metwally, H.M. Al-Mandhari, A. Gastli, A. Al-Bimani, Stray currents of ESP well casings, *Engineering Analysis with Boundary Elements*, 32 (2008) 32-40.
- [439] H.H. Uhlig, *Corrosion and Corrosion Control (Third Version)* [M]. Weng Yongji, Etc. Trans, (1985).
- [440] C.L. Wang, C.Y. Ma, Z. Wang, Analysis of stray current in metro DC traction power system, *Urban Mass Transit*, 3 (2007) 51-56.
- [441] M. Wu, Progress of the durability of concrete structure of the subway, 1st International Conference on Civil Engineering, Architecture and Building Materials, CEABM 2011 Haikou, 2011, pp. 1456-1459.
- [442] G. Malumbela, M. Alexander, P. Moyo, Interaction between corrosion crack width and steel loss in RC beams corroded under load, *Cem. Concr. Res.*, 40 (2010) 1419-1428.
- [443] Y. Zhao, H. Lin, K. Wu, W. Jin, Bond behaviour of normal/recycled concrete and corroded steel bars, *Construction and Building Materials*, 48 (2013) 348-359.
- [444] K. Lundgren, Bond between ribbed bars and concrete. Part 1: Modified model, *Magazine of Concrete Research*, 57 (2005) 371-382.
- [445] M. John Robert Prince, B. Singh, Bond behaviour of deformed steel bars embedded in recycled aggregate concrete, *Construction and Building Materials*, 49 (2013) 852-862.
- [446] M.F. Sulaiman, C.-K. Ma, N.M. Apandi, S. Chin, A.Z. Awang, S.A. Mansur, W. Omar, A Review on Bond and Anchorage of Confined High-strength Concrete, *Structures*, 11 (2017) 97-109.
- [447] K.H. Mo, U.J. Alengaram, M.Z. Jumaat, Bond properties of lightweight concrete – A review, *Construction and Building Materials*, 112 (2016) 478-496.
- [448] C. Van der Veen, Cryogenic bond stress-slip relationship, None (EN), 1990.
- [449] D. Darwin, J. Zuo, M.L. Tholen, E.K. Idun, Development length criteria for conventional and high relative rib area reinforcing bars, *ACI Structural Journal*, 93 (1996) 347-359.
- [450] T.P. Tassios, Properties of bond between concrete and steel under load cycles idealizing seismic actions, *Comité Euro-International Du Béton, Bulletin*, 131 (1979) 65-122.
- [451] G.M. Verderame, G. De Carlo, P. Ricci, G. Fabbrocino, Cyclic bond behaviour of plain bars. Part II: Analytical investigation, *Construction and Building Materials*, 23 (2009) 3512-3522.
- [452] Y.S. Choi, S.-T. Yi, M.Y. Kim, W.Y. Jung, E.I. Yang, Effect of corrosion method of the reinforcing bar on bond characteristics in reinforced concrete specimens, *Construction and Building Materials*, 54 (2014) 180-189.
- [453] R.A. Chapman, S.P. Shah, EARLY-AGED BOND STRENGTH IN REINFORCED CONCRETE, *ACI Mater. J.*, 84 (1987) 501-510.
- [454] E. Franzoni, H. Varum, M.E. Natali, M.C. Bignozzi, J. Melo, L. Rocha, E. Pereira, Improvement of historic reinforced concrete/mortars by impregnation and electrochemical methods, *Cem. Concr. Compos.*, 49 (2014) 50-58.
- [455] J.J. Chang, Bond degradation due to the desalination process, *Construction and Building Materials*, 17 (2003) 281-287.
- [456] L. Chung, J.-H. Jay Kim, S.-T. Yi, Bond strength prediction for reinforced concrete members with highly corroded reinforcing bars, *Cem. Concr. Compos.*, 30 (2008) 603-611.
- [457] C. Fang, K. Lundgren, L. Chen, C. Zhu, Corrosion influence on bond in reinforced concrete, *Cem. Concr. Res.*, 34 (2004) 2159-2167.
- [458] H. Yalciner, O. Eren, S. Sensoy, An experimental study on the bond strength between reinforcement bars and concrete as a function of concrete cover, strength and corrosion level, *Cem. Concr. Res.*, 42 (2012) 643-655.
- [459] L. Chung, J.H. Jay Kim, S.T. Yi, Bond strength prediction for reinforced concrete members with highly corroded reinforcing bars, *Cem. Concr. Compos.*, 30 (2008) 603-611.
- [460] "Bond and Development of Straight Reinforcing Bars in Tension (ACI 408R-03)", *Bond and Development of Straight Reinforcing Bars in Tension (ACI 408R-03)*, (2003).
- [461] Y. Huo, M.Y.J. Tan, M. Forsyth, Investigating effects of potential excursions and pH variations on cathodic protection using new electrochemical testing cells, *Corrosion Engineering Science and Technology*, 51 (2016) 171-178.
- [462] C. Wu, G. Chen, J.S. Volz, R.K. Brow, M.L. Koenigstein, Local bond strength of vitreous enamel coated rebar to concrete, *Constr Build Mater*, 35 (2012) 428-439.
- [463] A. Torre-Casanova, L. Jason, L. Davenne, X. Pinelli, Confinement effects on the steel-concrete bond strength and pull-out failure, *Eng. Fract. Mech.*, 97 (2012) 92-104.
- [464] Standard test method for comparing concrete on the basis of the bond developed with reinforcing steel, *ASTM annual book of standards: Section 4. Construction*, (1991).
- [465] J. Magnusson, Bond and anchorage of ribbed bars in high-strength concrete, *Bond and Anchorage of Ribbed Bars in High-strength Concrete*, (2000).
- [466] A. Torre-Casanova, L. Jason, L. Davenne, X. Pinelli, Confinement effects on the steel-concrete bond strength and pull-out failure, *EnFM*, 97 (2013) 92-104.

- [467] J. Magnusson, Bond and anchorage of ribbed bars in high-strength concrete, Chalmers University of Technology, (2000).
- [468] M.T.G. Barbosa, E. de Souza Sánchez Filho, T.M. de Oliveira, W.J. dos Santos, Analysis of the relative rib area of reinforcing bars pull out tests, *Materials Research*, 11 (2008) 453-457.
- [469] A.A. Almusallam, A.S. Al-Gahtani, A.R. Aziz, Rasheeduzzafar, Effect of reinforcement corrosion on bond strength, *Construction and Building Materials*, 10 (1996) 123-129.
- [470] A. Fattah-alhosseini, A. Saatchi, M.A. Golozar, K. Raeissi, The transpassive dissolution mechanism of 316L stainless steel, *Electrochim. Acta*, 54 (2009) 3645-3650.
- [471] D.A. Koleva, N. Boshkov, K. van Breugel, J.H.W. de Wit, Steel corrosion resistance in model solutions, containing waste materials, *Electrochim. Acta*, 58 (2011) 628-646.
- [472] A. Covelo, B. Díaz, L. Freire, X.R. Nóvoa, M.C. Pérez, Microstructural changes in a cementitious membrane due to the application of a DC electric field, *Journal of Environmental Science and Health - Part A Toxic/Hazardous Substances and Environmental Engineering*, 43 (2008) 985-993.
- [473] B. Díaz, L. Freire, P. Merino, X.R. Nóvoa, M.C. Pérez, Impedance spectroscopy study of saturated mortar samples, *Electrochim. Acta*, 53 (2008) 7549-7555.
- [474] G. Song, Equivalent circuit model for AC electrochemical impedance spectroscopy of concrete, *Cem. Concr. Res.*, 30 (2000) 1723-1730.
- [475] O. Poupard, A. Ait-Mokhtar, P. Dumargue, Corrosion by chlorides in reinforced concrete: Determination of chloride concentration threshold by impedance spectroscopy, *Cem. Concr. Res.*, 34 (2004) 991-1000.
- [476] M.F. Montemor, M.P. Cunha, M.G. Ferreira, A.M. Simões, Corrosion behaviour of rebars in fly ash mortar exposed to carbon dioxide and chlorides, *Cem. Concr. Compos.*, 24 (2002) 45-53.
- [477] V. Feliu, J.A. González, C. Andrade, S. Feliu, Equivalent circuit for modelling the steel-concrete interface. I. Experimental evidence and theoretical predictions, *Corros. Sci.*, 40 (1998) 975-993.
- [478] C. Andrade, L. Soler, C. Alonso, X.R. Nóvoa, M. Keddah, The importance of geometrical considerations in the measurement of steel corrosion in concrete by means of AC impedance, *Corros. Sci.*, 37 (1995) 2013-2023.
- [479] D.A. Koleva, A.G. Denkova, N. Boshkov, K. Van Breugel, Electrochemical performance of steel in cement extract and bulk matrix properties of cement paste in the presence of Pluronic 123 micelles, *JMatS*, 48 (2013) 2490-2503.
- [480] A.A. Sagüés, S.C. Kranc, E.I. Moreno, The time-domain response of a corroding system with constant phase angle interfacial component: Application to steel in concrete, *Corros. Sci.*, 37 (1995) 1097-1113.
- [481] A.A. Sagüés, M.A. Pech-Canul, A.K.M. Shahid Al-Mansur, Corrosion macrocell behavior of reinforcing steel in partially submerged concrete columns, *Corros. Sci.*, 45 (2003) 7-32.
- [482] A. Blagojevic, D.A. Koleva, J.C. Walraven, Monitoring steel corrosion in reinforced concrete beams with variable crack widths under sustained load, *EUROCORR 2014: European Corrosion Congress*, Pisa, Italy, 8-12 September 2014, 2014.
- [483] D.A. Koleva, Z. Guo, K. van Breugel, J.H.W. de Wit, Conventional and pulse cathodic protection of reinforced concrete: Electrochemical behavior of the steel reinforcement after corrosion and protection, *Mater. Corros.*, 60 (2009) 344-354.
- [484] J. Hu, D.A. Koleva, P. Petrov, K. van Breugel, Polymeric vesicles for corrosion control in reinforced mortar: Electrochemical behavior, steel surface analysis and bulk matrix properties, *Corros. Sci.*, 65 (2012) 414-430.
- [485] M. Castellote, C. Andrade, M.C. Alonso, Changes in concrete pore size distribution due to electrochemical chloride migration trials, *ACI Mater. J.*, 96 (1999) 314-319.
- [486] J. Garzón-Roca, J. Ruiz-Pinilla, J.M. Adam, P.A. Calderón, An experimental study on steel-caged RC columns subjected to axial force and bending moment, *Eng. Struct.*, 33 (2011) 580-590.
- [487] E. Esmaeli, F. Danesh, K.F. Tee, S. Eshghi, A combination of GFRP sheets and steel cage for seismic strengthening of shear-deficient corner RC beam-column joints, *CmpSt*, 159 (2017) 206-219.
- [488] C. Jørgensen, R. Grastveit, J. Garzón-Roca, I. Payá-Zaforteza, J.M. Adam, Bearing capacity of steel-caged RC columns under combined bending and axial loads: Estimation based on Artificial Neural Networks, *Eng. Struct.*, 56 (2013) 1262-1270.
- [489] G. Campione, L. Cavaleri, M. Papia, Flexural response of external R.C. beam-column joints externally strengthened with steel cages, *Eng. Struct.*, 104 (2015) 51-64.
- [490] B. Dolinšek, J. Duhovnik, Robotic assembly of rebar cages for beams and columns, *Automation in Construction*, 8 (1998) 195-207.
- [491] S. Spagnuolo, A. Meda, Z. Rinaldi, A. Nanni, Precast concrete tunnel segments with GFRP reinforcement, *J. Composite Constr.*, 21 (2017).
- [492] A. Kerimov, P. Spirin, R. Kerimov, Relationship between the parameters of stray current circuits and the traction load, *Prot. Met.*, 42 (2006) 409-411.
- [493] S. Memon, G. Clarner, P. Fromme, Stray Current Mitigation and Collection Techniques Adopted by a DC Transit Agency and Its Effectiveness in Controlling Stray Currents, *International Conference on Transportation and Development 2016: Projects and Practices for Prosperity - Proceedings of the 2016 International Conference on Transportation and Development*, 2016, pp. 640-650.

- [494] A. Susanto, D.A. Koleva, K. Van Breugel, The effect of water-to-cement ratio and curing on material properties of mortar specimens in stray current conditions, *Journal of Advanced Concrete Technology*, 15 (2017) 627-643.
- [495] Z. Chen, D. Koleva, K. van Breugel, Stray current vs anodic polarization in reinforced mortar: a comparative study on steel corrosion behaviour in both regimes, *European corrosion congress : Earth, Water, Fire, Air, Corrosion happens everywhere* 2015, pp. 1-10.
- [496] C.A. Charalambous, P. Aylott, D. Buxton, Stray Current Calculation and Monitoring in DC Mass-Transit Systems: Interpreting Calculations for Real-Life Conditions and Determining Appropriate Safety Margins, *IEEE Vehicular Technology Magazine*, 11 (2016) 24-31.
- [497] S. Xu, W. Li, F. Xing, Y. Wang, R. Wang, X. Wang, An elimination method of temperature-induced linear birefringence in a stray current sensor, *Sensors (Switzerland)*, 17 (2017).
- [498] S.R. Allahkaram, M. Isakhani-Zakaria, M. Derakhshani, M. Samadian, H. Sharifi-Rasaey, A. Razmjoo, Investigation on corrosion rate and a novel corrosion criterion for gas pipelines affected by dynamic stray current, *Journal of Natural Gas Science and Engineering*, 26 (2015) 453-460.
- [499] L.I. Freiman, Stray-Current Corrosion Criteria for Underground Steel Pipelines, *Prot. Met*, 39 (2003) 172-176.
- [500] E. Volpi, A. Olietti, M. Stefanoni, S.P. Trasatti, Electrochemical characterization of mild steel in alkaline solutions simulating concrete environment, *J. Electroanal. Chem.*, 736 (2015) 38-46.
- [501] D.A. Koleva, J.H.W. de Wit, K. van Breugel, Z.F. Lodhi, G. Ye, Investigation of Corrosion and Cathodic Protection in Reinforced Concrete, *JEIS*, 154 (2007) C261.
- [502] D.A. Koleva, Electrochemical behavior of corroded and protected construction steel in cement extract, *Mater. Corros.*, 62 (2011) 240-251.
- [503] M. Ormellese, S. Goidanich, L. Lazzari, Effect of AC interference on cathodic protection monitoring, *Corrosion Engineering Science and Technology*, 46 (2011) 618-623.
- [504] S. Sathiyarayanan, P. Natarajan, K. Saravanan, S. Srinivasan, G. Venkatachari, Corrosion monitoring of steel in concrete by galvanostatic pulse technique, *Cem. Concr. Compos.*, 28 (2006) 630-637.
- [505] P. Giménez, K. Mukai, K. Asaka, K. Hata, H. Oike, T.F. Otero, Capacitive and faradic charge components in high-speed carbon nanotube actuator, *Electrochim. Acta*, 60 (2012) 177-183.
- [506] F. Ciepiela, M. Jakubowska, Faradaic and capacitive current estimation by means of Independent Components Analysis and 1kHz sampling, *Talanta*, 170 (2017) 158-164.
- [507] J. Tu, W. Cai, X. Shao, Direct separation of faradaic and double layer charging current in potential step voltammetry, *Talanta*, 116 (2013) 575-580.
- [508] A.J. Bard, L.R. Faulkner, *Electrochemical Methods: Fundamentals and Applications*, 2nd Edition, John Wiley & Sons 2000.
- [509] L. Zhu, L. Zhang, A.V. Virkar, Measurement of ionic and electronic conductivities of Yttria-stabilized zirconia by an embedded electrode method, *JEIS*, 162 (2015) F298-F309.
- [510] V.B. Svetovoy, R.G.P. Sanders, M.C. Elwenspoek, Transient nanobubbles in short-time electrolysis, *Journal of Physics Condensed Matter*, 25 (2013).
- [511] A. Lamibrac, G. Maranzana, O. Lottin, J. Dillet, J. Mainka, S. Didierjean, A. Thomas, C. Moyne, Experimental characterization of internal currents during the start-up of a proton exchange membrane fuel cell, *JPS*, 196 (2011) 9451-9458.
- [512] L. Zhang, L. Zhu, A.V. Virkar, Electronic conductivity measurement of yttria-stabilized zirconia solid electrolytes by a transient technique, *JPS*, 302 (2016) 98-106.

List of Publications

Z. Chen, D. Koleva, **Corrosion Behavior of Reinforcing Steel Undergoing Stray Current and Anodic Polarization**, Materials, 14 (2021) 261. DOI: doi.org/10.3390/ma14020261

Z. Chen, D. Koleva, K. van Breugel, **A review on stray current-induced steel corrosion in infrastructure**, Corrosion Reviews, 35 (2017) 397-423. DOI: doi.org/10.1515/correv-2017-0009

Z. Chen, D. Koleva, K. van Breugel, **Electrochemical Tests in Reinforced Mortar Undergoing Stray Current-Induced Corrosion**, In: Concrete Durability (1st Ed), Springer International 2017, pp. 83-108. (Springer Cham). DOI: doi.org/10.1007/978-3-319-55463-1_5

Z. Chen, D. Koleva, E.A.B. Koenders, K. van Breugel, **Stray current induced corrosion control in reinforced concrete by addition of carbon fiber and silica fume**, Proceedings of the 23th international materials research congress 2014, Cambridge University Press 2015, pp. 1-6. DOI: doi.org/10.1557/opl.2015.320

Z. Chen, D. Koleva, K. van Breugel, **Properties of the steel-mortar interface derived by impedance spectroscopy in different environment and curing conditions**, Proceedings of the 24th international materials research congress 2015, Cancun, Mexico.

Z. Chen, D. Koleva, K. van Breugel, **Stray current vs anodic polarization in reinforced mortar: a comparative study on steel corrosion behaviour in both regimes**, EUROCORR 2015, 6 - 10 September 2015, Graz, Austria.

Z. Chen, D. Koleva, **Effect of stray current on corrosion behavior of reinforcing steel: importance of cell geometry and orientation with respect to the electrical field**, 2nd International Conference on Architecture, Materials and Construction (ICAMC 2016), 3-5 December 2016, Dubai, UAE. DOI: doi.org/10.18178/ijscer.6.2.93-100

Z. Chen, D. Koleva, E. Schlangen, **Bond of steel-mortar interface interfered by stray current**, submitted to Cement and Concrete Research.

Z. Chen, D. Koleva, **Stray current corrosion as determined by geometrical orientation of steel rebar**, submitted to Construction and Building Materials.

Acknowledgements

Time flies. In Oct 2013, a one-way ticket for PhD was given to me by TU Delft and CSC (China Scholarship Council). As the most exciting adventure in my life until now, this PhD has presented the biggest challenge. Without the help of many people during this long journey, reaching this destination would have been impossible.

This project/research was carried out in the Microlab, Faculty of Civil Engineering and Geosciences, TU Delft, and financially sponsored by TU Delft and CSC. TU Delft and CSC are gratefully acknowledged.

I would like to express my sincerest gratitude to my promotor - Prof.dr.ir. Klaas van Breugel. His valuable comments, inspiring discussions, and the freedom he gave me in the research helped me to complete this project. His suggestions for linking the test results to practical engineering, for concise writing, changed my views in both study and research. All his tireless efforts and constructive comments on this dissertation are highly appreciated.

I would like to give my deepest acknowledgement to my copromotor - Dr. ir. Dessi Koleva. In these years, her valuable suggestions and encouragement supported me to pursue a doctorate. Her suggestions for linking the discovered phenomena with each other, have improved me a lot. Her focus and patience on cycles of revisions of this thesis draft are highly appreciated.

I also would like to thank Dr. Guang Ye, for his patient help on applying for this PhD position. Appreciations also go to Prof.dr. H.E.J.G. Schlangen, for his worthy suggestions on the test plans related to this research.

Dissertation committee members of Prof. dr. B.M. Wang, Prof.dr.ir. E.A.B. Koenders, Prof. dr. C. Andrade, Prof.dr.ir. R.P.B.J. Dollevoet, Prof.dr.ir. H.E.J.G. Schlangen, are greatly acknowledged for their constructive comments and valuable feedback on this thesis. I would like to acknowledge the guidance and helpful advice from them.

I would like to thank all the technicians at TU Delft for their help during this research. Mr. Maiko van Leeuwen, Mr. Gerrit Nagtegaal, Mr. John van den Berg and Mr. Arjan Thijssen are highly appreciated for their help with my experimental work. Furthermore, I would like to thank Mr. Kees van Beek from TU Delft-UD-DEMO, of the excellent assistance and suggestions on electrical aspects involved in this work. Mr. Fred Schilperoort helped a lot for the pull-out tests, his support is also highly appreciated.

Our secretaries Jacqueline van Unen-Bergenhenegouwen, Claire de Bruin, Nynke Verhulst, Iris Batterham, and Franca Post from CICAT helped me a lot with various daily issues. They are greatly recognized as well.

I warmly acknowledge all the colleagues and former colleagues of Microlab. I want to thank Dr. Oguzhan Copuroglu, Dr. Henk Jonks, Dr. Branko Savija. The cooperation and discussions with Dr. Agus Susanto, Dr. Farhad Pargar, Dr. Hitham Amin Hassan, Dr. Wenhao Guo, Dr. Kai Zhang, Dr. Amir Zommodian, in both work and life are highly appreciated. Thank Dr. Zhiwei Qian, Dr. Zhengxian Yang, Dr. Zhuqing Yu, Dr. Tianshi Lu, Dr. Hua Dong, Dr. Peng Gao, Dr. Haoliang Huang, Hao Huang, Dr. Xiaowei Ouyang, Jiayi Chen, Dr. Yong Zhang, Bei Wu, Dr. Chunping Gu, etc, for their help and suggestions. Appreciations also go to Xuliang Hou, Dr. Leyang Lyu, Dr. Hongzhi Zhang, Dr. Xu Ma, Dr. Yibing Zuo, Dr. Wenjuan Lyu, Shizhe Zhang, Zhenming Li, Dr. Shi Xu, Yu Chen, Yidong Gan, Yading Xu, Zhiyuan Xu, Boyu Chen, Ze Chang, Yu Chen, Prof. Jiangxiong Wei, Dr. Fuhai Li, Renee Mors, Dr. Marija

Nedeljkovic, Dr. Damian Palin, Dr. Mladena Lukovic, Dr. Zichao Pan, Dr. Eirini Tziviloglou, Dr. Senot Sangadji, Stefan Chaves Figueiredo, Claudia Romero, Balqis MD Yunus, Luiz Miranda de Lima Junior, Irving Flores Beltran, etc., for their support and help.

I owe my thanks to Dr. Fanming Qu and Ben Zhu, the roommates in the Netherlands. Their friendship is a great pleasure I gained during this PhD period. And thank all other friends I met in Netherlands.

I would like to thank some friends from hometown. Xiao Ni, Ms. Yingying Mao and little Kaizheng Ni, our meeting and dinner in Brussels are unforgettable. This is one of the best memories over my stay in Europe. I want to say a special thank you to Ms. Hao Han, for the meetings and talks in Beijing. These moments are worthy to be kept in mind.

I want to express my greatest appreciation to my parents for bringing me up, for their unconditional love, support, and sacrifices. Without them I cannot be a human being/child of universe on this earth, not to mention I can finish this PhD thesis.

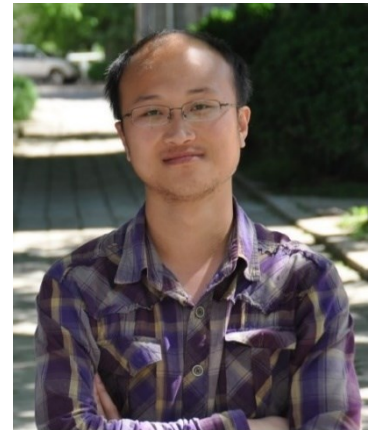
Mom, I miss you. You haven't left me, you are the fire burning in my heart, and warm me forever.

Zhipei Chen
Feb 2021
Delft, the Netherlands

Curriculum Vitae

Personnel Information:

Name: Zhipei CHEN (陈志裴)
Date of birth: 09 Oct, 1987
Place of birth: Hengshui, Hebei, P.R. China
Email: zhipeichen@outlook.com



Education Experience:

Oct 2013 – Feb 2021	PhD Candidate Microlab Faculty of Civil Engineering and Geosciences Delft University of Technology, the Netherlands
Sep 2010 – Jul 2013	Master of Engineering MSc in Structural Engineering (Excellent Master's Thesis) School of Civil Engineering Dalian University of Technology, P.R. China
Aug 2006 – Jul 2010	Bachelor of Engineering BSc in Civil Engineering School of Human Settlements and Civil Engineering Xi'an Jiaotong University, P.R. China

